Development of photoinitiating systems based on NHC-boranes for visible lightinduced emulsion and dispersion polymerization

Rémi Canterel

▶ **To cite this version:**

Rémi Canterel. Development of photoinitiating systems based on NHC-boranes for visible lightinduced emulsion and dispersion polymerization. Polymers. Université de Lyon, 2020. English. NNT : 2020LYSE1311 . tel-03506296

HAL Id: tel-03506296
https://theses.hal.science/tel-03506296

Submitted on 2 Jan 2022

HAL is a multi-disciplinary open access archive for the deposit and dissemination of scientific research documents, whether they are published or not. The documents may come from teaching and research institutions in France or abroad, or from public or private research centers.

L'archive ouverte pluridisciplinaire **HAL**, est destinée au dépôt et à la diffusion de documents scientifiques de niveau recherche, publiés ou non, émanant des établissements d'enseignement et de recherche français ou étrangers, des laboratoires publics ou privés.

N° d'ordre NNT : 2020LYSE1311

THESE de DOCTORAT DE L'UNIVERSITE DE LYON
opérée au sein de
l'Université Claude Bernard Lyon 1

Ecole Doctorale N° 206
Chimie, Procédés, Environnement

Spécialité de doctorat : **Polymérisation en milieux dispersés**

Soutenue publiquement le 08/12/2020, par :
Rémi CANTEREL

Development of photoinitiating systems based on NHC-boranes for visible light-induced emulsion and dispersion polymerization

---

Devant le jury composé de :

Chemtob Abraham Maître de Conférences, Université de Haute-Alsace	Rapporteur
Lacroix-Desmazes Patrick Directeur de Recherche, CNRS Montpellier	Rapporteur
Beyou Emmanuel Professeur des Universités, Université Lyon 1	Président du jury
Lalevée Jacques Professeur des Universités, Université de Haute-Alsace	Examinateur
Rieger Jutta Chargée de Recherche, CNRS Paris	Examinatrice
Lansalot Muriel Directrice de Recherche, CNRS Lyon	Directrice de thèse
Bourgeat-Lami Elodie Directrice de Recherche, Université Lyon 1	Co-directrice
Lacôte Emmanuel Directeur de Recherche, Université Lyon 1	Co-directeur

UNIVERSITE CLAUDE BERNARD – LYON 1

Administrateur provisoire de l'Université	M. Frédéric FLEURY
Président du Conseil Académique	M. Hamda BEN HADID
Vice-Président du Conseil d'Administration	M. Didier REVEL
Vice-Président du Conseil des Etudes et de la Vie Universitaire	M. Philippe CHEVALLIER
Vice-Président de la Commission de Recherche	M. Jean-François MORNEX
Directeur Général des Services	M. Pierre ROLLAND

COMPOSANTES SANTE

Département de Formation et Centre de Recherche en Biologie Humaine	Directrice : Mme Anne-Marie SCHOTT
Faculté d'Odontologie	Doyenne : Mme Dominique SEUX
Faculté de Médecine et Maïeutique Lyon Sud - Charles Mérieux	Doyenne : Mme Carole BURILLON
Faculté de Médecine Lyon-Est	Doyen : M. Gilles RODE
Institut des Sciences et Techniques de la Réadaptation (ISTR)	Directeur : M. Xavier PERROT
Institut des Sciences Pharmaceutiques et Biologiques (ISBP)	Directrice : Mme Christine VINCIGUERRA

COMPOSANTES & DEPARTEMENTS DE SCIENCES & TECHNOLOGIE

Département Génie Electrique et des Procédés (GEP)	Directrice : Mme Rosaria FERRIGNO
Département Informatique	Directeur : M. Behzad SHARIAT
Département Mécanique	Directeur M. Marc BUFFAT
Ecole Supérieure de Chimie, Physique, Electronique (CPE Lyon)	Directeur : Gérard PIGNAULT
Institut de Science Financière et d'Assurances (ISFA)	Directeur : M. Nicolas LEBOISNE
Institut National du Professorat et de l'Education	Administrateur Provisoire : M. Pierre CHAREYRON
Institut Universitaire de Technologie de Lyon 1	Directeur : M. Christophe VITON
Observatoire de Lyon	Directrice : Mme Isabelle DANIEL
Polytechnique Lyon	Directeur : Emmanuel PERRIN
UFR Biosciences	Administratrice provisoire : Mme Kathrin GIESELER
UFR des Sciences et Techniques des Activités Physiques et Sportives (STAPS)	Directeur : M. Yannick VANPOULLE
UFR Faculté des Sciences	Directeur : M. Bruno ANDRIOLETTI

Remerciements

Je voudrais tout d'abord remercier Timothy McKenna pour son accueil au laboratoire de Chimie, Catalyse, Polymères et Procédés (C2P2) et l'Agence Nationale de la Recherche pour le financement de ce projet de thèse. Ce travail est le fruit d'une étroite collaboration entre PnP, l'Institut de Science des matériaux de Mulhouse (IS2M) et les laboratoires C2P2 et LHCEP.

Je tiens à remercier les membres du jury pour avoir accepté d'évaluer mon travail de thèse. Merci à Patrick Lacroix-Desmazes et Abraham Chemtob en leur qualité de rapporteurs. Je remercie également Jutta Rieger et Jacques Lalevée pour leur présence en tant qu'examinateurs de mon travail de thèse, ainsi que Emmanuel Beyou pour avoir présidé le jury.

Ces trois années de thèse n'auraient pas pu se faire sans mes trois super encadrants. Je commencerai donc par remercier Emmanuel Lacôte pour ses connaissances sur la chimie du bore. Je remercie très sincèrement Elodie Bourgeat-Lami pour tout ce qu'elle a pu me transmettre scientifiquement. J'ai pu ainsi entreprendre un sujet complètement innovant que je ne maîtrisais pas lorsque je suis arrivé au laboratoire. Les réunions à deux dans ton bureau à parler Pickering et oxydes de cérium furent très enrichissantes. J'ai également apprécié le côté humain chez toi où on a pu avoir des discussions ouvertes. Pour terminer, je remercie chaleureusement ma directrice de thèse Muriel Lansalot. Merci d'avoir partagé toutes tes connaissances scientifiques (et il y en a beaucoup !). Maintenant, je me sens d'attaque pour faire des polymères en milieux dispersés. Outre l'aspect scientifique, nous avons pu partager de très bons moments autour d'un superbe barbecue ainsi que lors de nos divers congrès, je pense à la Crète en particulier ! J'espère sincèrement qu'on pourra travailler ensemble sur d'autres projets dans un futur proche !

Je voudrais remercier toutes les personnes qui ont contribué au bon déroulement de ces trois ans de thèse. Je pense bien évidemment à Pierre-Yves pour toutes ces heures passées en microscopie. Egalement un immense merci à Edgar qui a toujours été présent au labo quand quelque chose n'allait pas et surtout merci pour ta générosité et ta bienveillance. Je remercie Franck Collas pour les études de DMA. De manière générale, je remercie l'ensemble des permanents du laboratoire d'avoir rendu ces trois ans de thèse moins douloureux. Un très grand merci à Nathalie pour toutes nos discussions et rigolades. Je remercie Sébastien pour sa bonne

humeur, Vincent pour sa franchise et ses discussions autour du 7ème art et Jean pour nos petits débats lors des pauses café.

Durant ces trois ans, j'ai pu faire la rencontre de nombreux étudiants et je voudrais vous remercier pour tous les bons moments partagés comme la soirée bowling, la fondue savoyarde, le karakoé … Je remercie donc Marie, Yashmin, Ana, Alice, Roberta, Marianna, Arne, Felipe, Rhaman, Nicolas, Ambroise. Merci à mon homme idéal Flo, Paul le râleur qui n'arrive pas encore à mon niveau, James pour sa bonne humeur, Wilfried monsieur blague de c*l, Cédric mon second homme idéal, Matthieu H mon troisième homme idéal (décidemment ^^), Mathieu F (alors ce fameux doigt ?), Mathieu C ça va Mathieu ?, Aurélien pour toutes les bières et les jeux de société, et enfin Juliette pour tes valeurs dans lesquelles je me reconnais.

J'aimerais remercier quatre personnes en particulier, à commencer par Amel. J'apprécie beaucoup ton honnêteté et ta joie de vivre. Tu profites à fond de chaque moment de la vie et tu as bien raison. Nous avons rapidement partagé de très bons moments et cela tout le long de cette thèse. La vie au labo sans toi n'aurait clairement pas été aussi drôle, notamment lorsque tu as demandé à Damien de dépiauter ta cuisse de poulet ! Ca restera dans les annales. Je te souhaite de réussir tes projets futurs et à très vite pour faire la fête ou un Bang ! J'espère que cette fois-ci tu te souviendras des règles ;). Je continue ce paragraphe pour remercier Prisssss. Au début de la thèse, j'ai rencontré une Priscilla plutôt réservée et qui pensait que les séries et les films correspondaient à la réalité. Pendant ces trois ans, j'ai pu voir une nouvelle Priscilla gagner en maturité, qui profite de la vie et qui est devenue une « killeuse ». Ce fut un réel plaisir de t'avoir rencontré et d'avoir pu partager nos angoisses et nos moments de joie. Je garde un excellent souvenir de la Crète où on s'est tellement empiffré qu'on roulait pour aller aux conférences. Nos soirées jeux de société me manqueront énormément, surtout Shadow Hunter ! Bonne chance pour la suite, je suis certain que tu vas t'épanouir dans tes projets futurs. Astriiiiiiiiiiiiiid ! Quel bonheur de t'avoir connu. Tu es un véritable soleil, toujours souriante et d'une gentillessee absolue. Je garderai tellement de bons souvenirs, notamment à Ibiza et l'eau turquoise incroyable de la cala Comté, mais aussi la Corse et toutes les soirées que nous avons pu faire à se déhancher sur la piste de danse ! Vive la disco ! Je termine par la crème de la crème, ma doudou. Ca fait maintenant six ans qu'on se connait et quel hasard qu'on se retrouve dans le même labo. Je me souviens des débuts où on allait à la cafétéria Astrée pour manger un sandwich au pain car on n'osait pas manger avec les permanents. On en aura passé du temps ensemble, tellement de rigolades mais aussi quelques disputes et des larmes. Mais

nous avons pu surmonter cela, signe que notre amitié est très solide. Je crois que tu es la personne qui m'a fait le plus rire dans toute ma vie (je ne suis plus si jeune et oui !). Tu te souviens de notre retour du dîner avec Bernadette à Mulhouse, je crois que c'est la première fois que j'ai senti mes abdos ! Nos chemins vont malheureusement se séparer et je crois bien être triste sans toi à mes côtés mais tu restes toujours dans mon cœur et ma tête. Je te souhaite toutes les réussites possibles dans ta future carrière et en amour !

Il n'y a pas uniquement la vie au labo, et durant ces trois années de thèse, j'ai pu compter sur le soutien de ma famille MTX. Je remercie ainsi Alice, Elodie, Charlotte, Julie, Gomi, Hadrien, Gaetan et Thomas. Je remercie également mes deux crocos nimoises Emilie et Pauline. Un grand merci à ma Angela qui est venu me rendre visite et a découvert cette magnifique ville qu'est Lyon, toujours un bonheur de t'être en ta compagnie. Merci également à Lolo et Carine la team Givo ! Durant la dernière année (la plus difficile), j'ai pu faire la rencontre de Nahuel qui malgré tout a réussi à me supporter ! Ton soutien aura été d'une grande importance et maintenant que tu as survécu à la thèse, tu pourras affronter n'importe quelle situation à venir. Je te remercie énormément d'être à mes côtés tous les jours. Te amo muchisimo mi Opi.

C'est avec beaucoup d'émotions que remercie ma famille qui aura été d'un grand soutien pendant ces trois ans de thèse. Merci à mon frère Cédric et ma sœur Cécile. Je remercie tout particulièrement ma maman qui m'a procurée tout son amour et une excellente éducation. Si j'en suis là actuellement c'est en grande partie grâce à elle. Je ne te le dis pas très souvent mais je t'aime très fort.

Résumé

Les procédés de synthèse de latex occupent depuis des décennies une place importante dans l'industrie. En effet, les latex synthétiques, c'est-à-dire des dispersions colloïdales de polymère, sont utilisés dans de nombreux domaines tels que les revêtements, les peintures et les adhésifs, popularité qui s'explique par la vaste gamme de produits accessibles, en termes de taille, de composition, de morphologie et de fonctionnalité des particules. Parmi tous les procédés de polymérisation en milieu hétérogène, la photopolymérisation en milieu dispersé n'a été rapportée pour la première fois que dans les années 1980. Depuis, les études sur le sujet sont rares et seuls quelques travaux sur des monomères tels que le méthacrylate de méthyle et le styrène ont été publiés jusqu'ici. Toutefois, la photopolymérisation est attrayante car elle est amorcée par la lumière et permet donc un contrôle externe de la polymérisation, du point de vue spatial comme temporel. Des stratégies doivent donc être mises en place pour combiner les avantages de la photopolymérisation, en particulier dans le domaine du visible, avec ceux de la polymérisation en milieu dispersé.

Pour atteindre cet objectif, il a fallu franchir deux principaux obstacles. Premièrement, la majorité des systèmes photo-amorceurs sont lipophiles. Or, la polymérisation en émulsion est le plus souvent conduite dans l'eau, ce qui nécessite l'utilisation d'amorceurs hydrosolubles. De plus, la présence des gouttelettes de monomère ainsi que des particules de polymère formées au cours de la polymérisation vont, du fait de leurs tailles (gouttelettes et particules varient de 1 et 20 µm, et de 50 et 500 nm, respectivement) engendrer des phénomènes de diffusion de la lumière, notamment lorsqu'il s'agit de rayonnement UV. Il faut se tourner vers l'utilisation d'une source de lumière visible qui produit des photons ayant des longueurs d'onde plus grandes, ce qui permet de mieux adapter ce système aux milieux dispersés. En effet, les photons dans le visible sont moins soumis aux effets de diffusion induits par la présence de particules de quelques centaines de nm de diamètre, permettant ainsi une meilleure pénétration de la lumière.

Au sein des laboratoires C2P2 et LHCEP, F. Le Quéméner[1] et D. Subervie[2] ont développé au cours de leur thèse un nouveau système photo-amorceur hydrosoluble pour la polymérisation en émulsion absorbant la lumière visible à température ambiante. Il est composé d'un colorant (acridine orange), d'un composé disulfure et d'un carbène *N*-hétérocyclique-

[1] F. Le Quéméner, Utilisation de NHC-Boranes pour la synthèse de nanoparticules et l'amorçage de photopolymérisation en émulsion, phdthesis, Université de Lyon, 2016.
[2] D. Subervie, NHC-Boranes : amorceurs de photopolymérisation en émulsion et nouveaux matériaux énergétiques, phdthesis, Université de Lyon, 2018.

borane (NHC-BH_3) (Figure 1). L'utilisation de LEDs en tant que source de lumière visible par rapport à la lumière UV, est intéressante car les photons sont moins énergétiques. De plus la lampe est simple à mettre en place et apporte plus de sécurité pour l'opérateur. Ce système photo-amorceur a ainsi conduit à l'amorçage de la photopolymérisation en émulsion de monomères acryliques et du styrène. Les latex finaux obtenus sont très stables, avec des diamètres de particules compris entre 50 et 300 nm et avec des taux de solides allant jusqu'à 30%.

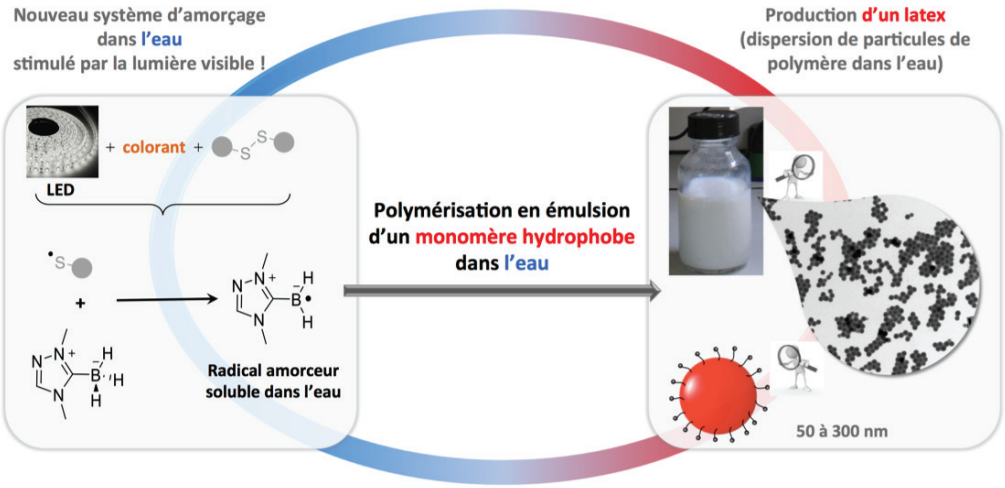

***Figure 1**. Photopolymérisation en émulsion : production de particules de polymère grâce à la lumière visible.*

Cependant, il a été également observé au cours de ces précédents travaux que les différentes espèces du système photo-amorceur, notamment le colorant et le NHC-BH_3 pouvaient se partager entre les deux phases (le monomère et l'eau), ce qui entraîne une large distribution de taille des particules. Dans ce travail, nous avons étudié différentes stratégies permettant de réduire cette distribution de tailles de particules. Un nouveau NHC-BH_3 fonctionnalisé par un groupe amine a été synthétisé puis testé pour la photopolymérisation en émulsion du styrène. Il conduit à un latex stable avec une amélioration significative de la distribution de tailles de particules. Puis, l'utilisation de colorants plus solubles dans l'eau que l'acridine orange a permis de synthétiser des latex de polystyrène très stables avec également des distributions de tailles très étroites. Enfin, nous avons étudié la photopolymérisation en émulsion du méthacrylate de méthyle amorcée par la lumière verte afin d'améliorer l'absorption des photons par le colorant en fonction de leur longueur d'onde maximale d'absorption. Les premiers résultats avec le colorant éosine Y semblent très prometteurs.

Dans une seconde partie, nous avons préparé des latex de polystyrène par photopolymérisation en dispersion en utilisant le système photo-amorceur d'origine (AO/NHC-

BH3 et un disulfure soluble dans l'eau – Figure 2) dans le but de préparer des particules plus grosses. En effet, la polymérisation en dispersion se distingue par sa capacité à atteindre une large gamme de tailles de particules (de quelques centaines de nm à quelques microns). De plus, le milieu réactionnel est initialement homogène, ce qui pourrait aider à augmenter la pénétration de la lumière au début de la réaction. Nous avons dans un premier temps étudié un poly(éthylène glycol) méthacrylate (PEGMA, M_n = 2 080 g mol^{-1}) en tant que stabilisant réactif dans un mélange éthanol/eau (70/30 en masse).

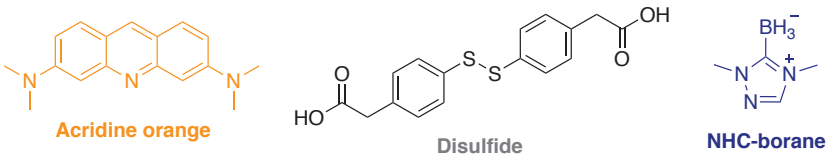

***Figure 2**. Structure chimique du système photo-amorceur d'origine composé d'un colorant acridine orange, d'une espèce disulfure et d'un NHC-borane.*

Des problèmes de reproductibilité lors de la photopolymérisation du styrène en dispersion ont été observés ainsi que de plus larges distributions de taille par rapport aux polymérisations en dispersion amorcées thermiquement (Figure 3). Ces problèmes s'expliqueraient par le fait qu'à partir d'une certaine taille de particules en croissance (de l'ordre de 200 nm), des phénomènes de diffusion impacteraient fortement la génération des radicaux, conduisant à des cinétiques stochastiques. Toutefois, la taille finale des latex reste similaire (*ca.* 200 nm). L'ajout d'une base organique a permis de mieux solubiliser le composé disulfure du système photo-amorceur (partiellement soluble dans le milieu hydro alcoolique) et donc d'améliorer les vitesses de polymérisation. Ainsi, nous avons pu obtenir des latex de polystyrène avec des tailles de l'ordre de 360 nm avec une excellente reproductibilité. Néanmoins, dans ces conditions expérimentales, il est difficile de dépasser cette taille de particule.

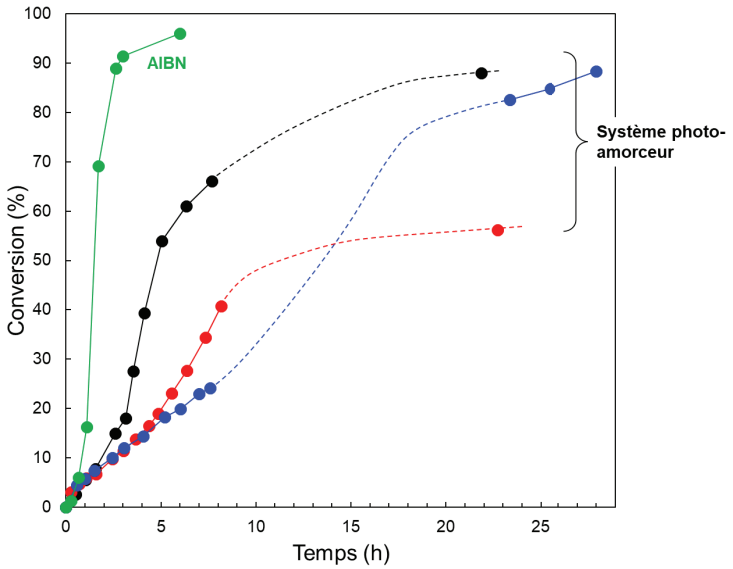

Figure 3. *Reproductibilité – Évolution de la conversion en fonction du temps pour des polymérisations en dispersion du styrène (courbes noire, rouge et bleue en photochimie et courbe verte en thermique) avec le stabilisant PEGMA (10 % en masse par rapport au styrène).*

Nous avons donc décidé de remplacer le stabilisant PEGMA par un homopolymère généralement utilisé en dispersion, la poly(*N*-vinylpyrrolidone) (PVP-K30, M_n = 40 000 g mol^{-1}) qui, *via* des réactions de transfert, permet de créer *in situ* un stabilisant du type PVP-*g*-PS. Nous montrons pour la première fois dans des conditions de photochimie la formation de particules très grosses (900 nm) avec une distribution de taille très étroite (Figure 4). Cependant, des problèmes de reproductibilité des cinétiques de polymérisation ont été à nouveau rencontrés. Durant les premières heures de la synthèse, les courbes de conversion suivent la même tendance. Cependant, lorsqu'une certaine taille critique (aux alentours de 200 nm) est atteinte à des conversions relativement faibles (< 20%), les cinétiques divergent à cause des phénomènes de diffusion de la lumière par les particules en croissance. Finalement, les tailles obtenues (> 800 nm), avec des conversions de 75–80%, supposent que la lumière continue à pénétrer dans le milieu réactionnel et génère des radicaux. Enfin, à une longueur d'onde sélectionnée (notamment dans le domaine du visible), la lumière est moins affectée par les particules de larges tailles et pénètre à nouveau.

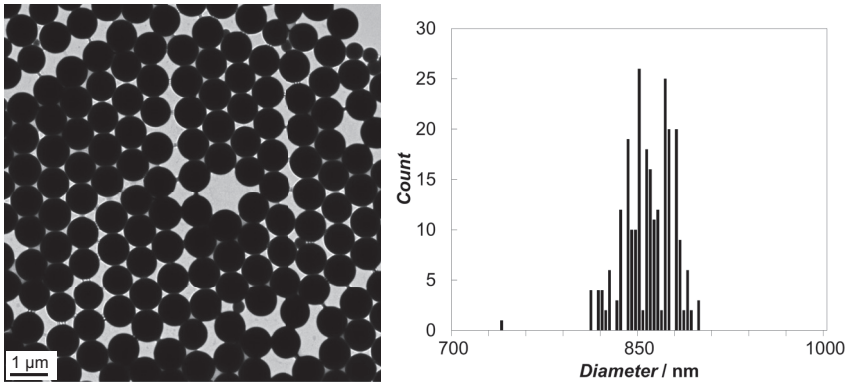

***Figure 4**. Image de microscopie électronique en transmission et la distribution de taille correspondante pour un latex de polystyrène obtenu par photopolymérisation en dispersion en présence de la PVP-K30 (10% en masse par rapport au styrène).*

Enfin, nous avons tiré avantage du photo-amorçage que permet la seule utilisation du composé disulfure dans le domaine du visible pour des monomères (méth)acryliques pour synthétiser des particules hybrides par photopolymérisation en dispersion de type Pickering, dans laquelle la stabilisation est apportée par des nanoparticules solides d'oxyde de cérium (CeO_2). La localisation du CeO_2 à la surface des particules de polymère s'appuie sur l'adsorption (par complexation) du composé disulfure à la surface des nanoparticules inorganiques *via* ses fonctions acides carboxyliques. A notre connaissance, il s'agit du premier exemple de formation de latex hybrides CeO_2–polymère par photopolymérisation en dispersion de type Pickering. Nous avons ainsi obtenu des latex stables de poly(acrylate de butyle-*co*-méthacrylate de méthyle) dont les tailles vont jusqu'à 400 nm et avec une excellente robustesse du système. Nous avons ensuite formé des films et étudié leurs propriétés mécaniques et anti-UV.

Table of content

ABBREVIATIONS 1

GENERAL INTRODUCTION 5

***CHAPTER 1.* PREAMBLE ON THE FUNDAMENTALS OF PHOTOPOLYMERIZATION IN DISPERSED MEDIA** 9

I. INTRODUCTION TO PHOTOINITIATED POLYMERIZATION 13

A. PHOTOPHYSICAL AND PHOTOCHEMICAL PROCESSES DURING PI EXCITATION 14
B. PHOTOINITIATORS: STRUCTURE AND EFFICIENCY 15

II. POLYMERIZATION IN DISPERSED MEDIA 17

III. PHOTOPOLYMERIZATION ADAPTED TO POLYMERIZATION IN DISPERSED MEDIA: MAIN CHALLENGES 19

A. INTERACTIONS BETWEEN LIGHT AND PARTICLE 19
B. FUNDAMENTALS OF LIGHT ABSORPTION AND SCATTERING BY PARTICLES 21
1. Key parameters *21*
2. Extinction cross-section of a spherical particle *23*
3. Efficiency factors *25*
4. Angular distribution of scattering intensity *26*
C. LIGHT ABSORPTION AND SCATTERING: CASE OF PHOTOPOLYMERIZATION IN DISPERSED MEDIA 28
1. Light penetration issue and consequences *28*
2. How to improve the light penetration within the reaction medium? *31*

IV. CONCLUSION 32

REFERENCES 33

CHAPTER 2. VISIBLE-LIGHT INDUCED EMULSION POLYMERIZATION OF STYRENE AND ACRYLATE MONOMERS 35

PART 1. STATE-OF-THE-ART 39

I. GENERALITIES 39

II. MECHANISM AND KINETICS OF EMULSION POLYMERIZATION 40

A. NUCLEATION STEP 41
B. GROWTH STEP 43

III. PHOTOPOLYMERIZATION IN EMULSION UNDER UV-VISIBLE LIGHT: STATE-OF-THE-ART 44

A. PIONEERING STUDIES ON PHOTOPOLYMERIZATION IN DISPERSED MEDIA 44
B. EMULSION PHOTOPOLYMERIZATION 45
1. UV light-induced oil-in-water emulsion polymerization *45*
2. UV light-induced inverse water-in-oil emulsion polymerization *54*
3. Visible light-induced oil-in-water emulsion polymerization *55*

IV. CONCLUSION 58

PART 2. REMINDERS OF PREVIOUS WORKS ON THE USE OF NHC-BORANES AS CO-INITIATORS FOR VISIBLE LIGHT-INDUCED EMULSION POLYMERIZATION 60

I. FORMATION OF NHC BORYL RADICALS UNDER VISIBLE LIGHT 60

II. EMULSION PHOTOPOLYMERIZATION OF STYRENE 61

A. OPTIMIZATION OF THE IRRADIATION SET-UP AND PHOTOINITIATING SYSTEM 61

B. Influence of several parameters on the particles size and polymerization kinetics 64
C. Comparison with thermally activated emulsion polymerization 66

II. EMULSION PHOTOPOLYMERIZATION OF MMA 68

A. Effect of reaction conditions on polymerization kinetics and particles size 68
B. Influence of the PIS composition for the emulsion photopolymerization of MMA 70

III. EMULSION PHOTO(CO-)POLYMERIZATION OF VARIOUS MONOMERS 74

A. Photopolymerization of other (meth)acrylate monomers with disulfide alone as photoinitiator 74
B. Synthesis of copolymers photoinduced by the three-component PIS vs. disulfide alone 75

IV. CONCLUSION 77

PART 3. STRATEGIES TO NARROW THE SIZE DISPERSITY OF LATEX PARTICLES PREPARED BY EMULSION PHOTOPOLYMERIZATION UNDER VISIBLE IRRADIATION 78

I. INFLUENCE OF THE TYPE OF STABILIZER 78

II. DEVELOPMENT OF MORE WATER-SOLUBLE PISS FOR EMULSION PHOTOPOLYMERIZATION 80

A. Impact of the reactor geometry and LED brightness on the outcome of the polymerization reaction 80
B. Determination of AO and NHC-BH_3 partition coefficients 81
C. New water-soluble dyes for the photoinitiating system 83
1. Case of styrene 83
2. Case of MMA 87
D. Synthesis of new co-initiator NHC-boranes 89
1. Sulfonated-functionalized NHC-boranes 89
2. Amino-functionalized NHC-borane 94
E. Summary 96

III. REACTOR OPTIMIZATION: NEW COLOR LED RIBBON 97

GENERAL CONCLUSIONS 99

REFERENCES 101

CHAPTER 3. VISIBLE LIGHT-INDUCED DISPERSION POLYMERIZATION OF STYRENE PERFORMED IN HYDROALCOHOLIC MEDIUM 105

PART 1. STATE-OF-THE-ART 109

I. HISTORICAL CONTEXT 109

II. FORMATION OF PARTICLES BY DISPERSION POLYMERIZATION 110

A. Structure of stabilizer in polar media 112
1. Graft copolymers 112
2. Block copolymers 114
a. Macroinitiators 114
b. Macromolecular chain transfer agents (macro-CTAs) 116
B. Mechanism of particle formation in dispersion polymerization 118
A. Solubility parameters 120
B. Influence of the stabilizer 124
C. Effect of initiator 126
D. Effect of the temperature 129

IV. KINETICS OF DISPERSION POLYMERIZATION 131

A. First theoretical model of dispersion polymerization 131
B. The overall rate of dispersion polymerization 132

C. Determination of the polymerization locus 134
D. Reactivity of macromonomers in copolymerization 136

V. PHOTO-INDUCED DISPERSION POLYMERIZATION: FROM FREE RADICAL PHOTOPOLYMERIZATION TO PHOTO-PISA 138

A. Free radical polymerization in photo-dispersion 139
B. Reversible-deactivation radical polymerization in photo-dispersion 141
C. Polymerization-induced self-assembly in photo-dispersion 144

PART 2. OUR THREE-COMPONENT PHOTOINITIATING SYSTEM APPLIED TO DISPERSION POLYMERIZATION 149

I. DISPERSION PHOTOPOLYMERIZATION OF STYRENE WITH PEGMA 150

A. Transposition from emulsion to dispersion: robustness of our photoinitiating system 150
B. Effect of the photoinitiator concentration 153
C. Effect of stabilizer concentration 156
D. Disulfide vs. three-component photoinitiation system 159
E. Particle size vs. light penetration: reproducibility issue? 162
F. Influence of an organic base 164
1. Effect of TBAH concentration 165
2. Effect of stabilizer concentration in presence of TBAH 169
3. Disulfide as type I photoinitiator in the presence of TBAH 172
G. Conclusions 174

II. DISPERSION PHOTOPOLYMERIZATION OF STYRENE WITH PVP 175

A. Robustness of our photoinitiating system 175
B. Effect of temperature 178
C. Effect of the PVP concentration 181
D. Conclusions 182

GENERAL CONCLUSIONS 183

REFERENCES 185

CHAPTER 4. POLYMER/INORGANIC HYBRID LATEX PARTICLES VIA HYDROALCOHOLIC DISPERSION PHOTOPOLYMERIZATION UNDER VISIBLE LIGHT IRRADIATION 189

PART 1. LITERATURE REVIEW 193

I. INTRODUCTION 193

II. FORMATION OF ORGANIC/INORGANIC HYBRID LATEXES BY PICKERING POLYMERIZATION IN DISPERSED MEDIA 196

A. Pickering emulsions 196
B. Pioneering studies on heterogeneous Pickering polymerization in dispersed media 198
C. Pickering dispersion polymerization 198
1. Silica 198
2. Clay 200
3. Iron oxide 202

PART 2. CERIUM DIOXIDE AS PICKERING STABILIZER 203

I. CERIUM DIOXIDE 203

A. Nature of the CeO_2 sol 203
B. Particle size and morphology 203
C. Crystalline structure 204
D. Surface chemistry 206

II. SYNTHESIS OF CeO_2-ARMORED HYBRID LATEXES BY POLYMERIZATION OF PICKERING MINIEMULSIONS 208

A. Stabilization of miniemulsion droplets by CeO_2 nanoparticles 208
B. Polymerization of CeO_2-stabilized miniemulsions 209
C. Conclusion 213

III. SYNTHESIS OF CeO_2-ARMORED HYBRID LATEXES BY PICKERING EMULSION POLYMERIZATION 213

A. Functionalization of CeO_2 nanoparticles by MAA 214
B. Pickering emulsion polymerization with CeO_2 nanoparticles 215
C. Characteristics of CeO_2-armored P(*n*-BA-*co*-MMA) latex films 218

IV. SYNTHESIS OF CeO_2-ARMORED HYBRID LATEXES BY PICKERING EMULSION PHOTOPOLYMERIZATION 222

A. Functionalization of CeO_2 nanoparticles by disulfide 223
B. Pickering emulsion photopolymerization with CeO_2 nanoparticles 225

PART 3. SYNTHESIS OF CeO_2-ARMORED LATEXES *VIA* VISIBLE LIGHT-INDUCED PICKERING DISPERSION POLYMERIZATION 228

I. PREPARATION OF DICARBOXYLIC ACID DIPHENYL DISULFIDE MODIFIED CeO_2 NANOPARTICLES 229

A. Stabilization of CeO_2 nanoparticles in hydroalcoholic medium 229
1. Choice of the hydroalcoholic medium 229
2. Surface modification of CeO_2 nanoparticles by disulfide 230

II. SYNTHESIS OF CeO_2-ARMORED HYBRID LATEXES BY PICKERING DISPERSION PHOTOPOLYMERIZATION 236

A. Efficiency of our disulfide-modified CeO_2 nanoparticles for Pickering dispersion photocopolymerization of *n*-BA and MMA 237
B. Influence of the CeO_2 content 239
C. Influence of the disulfide concentration 241
D. Influence of the luminous flux 244
E. Towards very low CeO_2 contents 245
F. Influence of the monomer concentration 248
G. Proposed mechanism for the particle formation 250
H. Disulfide vs. three-component photoinitiating system 252

III. CHARACTERIZATION OF CeO_2-ARMORED P(*N*-BA-*CO*-MMA) LATEX FILMS 253

A. Structural characterization 254
B. Optical properties 255
C. Mechanical properties 257

GENERAL CONCLUSION 259

REFERENCES 261

CHAPTER 5. EXPERIMENTAL PART 265

I. MATERIALS AND METHODS 269

II. OPERATING PROCEDURES 274

A. Syntheses of photoinitiating systems 274
*1. Synthesis of disulfide (**4**) 274*
2. Synthesis of NHC-BH_3 275
B. Preparation of synthetic latexes by emulsion photopolymerization 281
C. Preparation of synthetic latexes by dispersion photopolymerization 282
D. Preparation of hybrid latexes by Pickering dispersion photopolymerization 282
*1. Modification of the CeO_2 nanoparticles surface by disulfide **(4)** 282*
2. Pickering dispersion polymerization of n-BA/MMA 283
3. Film formation 283

Abbreviations

AAPH: 2,2'-azobis(2-amidinopropane) dihydrochloride
ACN: acetonitrile
ACS: acidic CeO_2 sol
ACVA: 4,4'-azobis(4-cyanovaleric acid)
ADVN: 2,2'-azobis(2,4-dimethyl)valeronitrile
AIBN: azobisisobutyronitrile
AMBN: 2,2′-azobis(2-methylbutyronitrile)
AO (**1**): acridine orange
AOT-100: Aerosol® OT-100
AO-1805: octadecylamine ethoxylates *N*-oxide
ATR-IR: attenuated total reflectance infrared spectroscopy
ATRP: atom transfer radical polymerization
BAG: bis(4-methoxy benzoyl)diethylgermanium
BAPO: bis(2,4,6-trimethylbenzoyl)phenylphosphine oxide
BAPO-AA: 2-(bis(2,4,6-trimethylbenzoyl)phosphoryl)acetic acid
BCS: basic CeO_2 sol
BET: Brunauer, Emmet and Teller
BPO: benzoyl peroxide
BZ: benzoin
ca.: circa (= about)
Cell: cellosolve (2-ethoxyethanol)
CMC: critical micelle concentration
CQ: camphorquinone
CTA: chain transfer agent
CTAB: cetyltrimethylammonium bromide
Đ: dispersity
DAAm: diacetone acrylamide
DBK: dibenzyl ketone
DCM: dichloromethane
DEG: diethylene glycol
D_h: average hydrodynamic particle diameter
Disulfide (**2**): 5,5′-dithiobis(1-phenyl-*1H*-tetrazole)
Disulfide (**4**): dicarboxylate functionalized diaryl disulfide
DLS: dynamic light scattering
DMA: differential mechanical analysis
DMAc: dimethylacetamide
DMF: dimethylformamide
DMPA: 2,2-Dimethoxy-2-phenylacetophenone
DMSO: dimethyl sulfoxide
D_n: number average particle diameter
DP_n: degree of polymerization
DTBA: 4-diethylthiocarbamoylsulfanylmethyl benzoic acid
DTBK: 4,4'-di-tert-butyldibenzyl ketone
DVB: divinylbenzene
D_w: mass average particle diameter
E': storage modulus
e.g.: exempli gratia (= for example)
EHMA: 2-ethylhexyl methacrylate

EB: erythrosin B
EtOH: ethanol
EY: eosin Y
FIB: focused ion beam
FLP: flash laser photolysis
FT-IR: Fourier transform infrared spectroscopy
HMDS: hexamethyldisilazide
HPC: hydroxypropyl cellulose
HSP: Hansen solubility parameters
i.e.: id est (= that is)
i-PrOH: isopropyl alcohol
IEP: isoelectric point
IR: infrared
KGA: ketoglutaric acid
KHMDS: potassium hexamethyldisilazide
KPS: potassium persulfate
LED: light-emitting diode
LiHMDS: lithium hexamethyldisilazide
LWZ: poly(oxy ethylene)$_n$ nonyl phenyl ether sodium sulfate
MA: methyl acrylate
MAA: methacrylic acid
MB: methylene blue
MeCell: methyl cellosolve (2-methoxyethanol)
MEK: methyl ethyl ketone (butanone)
MeOH: methanol
MMA: methyl methacrylate
M_n: number average molar mass
mol.%: molar percent
M_w: mass average molar mass
Na(BAPO-O): bis(mesitoyl)phosphinate sodium
NaHMDS: sodium hexamethyldisilazide
n-BA: *n*-butyl acrylate
n-BMA: *n*-butyl methacrylate
ND: not determined
NHC: *N*-heterocyclic carbene
NHC-BH_3 (**3**): dimethyl-triazolylidene-borane
NMP: *N*-methyl-2-pyrrolidone
NMR: nuclear magnetic resonance
NP: nanoparticle
PAA: polyacrylic acid
PDEA: poly((2-diethylamino)ethyl methacrylate)
PDI: polydispersity index
PDMA: poly(*N*,*N*-dimethylaminoethyl methacrylate)
PDMS: polydimethylsiloxane
PEG: poly(ethylene glycol)
PEGMA: poly(ethylene glycol) methacrylate
PEI: polyethyleneimine
PEO: poly(ethylene oxide)
PEO-SH: poly(ethylene oxide) macro-thiol
PEOX: poly(2-ethyl-2-oxazoline)

PET-RAFT: photoinduced electron transfer-reversible addition-fragmentation chain transfer
PHEA: poly(hydroxyethyl acrylate)
PHEMA: poly(2-hydroxyethyl methacrylate)
PHPMA: poly(2-hydropropylmethacrylamide)
PI: photoinitiator
PIC: polyion complexation
PIS: photoinitiating system
PISA: polymerization-induced self-assembly
PMMA: poly(methyl methacrylate)
PNAM: poly(*N*-acryloylmorpholine)
PNIPAAm: poly(N-isopropylacrylamide)
POENPE: poly(oxy ethylene)$_{10}$ nonyl phenyl ether
POENPEAS: poly(oxy ethylene)$_{10}$ nonyl phenyl ether ammonium sulfate
ppm: parts per million
PS: polystyrene
PSD: particle size distribution
PTFE: poly(tetrafluoroethylene)
PVA: poly(vinyl alcohol)
PVAc: poly(vinyl acetate)
PVP: polyvinylpyrrolidone
RAFT: reversible addition-fragmentation chain transfer
RB: rose Bengal
RDRP: reversible deactivation radical polymerization
SAXS: small angle X-ray scattering
$scCO_2$: supercritical CO_2
SDS: sodium dodecyl sulfate
SEC: size exclusion chromatography
SEM: scanning electron microscopy
SFEP: surfactant-free emulsion polymerization
SG1: *N*-tert-butyl-*N*-(1-diethylphosphono-2,2-dimethylpropyl) nitroxide
SPTP: sodium phenyl-2,4,6-trimethylbenzoylphosphinate
tan δ: loss factor
t-BMA: *t*-butyl methacrylate
TEM: transmission electron microscopy
TERP: organotellurium-mediated radical polymerization
T_α : relaxation temperature
TBAH: tetrabutylammonium hydroxide
T_g: glass transition temperature
TMC: trimethylated chitosan
THF: tetrahydrofuran
TTC: S-cyanomethyl-S-dodecyltrithiocarbonate
$t_{1/2}$: half-life
VAc: vinyl acetate
vol.%: volume percent
wt.%: weight percent
XRD: X-ray diffraction
ZnTPP: 5,10,15,20-tetraphenyl-21*H*,23*H* zinc porphyrin
4-VP: 4-vinylpyridine

General introduction

A latex is defined as a colloidal dispersion of polymer particles with diameters ranging between 1 nm and 1 µm, dispersed in a liquid medium. Synthetic latexes are amongst the most industrially produced polymer materials. Indeed, their global consumption was estimated at 25.2 million wet tons in 2017 with an annual growth rate estimated at around 4.1% from 2017 to 2022.[1] By contrast, the world plastic production almost reached 360 million tons in 2018.[2] They are used in many applications such as coatings, adhesives, textiles and paints.[3] Synthetic latexes are mostly obtained by heterophase polymerization of which emulsion and suspension polymerizations are the most widely used processes. Other processes such as microemulsion, miniemulsion or dispersion polymerizations highlight the variety in experimental conditions available in dispersed media.[4–7] Synthetic latexes are mainly prepared in water, which is a green solvent, and the polymerization of a wide range of monomers such as acrylates (*e.g.*, methyl methacrylate, butyl acrylate), styrene, vinyl acetate and butadiene can be achieved. In addition, the polymer particles can represent up to 50–60 wt.% of the final dispersion, while providing a low viscosity product.

Generally, the synthesis of latexes involves thermally or redox-initiated polymerizations. There have been only a few examples of photoinduced polymerization in aqueous dispersed medium since the 1980s.[8] However, photoinduced polymerization has many advantages compared to thermally activated polymerization. It enables rapid polymerization rates under mild reaction conditions, it offers an external temporal and spatial control of the reactions, and give access to the preparation of new materials.[9,10]

In this thesis, we wished to introduce an efficient and original way to the production of latexes using photo-induced polymerization in dispersed media *via* a simple and cheap device (a LED ribbon coiled around the external glass wall of a conventional double-wall reactor).[11] Mostly photopolymerizations have been investigated with photoinitiating systems (PIS) that are almost always lipophilic and sensitive to UV irradiation. Mini- and microemulsions take advantage of these conditions since they favor the localization of the PIS inside the micelles.[12–15] However, microemulsions require a large amount of surfactant and miniemulsions are formed through high-energy homogenization. In addition, to date, no report describes a successful synthesis of latexes using conventional emulsion polymerization under UV light because the monomer droplets strongly absorb the UV photons required to initiate the photopolymerizations.

In our groups, a new water-soluble PIS based on *N*-heterocyclic carbene boranes (NHC-boranes) was introduced for a sustainable visible-light photopolymerization in collaboration with the Institut de Science des Matériaux de Mulhouse (IS2M). Two previous PhD theses [16,17] have investigated the use of NHC-boranes in the emulsion photopolymerization of styrene and (meth)acrylic monomers and developed a robust photoinitiating system that allows the preparation of highly stable latexes with particle sizes ranging from 50 to 300 nm and solids contents up to 30%. In my thesis, the objective was twofold. First, we focused on the optimization of the photoinitiating system for the emulsion process, more specifically playing with its water solubility properties. Secondly, we have decided to adapt our photoinitiating system to dispersion polymerization and also to prepare hybrid latexes *via* Pickering dispersion photopolymerization using cerium dioxide as solid stabilizer.

The manuscript is divided into 4 chapters. **Chapter 1** introduces the basics of photochemistry and the main challenges related to the adaptation of photopolymerizations to dispersed media.

Chapter 2 reviews the principle of emulsion polymerization and the various photoinitiating systems developed for micro-, mini- and emulsion photopolymerization under UV-vis irradiation. Following the works of F. Le Quéméner and D. Subervie, we tried to overcome the particle size distribution issues obtained with our photoinitiating system. Our hypothesis is that the different species involved in our photoinitiating system partition between the water and monomer phases, which may cause these broad size distributions. We synthesized new more hydrophilic functionalized NHC-boranes and applied them to emulsion photopolymerization. Finally, a color LED ribbon was set up to work with the less energetic green and red lights.

Chapter 3 focuses on the synthesis of polystyrene latexes by dispersion photopolymerization. The aim was to study our photoinitiating system in conditions where all compounds are initially soluble, allowing the polymerization to start in a homogeneous medium (unlike emulsion polymerization). The effect of various parameters such as the type and concentration of stabilizers, the photoinitiator concentration, the solids content and the pH of the medium on the polymerization kinetics, the particles sizes and morphologies, was studied in detail.

Chapter 4 focuses on the synthesis of poly(*n*-butyl acrylate-*co*-methyl methacrylate) latexes armored with cerium dioxide as solid stabilizer *via* Pickering dispersion photopolymerization. First, a brief survey of Pickering dispersion polymerization using various inorganic particles as stabilizer is presented. Then, the characteristics of the acidic ceric sol and the interaction between the cerium dioxide nanoparticles and the photoinitiator were investigated. Here again, the influence of several parameters such as the cerium dioxide content, the photoinitiator

concentration and the solids content on the polymerization rates, the morphologies and diameters of the resulting cerium dioxide armored polymer latexes was investigated. Finally, the properties of films obtained formed from the cerium dioxide-armored poly(*n*-butyl acrylate-*co*-methyl methacrylate) latexes were investigated.

We finally draw some general conclusions and perspectives for future works in the last part of the manuscript.

References

[1] K. Team, "Growing Synthetic Latex Polymers Capacity vs. Consumption Ratios," **2019**.
[2] *Plastics – the Facts 2019*, PlasticsEurope, **2019**.
[3] J.-C. Daniel, C. Pichot, *Les latex synthétiques - Élaboration, Propriétés, Applications*, Lavoisier, **2006**.
[4] F. M. Pavel, *J. Dispers. Sci. Technol.* **2004**, *25*, 1–16.
[5] J. M. Asua, *Prog. Polym. Sci.* **2002**, *27*, 1283–1346.
[6] E. Vivaldo-Lima, P. E. Wood, A. E. Hamielec, A. Penlidis, *Ind. Eng. Chem. Res.* **1997**, *36*, 939–965.
[7] S. Kawaguchi, K. Ito, in *Polym. Part.* -- (Ed.: M. Okubo), Springer, Berlin, Heidelberg, **2005**, pp. 299–328.
[8] F. Jasinski, P. B. Zetterlund, A. M. Braun, A. Chemtob, *Prog. Polym. Sci.* **2018**, *84*, 47–88.
[9] C. Dietlin, S. Schweizer, P. Xiao, J. Zhang, F. Morlet-Savary, B. Graff, J.-P. Fouassier, J. Lalevée, *Polym. Chem.* **2015**, *6*, 3895–3912.
[10] P. Xiao, J. Zhang, F. Dumur, M. A. Tehfe, F. Morlet-Savary, B. Graff, D. Gigmes, J. P. Fouassier, J. Lalevée, *Prog. Polym. Sci.* **2015**, *41*, 32–66.
[11] F. Le Quéméner, D. Subervie, F. Morlet-Savary, J. Lalevée, M. Lansalot, E. Bourgeat-Lami, E. Lacôte, *Angew. Chem. Int. Ed.* **2018**, *57*, 957–961.
[12] J. Tonnar, E. Pouget, P. Lacroix-Desmazes, B. Boutevin, *Macromol. Symp.* **2009**, *281*, 20–30.
[13] J. Saadé, C. Bordes, G. Raffin, M. Hangouët, P. Marote, K. Faure, *Colloid Polym. Sci.* **2016**, *294*, 27–36.
[14] P. L. Kuo, N. J. Turro, C. M. Tseng, M. S. El-Aasser, J. W. Vanderhoff, *Macromolecules* **1987**, *20*, 1216–1221.
[15] K. Jain, J. Klier, A. B. Scranton, *Polymer* **2005**, *46*, 11273–11278.
[16] F. Le Quéméner, Utilisation de NHC-Boranes pour la synthèse de nanoparticules et l'amorçage de photopolymérisation en émulsion, phdthesis, Université de Lyon, **2016**.
[17] D. Subervie, NHC-Boranes : amorceurs de photopolymérisation en émulsion et nouveaux matériaux énergétiques, phdthesis, Université de Lyon, **2018**.

Chapter 1.

Preamble on the fundamentals of photopolymerization in dispersed media

Table of content

I. INTRODUCTION TO PHOTOINITIATED POLYMERIZATION 13

A. PHOTOPHYSICAL AND PHOTOCHEMICAL PROCESSES DURING PI EXCITATION 14
B. PHOTOINITIATORS: STRUCTURE AND EFFICIENCY 15

II. POLYMERIZATION IN DISPERSED MEDIA 17

III. PHOTOPOLYMERIZATION ADAPTED TO POLYMERIZATION IN DISPERSED MEDIA: MAIN CHALLENGES 19

A. INTERACTIONS BETWEEN LIGHT AND PARTICLE 19
B. FUNDAMENTALS OF LIGHT ABSORPTION AND SCATTERING BY PARTICLES 21
1. Key parameters 21
2. Extinction cross-section of a spherical particle 23
3. Efficiency factors 25
4. Angular distribution of scattering intensity 26
C. LIGHT ABSORPTION AND SCATTERING: CASE OF PHOTOPOLYMERIZATION IN DISPERSED MEDIA 28
1. Light penetration issue and consequences 28
2. How to improve the light penetration within the reaction medium? 31

IV. CONCLUSION 32

REFERENCES 33

To get a better picture of what this thesis involves, this chapter will introduce on the one hand some basics of photopolymerization and on the second hand, the fundamental characteristics of the polymerization in dispersed media. To understand the main challenges associated with the transposition of photopolymerization to dispersed media, the efficiency of the light penetration in the reaction medium and the interactions of light with particles will be briefly discussed. The last section of this chapter will attempt to unearth contributing factor and possible solutions to the light penetration issue.

I. Introduction to photoinitiated polymerization

The photopolymerization is a process that uses ultraviolet or visible light irradiation to initiate a polymerization reaction.[1] UV (100–400 nm) is the most commonly used and most energetic radiation followed by visible light (400–800 nm) and very recently infrared (IR), between 800 and 2500 nm. The initiation reaction is based on photogenerated reactive species (usually free radicals) which are produced from a photoinitiator (PI) (**Erreur ! Source du renvoi introuvable.**).

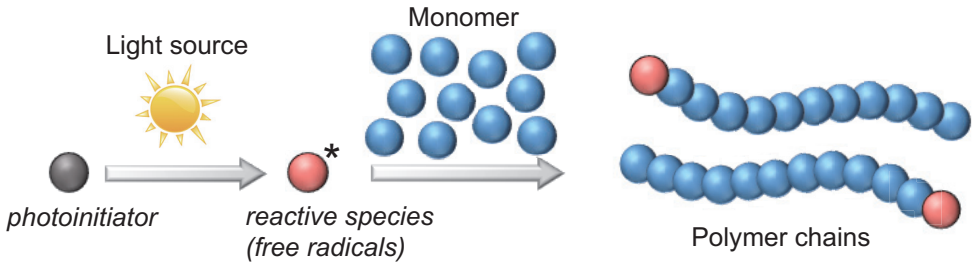

***Figure 5**. General presentation of photoinitiated polymerization.*

Photopolymerization offers many advantages compared to thermally activated free radical polymerization, providing high polymerization rates under mild reaction conditions and enabling the preparation of new materials.[2,3] Since the reaction can proceed at physiological temperature and pH, sensitive molecules such as enzymes or pharmaceutical compounds can be safely incorporated into the polymers during photopolymerization. Moreover, photopolymerizations are triggered by light and as such subject to external temporal and spatial control. When the light is switched off, the reaction stops almost instantaneously (initiating radicals cannot be generated without electronic excitation of a PI). Therefore, the risk of runaway reaction is reduced. In addition, the initiation and polymerization rates can be controlled by varying the light intensity or the PI concentration. Free radical

photopolymerization is the most commonly used process both in standard applications (adhesives, coating industry) and in advanced high technologies (microelectronics, photolithography, 3D printing).

A. Photophysical and photochemical processes during PI excitation

The mechanisms induced from the PI after absorption of a photon involve the absorbance (A). The absorbance relates the capacity of a PI to absorb incident light. According to the Beer–Lambert law:

$$A = \varepsilon l c \quad (Eq. 1.1)$$

where c is the PI concentration (mol L^{-1}), ε the molar extinction coefficient at a particular wavelength (L mol^{-1} cm^{-1}) and l the optical path length (cm). Furthermore, the absorbance is also related to the transmittance T by the following equation:

$$A = -\log(T) \quad (Eq. 1.2)$$

In this way, a high molar extinction coefficient leads to an increase in the absorbance and consequently, a reduction in the incident light transmission. For example, for an absorbance value of 0.6 only 25% of light penetrates the solution containing the PI.[4] The molar extinction coefficient is therefore a key parameter that influences the irradiated volume where the polymerization proceeds. Inner filter effects could then occur for systems when the absorbance is too high, resulting in a polymerization that can only proceed at a minimum irradiated volume close to the reactor wall.[5] This effect is a regular problem in photopolymerization.

The emission spectrum of the light source must coincide with the PI absorption. Indeed, after absorbing the light energy, the PI transitions from the ground state to the excited state. This usually corresponds to the transition of an electron from an occupied molecular orbital (highest occupied molecular orbital, HOMO) to an unoccupied molecular orbital (lowest unoccupied molecular orbital, LUMO) (**Erreur ! Source du renvoi introuvable.**).

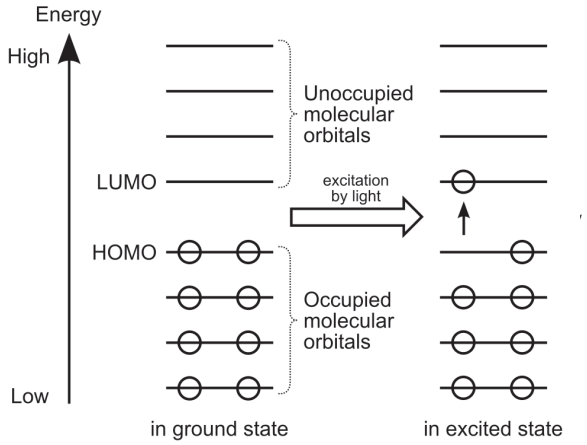

***Figure 6**. Diagram of the electronic transition of a PI from the HOMO to the LUMO when light is absorbed.*

B. Photoinitiators: structure and efficiency

Upon exposure to UV-vis light, PIs can generate active compounds *via* unimolecular dissociation (Type I) or in the presence of co-initiators in a multi-step reaction mechanism (Type II) (**Erreur ! Source du renvoi introuvable.**).

- A ***Type I unimolecular PI*** is subject to a homolytic bond cleavage due to the electronic transition from its ground to excited state, producing two free radicals. The PI must meet certain criteria to undergo an efficient homolytic cleavage: i) the bond dissociation energy (BDE) should be low enough so that the photon energy is sufficient to cleave the bond and generate free radicals, ii) the excited state energy must be higher than the bond energy in order that, during the relaxation of the PI, the scission can occur and iii) the activation energy of the scission should be as low as possible.
- In the case of ***Type II bimolecular PIs***, free radicals are formed *via* a hydrogen atom abstraction or a proton-coupled electron transfer mechanism between the PI long-lived triplet excited PI (the lifetime of the triplet state is longer than the singlet state) and a co-initiator that can provide the H atom or accept/donate an electron to the excited PI.[6–8] The co-initiators used as hydrogen donors are mostly aliphatic ethers with hydrogen in the α-position of hydroxyl, thiol and silane. The electron donor co-initiators are essentially tertiary aliphatic amines.

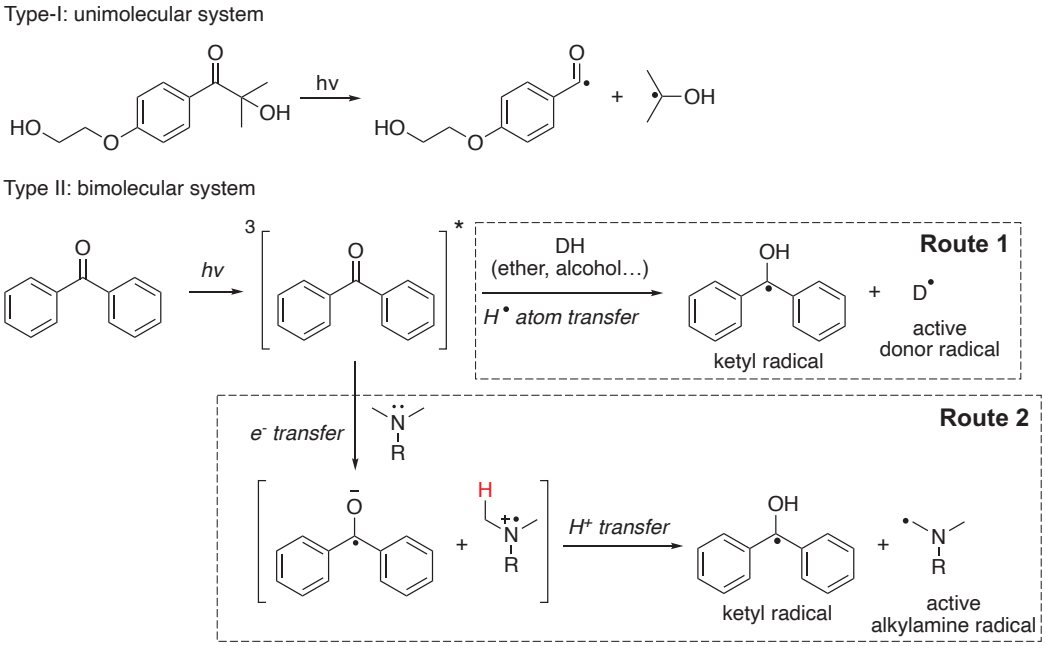

***Figure** 7. Examples of type I and II photoinitiator systems used in free radical photopolymerization.*

The main classes of unimolecular PIs are benzoin ethers, benzyl ketals, acetophenones, oxime esters, aminoalkyl phenones, and acylphosphine oxides. As will be discussed later in Chapters 2 (emulsion) and 3 (dispersion), type I PIs are the most commonly used for the production of latexes in aqueous media. Typical bimolecular PIs include benzophenones, thioxanthones, benzyls and quinones as photosensitizers with alcohols, amines, and thiols acting as hydrogen donors.[9,10]

Generally, the photoinitiation step rapidly generates reactive species with high efficiency by either varying the light intensity or the PI concentration.[11] The polymerizations are likely to be fast, although termination reactions could also be favored. Moreover, the polymerizations initiated by type II PIs are generally slower than those initiated by type I PIs. Indeed, the reaction mechanism of type II initiation is bimolecular, thereby free radicals are not intrinsically generated after absorption. It is thus necessary to take into account the diffusion of the species in the medium which is strongly dependent on the viscosity of the latter.

In the case of thermal initiation, which is widely used in radical polymerization in dispersed media, the thermal effusivity (ability to transfer thermal energy) and the gradual decomposition of the initiator reduce the generation of reactive species.

II. Polymerization in dispersed media

A broad range of polymers dispersed in a continuous phase are produced by polymerization in heterogenous media. Contrary to polymerization in homogeneous media (bulk or solution), polymerizations in dispersed media present various advantages:

- The production of high molecular weight polymers.
- The use of a relatively green solvent as continuous phase (water, supercritical CO_2).
- The low viscosity of the dispersed polymer allowing a better handling of the final polymer material.
- The formation of various particle morphologies and sizes.

A short description of different polymerization processes in dispersed media is mentioned in **Erreur ! Source du renvoi introuvable.**. We will briefly describe some of them (emulsion, microemulsion, miniemulsion and dispersion), and emulsion and dispersion polymerization will be discussed in detail later in the manuscript. It should be noticed that in the case of dispersion and precipitation polymerization, the initial reaction medium is completely homogeneous.

Table 1. *Several processes of radical polymerization in dispersed media.*

Process	Continuous phase	Initiator	Monomer droplet size	Particle size (generally obtained)	Note
Emulsion	Aqueous	Water-soluble	1 – 20 µm	50 – 500 nm	Dispersed medium
Microemulsion	Aqueous	Water-soluble	10 – 20 nm	10 – 50 nm	Thermodynamically stable
Miniemulsion	Aqueous	Water-soluble/ organosoluble	50 – 300 nm	50 – 300 nm	High-energy homogenization required
Dispersion	Organic	Organosoluble	Only one phase at the start	0.1 – 20 µm	Presence of stabilizer
Precipitation	Aqueous	Water-soluble	Only one phase at the start	Variable	Stabilizer-free
Suspension	Aqueous	Organosoluble	50 – 10 000 µm	50 – 10 000 µm	Very low amount of stabilizer

Aqueous ***emulsion polymerization*** is widely used industrially to synthesize large quantities of latexes for a multitude of applications, such as surface coatings and cosmetics.[12] The polymerization of one or several hydrophobic monomers, in the form of droplets, is initiated in the aqueous phase by a water-soluble initiator. A typical emulsion is thermodynamically unstable. The polymerization leads to a uniform colloidal dispersion stabilized by a surfactant. Several compounds are required for the emulsion polymerization process to work: monomer(s), an initiator able to generate free radicals, a surfactant to stabilize the particles. During an emulsion polymerization, several objects are present in the reaction medium (**Erreur ! Source du renvoi introuvable.**). Other compounds such as chain transfer agents, buffers, electrolytes or crosslinking agents can be added to the basic formulation for specific applications.

Table 2*. Characteristics of the dispersed objects during an emulsion polymerization.*

	Droplets	**Micelles**	**Particles**
Number of objects L^{-1}	6×10^{11}	10^{20}	10^{17}
Radius (nm)	5 000	4	30
Surface (m^2)	30	1 600	1 200

There are three types of emulsion polymerization processes.[13]

- Batch polymerization, in which all compounds are present at the start of the reaction.
- Semi-batch polymerization, in which some of the reactants (generally the monomer and/or the initiator) are added continuously or in increments.
- Continuous polymerization, in which all compounds are added continuously to the entry section of the reactor and the latex is continuously removed outside the reactor.

Two other techniques related to emulsion polymerization, micro- and miniemulsion polymerization, have been developed to obtain latex particles. In both cases, particle nucleation is forced in submicron monomer droplets, which have drastically decreased sizes in comparison with the droplet reservoirs of conventional emulsion polymerization.

In the case of ***microemulsion polymerization***[14,15], the use of a high amount of surfactant (in the range of 150–300 wt.% surfactant based on monomer), often in combination with a co-surfactant, leads to an extremely large number of small micelles (around 10 nm in diameter), making microemulsions thermodynamically stable. Therefore, the system contains surfactant stabilized monomer-swollen micelles in water. The monomer-swollen micelles capture the radicals generated in the aqueous phase. The diffusion of monomer is then ensured by the

unreacted monomer-swollen micelles acting as monomer reservoirs. The final particle size is typically in the range of 20–60 nm (slightly higher than the monomer-swollen micelles). It is important to notice that microemulsions are initially transparent.

In ***miniemulsion polymerization***[16,17], the size of the monomer droplets typically ranges from 40 to 400 nm. Contrary to what happens in microemulsion, the formation of these monomer droplets requires a high energy input (ultrasonifier, high-pressure homogenizer or static mixer). The monomer droplets are stabilized by a surfactant but are metastable. The amount of surfactant in that case is lower than the amount needed in microemulsion. A hydrophobic agent (n-hexadecane for instance) is required to prevent miniemulsions from Ostwald ripening (*i.e.*, the growth of the large particles at the expense of the small ones). The initiator can be either water-soluble or organosoluble. The polymerization proceeds mainly in the monomer droplets and the particle sizes obtained are generally similar to those of the monomer droplets.

In a typical ***dispersion polymerization*** process[12], contrary to what happens in emulsion, microemulsion, miniemulsion or suspension polymerizations, the reaction medium is initially homogeneous. The initial medium is composed of the monomer, the initiator, a stabilizer and the solvent (and sometimes a co-stabilizer). One critical characteristic of a dispersion polymerization reaction is that the monomer must be soluble in the dispersion medium to be polymerized, whereas the polymer must be insoluble.

The following section focuses on the combination of photopolymerization and polymerization in dispersed media, the identification of the challenges to overcome and suggestions for solutions. A bibliographic review on the photopolymerization in emulsion and dispersion will be presented in the dedicated chapters. There are also a lot of works that have been reported on the micro- and miniemulsion photopolymerization processes, but they will not be detailed in this thesis. The reader is referred to the publication of Jasinski and co-workers.[18]

III. Photopolymerization adapted to polymerization in dispersed media: main challenges

A. Interactions between light and particle

Light is an electromagnetic wave which consists of coupled vector fields, the electric field and the magnetic field. In the case of a plane wave, these vectors are perpendicular to each other and to the direction of propagation. The direction of the electric vector changes randomly over time for the natural light, it is therefore not possible to assign a direction to the electric field (unpolarized light). Conversely, polarized light has the particularity to present a precise direction for the electric field in the plane perpendicular to the direction of propagation. There are four kinds of interaction between light and particle: ***emission*** (the particle releases energy as light), ***extinction*** (the particle attenuates light by absorption of scattering), ***transmission*** (the particle allows light to pass) and ***reflection/refraction*** (the particle repels light in another direction) (**Erreur ! Source du renvoi introuvable.**). The following sections focus on the extinction since it the main factor that involves the attenuation of light.

The attenuation of the light intensity ($P_{t,\lambda}$ in photon L^{-1} s^{-1}) after passing through the particle can be expressed as a function of the incident photon flux ($P_{0,\lambda}$ in photon L^{-1} s^{-1}), the extinction coefficient (E_λ in cm^{-1}) and the thickness of the matter (l in cm), as follows:

$$P_{t,\lambda} = P_{0,\lambda} e^{-E_\lambda l} \quad (Eq. 1.3)$$

The extinction coefficient E_λ (cm^{-1}) is usually defined as the sum of the absorption K_λ (cm^{-1}) and scattering S_λ (cm^{-1}) coefficients:

$$E_\lambda = K_\lambda + S_\lambda \quad (Eq. 1.4)$$

- ***Absorption*** is a process that removes the light energy from an electromagnetic wave and transfers it to another form of energy (heat…). It is important to notice that for very small particles, light absorption dominates, whereas for particles larger scattering dominates.[19]
- ***Scattering*** is a process that does not remove energy from the electromagnetic wave but redirect it. When the electromagnetic field of an incident wave interacts with particle, the latter behaves like an oscillating dipole and in turn emits a secondary electromagnetic wave with the same frequency as the incident wave but in all directions.

Equation 1.4 can only be true for single scattering, in which process singly scattered light is effectively scattered out of the field of interest.[20]

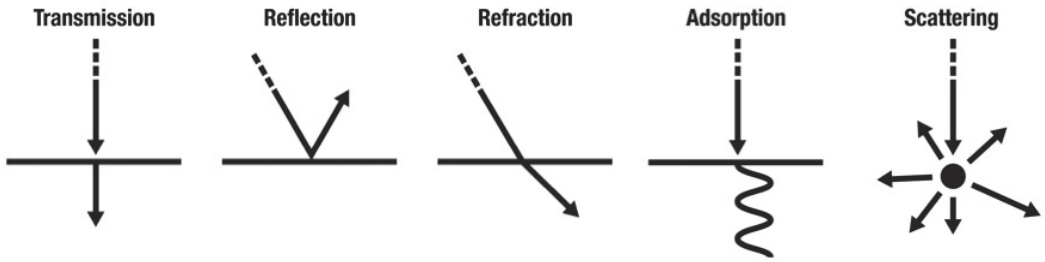

Figure 8. *Main phenomena that occur when the light interacts with matter.*

B. Fundamentals of light absorption and scattering by particles

1. Key parameters

There are three key parameters that govern the absorption and scattering of light radiation by a particle:

- The ***wavelength*** λ (nm) of the incident radiation.
- The size of the particles *r* (radius), expressed as a dimensionless ***size parameter*** *x*:

$$x = \frac{2\pi r}{\lambda} \quad (Eq.\,1.5)$$

- The ***complex refractive index*** of a particle:

$$m = m_r + im_i \quad (Eq.\,1.6)$$

  where m_r is the real part of the refractive index (responsible for scattering) and m_i is the imaginary part of the refractive index (responsible for absorption). Both m_r and m_i depend on the wavelength.

$$m_i = \frac{K_\lambda \lambda}{4\pi} \quad (Eq\ 1.7)$$

Several optical theories such as Rayleigh theory, Mie theory and the Kubelka-Munk model, have been implemented to describe the interaction of light with a single particle.[21–23] Each theory predicts the scattering coefficients as a function of λ, *r* and *m*.

In the case of a very small size parameter (*i.e.*, $r << \lambda$, $x << 1$ which corresponds to Rayleigh theory), there is complete symmetry in the patterns of the intensity of scattered light (forward scattering and backward scattering) from a single particle. In the case of a very large size parameter (*i.e.*, $r >> \lambda$, $x >> 1$ related to geometric optics), a nonselective scattering occurs

which can be considered as comprising a combination of Mie theory, absorption and multiple scattering (multiple scattering is too complex and not considered here). Between these two regimes, there is an intermediate state corresponding to the Mie theory. The summary of the different regimes of interaction between light and particle which depend on the size parameter are presented in **Erreur ! Source du renvoi introuvable.**.

Table 3. *Light scattering regimes by a spherical particle as a function of the size parameter x.*

$x \ll 1$	**Rayleigh regime**
$x \sim 1$	Mie regime
$x \gg 1$	Geometric optics

The graph below (**Erreur ! Source du renvoi introuvable.**) presents an overview of the different scattering behavior as a function of the wavelength and the particle radius considering atmospheric particles.[24] If we draw an analogy with solid/liquid dispersions, we can consider that in the case of emulsion photopolymerization under UV-vis light irradiation, Mie scattering mainly occurs. Indeed, for a particle with a diameter of 100 nm dispersed in water (n_{water} = 1.33) and an excitation source at 405 nm, the parameter size x is approximately equal to 1.

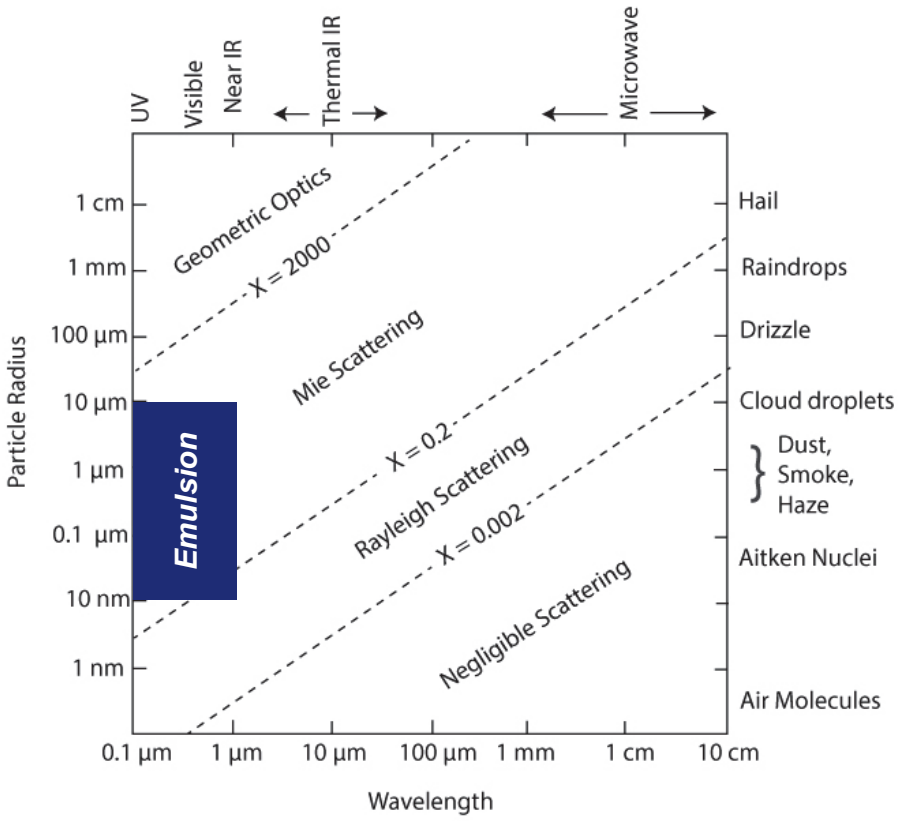

***Figure 9**. Relationship between particle size, radiation wavelength and scattering behavior for atmospheric particles. Diagonal dashed lines represent rough boundaries between scattering regimes.*[24]

2. Extinction cross-section of a spherical particle

The extinction coefficient E_λ for identical scatterers, *i.e.*, spherical particles, can then be calculated as a function of the extinction cross-section and the number of spherical particles per unit volume (N) by the following equation:

$$E_\lambda = N\sigma_E \quad (Eq.1.8)$$

The extinction cross section σ_E corresponds to the ratio of the energy flow absorbed and/or scattered by a spherical particle over the incident light intensity. In other words, the extinction cross section can be described as the effective area of interaction between the incident radiation and a spherical particle. According to the principle of energy conversation, the extinction cross section can be written as the sum of absorption and scattering cross-sections:

$$\sigma_E = \sigma_A + \sigma_S \quad (Eq.1.9)$$

Without going through the math or the reasoning, the extinction and scattering cross-sections, which are valid for spherical particles of any size according to the Mie theory, can be expressed as follows:[21,25]

$$\sigma_E = \left(\frac{2\pi r^2}{x^2}\right)\sum_{n=1}^{\infty}(2n+1)\,Re(a_n + b_n) \quad (Eq.1.10)$$

$$\sigma_S = \left(\frac{2\pi r^2}{x^2}\right)\sum_{n=1}^{\infty}(2n+1)(|a_n|^2 + |b_n|^2) \quad (Eq.1.11)$$

where a_n and b_n are complex coefficients expressed in terms of spherical Hankel functions and spherical Bessel functions of the first kind (more details in ref. [21,25]). These functions are dependent on the magnetic permeabilities of the particle, the size parameter and the refractive indices of the particle and the surrounding medium. Numerical values of cross sections can be calculated *via* a computer code.[26] The absorption cross-section is calculated from *Eq*. 1.9.

For example, Xie *et al.*[27] determined the extinction cross-section of polystyrene particles (1.06 µm in diameter and N_P = 2.31 x10^{13} m^{-3}) calculated by Mie theory as shown in **Erreur ! Source du renvoi introuvable.**. The authors found a very good agreement between their measured results and the calculated values by the Mie theory. The extinction cross section was plotted as a function of wavelength. As the wavelength increased, the extinction cross section reached a maximum value and then decreased. Note that the extinction cross-section can be extended to the scattering cross-section since the scattering dominates for large particles.

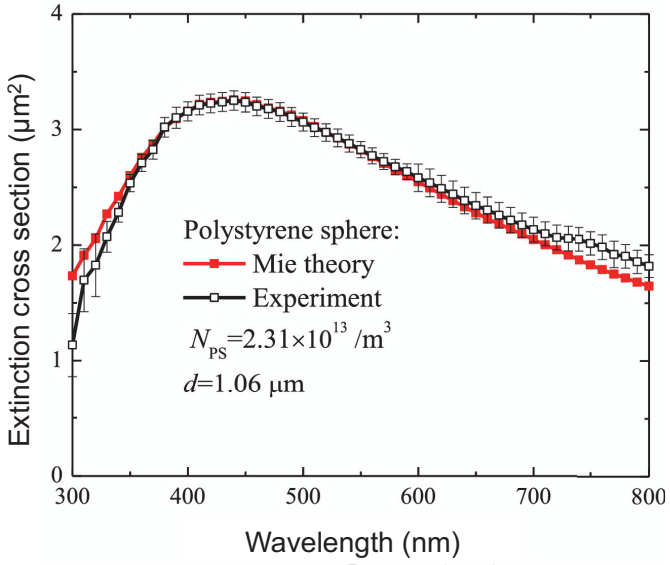

***Figure 10**. The extinction cross section of polystyrene particles calculated by the Mie theory.*[27]

In the simple case of very small particles (Rayleigh regime), the scattering cross-section can be expressed as follows:

$$\sigma_S = \frac{8\pi^2}{3}\left(\frac{2\pi n_{medium}}{\lambda_0}\right)^4 r^6 \left(\frac{m^2-1}{m^2+2}\right)^2 \quad (Eq.1.12)$$

The scattering cross-section coefficient is thus proportional to the wavelength and the particle radius as follows:

$$\sigma_S \propto \frac{r^6}{\lambda^4} \quad (Eq.1.13)$$

In the particular case where particles weakly absorb the incident light (*i.e.*, $\sigma_S \gg \sigma_A$), the single-scattering albedo (ω) of a particle can be defined for a given wavelength as follows:[23]

$$\omega = \frac{\sigma_S}{\sigma_E} \quad (Eq.1.14)$$

3. Efficiency factors

The extinction, scattering and absorption efficiencies (respectively Q_E, Q_S and Q_A) can be determined as follows:

$$Q_E = \frac{\sigma_E}{\pi r^2} \quad (Eq.1.15)$$

$$Q_S = \frac{\sigma_S}{\pi r^2} \quad (Eq.1.16)$$

$$Q_A = Q_E - Q_S \quad (Eq.1.17)$$

The scattering efficiency as a function of the size parameter x and imaginary refractive index m_i are shown in **Erreur ! Source du renvoi introuvable.**. The peak value at x = 4 exceeds the geometric cross section πr^2 by a factor of about 4, and an asymptotic value for very large non-absorbing particles is 2. According to the Mie theory, the scattering efficiency does not always increase with the size parameter.

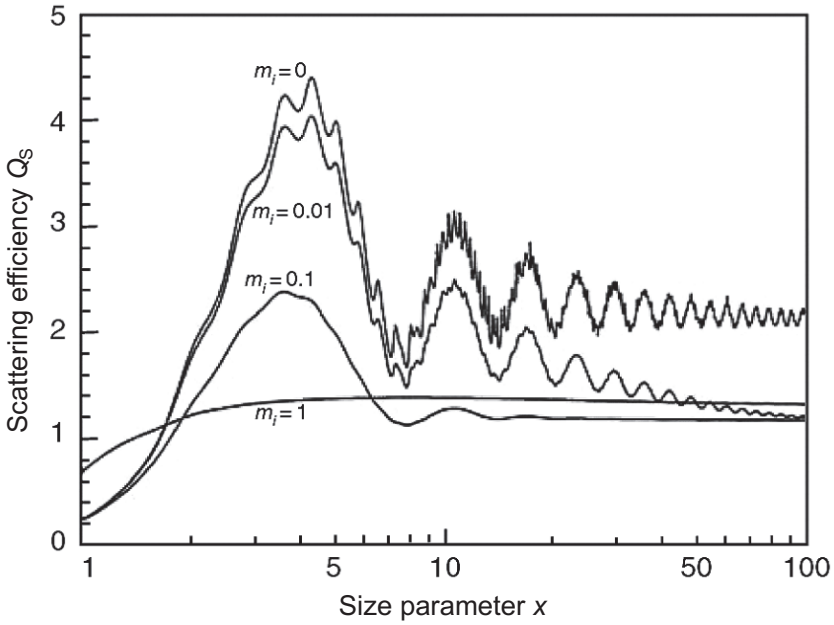

Figure 11. *Scattering efficiency as a function of size parameter and imaginary refractive index for m_r = 1.33.*[25]

Galpin *et al.*[28] developed a new method to retrieve complex refractive indices for polystyrene latexes in the 220 to 420 nm wavelength range, and then investigated the relationship between particle diameter, wavelength and extinction efficiency. Their experimental values were compared to the Mie theory. **Erreur ! Source du renvoi introuvable.** shows the extinction efficiency Q_E for polystyrene particles of different sizes dispersed in water with irradiation wavelengths of 228 and 351 nm.

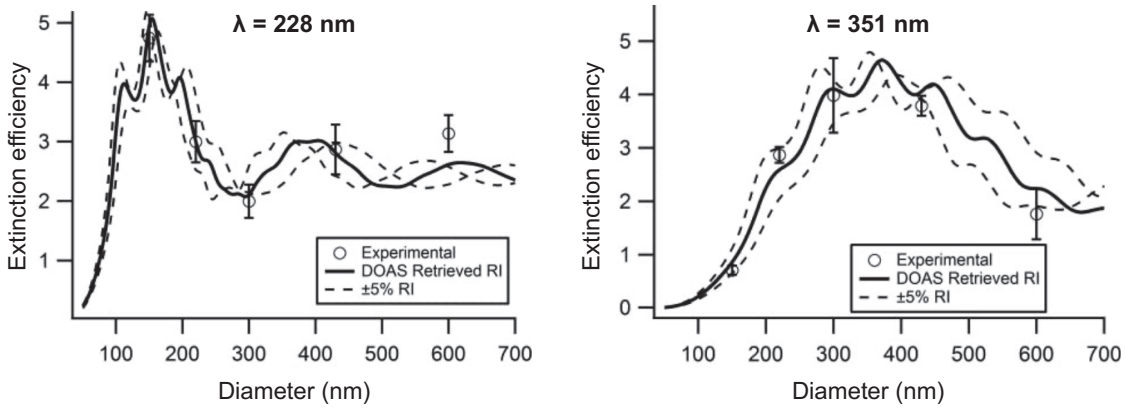

***Figure 12**. Scattering efficiency vs. diameter for polystyrene latexes measured at λ = 228 nm (left) and 351 nm (right). The solid black line represents the calculations from the Mie theory.*[28]

The experimental results were in agreement with what is found in the literature. In the case of small particles (diameter < 100 nm), the extinction efficiency can be minimized by shifting towards higher irradiation wavelengths (reduction of the scattering cross section). For larger particles (diameter >> λ), the extinction efficiency approaches a limiting value. Moreover, at λ = 228 nm, Q_E is maximal in the 100–200 nm range whereas at higher wavelength (351 nm), Q_E is more significant for sizes from 300 to 600 nm. This shows that by increasing the wavelength, the maximal extinction efficiency shifts toward higher particles sizes.

4. Angular distribution of scattering intensity

Another characteristic of scattered light if the angular distribution of scattering intensity which is dependent on the polarization of the incident light beam as well as on the parameters mentioned above (r, λ and m).[29] Different normalized scattering intensity distributions in a polar plot are represented in **Erreur ! Source du renvoi introuvable.**, for spherical polystyrene particles of several sizes and at λ = 600 nm. The red dashed lines (I_1) correspond to an incident beam linearly polarized along the direction perpendicular to the observation plane, the green

dash-dotted lines (I_2) correspond to an incident beam linearly polarized along the direction parallel to the observation plane and the dark solid lines correspond to the intensity distribution $I_{1,2} = (I_1 + I_2)/2$. For a polystyrene particle diameter ≤ 10 nm, a symmetric forward and backward scattering distribution is obtained. In this simple case of Rayleigh scattering, the angular distribution of the total scattering intensity can be expressed as a function of the scattering angle (θ):

$$I = \frac{1 + (\cos\theta)^2}{2} \quad (Eq.1.18)$$

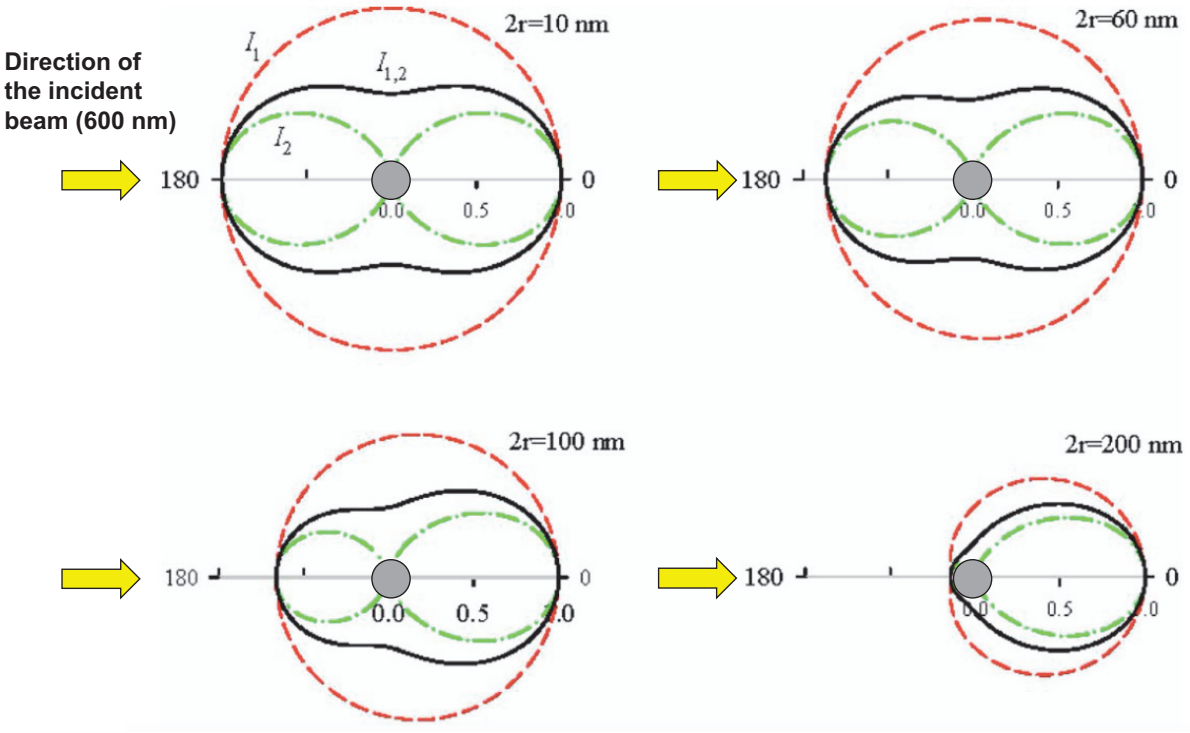

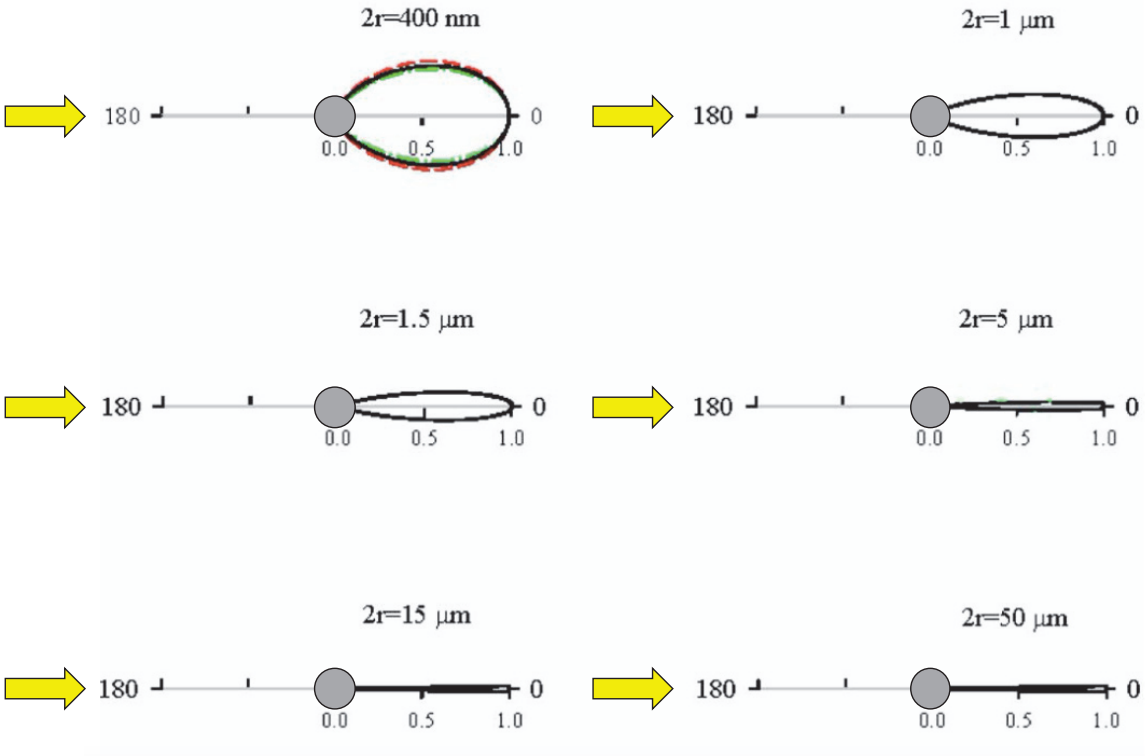

***Figure 13**. Calculated normalized angular distribution of scattering intensity for ten scattering samples with different particle sizes.*[29]

From a polystyrene particle diameter of 20 to 100 nm, the angular distribution of scattering intensity becomes gradually asymmetric between forward and backward directions. It is important to notice that when a threshold of 200 nm in diameter is exceeded, only forward scattering is obtained. In addition, beyond a particle diameter of 5 µm, the scattering intensities are concentrated on a very small angular range around the $\theta = 0$ direction. This result is useful for the understanding of the higher light penetration in polymer suspensions exhibiting a particle radius greater than 5 µm.

C. Light absorption and scattering: case of photopolymerization in dispersed media

1. Light penetration issue and consequences

Absorption (from the PI but also monomer and surfactant) and scattering represent the key issues to photoinduced polymerization in dispersed media because of the resulting attenuation of the radiation source inside the reactor. However, the absorption and scattering coefficients, K_λ and S_λ, are difficult to determine individually for dispersions. They can be

experimentally obtained by nonconventional spectrophotometric methods using diffusive reflectance and transmittance requiring spectrophotometers equipped with an integrating sphere.[30,31] Nevertheless, to demonstrate the impact of scattering on light penetration within emulsion systems, Jasinski *et al.*[18] simply used a UV-vis spectrophotometer to compare the internal transmittance (T_λ) between a PI emulsion system which combined scattering and absorption, and a homogeneous solution where only absorption occurred (**Erreur ! Source du renvoi introuvable.**).

$$T_\lambda = \frac{P_{t,\lambda}}{P_{0,\lambda}} \quad (Eq.\,1.19)$$

For the same PI concentration (only the PI absorbed at the incident wavelength 366 nm), the incident light passed through an optical path much larger in the solution than in the emulsion system. This showed empirically that the scattering highly impacted the light penetration. In the case of important optical path (typically the case for reactors used in conventional polymerization in dispersed media), the scattering effects have a considerable impact on the light penetration. Therefore, the particle size and the number of particles, the refractive indices of the medium and the polymer or the wavelength will influence the light penetration.

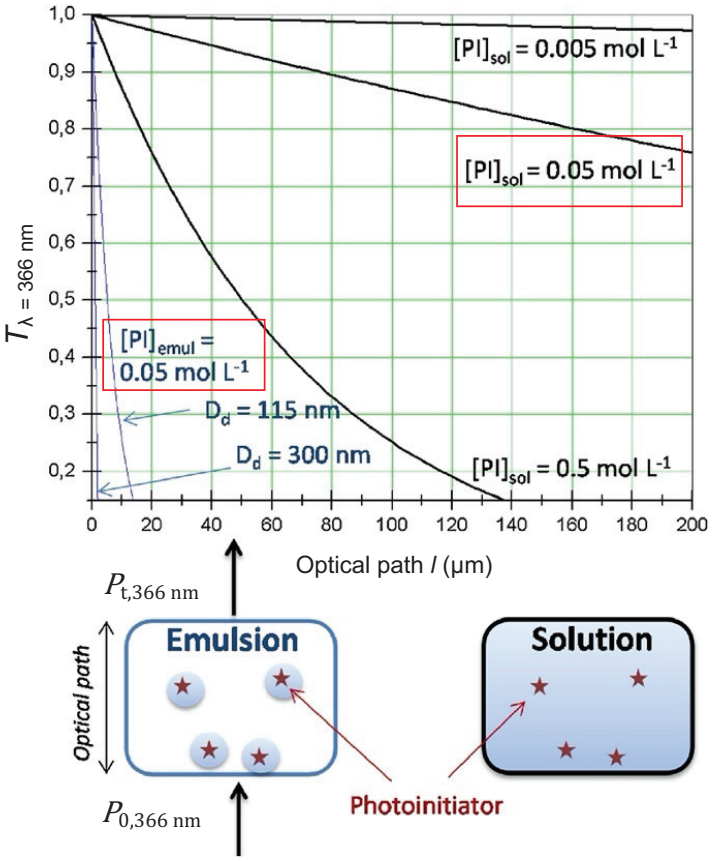

***Figure 14**. Internal transmittance measured at 366 nm for two concentration equivalent systems in solution and emulsion containing 2,2-dimethoxy-2-phenylacetophenone as PI. The droplet diameter is between 115 and 300 nm.*[18]

- ***Particle number***: Emulsions or suspensions of particles develop complex interactions with light that our eyes interpret by seeing a milky solution. In a milky environment, each particle behaves like a secondary source of light. Therefore, the light is subject, as mentioned above, to absorption and scattering phenomena. The extinction coefficient (E_λ) can be related to the number of particles (N) as indicated in *Eq*. 1.8. However, the industrialized processes of emulsion polymerization impose specifications that are not in the best interest of light penetration. Indeed, the solids contents are generally around 50%, resulting in a high particle concentration and thus an increase of scattering.

- ***Reactor design***: The geometry of the reactors used for the synthesis of polymers also presents a large optical path (except for microreactors), leading to a minimal irradiated reactor volume fraction. Indeed, the incident light can be absorbed at the location of irradiation by the PI or backscattered by the various objects present. Only forward scattering may contribute to light penetration at the center of the reactor. For example, the macroemulsions of acrylates characterized by a high solids content (> 50 wt.%) and broad droplet size distributions (10 – 100 µm) present a high scattering coefficient, resulting in very low irradiated volume (50 µm from the reactor wall) in the case of UVB (280–315 nm) and UVA (315–400 nm) light.[18]

Compared to thermally activated polymerizations where mixing ensures the reaction throughout the reactor, the photoinitiation thus occurs in a more or less important irradiated reactor volume fraction. Nevertheless, the limits encountered by light penetration can be attenuated by the stirring, which ensures efficient diffusion of the generated radicals in the whole reactor.

- ***Light absorption by the PI***: It is very important since it determines the reaction rate. This usually refers to the absorbed photon flux which corresponds to the number of photons absorbed per unit time and reaction volume. The absorbed photon flux can be calculated in applying the radiative transfer equation and by taking into account the attenuation of the incident light due to forward and backward scattering in the case of dispersed media. The resolution of this radiative transfer equation has already demonstrated its usefulness for heterogeneous photochemical systems but is barely used in photopolymerization. For example, by using Monte Carlo method, Moreira *et al.*[32] reported the optimization of an oxidation process. The aim was to control the water pollution by using a photochemical reactor containing

TiO_2 particles suspended in water. Currently, the use of this model has never been applied in the case of photopolymerization in dispersed media, but one day this may become essential.

In addition, the importance of absorption phenomena should not be underestimated since it may be one reason why it is very tricky to carry out emulsion polymerization under UV light. Indeed, the monomer such as acrylates or styrene present in the droplets (1 – 10 µm in diameter) may highly absorb in the UV range.

2. How to improve the light penetration within the reaction medium?

Despite the low light penetration due to the various parameters mentioned above, many syntheses have still been able to proceed in dispersed media in recent years as we will discuss in this thesis. The successful production of latexes can be explained by the fact that radical photoinitiations have rather high quantum yields Φ(λ).

$$\Phi(\lambda) = \frac{amount\ of\ reactant\ consumed\ or\ product\ formed}{number\ of\ photons\ absorbed} \quad (Eq.\ 1.20)$$

Therefore, the polymerization can even proceed in a locus where relatively few photons are absorbed per unit volume and at a low temperature, and the stirring can ensure efficient diffusion of the generated radicals in the whole reactor. Moreover, a small fraction of monomer contained in the droplets (or micelles if present) can diffuse through the aqueous phase and react with radicals generated in the aqueous phase.

In order to improve the light penetration within the reaction medium, various actions can be considered as follows:

- ***New photoreactors*** can be designed, to reduce the optical path lengths.[33]
- ***Increasing the irradiation wavelength***. The light scattering is considerably decreased when the wavelength is shifted to higher wavelength (visible and even near-infrared radiation), in particular for very small particles (< 50 nm). This parameter was studied by Boyer and co-workers to produce particles by miniemulsion polymerization in the presence of photo-redox systems activated under visible light.[34,35] Moreover, it is very tricky to carry out emulsion polymerization under UV light since the monomer droplets (1 – 10 µm in diameter) should highly absorb in the UV range and thus limiting the light penetration.

- ***Synthesizing latexes with reduced droplet sizes and size distributions***. Thereby, the droplet sizes must be correlated to the irradiation wavelength. Indeed, as previously mentioned, the reduction of the droplet size leads to the diminution of the scattering efficiency. Micro- and miniemulsions polymerization techniques successfully lead to the production of stable latexes under UV and visible light irradiation.[36–39]
- ***Decreasing the solids content*** because a high droplet/particle concentration may involve multiple scattering phenomena.
- ***Decreasing the difference of the refractive indices between the monomer phase and the aqueous phase***. This approach was used to form transparent miniemulsions of various vinyl monomers by use of the compressed gases CO_2 and ethylene[40] and in the case of Pickering emulsions[41], but it has never been tested in a photopolymerization reaction.
- ***Mathematical modeling*** could also be a way to better understand the scattering effects and optimize the systems under irradiation conditions.

IV. Conclusion

In addition to the various advantages of photochemical processes (such as spatial and temporal control, fast decomposition of the initiator), their adaptation to dispersed media can provide significant added value, in particular by producing polymer particles at room temperature, and more generally by broadening the range of currently available latexes. The visible light irradiation sources involved are easily accessible, inexpensive and not dangerous for the operators. Among the reaction media, water is the most commonly used green solvent.

However, one of the main issues facing the development of photoinduced polymerizations in dispersed media is the light attenuation that occurs as soon as the dispersed particle sizes exceed 50 nm. Therefore, the effectiveness of photochemical initiation strongly depends on the light penetration which is affected by the absorption and scattering phenomena. Several optical theories such as Rayleigh scattering, Mie scattering and the Kubelka-Munk model, have been implemented to predict the scattering coefficient as a function of the wavelength λ, the particle radius r, and the complex refractive index. Many actions have been tried to reduce the light scattering phenomenon.

Several studies showed the possibility to conduct photopolymerizations in dispersed media by using UV or visible light irradiation. However, the use of UV sources requires specific reactor and it is not safe for the operator. In addition, as will be shown in the next chapter, the few studies reported on the emulsion photopolymerizations under UV irradiation were not really successful, probably due to the fact that the large monomer droplets absorbed most of the UV light instead of the PI. Increasing the wavelength to visible light range may improve the photopolymerization in emulsion. But there are difficulties to be overcome, especially in terms of size range and photoinitiation efficiency in the turbid medium, which we propose to deal with during this thesis.

References

[1] Y. Yagci, S. Jockusch, N. J. Turro, *Macromolecules* **2010**, *43*, 6245–6260.
[2] C. Dietlin, S. Schweizer, P. Xiao, J. Zhang, F. Morlet-Savary, B. Graff, J.-P. Fouassier, J. Lalevée, *Polym. Chem.* **2015**, *6*, 3895–3912.
[3] P. Xiao, J. Zhang, F. Dumur, M. A. Tehfe, F. Morlet-Savary, B. Graff, D. Gigmes, J. P. Fouassier, J. Lalevée, *Prog. Polym. Sci.* **2015**, *41*, 32–66.
[4] B. Aubry, Développement de Nouveaux Systèmes Photoamorceurs Borés Pour Une Photopolymérisation Durable, Mulhouse, **2020**.
[5] S. Chen, Y.-L. Yu, J.-H. Wang, *Anal. Chim. Acta* **2018**, *999*, 13–26.
[6] X. Pan, M. A. Tasdelen, J. Laun, T. Junkers, Y. Yagci, K. Matyjaszewski, *Prog. Polym. Sci.* **2016**, *62*, 73–125.
[7] J. Shao, Y. Huang, Q. Fan, *Polym. Chem.* **2014**, *5*, 4195–4210.
[8] H. F. Gruber, *Prog. Polym. Sci.* **1992**, *17*, 953–1044.
[9] H. J. Hageman, *Prog. Org. Coat.* **1985**, *13*, 123–150.
[10] J.-P. Fouassier, J. Lalevée, *Photoinitiators for Polymer Synthesis: Scope, Reactivity, and Efficiency*, John Wiley & Sons, **2012**.
[11] N. S. Allen, Ed. , *Photopolymerisation and Photoimaging Science and Technology*, Springer Netherlands, Dordrecht, **1989**.
[12] J.-C. Daniel, C. Pichot, *Les latex synthétiques - Élaboration, Propriétés, Applications*, Lavoisier, **2006**.
[13] J. W. Vanderhoff, in *Future Dir. Polym. Colloids* (Eds.: M.S. El-Aasser, R.M. Fitch), Springer Netherlands, Dordrecht, **1987**, pp. 23–45.

[14] G. L. Rempel, H. Wang, in *Encycl. Polym. Nanomater.* (Eds.: S. Kobayashi, K. Müllen), Springer, Berlin, Heidelberg, **2015**, pp. 1241–1250.
[15] F. M. Pavel, *J. Dispers. Sci. Technol.* **2004**, *25*, 1–16.
[16] J. M. Asua, *Prog. Polym. Sci.* **2002**, *27*, 1283–1346.
[17] J. M. Asua, *Prog. Polym. Sci.* **2014**, *39*, 1797–1826.
[18] F. Jasinski, P. B. Zetterlund, A. M. Braun, A. Chemtob, *Prog. Polym. Sci.* **2018**, *84*, 47–88.
[19] M. H. Nayfeh, in *Opt. Our Time* (Eds.: M.D. Al-Amri, M. El-Gomati, M.S. Zubairy), Springer International Publishing, Cham, **2016**, pp. 223–264.
[20] P. Schwerdtfeger, *Nature* **1969**, *222*, 378–379.
[21] A. J. Cox, A. J. DeWeerd, J. Linden, *Am. J. Phys.* **2002**, *70*, 620–625.
[22] P. Kubelka, *JOSA* **1948**, *38*, 448–457.
[23] H. Moosmüller, W. P. Arnott, *J. Air Waste Manag. Assoc.* **2009**, *59*, 1028–1031.
[24] E. Johansson, **2019**.
[25] V. A. Krasnopolsky, Ed. , in *Spectrosc. Photochem. Planet. Atmospheres Ionos. Mars Venus Titan Triton Pluto*, Cambridge University Press, Cambridge, **2019**, pp. 52–64.
[26] S. Prahl, "Mie scattering calculator," can be found under https://omlc.org/calc/mie_calc.html, **2018**.
[27] B. W. Xie, L. X. Ma, J. M. Zhao, L. H. Liu, X. Z. Wang, Y. R. He, *J. Quant. Spectrosc. Radiat. Transf.* **2019**, *232*, 93–103.
[28] T. Galpin, R. T. Chartier, N. Levergood, M. E. Greenslade, *Aerosol Sci. Technol.* **2017**, *51*, 1158–1167.
[29] G. S. He, H.-Y. Qin, Q. Zheng, *J. Appl. Phys.* **2009**, *105*, 023110.
[30] L. Sun, J. R. Bolton, *J. Phys. Chem.* **1996**, *100*, 4127–4134.
[31] M. L. Satuf, R. J. Brandi, A. E. Cassano, O. M. Alfano, *Ind. Eng. Chem. Res.* **2005**, *44*, 6643–6649.
[32] J. Moreira, B. Serrano, A. Ortiz, H. de Lasa, *Chem. Eng. Sci.* **2011**, *66*, 5813–5821.
[33] V. Daniloska, R. Tomovska, J. M. Asua, *Chem. Eng. J.* **2012**, *184*, 308–314.
[34] J. Xu, C. Boyer, *Macromolecules* **2015**, *48*, 520–529.
[35] K. Jung, J. Xu, P. B. Zetterlund, C. Boyer, *ACS Macro Lett.* **2015**, *4*, 1139–1143.
[36] I. Capek, J. P. Fouassier, *Eur. Polym. J.* **1997**, *33*, 173–181.
[37] K. Jain, J. Klier, A. B. Scranton, *Polymer* **2005**, *46*, 11273–11278.
[38] A. Chemtob, B. Kunstler, C. Croutxé-Barghorn, S. Fouchard, *Colloid Polym. Sci.* **2010**, *288*, 579–587.
[39] F. Jasinski, E. Lobry, A. Chemtob, C. Croutxé-Barghorn, A. Criqui, *Macromol. Chem. Phys.* **2013**, *214*, 1669–1676.
[40] S. Dong, Y. Suzuki, N. H. N. Hadzir, F. P. Lucien, P. B. Zetterlund, *RSC Adv.* **2016**, *6*, 50650–50657.
[41] K. L. Thompson, J. A. Lane, M. J. Derry, S. P. Armes, *Langmuir* **2015**, *31*, 4373–4376.

Chapter 2.

Visible-light induced emulsion polymerization of styrene and acrylate monomers

Table of content

PART 1. STATE-OF-THE-ART 39

I. GENERALITIES 39

II. MECHANISM AND KINETICS OF EMULSION POLYMERIZATION 40

A. NUCLEATION STEP 41
B. GROWTH STEP 43

III. PHOTOPOLYMERIZATION IN EMULSION UNDER UV-VISIBLE LIGHT: STATE-OF-THE-ART 44

A. PIONEERING STUDIES ON PHOTOPOLYMERIZATION IN DISPERSED MEDIA 44
B. EMULSION PHOTOPOLYMERIZATION 45
1. UV light-induced oil-in-water emulsion polymerization 45
2. UV light-induced inverse water-in-oil emulsion polymerization 54
3. Visible light-induced oil-in-water emulsion polymerization 55

IV. CONCLUSION 58

PART 2. REMINDERS OF PREVIOUS WORKS ON THE USE OF NHC-BORANES AS CO-INITIATORS FOR VISIBLE LIGHT-INDUCED EMULSION POLYMERIZATION 60

I. FORMATION OF NHC BORYL RADICALS UNDER VISIBLE LIGHT 60

II. EMULSION PHOTOPOLYMERIZATION OF STYRENE 61

A. OPTIMIZATION OF THE IRRADIATION SET-UP AND PHOTOINITIATING SYSTEM 61
B. INFLUENCE OF SEVERAL PARAMETERS ON THE PARTICLES SIZE AND POLYMERIZATION KINETICS 64
C. COMPARISON WITH THERMALLY ACTIVATED EMULSION POLYMERIZATION 66

II. EMULSION PHOTOPOLYMERIZATION OF MMA 68

A. EFFECT OF REACTION CONDITIONS ON POLYMERIZATION KINETICS AND PARTICLES SIZE 68
B. INFLUENCE OF THE PIS COMPOSITION FOR THE EMULSION PHOTOPOLYMERIZATION OF MMA 70

III. EMULSION PHOTO(CO-)POLYMERIZATION OF VARIOUS MONOMERS 74

A. PHOTOPOLYMERIZATION OF OTHER (METH)ACRYLATE MONOMERS WITH DISULFIDE ALONE AS PHOTOINITIATOR 74
B. SYNTHESIS OF COPOLYMERS PHOTOINDUCED BY THE THREE-COMPONENT PIS VS. DISULFIDE ALONE 75

IV. CONCLUSION 77

PART 3. STRATEGIES TO NARROW THE SIZE DISPERSITY OF LATEX PARTICLES PREPARED BY EMULSION PHOTOPOLYMERIZATION UNDER VISIBLE IRRADIATION 78

I. INFLUENCE OF THE TYPE OF STABILIZER 78

II. DEVELOPMENT OF MORE WATER-SOLUBLE PISS FOR EMULSION PHOTOPOLYMERIZATION 80

A. IMPACT OF THE REACTOR GEOMETRY AND LED BRIGHTNESS ON THE OUTCOME OF THE POLYMERIZATION REACTION 80
B. DETERMINATION OF AO AND NHC-BH_3 PARTITION COEFFICIENTS 81
C. NEW WATER-SOLUBLE DYES FOR THE PHOTOINITIATING SYSTEM 83
1. Case of styrene 83
2. Case of MMA 87
D. SYNTHESIS OF NEW CO-INITIATOR NHC-BORANES 89
1. Sulfonated-functionalized NHC-boranes 89
2. Amino-functionalized NHC-borane 94
E. SUMMARY 96

III. REACTOR OPTIMIZATION: NEW COLOR LED RIBBON 97
GENERAL CONCLUSIONS 99
REFERENCES 101

In this chapter, the start-of-the-art of emulsion photopolymerization will be first discussed. Then, the results obtained by our group in the emulsion photopolymerization of styrene and acrylic monomers with a water-soluble photoinitiating system (PIS) based on a *N*-heterocyclic carbene borane (NHC-borane) will be presented. With the aim of improving the system, notably the particle size distribution, we developed novel NHC-boranes less susceptible to partition with the oil phase and studied different water-soluble dyes that absorb in the visible light domain.

Part 1. State-of-the-art

I. Generalities

Emulsion polymerization is a process enabling the production of polymers in (aqueous) dispersed media. Aqueous emulsion polymerization is widely used industrially to synthesize large quantities of latexes for a multitude of applications, such as surface coatings (paints), adhesives and cosmetics. The polymerization of one or several hydrophobic monomers, in the form of droplets, is initiated in the aqueous phase by a water-soluble initiator. A typical emulsion is thermodynamically unstable. The polymerization leads to a colloidal dispersion stabilized by a surfactant with uniform particles. Several compounds are required for the emulsion polymerization process to work: monomer(s) (*e.g.*, acrylic and styrenic monomers, conjugated dienes…), an initiator able to generate free radicals, a surfactant to stabilize the particles. The latter can be anionic (carboxylate, sulfate groups), cationic (ammonium group), zwitterionic (sulfobetaine-type) or neutral (polyethylene oxide, PEO). The surfactant can also be reactive, acting as a monomer (*surfmer*), an initiator (*inisurf*) or a chain transfer agent (*transurf*). Other compounds such as transfert agents, buffers, electrolytes or crosslinking agents can be added to the basic formulation for specific applications.

Three types of initiators are commonly used: thermal initiators such as peroxides or azo compounds lead to radicals by heat-induced decomposition, redox initiator systems (*e.g.*, H_2O_2/Fe(II), $K_2S_2O_8$/$Na_2S_2O_5$) lead to radicals by single electron transfer, and finally PIS which generate radicals when irradiated.

There are three types of emulsion polymerization processes.

- Batch polymerization, in which all compounds are present at the start of the reaction.

- Semi-batch polymerization, in which some of the reactants (generally the monomer and/or the initiator) are added continuously or in increments.
- Continuous polymerization, in which all compounds are added continuously to the entry section of the reactor while the latex is continuously removed outside the reactor.

II. Mechanism and kinetics of emulsion polymerization

The first qualitative mechanism for emulsion polymerization was proposed by Harkins in 1945.[1–3] The authors studied the formation of polystyrene (PS) particles by using potassium persulfate (KPS) as initiator and sodium dodecyl sulfate (SDS) as surfactant with a concentration above the critical micelle concentration (CMC), i.e., in the presence of micelles. According to Harkins, the main locus of polymerization is the stabilized polymer particles rather than the monomer droplets. Based on this postulate, Smith and Ewart elaborated a quantitative model.[4,5] The process can be divided in three distinctive intervals (Figure 15):

- **Interval I**: the nucleation step. After the formation of free radicals in the aqueous phase, primary particles (*nuclei*) are produced in water, and their number increases as the polymerization proceeds until micelles of surfactant completely disappear.
- **Interval II**: when the particles are well stabilized (*i.e.*, no more formation of *nuclei*), the particle number and the polymerization rate remain constant. The particles grow by diffusion of monomer from the monomer droplet reservoirs to the particles through the continuous phase. During this period, the monomer concentration within the particles is assumed to be constant.
- **Interval III**: this period starts when the monomer droplet reservoirs are exhausted. The remaining monomer contained within the particles is polymerized and its concentration decreases. A lower polymerization rate is observed. Moreover, above a certain weight fraction of polymer in the particles, a gel effect can occur, where the effective termination rate is reduced.[6] This is attributed to the greatly reduced bimolecular termination reaction between two polymeric radicals within the very viscous particles.

Intervals I and II are described in more details in the following sections.

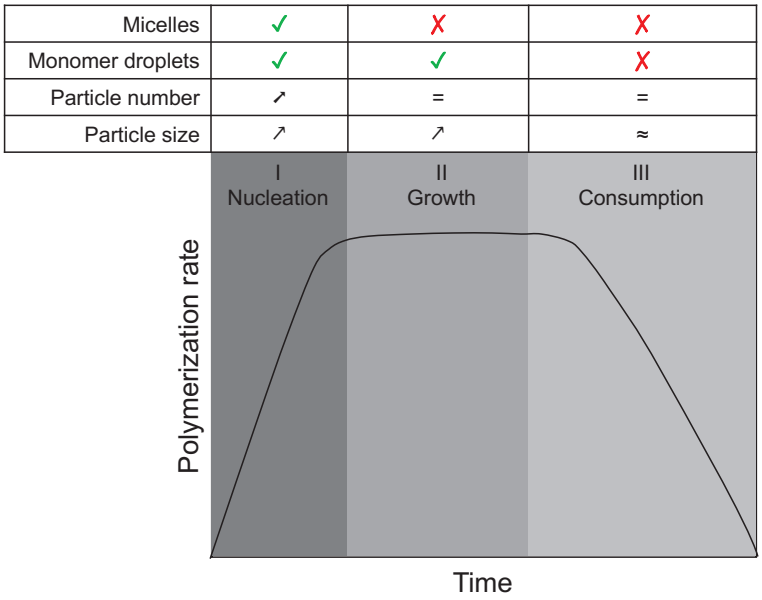

Figure 15. *Evolution of the polymerization rate during the three intervals of a typical emulsion polymerization as a function of time.*

A. Nucleation step

The nucleation step is complex but highly important for the determination of the particle number and the polymerization rate. The number of particles depends on the type of monomer, the type and concentration of the surfactant, the type and concentration of the initiator, the temperature of reaction and the type of process.

At the beginning of the reaction, the monomer is mainly localized in the emulsified 1 – 20 µm monomer droplet reservoirs. Above the CMC of the surfactant, micelles are present in the reaction mixture. Some of the monomer, which must be partially soluble in water, migrates in the micelles and some is in the water phase where the initiation takes place. Indeed, the initiator is soluble in water, where it decomposes and forms active free radicals.

At this point, several nucleation mechanisms are proposed to form primary polymer particles. Three major mechanisms for particle formation have been reported to date.

- ***Micellar nucleation***: proposed by Harkins in 1947, this mechanism occurs when the concentration of surfactant is above its CMC and/or the solubility of the monomer is very low (Figure 16). The hydro-soluble oligoradicals formed in the water phase reaches a degree of polymerization (denoted z) where it becomes surface-active, namely "z-mer", and enters into the micelles to form primary particles. The oligoradical can also enter within an existing particle.

- ***Homogenous nucleation***: the mechanism was proposed by Roe[7] in 1968 and detailed by Fitch and Tsai.[8] It can take place independently of the concentration of the surfactant. It is however generally admitted as the predominant mechanism for concentration of surfactant below the CMC and/or monomer with high water solubility. At a critical degree of polymerization, namely j_{crit}, the oligoradicals precipitate to form unstable primary particles (*nuclei*), which grow by monomer swelling or aggregation of other *nuclei* (Figure 16). The polymer particles are stabilized by the presence of surfactant or, if there is no surfactant, by charges present at the initiator fragment.

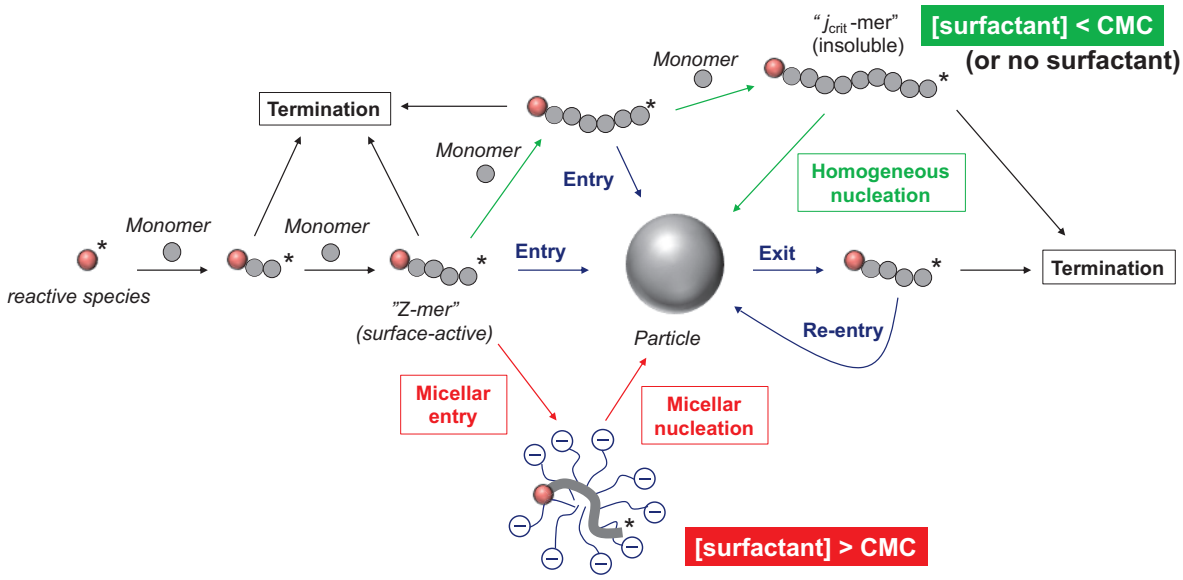

Figure 16. *Description of particle formation in emulsion polymerization below (green) and above (red) the CMC, corresponding to respectively homogeneous and micellar nucleation (adapted from ref. [9]).*

- ***Coagulative nucleation***: Gilbert and co-workers[10] proposed a mechanism of coagulative nucleation in two steps. First, either of the previous mechanisms occur to form nuclei. These nuclei are unstable and very small (around 2 – 3 nm in diameter), and thus it is unlikely that they are swollen by monomer. The authors suggested that the primary particles coagulate to form more stable particles (heterocoagulation).

It should be noticed that free radicals can enter monomer droplets to form polymer. However, this event is not favored as the specific surface area offered by the droplets is significantly smaller than that offered by the micelles.

In any event, at the end of the nucleation stage, the number of polymer particles and the rate of polymerization are constant. All surfactant in the reaction mixture is absorbed on the polymer

particles and no new particles are formed. The number of particles is calculated from their average diameter according to the following equation 2.1:

$$N_p = \frac{6m}{\pi D^3 \rho_P} \quad (Eq. 2.1)$$

with N_p the number of particles (L_{latex}^{-1}), m the mass of the polymer per unit volume of the aqueous phase (g L_{latex}^{-1}), D the average diameter of the particle (cm) and ρ_P the density of the polymer (g cm^{-3}).

B. Growth step

The second step of emulsion polymerization is the particle growth. The polymerization proceeds by the entry of new radicals within the polymer particles and by diffusion of monomer from the droplet reservoirs to the particles. The rate of polymerization is given by the following equation 2.2:

$$R_p = -\frac{d[M]}{dt} = k_p[M]_p[P^\circ] = k_p[M]_p \frac{\tilde{n}N_p}{N_A} \quad (Eq. 2.2)$$

with R_p the rate of polymerization (mol L_{latex}^{-1} s^{-1}), $[M]_p$ the monomer concentration in the particles (mol $L_{particle}^{-1}$), t the time (s), k_p the rate constant of propagation (L mol^{-1} s^{-1}), [P•] the radical concentration (mol L_{latex}^{-1}), ñ the average number of radicals per particle, N_p the number of particles (L_{latex}^{-1}) and N_A the Avogadro's number (6.02 10^{23} mol^{-1}).

The monomer concentration remains constant during this step and thus, the emulsion follows zero order kinetics. The average number of radicals $\tilde{n}$ is the key factor of the kinetics. Smith and Ewart have developed a theory to describe the kinetics according to the value of $\tilde{n}$:[4]

- **ñ << 0.5**: radicals enter and exit the particles, but they terminate in the water phase. The rate of polymerization is also independent of the number of particles.
- **ñ = 0.5**: the exit rate is negligible, and, in this case, instantaneous termination occurs when a second radical enters the particle already containing a radical. Indeed, only one radical per particle can be present because of the confined space. This case is also known as the zero-one limit. The polymerization rate depends on the number of particles and thus, on the concentration of surfactant and initiator.

- **ñ >> 0.5**: when the particles are large enough, two radicals (or more) can coexist within the same particle without instantaneously terminating. The polymerization rate is therefore independent of the number of particles and the kinetics is similar to that of bulk polymerization (pseudo-bulk kinetics).

However, the Smith-Ewart theory is limited to the micellar nucleation and does not take into account the phenomena occurring when the concentration of surfactant is below the CMC, when the ionic strength varies, or when polar monomers such as methyl methacrylate (MMA), methyl acrylate (MA) or vinyl acetate (VAc) are used.

III. Photopolymerization in emulsion under UV-visible light: state-of-the-art

A. Pioneering studies on photopolymerization in dispersed media

There are many and varied PISs used in free radical photopolymerizations.[11] The first studies on photoinitiated polymerizations in dispersed media were realized under particular experimental conditions that are quite different from those of conventional emulsion polymerization, *i.e.*, surfactant concentration around the CMC, a water-soluble initiator and a monomer slightly miscible with water. However, these works are of interest because they connect photoinitiation and polymerization in dispersed media.

Takeishi *et al.*[12] reported for the first time the photopolymerization of styrene in water in 1978, in conditions comparable to those of microemulsion polymerization. The photoinitiation takes place in the micelles of *N*-laurylpyridinium azide. The polymerization is initiated by addition of the triplet nitrene produced by the photolysis of the azide adduct which is formed during the ion-exchange reaction between *N*-laurylpyridinium chloride and sodium azide in THF solution under reflux (Figure 17).

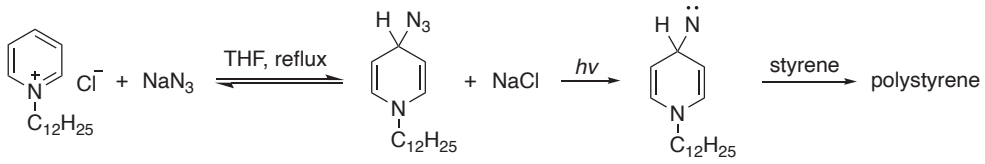

Figure 17. *Addition of the azide ion to N-laurylpyridinium, and decomposition of the adduct to an initiating triplet nitrene.*[12]

According to the authors, the micelles are the reaction locus. However, other cationic surfactants such as lysophosphatidylcholine, cetyltrimethylammonium chloride and cetyltrimethylammonium acetate did not lead to initiation of the photopolymerization, indicating that both the pyridinium ring and the azide ion are necessary. Moreover, the pyridinium ring possibly interacts with styrene to form charge-transfer complexes and this interaction in the highly polar surface area of the micelle might play an important role.

The initiation of styrene polymerization by a triplet nitrene within the *N*-laurylpyridinium azide micelles was supported by addition of a radical scavenger in the reaction mixture. However, the final conversions obtained were low (around 20 %) due to the decrease of the light penetration during the emulsion photopolymerization. Consequently, a small amount of photoinitiating species absorbed photons limiting the monomer conversion. Besides, the formation of PS particles and their characterization were not mentioned and this PIS was limited to styrene.

This pioneering study however showed the feasibility of photoinduced polymerization in dispersed media. In the following sections, we will give example of conventional emulsion photopolymerization reactions, initiated by UV and visible light irradiations.

B. Emulsion photopolymerization

1. UV light-induced oil-in-water emulsion polymerization

In 1980, Turro *et al*.[13,14] reported for the first time a photochemically initiated emulsion polymerization under UV light. The system was composed of styrene, SDS and various ketone photoinitiators, such as dibenzyl ketone (DBK), benzoin (BZ), β-ketoglutaric acid (KGA) and 4,4'-di-tert-butyldibenzyl ketone (DTBK) (Figure 18). The typical initial solution contained 2-3 mL of styrene in 5-6 mL of water with a concentration of SDS from 4 to 8 times the CMC. The molecular weight and yield of emulsion photopolymerization were compared with those obtained with conventional water-soluble thermal initiators, and they were similar or slightly higher. However, the final particle sizes were not analyzed.

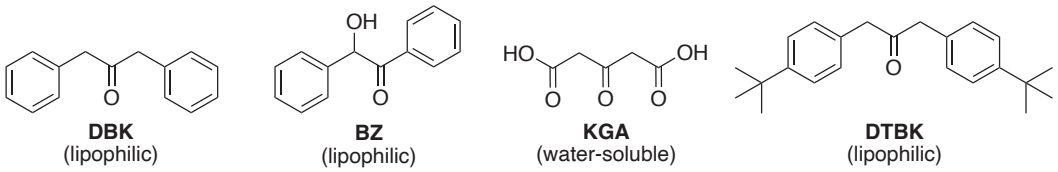

Figure 18. *Chemical structures of photoinitiators used for the emulsion photopolymerization of styrene under UV irradiation.*[13,14]

Under irradiation at 313 nm, the photopolymerization of styrene reached a final conversion of 80 % after 8 h with DBK, BZ and KGA as photoinitiators. The photopolymerizations of styrene were carried out with both lipophilic (DBK, BZ and DTBK) and water-soluble (KGA) photoinitiators. The hydrophobic ones however required a magnetic field to proceed. Indeed, according to the authors, in the presence of surfactant above the CMC, the polymer particles are produced in micelles (micellar nucleation), and due to their low solubility in water, the radicals generated from the initiators are located within the micelles. The hydrophobic photoinitiators are ineffective in emulsion polymerization since they are subject to fast recombination of the radical pair generated in the monomer-swollen micelles. The use of a magnetic field apparently increased the ability of radicals to escape from the micelles and thus led to a more effective overall initiation in the aqueous phase.

The authors also demonstrated that the use of a magnetic field was efficient only in the case of photoinitiators generating triplet radical pairs *via* homolytic cleavage and decarbonylation. For example, there was no effect of the application of a magnetic field for the thermal initiators azobisisobutyronitrile (AIBN) or KPS, or for the water-soluble KGA because the formation of radicals in this case involves a singlet radical pair.

Turro's group investigated in more detail the effect of the magnetic field on the inside recombination or escape from the micelles of benzyl radicals (Figure 19).[15] They paid particular attention to the coupling of benzyl radicals to form benzyl radical pairs in micelle cages and defined the cage effect as the ratio of the rate constant for cage recombination of benzyl radical to the sum of the rate constants for all cage processes. This allowed determining the efficiency of recombination of benzyl radicals and thus the initiation efficiency after radical escape from the micelles. The cage effect in aqueous hexadecyltrimethylammonium chloride micellar solutions was 32% at earth's magnetic field (in the range of 0.25–0.65 G) and 17% at 500 G.

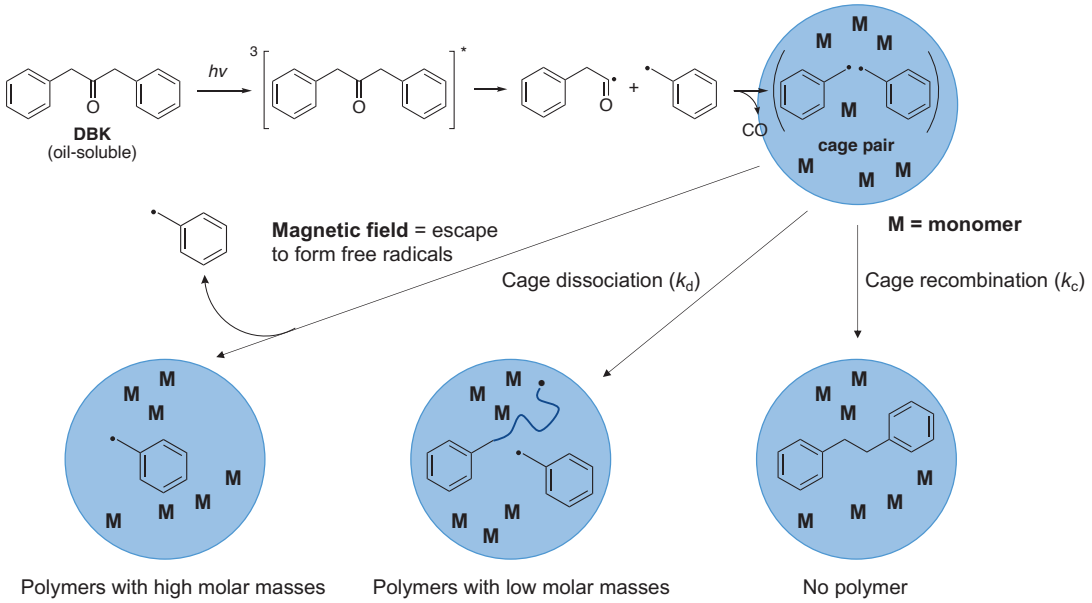

Figure 19. *Schematic representation of the reaction pathways for a radical pair (bis-benzyl) in emulsion polymerization during the initial stages of polymerization.*[15]

Then, the authors studied the ^{13}C isotope effect on the cage effect for DBK. In the case of DBK enriched in ^{13}C at the two α-carbon positions (90%), a higher cage effect (46%) was observed than for ^{12}C-DBK (32%) and DBK ^{13}C enriched in the carbonyl carbon position (33%). This result is in agreement with the postulate that germinal ^{13}C-radical centers undergo rapidly triplet-singlet intersystem crossing followed by rapid recombination.[16] The authors also performed emulsion photopolymerization of methyl methacrylate and acrylic acid under the same experimental conditions and observed similar efficiencies.[17]

In order to obtain high molecular weight poly(vinyl alcohol) (PVA), Yamamoto *et al.*[18] described in the 1990's, the emulsion photopolymerization of VAc, which are precursors for PVA under mild conditions (-5 °C < T < 5 °C) in the presence of SDS as surfactant and poly(oxy ethylene)$_n$ nonyl phenyl ether sodium sulfate (LWZ – see Figure 20) as photoactive surfactant. The polymerizations took place by irradiation at 300 or 313 nm. Even if LWZ has a low absorbance at these wavelengths, resulting in an inefficient decomposition by UV irradiation, poly(vinyl acetate) (PVAc) was obtained with good yield (96% in the optimal case). In addition, by removing LWZ from the reaction mixture, the polymerization did not start. Once LWZ decomposes, the hydrophilic part goes to the aqueous phase, and the hydrophobic part is captured by the micelles to initiate polymerization. PVAc with a high degree of polymerization (DP_n) was obtained, which was not the case when KPS was used. When the irradiation wavelength was increased to 365 nm, the photopolymerization of VAc did not start.

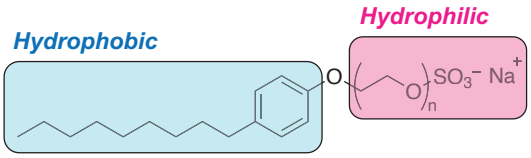

LWZ as photoreactive surfactant

Figure 20. *Chemical structure of LWZ used as photoactive surfactant (n was not provided).*[18]

The authors also observed that the DP_n increased when the temperature was lowered from 5 to 0°C (13 000 at 5 °C *vs* 20 000 at 0 °C). But the polymerization rate was lower. The increase in molecular weight was attributed to the low rate of chain transfer to polymer at lower temperatures. In addition, at 0 °C, the authors varied the LWZ concentration and the DP_n reached its highest value of 26 300 with a conversion of about 69% after 10 h and solids content of 30%. But the particles size was not discussed.

When 2,2'-azobis(2-amidinopropane) dihydrochloride (AAPH) was added as photoinitiator and irradiated at 365 nm through a UV-filter, a PVAc with a high DP_n (26 700) was obtained in good yield (84%) after 10 h at 0 °C. This technique therefore led to high molecular weights PVAc without thermal initiation.

In 2002, Mah *et al.*[19,20] also considered emulsion photopolymerization as a method to prepare high molecular weight PVAc. They used both a photoreactive anionic surfactant, poly(oxy ethylene)$_{10}$ nonyl phenyl ether ammonium sulfate (POENPEAS) and a photoreactive nonionic surfactant, poly(oxy ethylene)$_{10}$ nonyl phenyl ether (POENPE), and KPS as co-initiator. The authors observed fast polymerization rates which they attributed to complex formation between the emulsifier and KPS. They postulated that complex formation increased the rate of KPS dissociation, and thus the polymerization rate ($k_{ds} >> k_d$ – see Figure 21).

$$K_2S_2O_8 \xrightarrow{k_d} 2SO_4^{\bullet -}$$

$$K_2S_2O_8 + E \longrightarrow \text{Complex} \xrightarrow{k_{ds}} SO_4^{\bullet -} + SO_4^{2-} + E^{\bullet +}$$

Figure 21. *Formation of initiating radicals from a KPS/emulsifier complex.*[19,20]

In the case of the POENPEAS anionic surfactant, the DP_n obtained and the degree of branching were respectively 9 030 and 0.3 at 71% conversion. The degree of branching for the acetyl group of PVAc was calculated by equation 2.3:

$$Degree\ of\ branching = \frac{number\ average\ degree\ of\ original\ PVAc}{number\ average\ degree\ of\ PVA\ prepared\ by\ saponifying\ PVAc} - 1 \quad (Eq.\ 2.3)$$

Similar results were observed with the nonionic emulsifier, POENPE, which led to PVAc having a DP_n = 8 600 and a degree of branching of 0.52 at 78% conversion. A lower degree of branching was achieved when the temperature was lowered to 0 °C in order to inhibit chain transfer reactions during the polymerization.

In 2003, Robin and co-workers reported for the first time the synthesis of poly(methyl methacrylate) (PMMA) by controlled/living radical photopolymerization in emulsion using 4-diethylthiocarbamoylsulfanylmethyl benzoic acid (DTBA) as "*surf-photo-iniferter*" agent (meaning SURFactant INItiator-transFER agent-TERminator). The latter was reported to act at the same time as surfactant, photoinitiator and control and termination agent (Figure 22).[21] After the decomposition of DTBA into two radicals, the initiating benzyl radical adds to the monomer while the xanthyl radical traps the oligoradicals, leading to a dormant specie. The transition from the dormant specie to the active specie proceeded *via* the homolytic cleavage of the C-S bond under UV irradiation.[22]

The authors showed a good control of the photopolymerization. Indeed, the molecular weight increased linearly with monomer conversion up to 60%. Beyond this value, the control was lost. In addition, the presence of an additional surfactant (SDS) also led to a poor control of the polymerization with a very high molecular weight (M_n = 26 0000 g mol^{-1} against M_n = 49 000 g mol^{-1} without SDS). One possible reason is that the SDS micelles are nucleated by active species resulting from DTBA to form particles. In these precursor particles, the concentration of DTBA is probably very low making it impossible to control the polymerization. The advantage of using DTBA is that it allows the functionalization of the PMMA chain ends by carboxylic acid groups, therefore opening the possibility to graft PMMA (10 wt.%) in the molten state on a poly(ethylene-*co*-glycidyl methacrylate) copolymer.

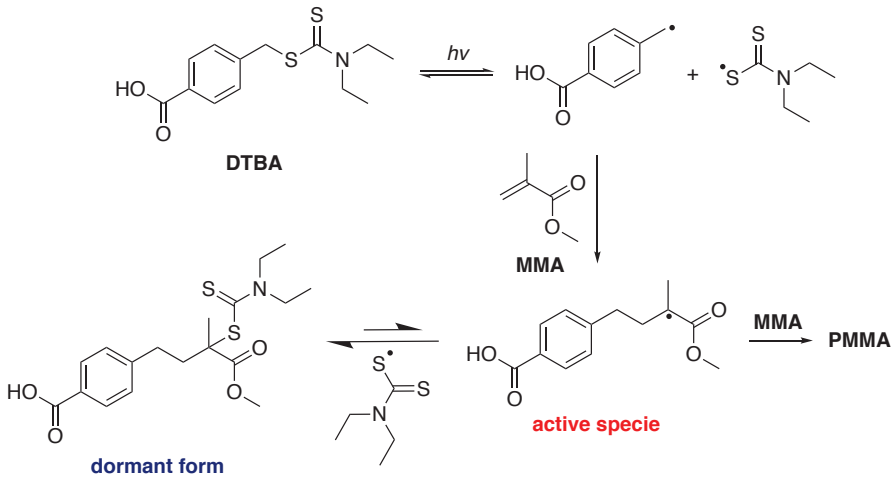

Figure 22. *Emulsion photopolymerization of MMA with DTBA as "surf-photo-iniferter" agent.*[21]

The same year, Shim *et al*.[23] also reported the synthesis of 4-thiobenzoyl sulfanylmethyl sodium benzoate as a "*surf-photo-iniferter"* (Figure 23) for the controlled/living radical photopolymerization of MMA in emulsion under UV irradiation. The authors studied the effects of "*surf-photo-iniferter"* concentration and of temperature on monomer conversion, molecular weight and particles size. The higher the "*surf-photo-iniferter"* concentration, the higher the conversion and the lower the molecular weight and final particles size obtained. A linear increase in molecular weight as a function of conversion was observed, demonstrating a good control of the polymerization. Final particle sizes in the 304 – 407 nm range were obtained depending on the experimental conditions.

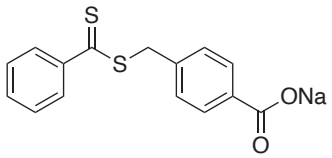

Figure 23. *Chemical structure of the 4-thiobenzoyl sulfanylmethyl sodium benzoate "surf-photo-iniferter".*

Then, Yang and co-workers compared the performance of photoinitiating systems: Irgacure 2959 and 2,2-Dimethoxy-2-phenylacetophenone (DMPA), with KPS (thermal initiator) in the emulsion polymerization of styrene in the presence of cetyltrimethylammonium bromide (CTAB) as surfactant.[24] After irradiation for 2 h, the styrene (10 wt.%) emulsion polymerized with KPS and DMPA seemed highly turbid with an average particle size of 90 and 60 nm respectively, whereas it was surprising that the one photoinitiated by Irgacure 2959 was transparent with particles size of 28 nm (Figure 24). However, it should be noticed that the CTAB concentration was not identically (1 wt.% based on styrene for KPS vs. 0.4 wt.% for DMPA and Irgacure 2959,).

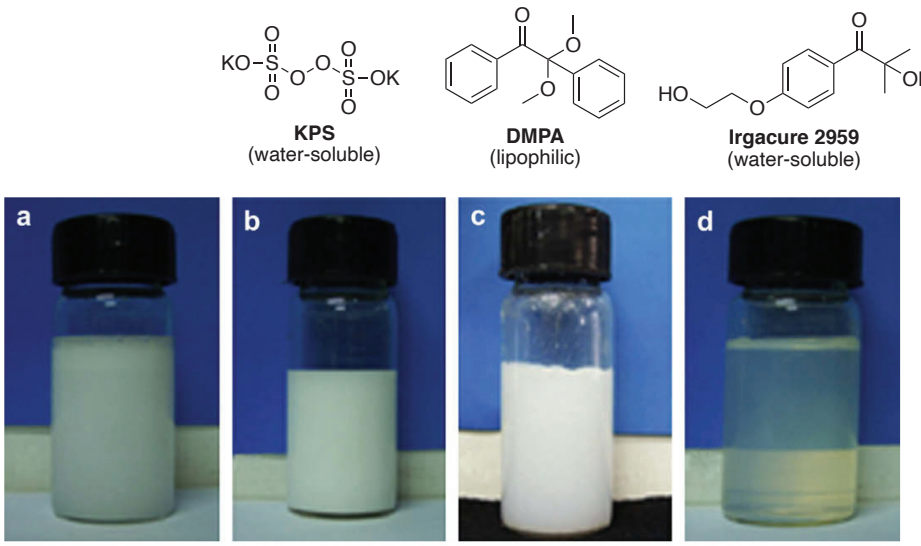

Figure 24. *Photos of (a) the styrene emulsion before polymerization, (b) the PS latex with KPS and CTAB (1 wt.% based on styrene), and (c, d) the PS latex photoinitiated by DMPA (c) and Irgacure 2959 (d) using 0.4 wt.% of CTAB based on styrene.*[24]

According to the authors, the formation of very small particles was caused by the *in situ* formed end-hydroxyl functionalized PS chains present on the latex surface and acting as a co-surfactant (Figure 25). They also studied the effect of the surfactant concentration in the case of the water-soluble Irgacure 2959. The particles size increased with increasing the surfactant concentration. This result was unexpected since the opposite is usually observed in emulsion polymerization. The authors argued that the formation of the nuclei was obtained by both homogeneous and micellar nucleation. Indeed, the precursor particles presented a colloidal instability and a very low polymerization rate. After the formation of the nuclei, they coagulated with other precursor particles or existing particles to form stable particles. Finally, the polymerization rate and the particles size increased with increasing the UV light intensity from 1.3 to 8 mW cm^{-2}. This was explained by the increased rate of formation of radicals and thus by a larger number of initially formed particles.

Zhang *et al.*[25] reported the preparation of PMMA nanolatexes *via* UV irradiation in the presence of $FeCl_3$ as photoinitiator and CTAB as surfactant at a light intensity fixed at 20 mW cm^{-2}. The monomer conversion reached up to 95% in a very short time (10 min) due to the strong photocatalytic activity of iron (III) chloride. Particle diameters in the 20–90 nm range were successfully obtained.

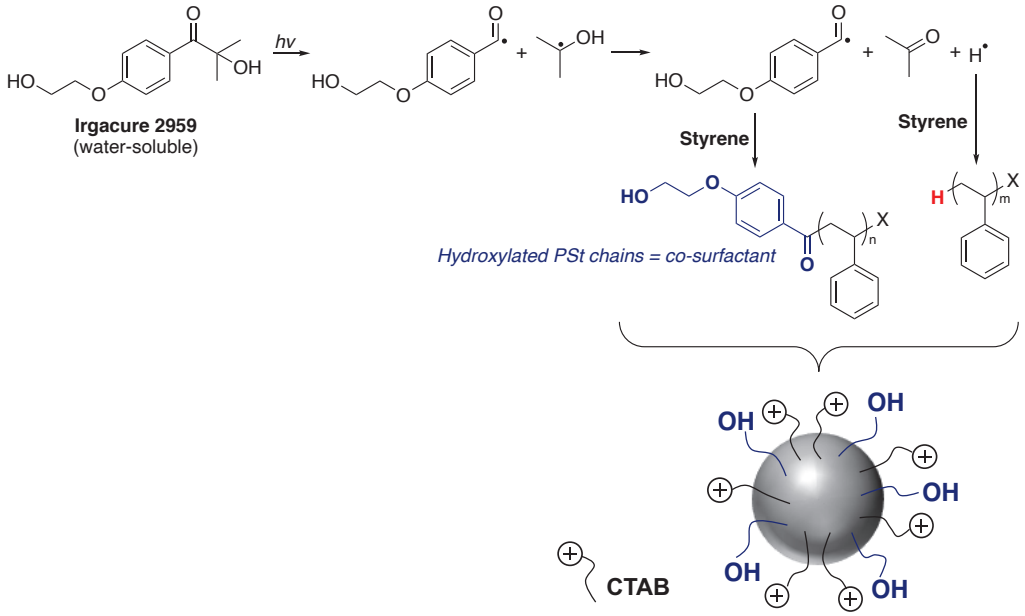

Figure 25. *In situ formation of end-hydroxyl functionalized PS chains at the latex surface acting as a co-surfactant for the production of very small particles.*[24]

In 2011, Tauer and co-workers studied the photoinitiating behavior of two bisacyl photoinitiators, namely bisacylphosphine oxide (bis(2,4,6-trimethylbenzoyl)phenylphosphine oxide, BAPO) and bisacylgermanium (bis(4-methoxy benzoyl)diethylgermanium, BAG – see Figure 26), in the emulsion photopolymerization of styrene under UV irradiation.[26] These two photoinitiators are hydrophobic and as a consequence, two types of mechanisms were taken into account: i) a small fraction of radicals was generated in the aqueous phase and then transported in the growing particles, and ii) the photoinitiators decomposed in the monomer droplets which became the polymerization locus. As a result, some coagulum (comprising particles between 100 nm and 200 µm in size) was formed in addition to latex particles with final particle diameters of around 100 nm.

The authors observed that the polymerization continued after consumption of all the photoinitiators or even occurred in their absence. In the case of BAPO, the reaction ended after 22 h reaching a conversion close to 70%, whereas for BAG, 80% conversion was reached after 40 h. It is obvious that for such long reaction times, the photoinitiators were completely consumed before the end of the polymerizations. A linear increase of the molecular weight as a function of the conversion, similar to a controlled/living radical polymerization was observed. This was attributed to the photoactive chain ends of oligoradicals/terminated polymer. The subsequent photocleavage of the polystyrene with monoacylphosphine oxide terminal groups was previously used by Günersel *et al.*[27] to produce block copolymers in the presence of MMA. In comparison with photoinitiated bulk polymerization, the authors obtained a higher

polymerization rate in emulsion probably due to the compartmentalization of the propagating radicals.

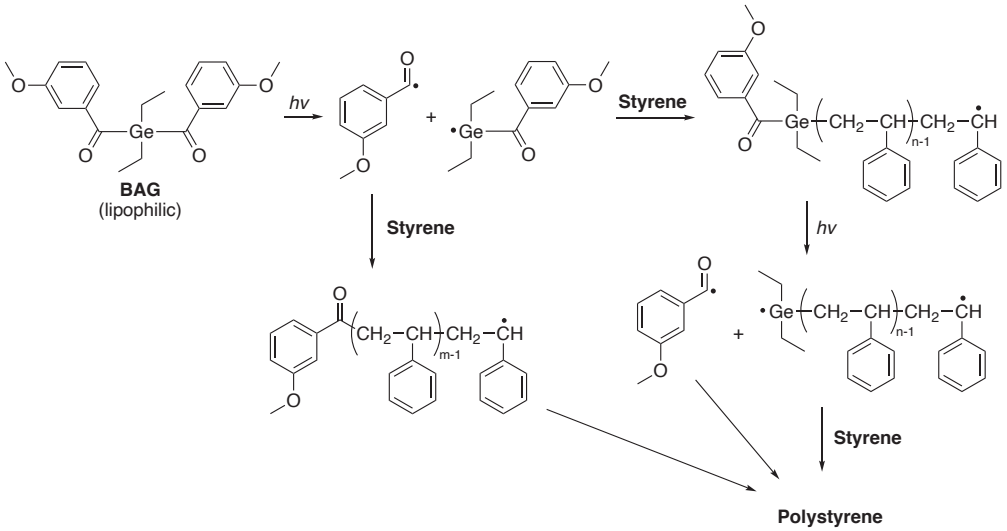

Figure 26. *Photoinduced a-cleavage of BAG under UV irradiation.*[26]

Tauer and co-workers later reported an emulsion polymerization of styrene that does not follow zero-one kinetics with 2-(bis(2,4,6-trimethylbenzoyl)phosphoryl)acetic acid (BAPO-AA) as a water-soluble photoinitiator.[28] They carried out the photopolymerization in a flow reactor under UV irradiation. Ultrahigh polymerization rates and molecular weights were obtained. The phosphine oxide was incorporated into the polymer backbone, resulting in repeated "snowballing" radical generation upon photolysis (Figure 27). The authors suggested that the bond cleavage of the oligoradical (1) could produce diradicals by routes a and b. As a consequence, there was an excessive concentration of radicals within the particles, leading to faster polymerization rates than observed in conventional emulsion polymerization to reach complete monomer conversions. Diradicals have been reported for the first time in 1920.[29] However, no experimental data was found regarding their formation.[30–32] Since then, it has been shown that when initiators "bearing" diradicals are used, the polymer chains grow from both sides.[33–35]

In their continuous flow reactor under UV irradiation, the authors reached complete conversion after only 36 seconds against 25 min in the case of the conventional thermal activation emulsion polymerization of styrene. In addition, diradicals (2) and (5) can undergo polymerization from each end of the polymers and thus, the final polymers have high molecular weight (around 10^7 g mol^{-1}).

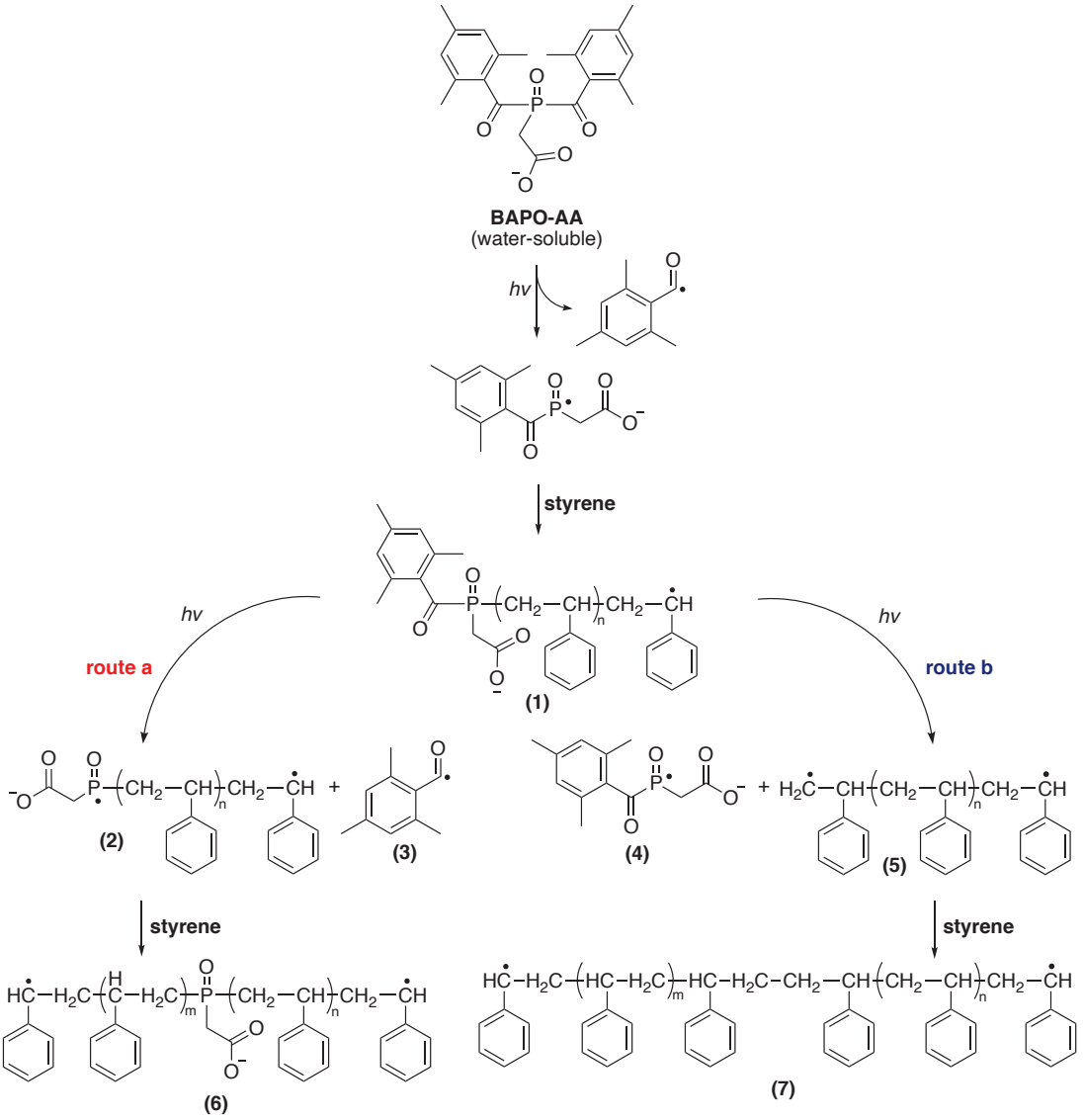

Figure 27. *Photochemical decomposition of BAPO-AA and subsequent polymerization of styrene leading to polymer chains enabling "snowballing" radical generation.*[28]

2. UV light-induced inverse water-in-oil emulsion polymerization

Two examples of inverse water-in-oil emulsion photopolymerization of acrylamide under UV irradiation have been reported in the literature. The first one is from Mandal and Ghosh.[36] who used α-Ketoglutaric acid (α-KGA) as a water-soluble photoinitiator, sorbitan monooleate (Span 80) as a surfactant and toluene as the oil phase. The authors studied the kinetics and concluded that the polymerization of acrylamide followed a reverse microsuspension mechanism. However, a second study conducted by Liu and Yang disagreed with this previous work.[37] The inverse emulsion polymerization of acrylamide was carried out with DMPA as a photoinitiator, Span 80 and Op10 as surfactants and kerosene as the oil phase.

The authors surprisingly obtained a sharp increase of absorption of the acrylamide solution by increasing its initial concentration (from 0.005 to 2.96 mol L^{-1}). Therefore, at the highest monomer concentration, self-initiation of acrylamide was observed throughout a wide UV–visible range (250–450 nm). When a UV filter was used, no polymerization took place in the absence of a photoinitiator. This shows that in UV-photopolymerization of acrylamide, it is important to take into account the self-initiation, especially at high concentration in the continuous phase.

3. Visible light-induced oil-in-water emulsion polymerization

In 2013, Ratanajanchai *et al.*[38] reported a visible light-induced surfactant-free emulsion polymerization (SFEP) of MMA for the preparation of amine-functionalized nanoparticles in the presence of a photoinitiating system consisting of camphorquinone (CQ) as a photoinitiator coupled with a hyperbranched tertiary amine, polyethyleneimine (PEI – M_n = 60 000 g mol^{-1} and M_w = 750 000 g mol^{-1}). Under visible light (460 nm), the CQ was subject to electron transfer reactions with α-tertiary amine containing polymers, resulting in the formation of free radicals on the polymer chains of PEI and on CQ molecules (Figure 28). These radicals initiated the polymerization of MMA and led to amphiphilic PMMA-PEI grafted copolymers. The PEI polymer chains acted as a surfactant and the nanoparticles formed carried amine functionalities on their surface.

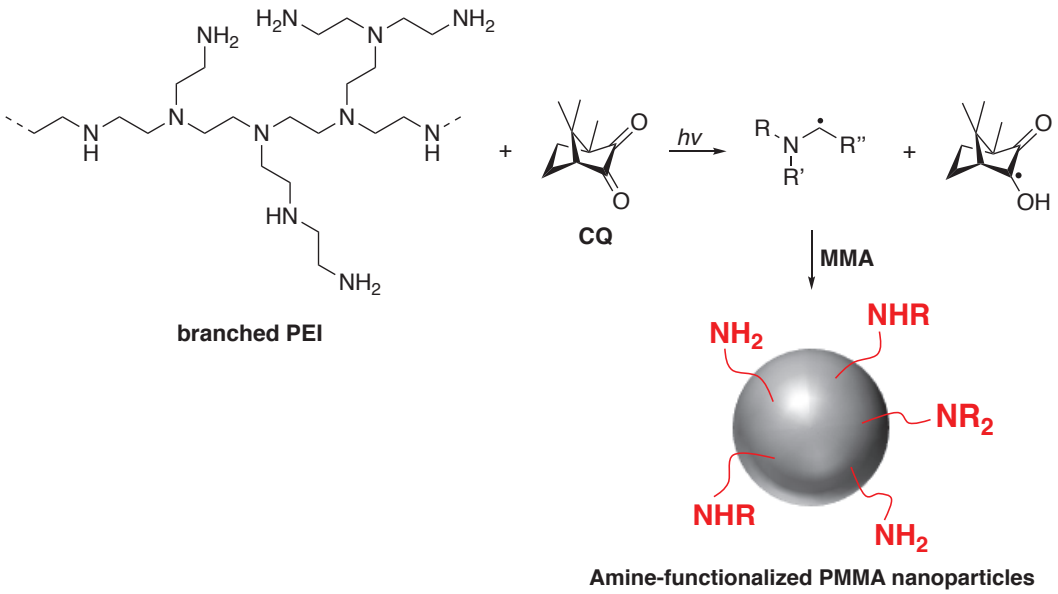

Figure 28. *Synthetic scheme illustrating the synthesis of amine-functionalized PMMA nanoparticles by the visible light-induced SFEP method using a CQ/PEI photo-redox system.*[38]

The authors obtained stable particles with size in the 100–230 nm range. They varied the weight ratio of monomer to PEI and found an optimal value of PEI:MMA = 1:4 to prepare amine-functionalized nanoparticles with high solids content and a final conversion around 80%. However, it was not possible to achieve more than 12% solids content. Moreover, for a weight ratio of PEI:MMA = 1:10, only 60% monomer conversion was reached. Then, the authors studied other polymers with tertiary amine groups, such as poly(*N*,*N*-dimethylaminoethyl methacrylate) (PDMA) and trimethylated chitosan (TMC), and observed a strong decrease of the monomer conversions to 67 and 26% for PDMA and TMC, respectively.

In 2015, Müller *et al*.[39] synthesized monodisperse PS nanoparticles photoinitiated by water-soluble bis(mesitoyl)phosphinate sodium Na(BAPO-O) *via* SFEP under UV irradiation and with a blue LED (λ = 465 nm). Polymer particles with diameter in the 209–228 nm range in the case of UV irradiation and in the 80–380 nm range using a blue LED were obtained. However, the molecular weights were unusually low (M_n = 1 500–3 500 g mol^{-1}).

Li and co-workers reported the emulsion photopolymerization of styrene based on amphiphilic octadecylamine ethoxylates *N*-oxide (AO-1805), which acted both as a surfactant and a co-initiator, using a thiocarbocyanine dye as photoinitiator under visible light irradiation (Figure 29).[40]

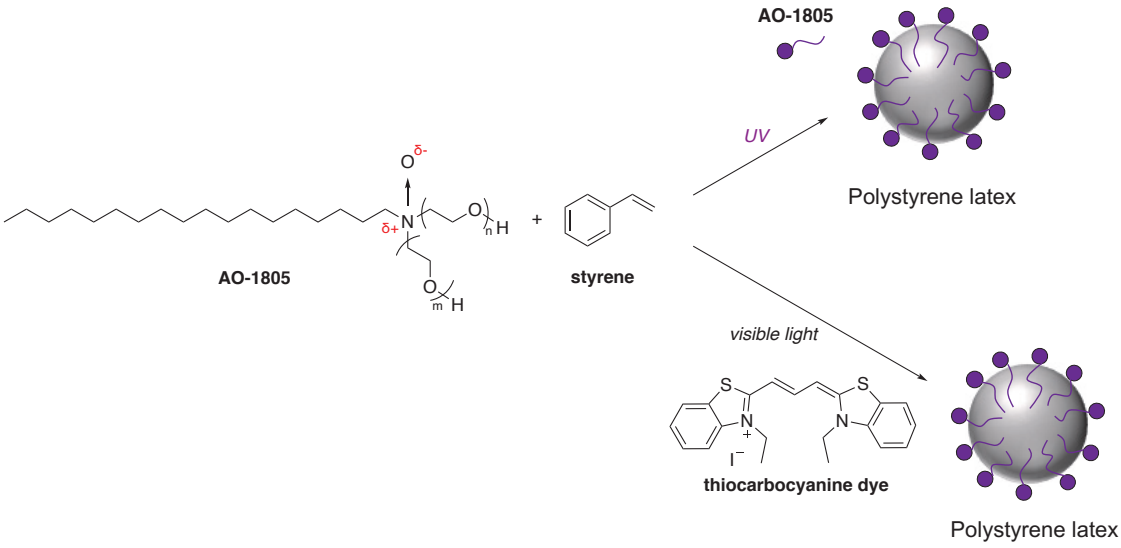

Figure 29. *Schematic reaction for the UV-visible induced emulsion polymerization of styrene based on AO-1805 and thiocarbocyanine dye (m + n = 5).*[40]

Upon UV irradiation, without dye, the generation of the active free radicals occurred at the interface of the AO-1805 micelles and then at that of the polymer particles formed. In optimal conditions, styrene conversion reached 65% after 8 h with ultra-high molecular weight

(M_n = 1 770 000 g mol^{-1}, M_w/M_n = 1.7). With the thiocarbocyanine dye, visible light-induced emulsion polymerization of styrene was possible and after 8 h, the final conversion of monomer was around 76% with M_n = 270 000 g mol^{-1} (M_w/M_n = 1.87). However, the study contains no indication as to the particle size or stability of the latexes formed. The solids content would be near 40%.

In 2018, Yamago and co-workers reported a controlled/living radical photopolymerization of MMA in emulsion using an organotellurium-mediated radical polymerization (TERP) process under visible light irradiation in the presence of an organotellurium chain transfer agent (CTA).[41] The polymerization was initiated through a cheap white LED involving the reversible photoinduced homolytic cleavage of the Te–C bond (Figure 30). The authors added the nonionic surfactant Brij 98 (polyoxyehylene (20) oleyl ether). Dimethyl ditelluride was added to the solution in order to increase the control in the polymerization of MMA.

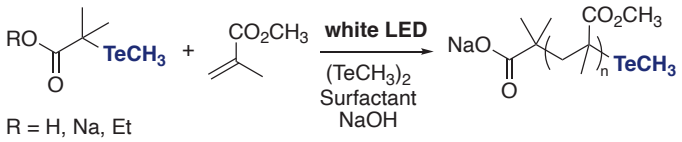

Figure 30. *Emulsion photo-TERP of MMA using an organotellurium CTA under visible light irradiation (solids content of 15%).*[41]

The authors demonstrated the controlled/living characteristics as well as a good temporal control according to a series of "ON–OFF" experiments. First, they compared the control of emulsion polymerization thermally initiated by 4,4'-azobis(4-cyanovaleric acid) (ACVA) with the photo-TERP. A slightly better M_w/M_n under photoinduced TERP than under thermal conditions (from 1.43 to 1.36) was observed. This was attributed to the decrease of dead polymer chains formation derived from the influx of ACVA radical species.[42] The particle size decreased from 342 nm (thermal initiation) to 267 nm (photo-TERP process). A hydrophilic photoinitiator was needed to obtain a stable latex. When the carboxylic acid group of the organotellurium CTA was converted into an ester and thus made hydrophobic, a less stable latex (with the presence of some coagulum) was obtained, while the control of the polymerization was poorer (M_w/M_n = 1.73). Photo-TERP emulsion polymerization enabled the synthesis of block copolymers by sequential addition of MMA and *t*-butyl methacrylate (*t*-BMA). The authors obtained the desired PMMA-*b*-poly(*t*-BMA) block copolymer with a narrow mass distribution (M_w/M_n = 1.37) and a particle size of about 98 nm with a polydispersity index (PDI) of 0.034. However, the conditions to control the molecular weights

were challenging requiring a precise radiation filtering and heat (65 °C) for 9 h to obtain full conversions.

Very recently, Su *et al.*[43] prepared PMMA and PMMA-*b*-poly(*t*-BMA) latexes via photo-TERP in emulsion at 65 °C under visible light irradiation (LED light) in the presence of an organotellurium CTA (Figure 31). The authors noticed that the reaction mixture became opaque resulting in a possibly retarding polymerization due to the weak light penetration. However, after 100 min the final monomer conversion reached 95%. This was attributed to the presence of the organic Te-dormant species on the particle surface (due to the cationic ammonium groups), facilitating the photoactivation of the Te species at a very thin irradiated surface. The living polymerization was well controlled with M_n = 11 800 g mol^{-1} and M_w/M_n = 1.16, and with particles size of around 61 nm (PDI = 0.058).

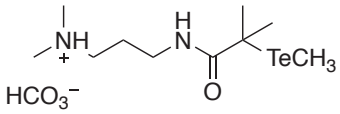

***Figure 31**. Chemical structure of the organotellurium CTA used for the emulsion photo-TERP of MMA and t-BMA.[43]*

Under the same conditions, *t*-BMA was added to the PMMA latex in the presence of dimethyl ditelluride. After 100 min, the photopolymerization was stopped and a block copolymer with M_n = 19 700 g mol^{-1} and M_w/M_n = 1.21 was obtained. The final diameter of the PMMA-*b*-poly(*t*-BMA) latex was 87 nm (PDI = 0.052). The authors also reported a series of "ON–OFF" experiments demonstrating the good temporal control of the polymerization.

IV. Conclusion

In conclusion, the studies presented in this section demonstrate the feasibility of emulsion photopolymerization processes under UV and visible lights. UV light can be however a limitation for scaling-up (except in specific microfluidic reactors). In addition, the formation of large particles (typically > 100 nm) is not possible with UV light due to increased scattering effects. Also, UV irradiation can trigger self-initiation of the monomers. In order to reduce these phenomena, emulsion polymerization was carried out under visible light irradiation. Some examples of photoinitiation in the visible region have been presented but very few of them

actually meet the conditions of conventional emulsion polymerization. Indeed, they either require large amounts of surfactants or rely on photoinitiators that are not soluble in water.

To overcome these issues, new water-soluble boron centered PISs for a sustainable emulsion photopolymerization under visible irradiation have been developed by our group and will be studied in this PhD thesis. Our water-soluble PIS was indeed capable of photoinitiate styrene and various (meth)acrylate monomers in emulsion under visible light irradiation. The obtained latexes were highly stable and the studies of the two previous works on this subject will be detailed in the following part.

As already mentioned in Chapter 1, micro- and miniemulsion polymerizations are two other techniques to prepare polymer latexes. However, we decided to do not detail them further here since microemulsion has several drawbacks: the large excess of surfactant needed and low solids content latexes (below 10%), and miniemulsion is difficult to scale-up. Moreover, miniemulsion formulations mostly involve a hydrophobic agent as co-stabilizer and the formation of monomer droplets requires a significant energy cost (ultrasonication).

Part 2. Reminders of previous works on the use of NHC-boranes as co-initiators for visible light-induced emulsion polymerization

I. Formation of NHC boryl radicals under visible light

In 2013, Lacôte and Lalevée demonstrated the successful polymerization of acrylates such as hydroxyethyl acrylate and hydroxyethyl methyl acrylate in water.[44] They used a three-component PIS consisting of a dye, namely acridine orange (AO, **1**), 5,5′-dithiobis(1-phenyl-*1H*-tetrazole) (disulfide, **2**) and dimethyl-triazolylidene-borane (NHC-BH_3, **3**) under visible light. They proposed a multi-step reaction mechanism as illustrated in Figure 32: i) under visible light, AO undergoes an electron transfer to the disulfide to form the radical-cation $AO^{\bullet+}$ and radical-anion $[Ar–S–S–Ar]^{\bullet-}$, which ii) fragments into the thiyl radical and the thiolate anion and then, iii) the thiyl radical rapidly abstracts a hydrogen atom from the nucleophilic NHC-BH_3, generating a NHC-boryl radical (**3•**) which initiates the polymerization.

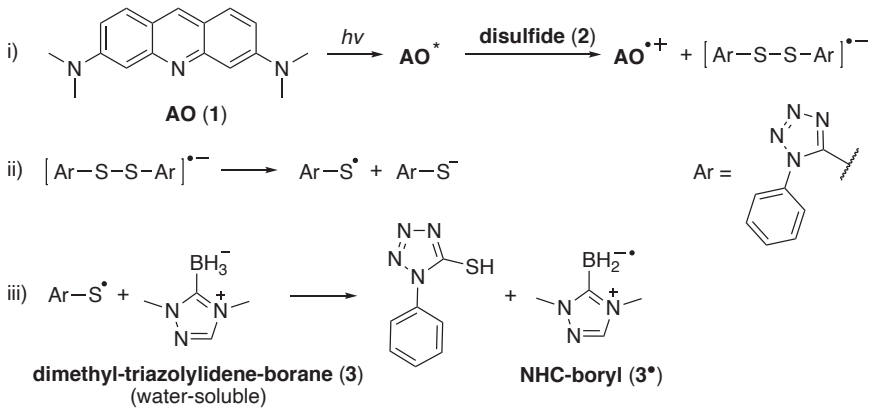

Figure 32. *Mechanism of NHC-boryl radical formation under visible light.*[44]

Encouraged by these first results, F. Le Quéméner and D. Subervie developed a water-soluble PIS for emulsion photopolymerization of styrene composed of AO (**1**), a dicarboxylate functionalized diaryl disulfide (**4** – see Figure 34) and NHC-BH_3 (**3**).[45–47] The following paragraphs will summarize the main results of these two theses, especially the mechanistic features of the photopolymerization of styrene and MMA with the PIS presented above. Finally, I will discuss my contribution to this topic.

II. Emulsion photopolymerization of styrene

A. Optimization of the irradiation set-up and photoinitiating system

The reactor used during my thesis for the emulsion photopolymerizations was optimized by F. Le Quéméner. For this purpose, a LED ribbon composed of 94 LEDs equivalent to an overall brightness of 1692 Lumens (170 W) was wrapped all around the double-wall of a glass reactor in order to maximize the light exposure within the reactor (Figure 33a). The emission spectrum of the white LEDs was measured in Mulhouse in the laboratory of J. Lalevée (Figure 33b). It clearly shows that the LEDs only emit in the visible region.

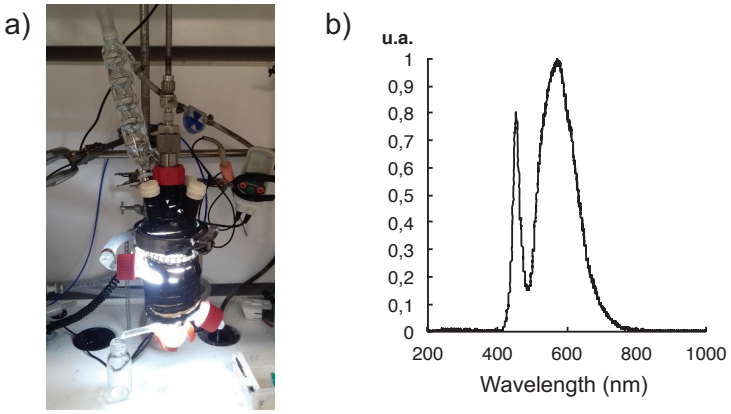

Figure 33. *a) Photoreactor powered with a LED ribbon as source of irradiation (170 W) and b) the LED emission spectrum.*

F. Le Quéméner then studied the solubility of the PIS in water starting from previously developed systems in bulk photopolymerizations.[48,49] He selected the water-soluble NHC-BH_3 (**3**) as the boron reagent and synthesized a dicarboxylic acid functionalized diphenyl disulfide (**4**), which is totally soluble in water above its p*K*a (3.8). Latex synthesis was carried out at 2 CMC of SDS targeting 20% solids content. After 6 h of LED irradiation, a highly stable polystyrene latex was obtained with complete monomer conversion, with particles around 110 nm in diameter (determined by DLS).

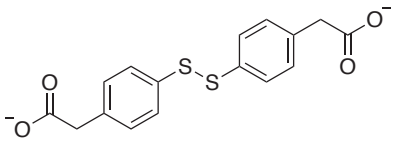

dicarboxylate functionalized diaryl disulfide (4)
(water-soluble at basic pH)

Figure 34. *Structure of the diaryl disulfide used in this work.*[45]

D. Subervie changed the LED ribbon, and used a more radiant one with 3133 Lumens (315 W) but with the same emission spectrum. The syntheses were reproduced with this new ribbon in order to compare the results in terms of kinetics and particles size. Very similar results were obtained, albeit the exact light intensity received inside the reactor could not be determined. Indeed, there is no reliable *in situ* technique to determine the light intensity transmitted within the reactor.

D. Subervie next studied the effect of each of the components of the PIS on the emulsion photopolymerization of styrene and showed that without NHC-BH_3 (**3**) or disulfide (**4**), the final conversions were limited. But surprisingly, by removing AO (**1**), the polymerization was completed after 8 h. In this case, the homolytic S–S bond likely cleaved to produce thiyl radicals in the visible region that rapidly abstracts a hydrogen atom from the nucleophilic NHC-BH_3, generating a NHC-boryl radical (**3•**) which initiates the polymerization. The photoinitiation occurred even if the maximum absorption of disulfide (**4**) is at 244 nm. Indeed, Barner-Kowollik and co-workers observed that some photoinitiators were also efficient at much longer and less energetic wavelengths than their maximum absorbance.[50]

Moreover, the disulfide (**4**) alone did not photoinitiate the polymerization of styrene. The corresponding bulk photopolymerization of styrene was performed in the presence of a lipophilic diphenyl disulfide and after 2.5 h of visible light irradiation, a conversion of 45% was reached. The different outcome between bulk and emulsion photopolymerization has several causes.

1) Ito studied the reversible addition reaction of benzenethiyl radical PhS• with styrene (Figure 35) and demonstrated that the addition rate constant was 20 times higher than that for the reverse *β*-fragmentation.[51] The study on solvent effect in the case of the *p*-NH_2-PhS• thiyl radical showed that the rate constant k_1 in cyclohexane was 2.2 x10^5 M^{-1} s^{-1}, which decreased to 3 x10^2 M^{-1} s^{-1} in dimethyl sulfoxide. There was a general tendency that the k_1 value decreased with an increase in the solvent polarity. This could explain our observations in emulsion conditions.

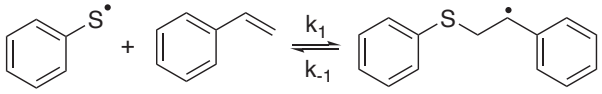

k_1 = 2 x10^7 M^{-1} s^{-1}
k_{-1} = 1.4 x10^6 M^{-1} s^{-1}
K = k_1/k_{-1} = 20 in cyclohexane

Figure 35. *Reversible addition reaction of thiyl radical PhS• with styrene and corresponding rate constants.*

2) The local styrene concentration in the bulk and emulsion photopolymerization, with respectively 8.7 mol L^{-1} and 4.3 10^{-3} mol L^{-1}, obviously had a different impact on the rate of polymerization.

Therefore, the reversible addition reaction of thiyl radicals with styrene, the solvent effect and the solubility of styrene in water are the main parameters that can explain the absence of styrene polymerization when the disulfide (**4**) is used alone (*i.e.*, in the absence of NHC-BH_3 (**3**)).

In addition, the group of Lalevée determined the rate constants of the PIS in water using flash laser photolysis (FLP). The different values are in agreement with the observations made. The rate constant for the addition of the thiyl radical with styrene was below the detection limit (k_{add} < 10^6 M^{-1} s^{-1}) whereas the rate constant for the hydrogen atom transfer from NHC-BH_3 (**3**) to the ArS• thiyl radical and the addition of the NHC-boryl radical with styrene were high (k_H = 5 x10^7 M^{-1} s^{-1} and k_{add} = 5 x10^6 M^{-1} s^{-1}, respectively), making the full system a good PIS also in water (Figure 36).

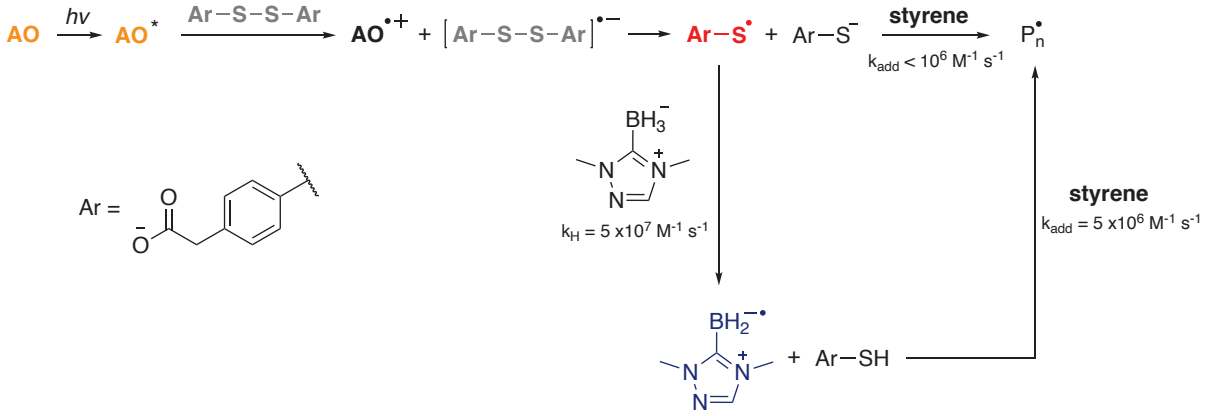

Figure 36. *The most efficient PIS for the emulsion photopolymerization of styrene.*

Therefore, the full three-component PIS was the most effective for the emulsion photopolymerization of styrene. The NHC-boryl radicals are essential for the polymerization to proceed.

B. Influence of several parameters on the particles size and polymerization kinetics

F. Le Quéméner investigated the influence of SDS concentration, solids content and NHC-BH_3 (**3**) and disulfide (**4**) concentrations on the photopolymerization rate and the final particles size. All the results are presented in Table 4.

Table 4. *Influence of several parameters (surfactant concentration, solids content, and NHC-BH_3 (**3**) and disulfide (**4**) concentrations) on the polymerization rate and the particles size in the case of styrene.*

Parameters		**Time (h)**	**Conv. (%)**	D_n[e] **(nm)**	D_w/D_n[e]	N_p **(x10^{17} cm^{-3})**
***c*(SDS) (xCMC)**[a]	0.5	50	86	294	1.01	0.2
	0.75	16	100	153	1.03	0.8
	1	9	92	94	1.32	4.0
	1.5	8	100	80	1.24	6.8
	2	6	100	67	1.30	9.9
Solids content (%)[b]	13	4	97	46	1.52	2.4
	20	6	100	67	1.30	9.9
	26	10	100	81	1.37	0.9
	31	11	100	68	1.71	1.8
***c*(NHC-BH_3) (mmol L^{-1})**	2[c]	50	75	277	1.01	0.01
	2[d]	6	96	91	1.10	0.64

[a] Experimental conditions: the solids content was fixed at 20 wt.%. [AO] = 1 x10^{-2} mmol L^{-1} (1 mol.% based on NHC-BH_3), [disulfide] = 0.5 mmol L^{-1} (50 mol.% based on NHC-BH_3) and [NHC-BH_3] = 1 mmol L^{-1}.
[b] Experimental conditions: the SDS concentration was fixed at 2 CMC. [AO] = 1 x10^{-2} mmol L^{-1} (1 mol.% based on NHC-BH_3), [disulfide] = 0.5 mmol L^{-1} (50 mol.% based on NHC-BH_3) and [NHC-BH_3] = 1 mmol L^{-1}.
[c] Experimental conditions: the solids content was fixed at 20 wt.%. The SDS concentration was fixed at 0.5 CMC. [AO] = 2 x10^{-2} mmol L^{-1} (1 mol.% based on NHC-BH_3), [disulfide] = 1 mmol L^{-1} (50 mol.% based on NHC-BH_3) and [NHC-BH_3] = 2 mmol L^{-1}.
[d] The same experimental conditions as [c] excepted for the SDS concentration fixed at 0.5 CMC.
[e] Determined by dynamic light scattering (DLS).

- ***Surfactant concentration***: a lower SDS concentration led to larger particles (from 67 nm at 2 CMC to 294 nm at 0.5 CMC, determined by TEM). The particles number decreased accordingly. Indeed, the lower the concentration of SDS, the less surface can be stabilized and thus, the larger the particles size and the lower their number. A drastic decrease of the polymerization rate was noticed at lower SDS concentrations. At 2 CMC, a complete conversion was reached after 6 h whereas at 0.5 CMC, the monomer conversion was only 86%

after 50 h. The polymerization rate is lower when the number of particles decreases, *i.e.*, when the concentration of SDS is low (*Eq.* 2.1). Moreover, the authors observed an increase of the size dispersity (D_w/D_n) below the CMC of SDS, from 1.01 at 0.5 CMC to 1.3 at 2 CMC, respectively.

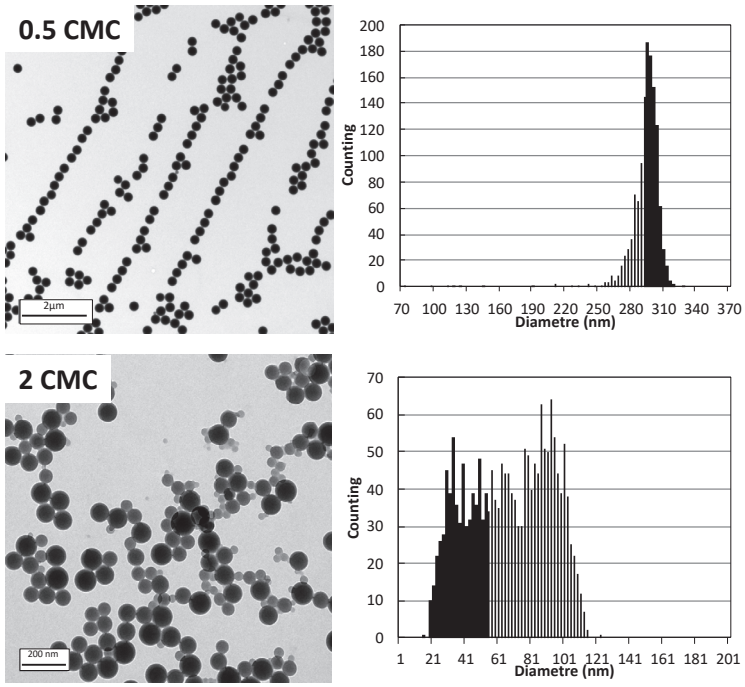

Figure 37. *TEM images and corresponding histograms for a concentration of 0.5 and 2 CMC of SDS respectively, during the emulsion photopolymerization of styrene.*

It was argued that the PIS generates radicals rather slowly resulting in a low and probably continuous nucleation rate. This means new particles are continuously formed. Above the CMC, the presence of micelles would promote this continuous nucleation. Conversely, below the CMC of SDS, the number of particles formed is lower, therefore the nucleation step is reduced compared to above the CMC where micellar nucleation is effective as long as surfactant micelles are present. In general, for conventional emulsion polymerization of styrene, the size dispersity is narrow regardless of the concentration of surfactant and this feature is specific to the present photopolymerization process.

- ***Solids content***: in each case, stable latexes were obtained without coagulum even at high solids contents. Furthermore, the polymerization rate decreased with increasing the solids content. This was attributed to the fewer number of radicals generated relative to the larger quantity of monomers at high solids content (*i.e.*, the initiator/monomer molar ratio decreased with increasing solids content). At a fixed SDS concentration, the particles size increased from 46 to 81 nm when increasing the solids content from 13 to 26 wt.%. However, at a solids content

of 31 wt.% the particle size decreased (D_n = 68 nm) and the size distribution broadened. It was assumed that the turbidity of the reaction medium, which should be significantly more important at high solids content due to the increase of the particles number prevented light penetration within the reactor (multiple scattering).

- ***PIS concentration***: as previously mentioned, the three-component PIS led to a slow and continuous nucleation and produced particles with a broad size distribution above the CMC. The next step thus aimed to boost the nucleation by increasing the photoinitiator concentration. D. Subervie opted for a twofold increase of the initial NHC-BH_3 (**3**) and disulfide (**4**) concentrations (NHC-BH_3:disulfide molar ratio = 2:1) while the AO (**1**) concentration was kept unchanged (10^{-5} mol L^{-1}), and studied the effect of the PIS concentration both below and above the CMC.

At 0.5 CMC of SDS, no enhancement has been noted in terms of size dispersity as the latex was already considered to be monodisperse. However, the final conversion was lower when the concentrations of NHC-BH_3 (**3**) and disulfide (**4**) were doubled, from 86% in standard conditions to 75%. On the contrary, at 2 CMC of SDS, the size dispersity was improved when doubling the photoinitiator concentration. The particles size was larger, and hence, the particle number was lower. This was explained by the fact that at the end of the polymerization, coagulation can occur. Indeed, by increasing the photoinitiator concentration, the oligoradicals are formed in larger amounts leading to faster formation of primary particles. The charges of the surfactant are not sufficient to stabilize the final latexes and thus, the particles coagulate to reduce the surface to be stabilized which causes an increase in particles size. The size dispersity remained however too high for the latex to be considered monodisperse.

C. Comparison with thermally activated emulsion polymerization

Then, D. Subervie compared the PIS with a conventional emulsion polymerization reaction thermally initiated by KPS. The polymerization with KPS was carried out in the same reactor as the photopolymerization for three different SDS concentrations (0.75, 1 and 2 CMC) and a targeted solids content of 20 wt.% at 70 °C. All the results are reported in Table 5. KPS was used at a concentration of 4.6 10^{-3} mol L^{-1}, that is, at a concentration 4.6 times higher than that used in photoinitiation conditions.

Table 5. *Comparison between photoinitiation and thermal initiation for several SDS concentrations (targeted solids content = 20%).*

Initiation	***c*(SDS) (xCMC)**	**Time (h)**[c]	D_n **(nm)**	D_w/D_n	M_n **(kg mol^{-1})**[d]	M_w/M_n[d]
Photo[a]	0.75	16	153	1.03	3400	-[e]
Photo[a]	1	9	94	1.32	2700	-[e]
Photo[a]	2	6	67	1.30	1600	-[e]
Thermal[b]	0.75	3.5	79	1.06	1200	1.75
Thermal[b]	1	0.8	69	1.06	340	2.29
Thermal[b]	2	0.6	52	1.06	330	2.07

[a] Experimental conditions: the initial temperature was measured at 21 °C and the solids content was fixed at 20 wt.%. [AO] = 1 x10^{-2} mmol L^{-1} (1 mol.% based on NHC-BH$_3$), [disulfide] = 0.5 mmol L^{-1} (50 mol.% based on NHC-BH$_3$) and [NHC-BH$_3$] = 1 mmol L^{-1}.
[b] Experimental conditions: the temperature was fixed at 70 °C and the solids content was fixed at 20 wt.%. [KPS] = 4.6 10^{-3} mol L^{-1}.
[c] The time it takes to reach complete monomer conversion.
[d] Determined by size exclusion chromatography in THF (SEC-THF).
[e] not determined because above the SEC detection limit.

Polymerizations initiated by KPS were systematically faster than those initiated by the photoinitiating system (from 4 to 10 times faster depending on the surfactant concentration). Moreover, at a specific concentration of SDS, the particle size was always smaller in the presence of KPS (Figure 38). A narrow size distribution was obtained below and above the CMC in the case of thermal initiation as expected.

Furthermore, the polymers obtained were characterized by SEC and the results showed that the number average molar mass M_n was considerably higher under the photoinitiation conditions than under the thermal ones, regardless of the surfactant concentration. Moreover, the "photochemical" molar masses were even above the size exclusion limits of the SEC device.

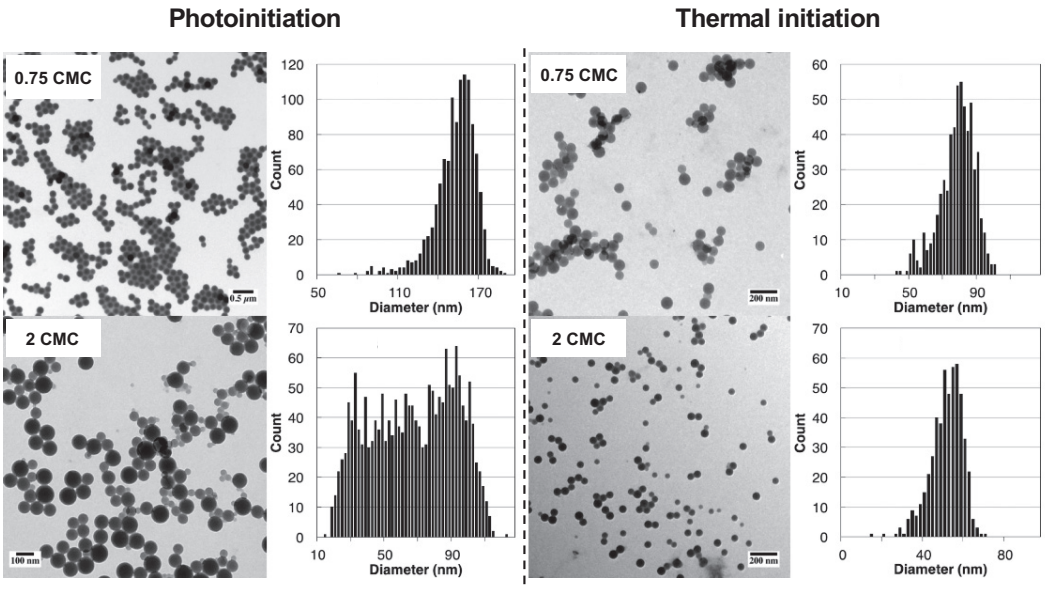

Figure 38. *TEM images and particle size distributions of the latexes obtained in two conditions: photoinitiation (left) vs thermal initiation (right); statistical analyses were performed on an average of 600–1 000 particles per batch.*

It is important to underline, however, that both systems chemically operate in a different way (T = 70 °C in thermal initiation whereas the photopolymerization proceeds at room temperature) and thus, it is difficult to provide a rationale for the observations. Another perspective considered is to design a photoreactor with an enhanced light penetration.

II. Emulsion photopolymerization of MMA

A. Effect of reaction conditions on polymerization kinetics and particles size

The three-component PIS was further extended to the emulsion polymerization of MMA and other acrylate monomers. As for styrene, several parameters were studied to observe their impact on the particles size and the kinetics. All the results are presented in Table 6.

Table 6. *Influence of several parameters (surfactant concentration, solids content, and NHC-BH$_3$ (**3**) and disulfide (**4**) concentrations) on the polymerization rate and the particle size in the case of MMA.*[a]

Parameters		Time (h)	Conv. (%)	D_n[d] (nm)	D_w/D_n[d]	N_p (x10^{17} cm^{-3})
***c*(SDS) (xCMC)**	0.25	7.5	89	128	1.17	1.4
	0.5	5	100	66	1.45	12.0
	1	4	100	54	1.37	20.5
	1.5	2.5	100	34	1.50	86.7
	2	2.25	100	35	1.37	78.0
Solids content (%)[b]	20	2.25	100	35	1.37	78.0
	26	2.25	100	30	1.62	159.0
	31	3	100	59	1.49	79.0
***c*(NHC-BH$_3$) (mmol L^{-1})**	5[c]	4	96	29	1.47	ND

[a] Experimental conditions: the solids content was fixed at 20 wt.%. [AO] = 1 x10^{-2} mmol L^{-1} (1 mol.% based on NHC-BH$_3$), [disulfide] = 0.5 mmol L^{-1} (50 mol.% based on NHC-BH$_3$) and [NHC-BH$_3$] = 1 mmol L^{-1}.
[b] Experimental conditions: the SDS concentration was fixed at 2 CMC. [AO] = 1 x10^{-2} mmol L^{-1} (1 mol.% based on NHC-BH$_3$), [disulfide] = 0.5 mmol L^{-1} (50 mol.% based on NHC-BH$_3$) and [NHC-BH$_3$] = 1 mmol L^{-1}.
[c] Experimental conditions: the solids content was fixed at 20 wt.%. The SDS concentration was fixed at 2 CMC. [AO] = 5 x10^{-2} mmol L^{-1} (1 mol.% based on NHC-BH$_3$), [disulfide] = 2.5 mmol L^{-1} (50 mol.% based on NHC-BH$_3$) and [NHC-BH$_3$] = 5 mmol L^{-1}.
[d] Determined by dynamic light scattering (DLS).

- ***Surfactant concentration***: as observed for the emulsion photopolymerization of styrene, the size of the PMMA particles decreased with increasing the SDS concentration. And a faster polymerization rate ensued. Likewise, highly stable PMMA latexes were obtained with complete monomer conversion after 5 h for 0.5 CMC and 2.25 h for 2 CMC (except at 0.25 CMC of SDS). It must be noticed that the polymerization rate was faster in the case of MMA than with styrene (complete styrene conversion was reached after 6 h, at 2 CMC of SDS) and the particle sizes of the PMMA latexes were smaller than those of the PS particles. The size distribution was broad for all SDS concentrations contrary to what happened for styrene and increased with increasing the amount of SDS (from 1.17 at 0.25 CMC of SDS to 1.37 at 2 CMC of SDS, as was also the case for styrene). As a reminder, the broad size distribution of the PS particles above the CMC was attributed to the slow production of initiating radicals leading to a slow and continuous nucleation. One possible explanation of the difference in polymerization rates between MMA and styrene is that MMA is much more soluble in water than styrene with a solubility of 15 g L^{-1} [52] and 0.45 g L^{-1} [53] at 50 °C, respectively. Therefore, the photopolymerization is probably faster for MMA as a result of its higher concentration in water.

Since the initiation of the emulsion process takes place in the water phase, the nucleation rate must be faster. This observation is in agreement with the large number of PMMA particles (4 to 12 times larger than the number of PS particles). In addition, the propagation rate constant of MMA is higher than that of styrene in bulk polymerization (for MMA, k_p = 323 M^{-1} s^{-1} and for styrene, k_p = 86 M^{-1} s^{-1}) which thus is to styrene's disadvantage in terms of kinetics of polymerization.

- ***Solids content***: the final monomer conversions were total in the three cases and highly stable PMMA latexes were obtained. Moreover, as already observed in the case of styrene, the polymerizations were slower when the solids content increased. The particle sizes were not compared because of the very broad size distributions obtained.

- ***PIS concentration***: here again, the objective was to boost the nucleation by increasing the PIS concentration. The NHC-BH_3 concentration was increased at 5 mmol L^{-1}, with the molar ratio between the component of the PIS detailed in Table 6, and studied the outcome at 2 CMC of SDS. By increasing the PIS concentration, polymerization kinetics comparable to the ones in standard conditions were observed, but with a slight decrease in the final monomer conversion (96% conversion after 4 h). In addition, the size dispersity increased with increasing the amount of photoinitiator and there was therefore no improvement of the particle size distribution contrary to what was observed for styrene.

B. Influence of the PIS composition for the emulsion photopolymerization of MMA

Next, D. Subervie studied the benefit of each of the components of the PIS by removing them from the formulation one by one (Table 7). All the syntheses were carried out at 1 CMC of SDS with a targeted solids content of 20 wt.%, and a constant concentration of the three-component PIS, unless otherwise indicated in the section.

Table 7. *Effect of the composition of the PIS during the emulsion photopolymerization of MMA ([SDS] = 1x CMC, solids content = 20 wt.%).*[a]

PIS	Time (h)	Conv. (%)	D_n[b] (nm)	D_w/D_n[b]	N_p ($x10^{17}$ cm^{-3})
AO/disulfide/NHC-BH_3	4	100	54	1.37	20.5
Disulfide/NHC-BH_3	5.5	94	30	2.62	110
AO/disulfide	1.75	100	36	1.59	67
AO/NHC-BH_3	18	5.5	-	-	-
Disulfide	1.5	100	86	1.14	5

[a] Experimental conditions: the solids content was fixed at 20 wt.% and the SDS concentration at 1 CMC. [AO] = 1 $x10^{-2}$ mmol L^{-1} (1 mol.% based on NHC-BH_3), [disulfide] = 0.5 mmol L^{-1} (50 mol.% based on NHC-BH_3) and [NHC-BH_3] = 1 mmol L^{-1}.
[b] Determined by TEM.

When AO (**1**) was removed from the PIS, the photopolymerization of MMA still proceeded (likely *via* the homolytic cleavage of the S–S bond of the disulfide (**4**)), as already observed in the case of styrene. The generation of thiyl radicals remained however less effective under visible light irradiation than the photoreduction of disulfide (**4**) by AO (**1**). The photoinitiation was low which led to a lower polymerization rate than for the full PIS. Also, without disulfide (**4**), the formation of NHC-boryl radicals is impossible and the photoinitiation was ineffective (monomer conversion reached 5.5% after 18 h). This low conversion may be due to the direct photoreduction of MMA by AO (**1**), but this reaction was inefficient.

What was more startling was that without NHC-BH_3 (**3**), and thus with the disulfide (**4**) alone, the photopolymerization was much faster and monomer conversion reached 100% in less than 2 h. The mechanism of photoinitiation is in this case different and must involve the thiyl radicals as initiating species (Figure 39). The disulfide compound (**4**) acts as a type I photoinitiator and led to a fast photopolymerization with a complete conversion after 1.5 h. The homolytic cleavage of the S–S bond generates two thiyl radicals unlike the photoreduction of disulfide (**4**) by AO (**1**) that generates only one thiyl radical (Figure 36). This may explain the faster photopolymerization observed, considering that the homolytic cleavage of the S–S bond in the blue region must be nonetheless less favorable than the photoreduction of disulfide (**4**) by AO (**1**).

This result was all the more remarkable that the measurements by laser flash photolysis performed in the laboratory of IS2M by J. Lalevée in water showed that the reversible addition of carboxylate-functionalized benzenethiyl radicals with MMA ($k_{add} \approx 10^5$ M^{-1} s^{-1}, near the

threshold of detection by LFP) was slower than the subsequent reactions of the hydrogen transfer from the NHC-BH_3 (**3**) to the thiyl radicals (k_H = 5 x10^7 M^{-1} s^{-1}) and the addition of NHC-boryl radicals with MMA (k_{add} = 2 x10^7 M^{-1} s^{-1}). Also the previous studies on the photopolymerization of HEA and HEMA in laminar conditions, bulk, or in water showed that the addition of NHC-BH_3 (**3**) made the photoinitiation more efficient than the disulfide (**2**) alone and AO (**1**) as PIS.[44,54]

In contrast to these experiments, the reaction medium of emulsion photopolymerization is heterogeneous. Consequently, these differences in reactivity may be due to the partitioning of NHC-BH_3 (**3**), which has an amphiphilic character, between the water and the organic phases. Therefore, the photoinitiation reaction with the three-component PIS may be complicated and influenced by this partitioning.

As a reminder, the thiyl radicals were ineffective in the emulsion photopolymerization of styrene. However, Ito and Matsuda determined the rate constants for the addition reactions of benzenethiyl radicals (PhS•) to MMA by means of flash photolysis.[55] They estimated a k_{add} = 3.2 x 10^6 M^{-1} s^{-1} for MMA and k_{add} = 2 x 10^7 M^{-1} s^{-1} for styrene in cyclohexane at 23 °C, suggesting that probably carboxylate-functionalized benzenethiyl radical would add faster to styrene than to MMA in water. The mechanism of particle formation was investigated in order to explain why the carboxylate-functionalized benzenethiyl radicals produced PMMA latexes but failed to initiate the emulsion polymerization of styrene.

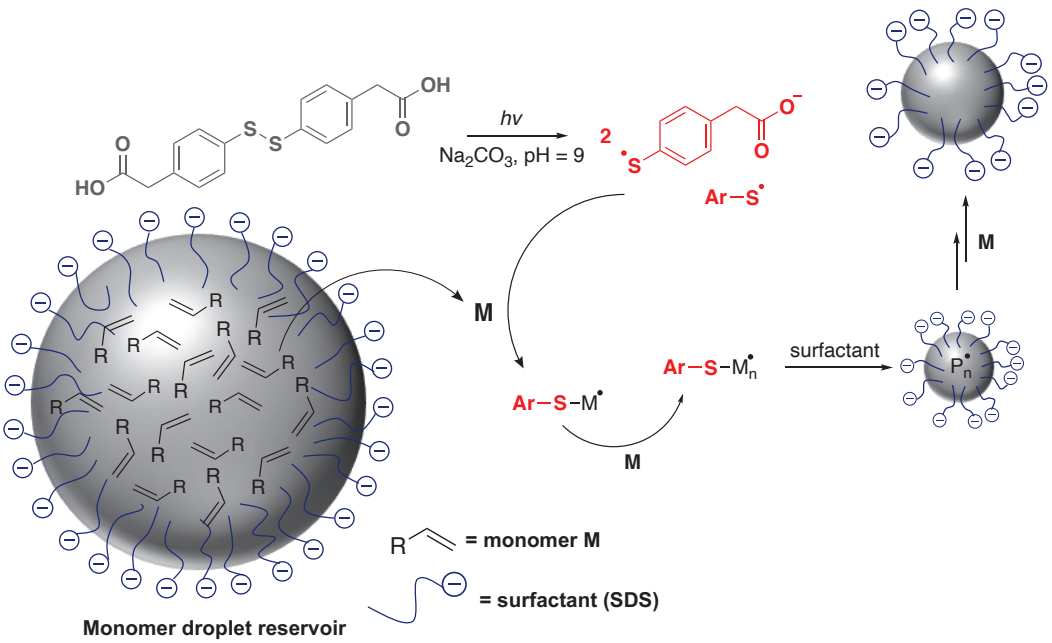

Figure 39. *Disulfide acting as type I photoinitiator to initiate the emulsion photopolymerization of MMA.*

It was then assumed that in the case of MMA, the photoinitiation without NHC-BH_3 (**3**) could probably be achieved by the combination of a greater solubility of MMA in water and a higher k_p than for styrene. In the latter case, the formation of thiyl radicals must occur, but the radicals generated likely died by recombination reactions before leading to efficient nucleation.

The two PIS (AO/disulfide and disulfide alone) were compared to demonstrate that the generation of thiyl radicals was more efficient *via* photoreduction of disulfide (**4**) by AO (**1**). For that purpose, an experiment was devised where the concentration of disulfide was halved. The polymerization rate was lower than the previous ones with only disulfide and AO/disulfide, and complete monomer conversions were reached after 3 h instead of 1.5 h and 1.75 h respectively, demonstrating that for a same formally equivalent number of thiyl radicals, the AO/disulfide PIS was the most efficient. However, the polymerization rates in each case remained faster than with the three-component PIS.

The PIS composed of AO (**1**) and disulfide (**4**) produced smaller particle sizes than the three-component PIS, with D_n = 36 and D_n = 54 nm respectively. But a broad size dispersity was obtained with D_w/D_n = 1.59 (vs. D_w/D_n = 1.37). However, in the case of the type I disulfide (**4**) polymerization, the PMMA particles were obtained with a diameter of 86 nm and a narrow size distribution (D_w/D_n = 1.14) in comparison with the other PISs, as illustrated in Figure 40. In the case of the disulfide/NHC-BH_3 system, an even broader particle size distribution was obtained (D_w/D_n = 2.62).

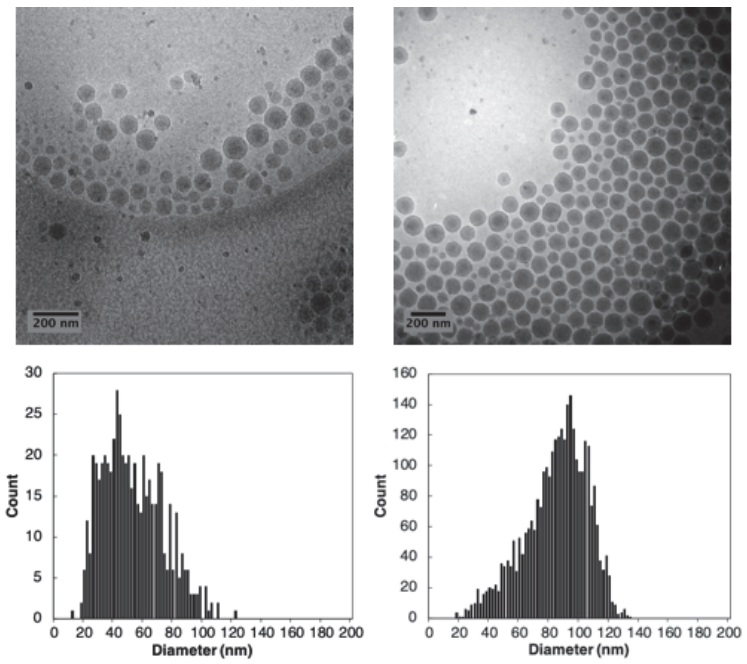

Figure 40. *Cryo-TEM images and particle size distributions of the latexes obtained with the full photoinitiating system (on the left) and the disulfide compound only (on the right).*

In conclusion, the use of disulfide alone as photoinitiator led to faster polymerization of MMA in emulsion compared to the full PIS. In addition, the disulfide alone produced larger particles with a narrow size distribution. D. Subervie studied the effect of several parameters for the emulsion photopolymerization of MMA with the simple disulfide type I photoinitiator.[46]

III. Emulsion photo(co-)polymerization of various monomers

A. Photopolymerization of other (meth)acrylate monomers with disulfide alone as photoinitiator

D. Subervie studied the photopolymerization of other (meth)acrylate monomers beyond MMA. For that purpose, he selected two different monomers: *n*-butyl methacrylate (*n*-BMA) and 2-ethylhexyl methacrylate (EHMA), and I, for my part, have completed this study by using two other monomers, methyl acrylate (MA) and *n*-BA. All the results are reported in Table 8.

The aim of this study was to observe the reactivity of the monomers with very different solubilities in water using the disulfide (**4**) as PIS. In all syntheses, the solids content was fixed at 20% and the concentration of SDS was fixed at 2 CMC.

Table 8. *Emulsion photopolymerization of (meth)acrylate monomers initiated by the disulfide alone under visible light irradiation.[a]*

Monomer	**Time (h)**	**Conversion (%)**	D_n[b] **(nm)**	D_w/D_n[b]	N_p **(x10^{17} cm^{-3})**	**Solubility in water (g L^{-1})[a]**
Styrene	-	-	-	-	-	0.45[53]
MMA	1.5	100	86	1.14	5	15.0[52]
n-BMA	1.5	100	87	1.13	5.5	0.36[56]
EHMA	8	93	90	1.23	5.1	< 0.1
MA	3	86	57	1.63	14.7	52.5[57]
n-BA	6.5	84	87	1.39	4.5	0.8[58]

[a] Experimental conditions: the solids content was fixed at 20 wt.% and the SDS concentration at 2 CMC. [disulfide] = 0.5 mmol L^{-1}.
[b] Determined by TEM.

First, *n*-BMA led to an efficient photopolymerization with a complete conversion reached after 1.5 h, which was much faster than for all the other monomers. The final particles size was about

87 nm with a size distribution D_w/D_n = 1.13, very similar to what was obtained for MMA (D_n = 86 nm and D_w/D_n = 1.14). The photopolymerization of the much less soluble EHMA and the very highly soluble MA in water (3.1 mg L^{-1} at 20 °C and 52.5 g L^{-1} at 50 °C respectively compared to 0.36 g L^{-1} for *n*-BMA at 50 °C), induced two different kinetics: a low polymerization rate for EHMA (the monomer conversion reached 93% after 8 h) and a very fast polymerization for MA, which reached a plateau after 1 h of irradiation with 85% conversion. And in the case of *n*-BA (0.8 g L^{-1} at 50 °C), the final monomer conversion reached 84% after 6.5 h with (D_n = 87 nm).

However, the example of HEMA shows that the water solubility of the monomers is not determining to explain the fact that MMA was photoinitiated by the disulfide (**4**) alone, but not styrene. Indeed, EHMA is less soluble than styrene and yet the polymerization is efficient. The monomer solubility in water contributes to the overall reaction because the polymerization rate with EHMA is much lower than with MMA although its k_p is higher. It was assumed that the main reason why there is such a difference between MMA and styrene involves the k_p of the monomers. Indeed, at 25°C, the k_p of styrene is 86 M^{-1} s^{-1} vs. 323 M^{-1} s^{-1} for MMA, 370 M^{-1} s^{-1} for *n*-BMA and 501 M^{-1} s^{-1} for EHMA. Therefore, even if the initial addition of the thiyl radicals in the case of the (meth)acrylates are less favorable than for styrene, the adduct radicals in this last case are not conducive to the formation of oligoradicals and nucleation in the case of styrene because of its lower k_p.

In conclusion, these results demonstrated the feasibility of the emulsion polymerization of other (meth)acrylate monomers with the use of disulfide alone under visible light irradiation. The k_p was one possible reason explaining why the photopolymerization of styrene was not efficient in emulsion. D. Subervie then decided to synthesize copolymers by emulsion photopolymerization under visible light irradiation.

B. Synthesis of copolymers photoinduced by the three-component PIS vs. disulfide alone

In order to determine further the mechanism, D. Subervie worked on the synthesis of copolymers based on styrene and MMA to see whether the mix behaved more like styrene or more like MMA. A comparison between both PISs was done, and the results are reported in

Table 9. The MMA to styrene weight ratio was varied at a fixed solids content of 20 wt.% and 2 CMC of SDS.

Table 9. *Copolymerization of MMA and styrene at various weight fractions photoinduced by the full system and the disulfide only.*

PIS	MMA/styrene (wt.%/wt.%)	Time (h)	Conv. (%)	D_n[c] (nm)	D_w/D_n[c]	N_p (x10^{17} cm^{-3})
Disulfide[a]	80:20	2	100	74	1.12	8.4
	20:80	2.5	100	74	1.08	8.9
	10:90	22	100	77	1.11	7.9
	2:98	36	88	88	1.17	5.4
AO/disulfide/NHC-BH_3[b]	80:20	5.2	100	45	1.46	35.0
	20:80	5.2	100	63	1.18	14.0
	10:90	7.8	100	70	1.20	10.0

[a] Experimental conditions: the solids content was fixed at 20 wt.% and the SDS concentration at 2 CMC. [disulfide] = 0.5 mmol L^{-1}.
[b] Experimental conditions: the solids content was fixed at 20 wt.% and the SDS concentration at 2 CMC. [AO] = 1 x10^{-2} mmol L^{-1} (1 mol.% based on NHC-BH_3), [disulfide] = 0.5 mmol L^{-1} (50 mol.% based on NHC-BH_3) and [NHC-BH_3] = 1 mmol L^{-1}.
[c] Determined by TEM.

Stable latexes with complete conversions were obtained regardless of the PIS used (expected for a MMA/styrene ratio of 2/98 in wt.%). At 80 wt.% of MMA, the disulfide system led to faster polymerization than the full system. Furthermore, the higher the amount of styrene in the mixture, the slower the polymerization. Interestingly, at 80 wt.% styrene, the polymerization photoinitiated by disulfide was over in 2.5 h, whereas with 90 and 98 wt.% of styrene, the polymerization took 22 and 36 h, respectively. In the case of the full PIS, the polymerization ended at 5.2 and 7.8 h for 80 and 90 wt.% of styrene, respectively. It was argued that above 80 wt.% of styrene, the nucleation step was slowed down by the low amount of MMA localized in the water phase, leading to a less effective nucleation in the case of the disulfide alone. Therefore, at 90 wt.% of styrene, the copolymerization was more efficient with the full PIS than the disulfide alone. It should be noticed that the copolymerization of styrene and MMA proceeds even below 10 wt.% of MMA because the first radical adducts formed by addition of the thiyl radicals to either styrene or MMA, can add fast enough to MMA in the early stages of the photopolymerization so that effective nucleating oligoradicals are formed.

Th full PIS led to smaller particles than the disulfide used alone, and this effect was more pronounced at 80 wt.% of MMA (D_n = 45 vs. 74 nm for the full PIS vs. disulfide, respectively).

However, since the disulfide is charged, and not the NHC-Borane, we expected that the thiyl radical residue should likely participate to the stabilization of the particles making them smaller, but we observed the opposite. Moreover, the size distribution obtained by using the full PIS was much higher than with the disulfide alone (D_w/D_n = 1.46 vs. 1.12), suggesting a better stabilization in the latter case. In addition, the particle sizes and the size distributions remained constant above 80 wt.% of styrene in both cases of photoinitiation (see Table 9).

IV. Conclusion

In this part, the efficiency of the NHC-BH_3 used as co-initiator in the emulsion photopolymerization of styrene and (meth)acrylate monomers under visible light irradiation was demonstrated. It was also found that the use of disulfide alone (one of the three-component PIS) was capable of photoinitiated (meth)acrylate monomers. These two PISs led to stable latexes with total conversions. However, significant differences were observed between the two PISs in terms of polymerization kinetics and final particle size and size distributions. For example, the use of disulfide alone led to faster (co-)polymerization than the full PIS.

A number of issues had been raised concerning the broad particle size distributions obtained for the emulsion photopolymerization of styrene at a concentration of surfactant above the CMC, and with MMA regardless of the surfactant concentration. This was attributed to the slow and continuous generation of radicals in solution. Another possible explanation might be that AO and NHC-BH_3, which have an amphiphilic character, partition between the water and monomer phases. Indeed, when the disulfide (which is soluble in water due to the carboxylate groups) was used alone as photoinitiator, an improvement in the size distributions was observed in the case of MMA. But, compared to emulsion polymerizations thermally initiated, these size distributions remained relatively high. The combination of the PIS partitioning, the slow and continuous generation of radicals, and the monomer k_p might have an impact on the size distribution.

In the following part, the partitioning of the different components of our PIS will be highlighted and then several strategies will be attempted to improve the particle size distribution of the latexes prepared by emulsion photopolymerization under visible light irradiation and above the CMC.

Part 3. Strategies to narrow the size dispersity of latex particles prepared by emulsion photopolymerization under visible irradiation

I. Influence of the type of stabilizer

In this section, SDS was replaced by a macromonomer of poly(ethylene glycol) methacrylate (PEGMA, M_n = 2 080 g mol^{-1}), able to ensure particle stabilization *via* the steric repulsion brought by the PEG chains.[59,60] The absence of any charge provides the latex with an insensitivity to ionic strength. Moreover, the PEG chains can increase the latex stability against freeze-thaw or shear.[61] It is also well known that this nonionic stabilizer is strongly anchored to the polymer particles, thus limiting its diffusion over time. For example, in the case of film formation, the migration of low molecular weight surfactants may deteriorate the material properties.[62,63]

We varied the PEGMA concentration in order to find optimal conditions leading to stable PS latexes. The syntheses were carried out under the same conditions as for SDS. The solids content was fixed at 10 wt.% and PEGMA concentrations between 0.26 and 9.37 mmol L^{-1}. Note that in the previous study, the concentration of SDS was 16.4 mmol L-1 (equivalent to 2 CMC). A colloidally stable PS latex was successfully obtained only at 9.37 mmol L-1 of PEGMA. After 5 h, the conversion reached 93% and the particles size was 76 nm with a narrow size distribution (D_w/D_n = 1.03 – see Figure 41).

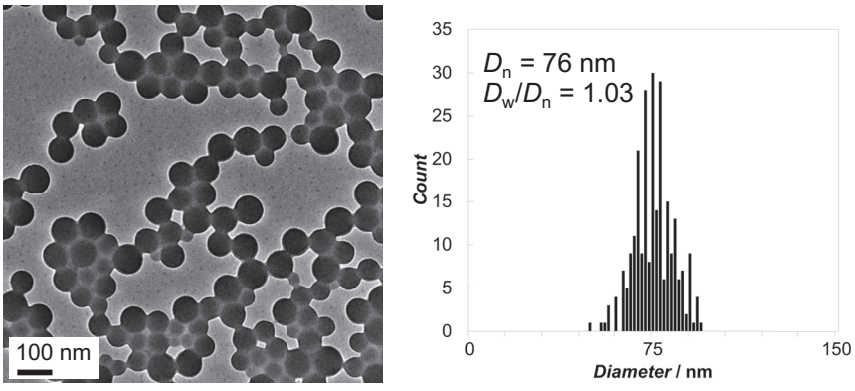

***Figure 41**. TEM image of the PS latex prepared by emulsion polymerization under visible light irradiation in the presence of [PEGMA] = 9.37 mmol L^{-1} at a fixed solids content of 10 wt.% and [AO] = 1 x 10^{-2} mmol L^{-1} (1 mol.% based on NHC-BH$_3$), [disulfide] = 0.5 mmol L^{-1} (50 mol.% based on NHC-BH$_3$) and [NHC-BH$_3$] = 1 mmol L^{-1}.*

The introduction of PEGMA in the emulsion photopolymerization of styrene resulted in an improvement of the size distribution in comparison with the synthesis carried out in the presence of SDS at 2 CMC (see Table 4). Indeed, in the latter case, under similar conditions, the final particle size was around 46 nm in diameter with a broad size distribution (D_w/D_n = 1.52).

At this concentration of 9.37 mmol L^{-1} in water, we believe that the PEGMA macromonomers will aggregate in micelles with their hydrophobic group (methacrylate) in the core and the hydrophilic PEG in the surrounding shell. Ito *et al.*[64] described the formation of those micelles with different PEO carrying polymerizable function and their homo-polymerization which was much faster than the model monomers because of the greater local concentration of polymerizable groups confined in the core of the micelles. In our case, the PEGMA micelles should be swollen by the styrene and the particles are therefore produced by micellar nucleation. Conversely to the SDS micelles, the PEGMA macromonomers exhibit frozen micellar-like structures that all lead to the formation of a particle, which may explain the significantly narrower particle size distribution compared with SDS. Indeed, the exchange dynamics of such structures must be lower than in the case of SDS micelles since the macromolecules are covalently bonded to the precursor particles.

As the PEGMA concentration decreases, destabilization phenomena were observed with very poor monomer conversions. It is possible that the macromonomers remain soluble in water (no micelle) and did not participate to the stabilization. Indeed, Ito *et al.*[65] calculated the reactivity ratios for copolymerization of styrene with PEO-MA and concluded that the relative reactivity of PEO-MA decreased with increasing the EO units (for example, EO = 62 corresponded to a $r_{styrene} = 1.18 \pm 0.11$). The PEO chains seem to reduce the reactivity of the terminal methacrylate.

This study showed that the type of stabilizer has a significant impact on the size distribution. As reminder, the first hypothesis to explain the obtention of narrow size distributions was a slow and continuous nucleation. The presence of PEGMA macromonomers could lead to a fast nucleation where all the PEGMA micelles form particles (the number of particles is thus rapidly fixed), resulting in narrow size distribution.

II. Development of more water-soluble PISs for emulsion photopolymerization

A. Impact of the reactor geometry and LED brightness on the outcome of the polymerization reaction

During the first period of this thesis, we were faced with reproducibility issues. Both F. Le Quéméner and D. Subervie had used the same double-wall reactor with a round bottom and obtained very similar results. In this work, we first used a double-wall reactor with a flat bottom and a different anchor stirrer. Using the exact same recipes as those of F. Le Quéméner and D. Subervie, we observed a high destabilization of the latex, with solid polymer formed on the anchor stirrer. We decided to vary the stirring rate between 200 and 400 rpm, but to no avail.

Then, we changed the reactor back to a round bottom and no more destabilization of the latex suspension occurred. However, the polymerization rates were lower than the ones observed in the previous works. This shows that the reactor geometry influences the photopolymerization process. For this purpose, a double-wall reactor with a round bottom was designed similar in all respects to the reactor of F. Le Quéméner and D. Subervie. In this case, the results were consistent with the previous ones.

Another key device in our system is the irradiation source. Indeed, the LED ribbon was changed to a more powerful one with 320 LEDs corresponding to an overall brightness of 6 156 Lumens (42 W) with the same emission spectrum (vs. 3 133 Lumens for D. Subervie). (NB: Obviously, caution should also be advised on the brightness of the LEDs ribbon, which will inevitably fade/decrease with time and use.) The syntheses were therefore reproduced to calibrate the results in terms of kinetics and particle size. We obtained very similar results in the case of MMA (D_n = 35 nm and D_w/D_n = 1.41 vs. D_n = 35 nm and D_w/D_n = 1.37 obtained by D. Subervie) but much better ones in terms of kinetics for styrene (Figure 42). Whereas F. Le Quéméner and D. Subervie observed the same trend for the styrene conversion profiles (complete conversion reached after 6 h with D_n = 67 nm and D_w/D_n = 1.30), with the new LED ribbon we obtained a faster photopolymerization whereby complete conversion was reached after 2.6 h. We also obtained similar particle sizes (D_n = 68 nm and D_w/D_n = 1.35). We believe that a more important number of radicals was generated, leading to a higher number of particles than with a less powerful LED ribbon, thus explaining the faster polymerization. The fact that the final colloidal features of the PS latexes were so similar remains however unclear at this point. Combined with

the very good reproducibility of the PMMA syntheses, these 4 experiments at least highlight the critical role of the events occurring in water on the outcome of the nucleation step.

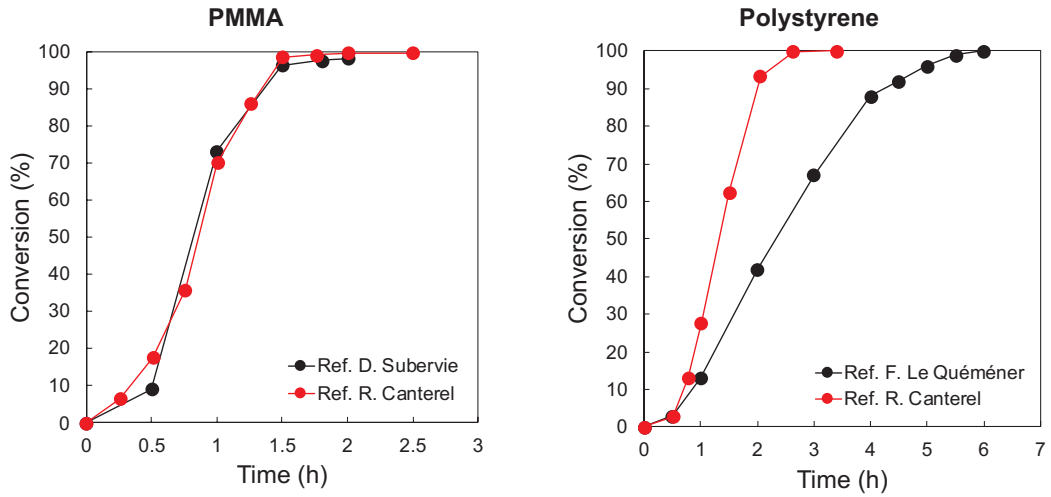

Figure 42. *Conversion profiles of the emulsion photopolymerization of MMA (left) and styrene (right) photoinitiated by the three-component system under visible light with a more radiant LED ribbon used in this thesis work. The solids content was fixed at 20 wt.% and the SDS concentration at 2 CMC.*

B. Determination of AO and NHC-BH_3 partition coefficients

To gain more information on the nucleation step, for which the solubility of the PIS is obviously crucial, we have used the traditional shake-flask method[66] at room temperature to estimate the partitioning coefficient P of AO (**1**) and NHC-BH_3 (**3**). The organic phase was either styrene or MMA, and the aqueous one a solution of sodium carbonate buffer (pH = 8). AO (**1**) was solubilized in the monomer, while NHC-BH_3 (**3**) was dissolved in water. It should be stressed that the determination of the partitioning coefficients was carried out without surfactant (simple case of a two-phase system). Both phases were mixed keeping the weight ratio used for the emulsion photopolymerizations (25 g of monomer per 100 g of water), and the mixture containing AO (**1**) or NHC-BH_3 (**3**) was stirred for 30 min and finally decantated for 2 h. After separation, the organic phase was analyzed by UV-vis to determine the concentration in each phase using pre-established calibration curves (see Chapter 5). The partition coefficient P is defined as the ratio between the concentration of the solute in the organic phase and its concentration in water. The logarithm of the ratio, log P (*Eq*. 2.4), represent the measure of the lipophilicity or hydrophobicity of AO (**1**) or NHC-BH_3 (**3**). If log P

< 0, the solute is hydrophilic and conversely for log P > 0, the solute is lipophilic. The results are shown in Table 10.

$$\log P = \log \frac{C_{org.}}{C_{water}} \quad (Eq. 2.4)$$

Table 10. *Partitioning of AO (**1**) and NHC-BH_3 (**3**) in styrene/water and MMA/water.*

Organic phase	Compound	Absorbance in organic phase	*c*(water phase) (mol L^{-1})	*c*(organic phase) (mol L^{-1})	Log P
Styrene	AO	1.032	3.3 x10^{-7}	4.3 x10^{-5}	1.11
	NHC-BH_3	0.305	8.1 x10^{-4}	8.3 x10^{-4}	0.01
MMA	AO	0.714	9.5 x10^{-8}	5.7 x10^{-5}	2.77
	NHC-BH_3	0.631	8.2 x10^{-4}	7.1 x10^{-4}	-0.06

The AO (**1**) concentrations were found to be 4.3 x10^{-5} in styrene and 5.7 x10^{-5} mol L^{-1} in MMA, corresponding to a concentration of 3.3 x10^{-7} and 9.5 x10^{-8} mol L^{-1} in the water phase, respectively, leading to log P values above 1 for both monomers. These values indicate that AO (**1**) can be considered as mainly soluble in the monomer phase. Note that after the decantation, we can clearly see a stronger orange coloration in styrene and MMA than in water.

NHC-BH_3 (**3**) behaves differently from AO (**1**). Indeed, for both styrene and MMA, it partitions between the monomer and water phases, with roughly equivalent concentrations (8.3 x10^{-4} in styrene and 7.1 x10^{-4} mol L^{-1} in MMA, which represents a concentration of 8.1 x10^{-4} and 8.2 x10^{-4} mol L^{-1} in the water phase, respectively). Consequently, the Log P was found to be close to 0, meaning that the NHC-BH_3 (**3**) is equally partitioned between the monomer and water phases.

In summary, AO (**1**) is mostly soluble in the monomer phase, especially in MMA, and the NHC-BH_3 (**3**) partitions between the monomer and water phases. As mentioned above, in emulsion polymerization, the initiation step takes place in the aqueous phase. The partition coefficients could explain the important size dispersity obtained for the PS latexes in the case where the surfactant concentration was above the CMC (see Table 4), and for the PMMA latexes independently of the surfactant concentration (see Table 6). The aim of the following sections was to introduce a more water-soluble PIS by either replacing AO (**1**) by more water-soluble dyes or developing new NHC-BH_3 functionalized with sulfonate or amino groups that should increase their water solubility.

C. New water-soluble dyes for the photoinitiating system

1. Case of styrene

As previously mentioned above, AO (**1**) is mostly present in the monomer phase. But in conventional emulsion, the initiation step must occur in the aqueous phase and consequently, the dye must be soluble in water since this is the specie that will lead to the generation of radicals under visible light irradiation. We thus decided to replace AO (**1**) by new water-soluble dyes. In collaboration with the group of J. Lalevée, we have selected different dyes, riboflavin (**6**), erythrosin B (EB) (**7**), rose Bengal (RB) (**8**) and methylene blue (MB) (**9**), that are more water-soluble than AO (**1**) and have listed in Table 11 their maximum absorption, extinction coefficient and water solubility. We have also indicated whether the pH plays a role or not on the absorption of the dyes in water. The UV-visible absorption spectra of these dyes, presented in Figure 43, allowed the determination of their molar extinction coefficients. Each dye was dissolved in water at pH = 8, which is the pH set in our experimental conditions to solubilize the disulfide (**4**) in water.

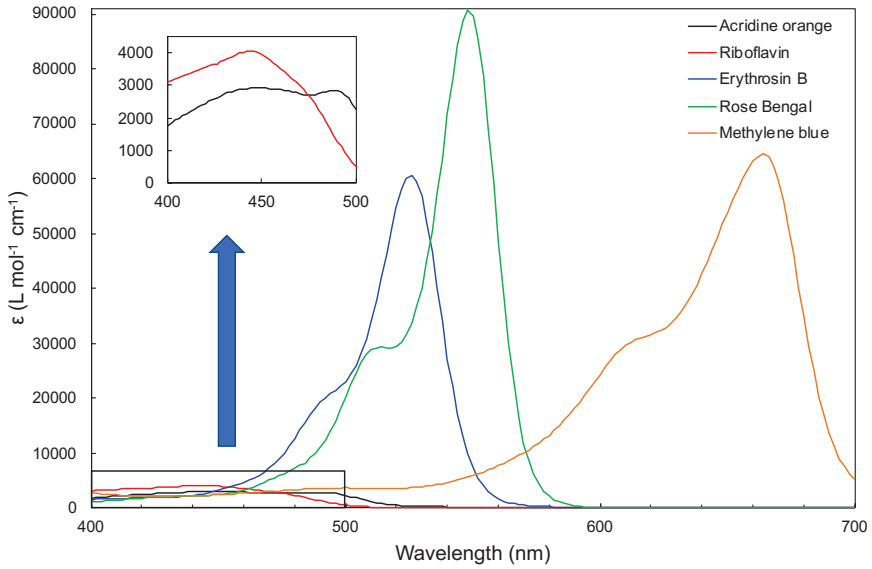

***Figure 43**. Molar extinction coefficient curves as a function of the wavelength for several dyes in basic water (pH = 8).*

Table 11. *List of potential dyes and their characteristics for the water-soluble photoinitiating system. The absorbance values were determined in basic water (pH = 8).*

Dyes	λ_{max} (nm)	Extinction coefficient at λ_{max} (L mol^{-1} cm^{-1})	pH effect	Solubility in water
AO (1) 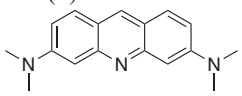 (**1**)	446	2 922	pH < 3.5: aggregation Not stable at pH > 10	ND
Riboflavin (6) 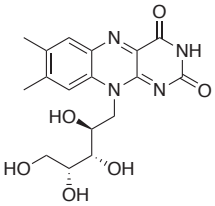 (**6**)	443	4 057	No effect	ND
EB (7) 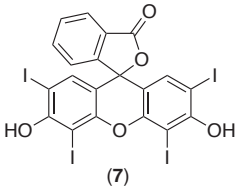 (**7**)	525	60 663	pH 3-5: insoluble pH 7-8: stable	1 g L^{-1} (at 1M NH_4OH)
RB (8) 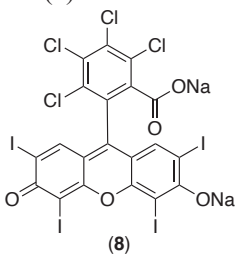 (**8**)	548	90 844	pH < 4: insoluble in water.	100 g L^{-1}
MB (9) 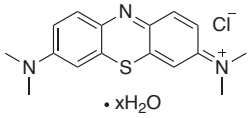 (**9**)	663	64 454	No effect	43 g L^{-1} at 25 °C

The dyes were then used in the production of PS latex particles in emulsion polymerization under visible irradiation. It should be noticed that we decided to keep the exact concentration that was used for AO (**1**), *i.e.*, [AO] = 10^{-5} mol L^{-1}, regardless of their molar extinction coefficient. All the results are reported in Table 12.

Table 12. Effect of the type of dye on the emulsion polymerization of styrene under visible light irradiation ([SDS] = 2x CMC and 20 wt.% solids content). *[a]*

Dyes	Time (h)	Conversion (%)	D_h[b] (nm)	PDI[b]	D_n[c] (nm)	D_w/D_n[c]	N_p (x10^{16} cm^{-3})
AO	2.6	100	110	0.02	68	1.35	11.4
Riboflavin	2.5	98	112	0.03	90	1.10	4.9
EB	2	100	100	0.03	76	1.12	9.8
RB	2.1	100	87	0.05	69	1.15	11.1
MB	2.1	99	107	0.05	84	1.10	6.0

[a] Experimental conditions: the solids content was fixed at 20 wt.% and the SDS concentration at 2 CMC. [dye] = 1 x 10^{-2} mmol L^{-1} (1 mol.% based on NHC-BH_3), [disulfide] = 0.5 mmol L^{-1} (50 mol.% based on NHC-BH_3) and [NHC-BH_3] = 1 mmol L^{-1}.
[b] Determined by DLS.
[c] Determined by TEM.

The use of the new dyes led to stable PS latexes with complete conversions in all cases. The polymerization rates were faster when EB (**7**), RB (**8**) or MB (**9**) were used than for AO (**1**) or riboflavin (**6**) (Figure 44). This can be attributed to the higher molar extinction coefficient of these dyes (60 663, 90 844 and 64 454 L mol^{-1} cm^{-1} at λ_{max} = 525, 548 and 663 nm, respectively) compared to AO (**1**) and riboflavin (**6**) (2 922 and 4 057 L mol^{-1} cm^{-1} at λ_{max} = 446 and 443 nm, respectively). Indeed, the molar extinction coefficient is a measure of how strongly a dye absorbs light at a particular wavelength. Therefore, the dye rapidly reaches its excited state and could photo-reduce the disulfide (**4**), resulting in a fast generation of thiyl radicals. Actually, we expected much faster photopolymerization than observed experimentally as the gap between the molar extinction coefficients was very large. However, if the absorption of a dye is too high, an inner filter effect may occur, therefore reducing the light penetration and consequently the efficiency of radical production. For a same dye concentration, the higher the molar extinction coefficient, the greater the absorption and therefore the optical path crossed by the light will be reduced. Moreover, at 635 nm (red light), the light is composed of photons that are less energetic than the photons from the blue light (400 nm). This can explain the observations concerning the polymerization rates. It is then essential to properly adjust the dye concentration for an optimal photopolymerization.

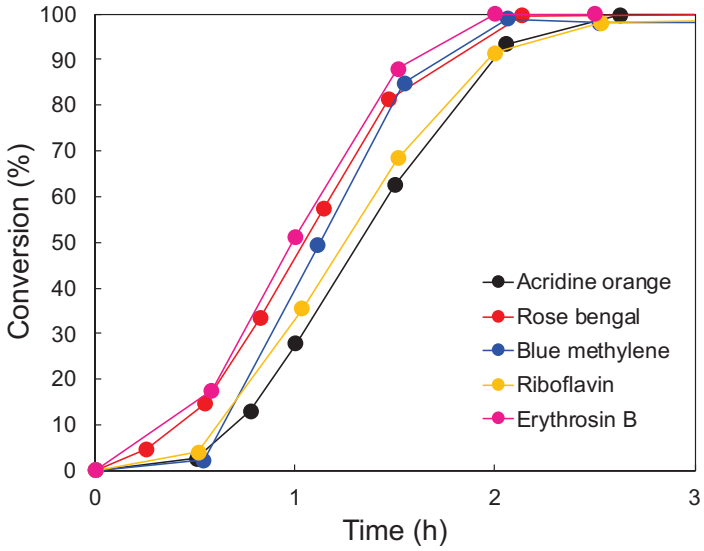

***Figure 44**. Conversion curves as a function of time for the emulsion polymerization of styrene using different water-soluble dyes. See Table 12 for more experimental details.*

Depending on the dye used, we obtained PS latexes with different particle sizes, from 69 nm with RB (**8**) to 90 nm with riboflavin (**6**) (Figure 45). Therefore, the type of dye also had an influence of the particles size. In addition, the size dispersity was significantly narrowed. Indeed, when AO (**1**) was used to produce PS particles, the size dispersity was very broad (D_w/D_n = 1.35) whereas with the other dyes we obtained narrower size distributions with D_w/D_n = 1.10, 1.12, 1.15 and 1.10 for riboflavin (**6**), EB (**7**), RB (**8**) and MB (**9**), respectively. This study demonstrates that the type of dye clearly impacts the initiation step and thus the particle formation, and consequently the size distributions. More specifically, the dye efficiency will depend both on its water solubility and on its molar extinction coefficient. In the most favorable cases, the new dyes can generate radicals more rapidly than AO (**1**) leading to more efficient nucleation and ultimately to narrower size distribution. Obviously, the next step would then be to optimize the concentration of each dye.

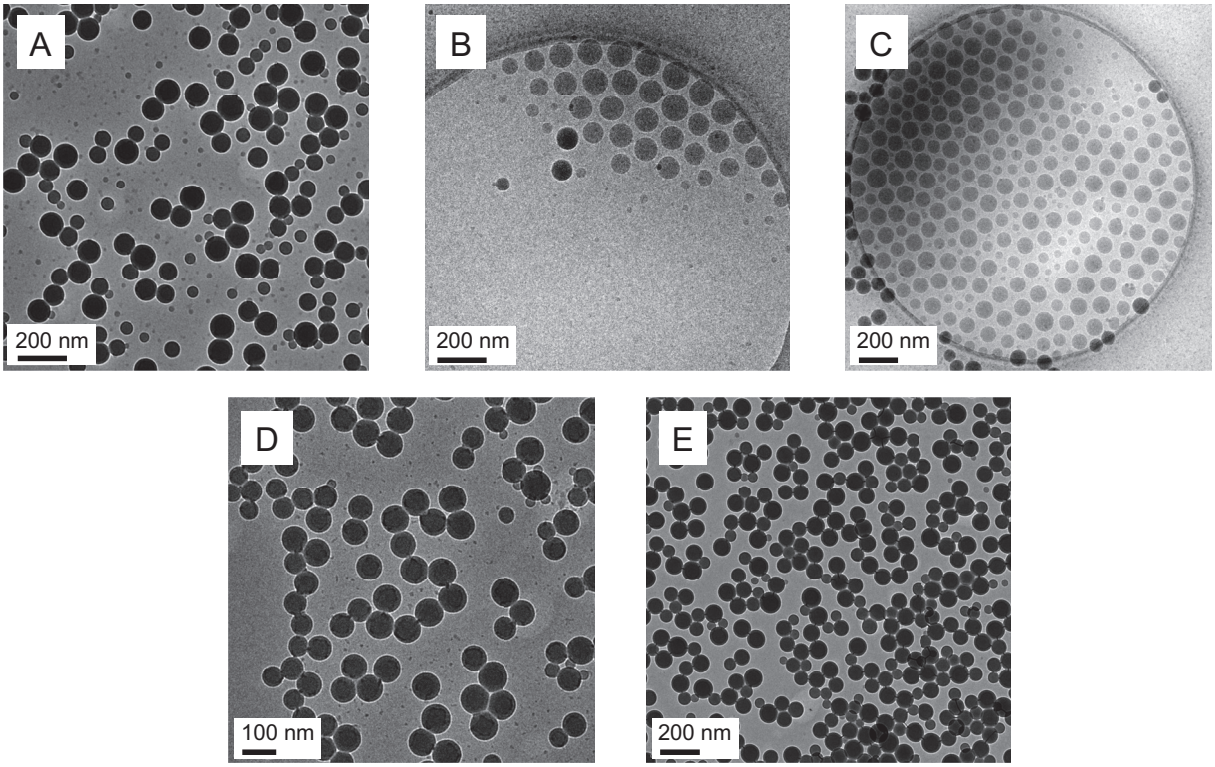

***Figure 45**. TEM and cryo-TEM images of PS latexes synthesized using several dyes. (A): Acridine orange, (B): Riboflavin, (C): Erythrosin B, (D): Rose Bengal and (D): Methylene blue. See Table 12 for more experimental details.*

2. Case of MMA

We then investigated the emulsion photopolymerization of MMA. AO (**1**) was replaced by RB (**8**) and MB (**9**). The experimental conditions were similar to the ones in the case of styrene. The results are presented in Table 13.

***Table 13**. Effect of the type of dye on the emulsion polymerization of MMA under visible light irradiation ([SDS] = 2x CMC and 20 wt.% solids content). [a]*

Dyes	Time (h)	Conversion (%)	D_h[b] (nm)	PDI[b]	D_n[c] (nm)	D_w/D_n[c]	N_p (x10^{17} cm^{-3})
AO	1.75	100	66	0.09	35	1.41	7.5
RB	2	100	65	0.15	40	1.48	5.6
MB	2	100	73	0.13	31	1.85	12.2

[a] Experimental conditions: the solids content was fixed at 20 wt.% and the SDS concentration at 2 CMC. [dye] = 1 x 10^{-2} mmol L^{-1} (1 mol.% based on NHC-BH_3), [disulfide] = 0.5 mmol L^{-1} (50 mol.% based on NHC-BH_3) and [NHC-BH_3] = 1 mmol L^{-1}.
[b] Determined by DLS.
[c] Determined by TEM.

The use of the new dyes led to stable PMMA latexes with complete conversions. Unlike the case of styrene, the polymerization of MMA was faster when AO (**1**) was used than with RB (**8**) and MB (**9**) (Figure 46). This may be due to the higher molar extinction coefficient of these new dyes (90 844 and 64 454 L mol^{-1} cm^{-1} at λ_{max} = 548 and 663 nm, respectively) compared to AO (**1**) (2 922 L mol^{-1} cm^{-1} at λ_{max} = 446, respectively) which involves an important absorption of the new dyes. Consequently, an inner filter effect may occur resulting in a reduction of the optical path crossed by the incident light. In addition, as the wavelength increases, the light is composed of photons that are less energetic. This can explain the observations concerning the polymerization rates.

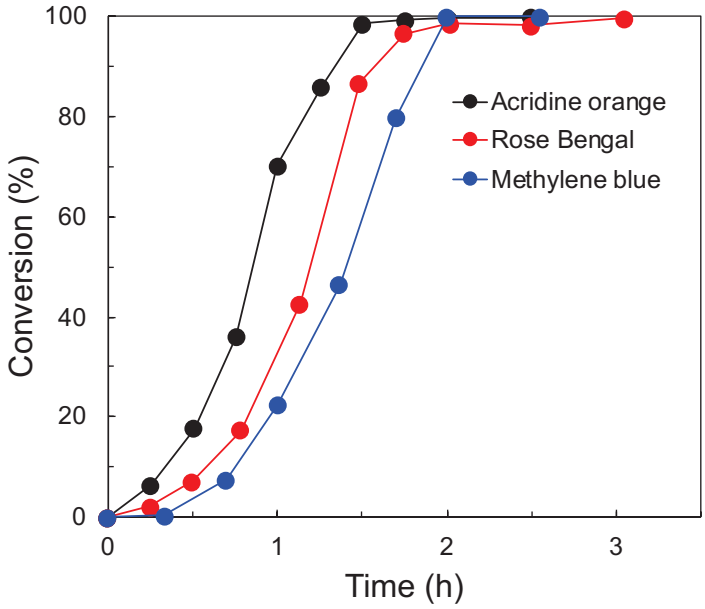

***Figure 46**. Conversion curves as a function of time for the emulsion polymerization of MMA by using different more water-soluble dyes. See Table 13 for more experimental details.*

Whatever the dye, the size of the PMMA particles is not particularly impacted (*ca.* 35 nm), and the size distributions remain very broad in all cases (Figure 47). This result differs from what was obtained in the case of styrene. Indeed, in the latter case, the size distributions were narrowed by replacing AO (**1**) by new more water-soluble dyes.

As mentioned above (in Part 2.III.A), we believe that the three-component PIS (*i.e.*, AO (**1**) /NHC-BH_3 (**3**) /disulfide (**4**)) generates radicals rather slowly leading to the continuous formation of new particles. This is even more significant with MMA, which is more soluble in water than styrene and all the more prone to homogeneous nucleation. Its k_p is also higher than that of styrene. All in all, it seems that for MMA, the reactions leading to particle nucleation in water are not really impacted between the 3 dyes tested. In each case, there is enough dye to

trigger the three-step cascade leading to initiation. We then believe that the broad size distributions might be attributed to the partition of NHC-BH_3 (**3**). This is why the synthesis of more water-soluble NHC-BH_3 was undertaken.

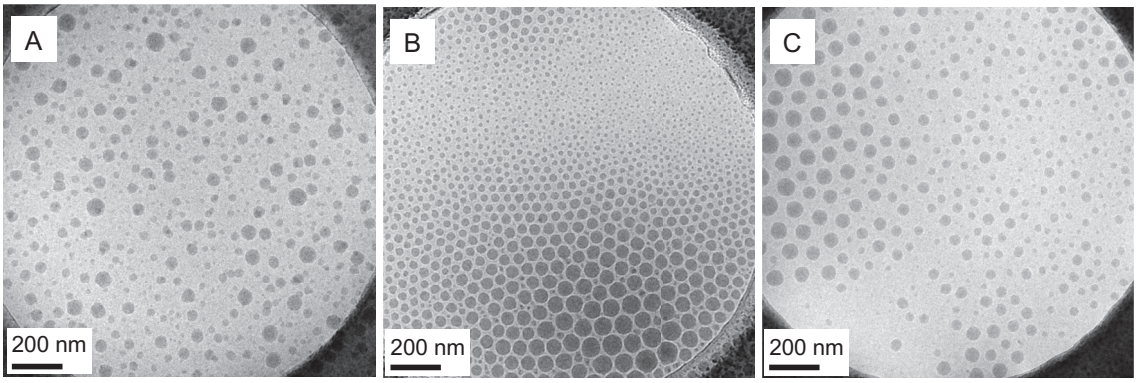

Figure 47*. Cryo-TEM images of PMMA latexes synthesized using several dyes. (A): Acridine orange, (B): Rose Bengal and (C): Methylene blue. See Table 13 for more experimental details.*

D. Synthesis of new co-initiator NHC-boranes

The second leverage to improve the efficiency of the PIS in water is to increase the water solubility of the NHC. Indeed, as demonstrated with the calculation of the partition coefficient, NHC-BH_3 (**3**) partitions between water and the monomer phase. The aim of this study was to prepare functionalized NHC-boranes in order to make them more water-soluble without altering their reactivity (the BH_3 group).

1. Sulfonated-functionalized NHC-boranes

For this purpose, we first identified sulfonate groups as a handle to improve NHC-borane water solubility. There are several examples in the literature supporting this choice. For instance, *m*-trisulfonated triphenylphosphine is highly soluble in water (1.100 g L^{-1} at 25 °C)[67] while triphenylphosphine is insoluble. Moreover, metal-based complexes that contains a sulfonate NHC ligand were recently developed in order to perform catalytic reactions in aqueous solution.[68,69]

We thus report in this section the syntheses of novel sulfonated NHC-boranes shown in Figure 48. We considered both 1-methylimidazole (**10**) and 1-methyl-1,2,4-triazole (**14**) structures as starting compounds to prepare two sulfonated-functionalized NHC-BH_3 (imidazole and triazole derivatives). The reaction scheme comprises two steps. First, imidazolium and triazolium

sulfonate zwitterions (**12**) and (**15**) were obtained by *N*-alkylation of (**10**) and (**14**) with propanesultone (**11**) in dichloromethane. In both cases, the first step led to pure products (**13**) and (**16**) with excellent yields (100%).

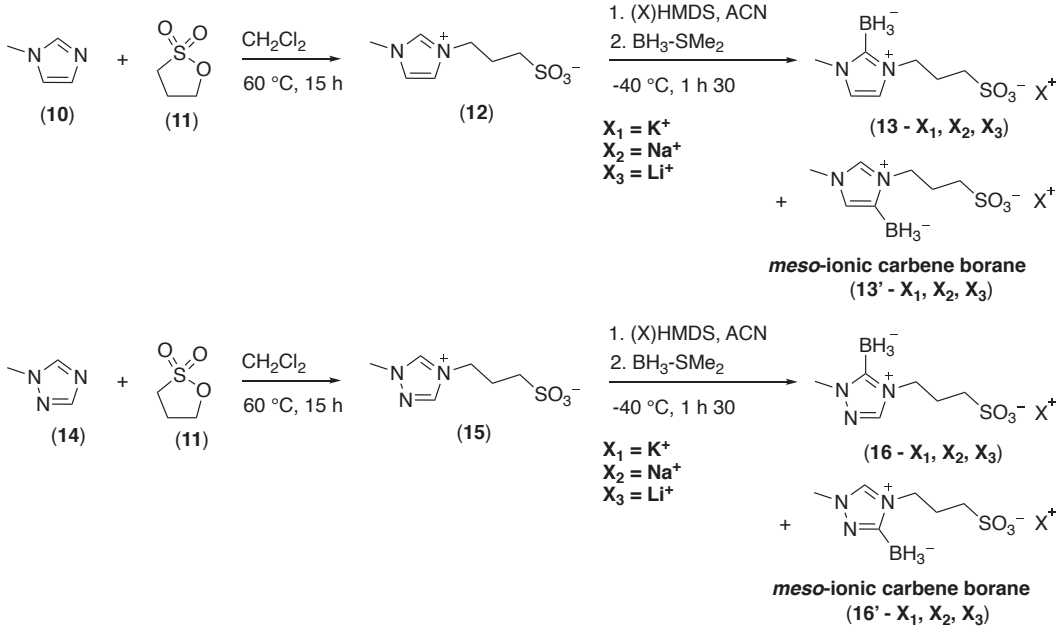

Figure 48. *Synthesis of sulfonated-functionalized NHC-boranes.*

Then, carbenes were formed by adding a strong base, potassium hexamethyldisilazide (KHMDS) and borane-dimethylsulfide was subsequently added. We obtained raw products (**13, – X_1 = K^+**) and (**16, – X_1 = K^+**) with good yields (90% and 70%, respectively). The obtention of the sulfonated NHC-boranes was confirmed by ^{11}B NMR characterization (δ = -36.9 (q) and -37.2 (q) ppm for (**13 – X_1 = K^+**) and (**16 – X_1 = K^+**), respectively – see Figure 49). However, the ^{1}H (see Chapter 5) and ^{11}B NMR spectra showed the formation of the *meso*-ionic carbene borane (MIC-BH_3) (see Figure 49), for both imidazole and triazole borane derivatives (**13'** and **16' – X_1 = K^+**). We believe that the presence of the sulfonate group had a strong impact on the reaction between the carbene and BH_3 due to the negative charge. It is possible that some flexibility of the chain –(CH_2-CH_2-CH_2-SO_3^-) may favor one reaction site over another. Note that by using BH_3-SMe_2 in excess, the imidazole and triazole NHC-BH_3 derivatives (**13** and **16 – X_1 = K^+**) were obtained without any trace of MIC-BH_3.

We then used other strong bases with different counterions (NaHMDS and LiHMDS) but with almost the same pK_a ≈ 26. The aim was to form the carbene corresponding to the NHC-BH_3 structure. By using LiHMDS, the MIC-BH_3 structure was only obtained. Some residues of borohydride were also observed. In the case of NaHMDS, imidazole borane derivative **(13 – X_2 = Na^+**) was predominant compared to MIC-NH_3 (**13' – X_2 = Na^+**), whereas both structures

were obtained for triazole borane derivative (**16, 16' – X_2 = Na^+**) with some residues of borohydride. The NHC-BH_3 structure was not exclusively formed. However, it was impossible to purify all the crude products. Therefore, after several unsuccessful purification attempts such as flash chromatography, evaporation or recrystallization, we decided to use the crude products.

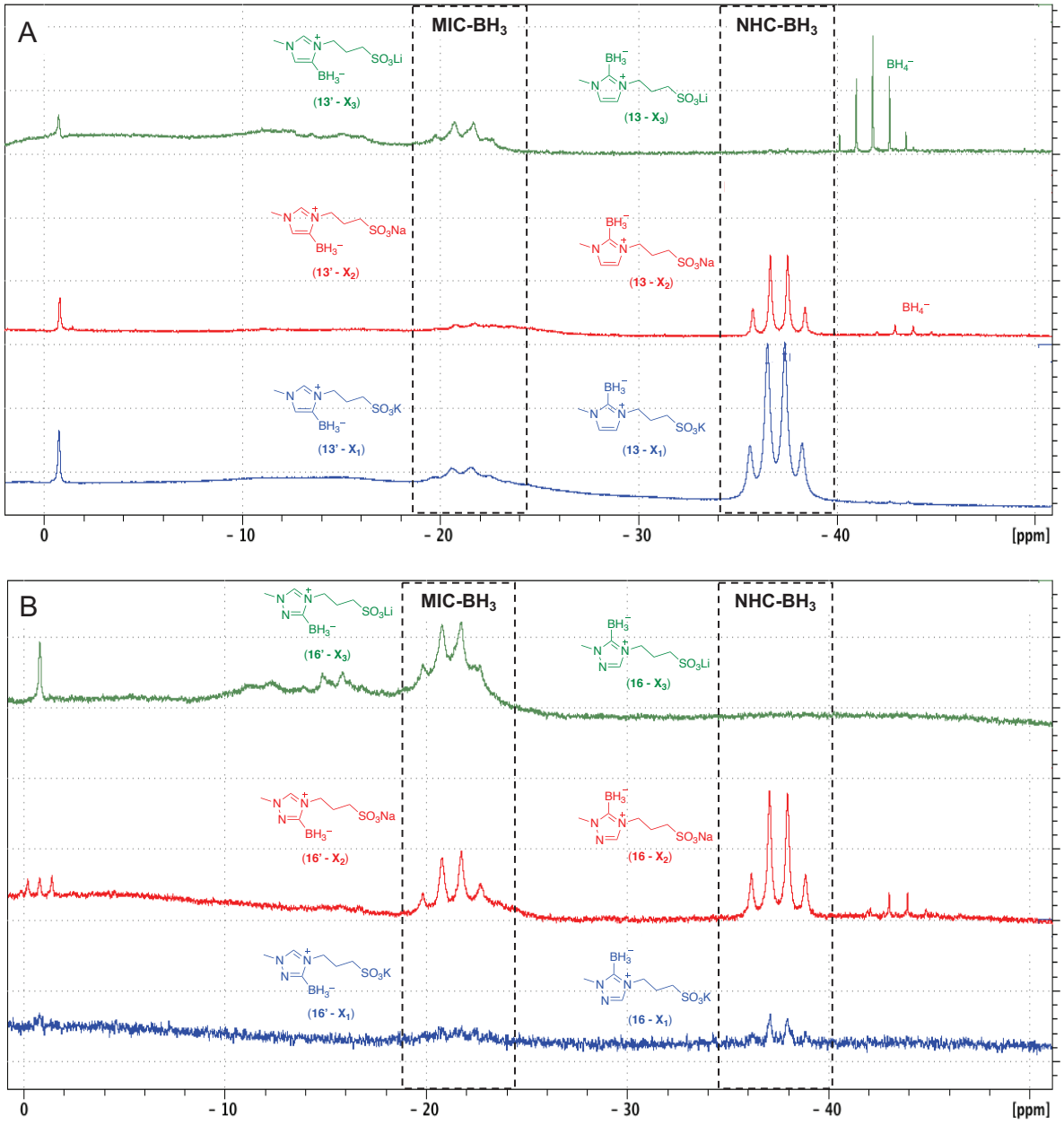

***Figure 49**. [11]B NMR spectra of (A) compounds **13 – X_1, X_2 and X_3** and (B) compounds **16 – X_1, X_2 and X_3**, with **X_1 = K^+**, **X_2 = Na^+** and **X_3 = Li^+**.*

By using the new NHC-BH_3 as crude products (*i.e.*, **13, 13' – X_1 = K^+, 16 – X_1 = K^+** and **16' – X_3 = Li^+**), the emulsion photopolymerization of styrene did not work. The impurities present in the samples may have quenched free radicals. In addition, the ineffectiveness of the crude sulfonated NHC-BH_3 to initiate the polymerization may be probably due to the presence of the

MIC-BH_3 structure. According to Crudden and co-workers, MIC-BH_3 have greater hydricity of the B–H bond (which is defined as its propensity to transfer a hydrogen atom along with an electron) than NHC-BH_3 and could lead to side reactions.[70] Indeed, it was reported that the X–H bond cleavage could enable the reduction of various unsaturated substrates such as carbonyl compounds or aromatics.[71]

On the contrary, the use of unpurified sulfonated NHC- and/or MIC-BH_3 produced stable PMMA latexes. Three crude products were used (**13, 13' – X_1 = K^+, 16 – X_1 = K^+** and **16' – X_3 = Li^+**) with AO (**1**) and disulfide (**4**) under similar concentrations as for the reference conditions. The solids content was fixed at 20 wt.% and the SDS concentration was fixed at 2 CMC. All the results are reported in Table 14.

***Table 14**. Emulsion photopolymerization of MMA with sulfonate-functionalized boron-based co-initiators under visible irradiation at 20 wt.% solids content and 2 CMC.[a]*

Boron compound	Time (h)	Conv. (%)	D_h[b] (nm)	PDI[b]	D_n[c] (nm)	D_w/D_n[c]	N_p (x10^{17} cm^{-3})
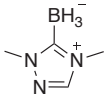 (**3**)	1.75	100	66	0.09	35	1.41	7.5
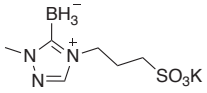 (**16 - X_1 = K^+**)	2.1	100	65	0.08	40	1.25	5.1
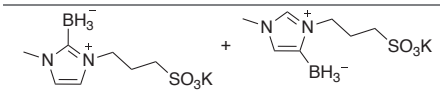 (**13 - X_1 = K^+**) (**13' - X_1 = K^+**)	2.1	100	65	0.11	43	1.29	4.1
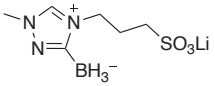 (**16' - X_3 = Li^+**)	2.1	100	68	0.6	37	1.47	6.5

[a] Experimental conditions: the solids content was fixed at 20 wt.% and the SDS concentration at 2 CMC. [AO] = 1 x 10^{-2} mmol L^{-1} (1 mol.% based on NHC-BH_3), [disulfide] = 0.5 mmol L^{-1} (50 mol.% based on NHC-BH_3) and [NHC-BH_3] = 1 mmol L^{-1}.
[b] Determined by DLS.
[c] Determined by TEM.

The polymerization rates obtained with the sulfonated NHC- and/or MIC-BH_3 were faster than with the NHC-BH_3 (**3**) (Figure 50). However, it is difficult to draw conclusions since D. Subervie showed that the PIS composed of disulfide (**4**) alone led to a faster photopolymerization of MMA (orange curve) than the full PIS, and in the present study, we cannot discriminated which of the co-initiators, disulfide (**4**) or sulfonated NHC-BH_3, started the polymerization of MMA.

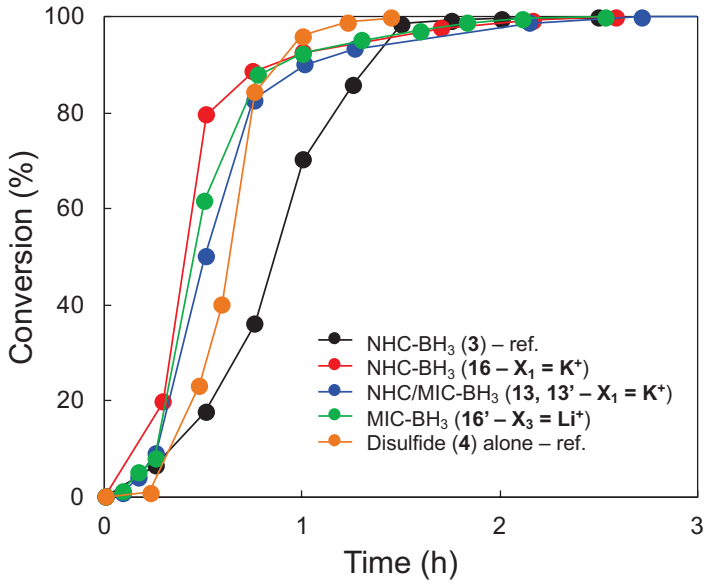

***Figure 50**. Conversion curves as a function of time for 3 sulfonated functionalized boron-based co-initiators used with AO (**1**) and disulfide (**4**) to photoinitiate the emulsion polymerization of MMA.*

The particle sizes with each sulfonated NHC-BH_3 were about 40 nm, similar to the size obtained with the NHC-BH_3 (**3**), but the size distribution was narrowed when **13, 13' – X_1 = K^+** and **16 – X_1 = K^+** was used (D_w/D_n = 1.25 and 1.29, respectively). However, the size distribution remained broad compared to what is obtained in conventional emulsion (*i.e.*, using a thermal initiator) carried out above CMC. We believe that the presence of sulfonate group in NHC- and/or MIC-BH_3 could have contributed to the stabilization of the particles even if it did not react with the thiyl radicals generated beforehand, resulting in a narrower size distribution. Nevertheless, D. Subervie obtained a narrower size distribution (D_w/D_n = 1.15) and particle size of 70 nm when disulfide (**4**) was used alone as photoinitiator for the emulsion polymerization of MMA

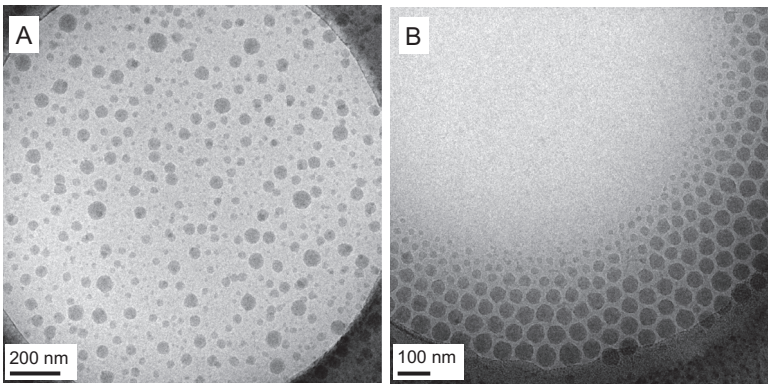

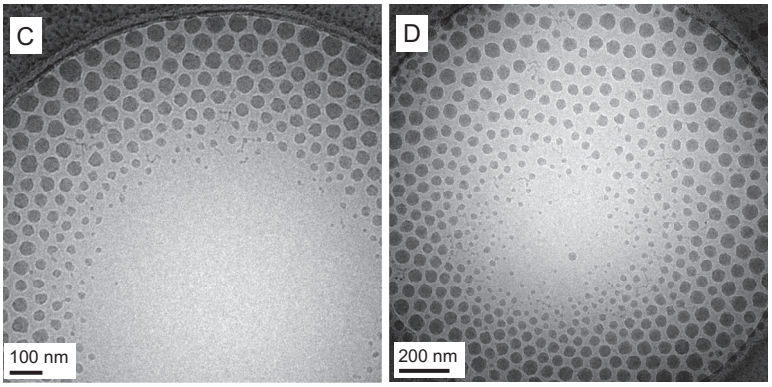

***Figure 51**. Cryo-TEM images of the PMMA latexes prepared with (A) NHC-BH₃ (**3**), (B) sulfonated NHC-BH₃ (**16 – X₁ = K⁺**), (C) sulfonated NHC/MIC-BH₃ (**13, 13' – X₁ = K⁺**) and (D) sulfonated MIC-BH₃ (**16' – X₃ = Li⁺**).*

To sum up, although promising, the use of sulfonated-functionalized NHC-BH₃ did not allow the synthesis of PMMA latexes with narrow size distribution. In addition, styrene polymerization was not even possible. Combined with the issues encountered with the synthesis of the NHC-BH₃ compounds, we thus changed our strategy.

2. Amino-functionalized NHC-borane

Still with the aim of increasing the water solubility of the NHC-BH₃ specie, a new compound functionalized with an amino group was synthesized (Figure 52). Its synthesis involves four steps (a more detail description of the procedure and characterizations is given in Chapter 5), and we obtained a pure NH_2-functionalized NHC-BH₃ (**21**) with a yield of 10%. The protection of the amino group was necessary to avoid side reactions between the hydrogen atoms from the amino group and the strong base KHMDS, and BH_3-SMe_2.

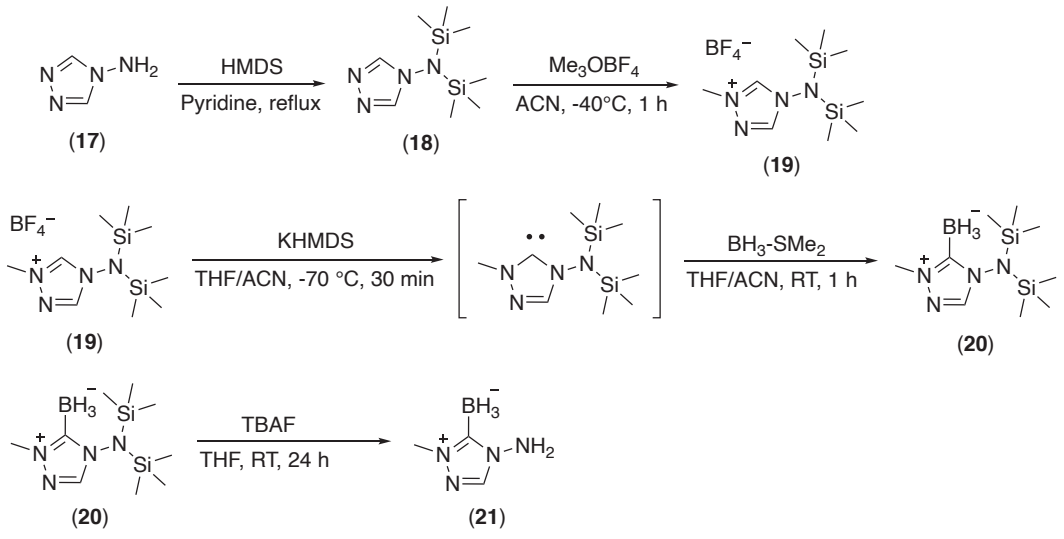

Figure 52. *reaction scheme for the synthesis of the amino-functionalized NHC-borane.*

We assumed that this amino-functionalized NHC-BH_3 (**21**) could be more soluble than the dimethyl-triazolylidene borane (**3**) because of the amino substituent that is more hydrophilic than the methyl group (the amino groups can form hydrogen bonds with water). This NH_2-functionalized NHC-BH_3 (**21**) was used for the polymerization of styrene at a fixed solids content (20 wt.%) and a SDS concentration of 2 CMC in the presence of AO (**1**) and disulfide (**4**). The results are reported in Table 15.

Table 15*. Emulsion photopolymerization of styrene with NHC-BH_3 (**3**) (reference) and (**21**) (amino-functionalized) under visible irradiation at 20 wt.% solids content and 2 CMC.*[a]

Boron compound	**Time (h)**	**Conv. (%)**	D_h[b] **(nm)**	**PDI**[b]	D_n[c] **(nm)**	D_w/D_n[c]	N_p **(x10^{16} cm^{-3})**
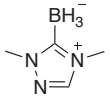 (**3**)	2.6	100	110	0.024	68	1.35	11.4
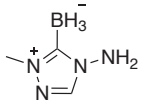 (**21**)	3	100	99	0.04	83	1.09	6.3

[a] Experimental conditions: the solids content was fixed at 20 wt.% and the SDS concentration at 2 CMC. [AO] = 1 x 10^{-2} mmol L^{-1} (1 mol.% based on (amino-functionalized) NHC-BH_3), [disulfide] = 0.5 mmol L^{-1} (50 mol.% based on (amino-functionalized) NHC-BH_3) and [(amino-functionalized) NHC-BH_3] = 1 mmol L^{-1}.
[b] Determined by DLS.
[c] Determined by TEM.

A stable latex was obtained with complete monomer conversion after 3 h. The polymerization rate was very similar to the one obtained with the reference NHC-BH_3 (**3**) (Figure 53). The particles had a size of 84 nm *vs.* 68 nm for NHC-BH_3 (**3**). Interestingly, the use of this new amino-functionalized NHC-BH_3 (**21**) led to a significant decrease of size dispersity with D_w/D_n = 1.09 (vs. D_w/D_n = 1.35 for NHC-BH_3 (**3**)). This result, combined with those obtained when varying the dye nature, demonstrate that the key to narrow the PSD is to be able to work with a fully water soluble PIS. Indeed, the amino-functionalized NHC-BH_3 (**21**) is likely more soluble in water than NHC-BH_3 (**3**), resulting in a more efficient initiation stage in water.

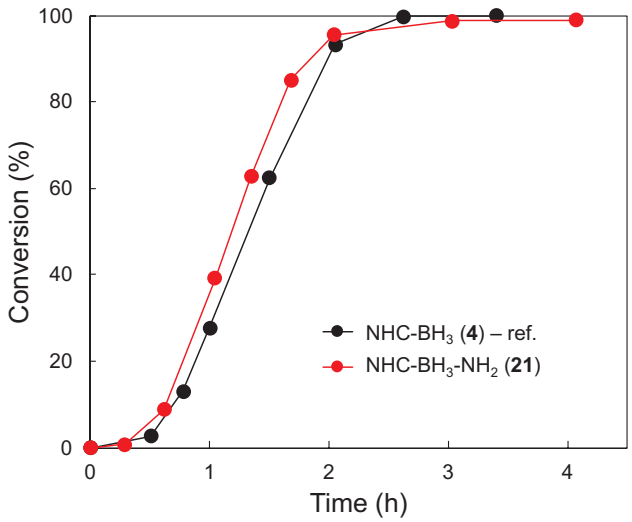

***Figure 53**. Conversion curves as a function of time for the amino-functionalized NHC-BH₃ (**21**) used with AO (**1**) and disulfide (**4**) to photoinitiate the emulsion polymerization of styrene in comparison with the reference NHC-borane (**3**).*

However, despite these encouraging results, the amount of amino-functionalized NHC-BH$_3$ (**21**) was not sufficient (very low yield obtained for the last step of synthesis 10%) to carry out an in-depth study with this new NHC-borane, and in particular to investigate its efficiency in MMA polymerization.

E. Summary

- ***Case of styrene***: We demonstrated that replacing AO (**1**), which is mostly located in the styrene phase, by new water-soluble dyes led to an important narrowing of the size distributions of the PS particles. Then, the NHC-BH$_3$ was functionalized with an amino group (**21**) and assuming that this specie was more soluble in water than the NHC-BH$_3$ (**3**), we carried out the emulsion photopolymerization of styrene with the PIS composed of AO (**1**), disulfide (**4**) and amino-modified NHC-BH$_3$ (**21**). Interestingly, the particle size distribution was narrowed, even with AO (**1**), suggesting that both the dye and the NHC-BH$_3$ independently have an influence of the particle size distributions.

- ***Case of MMA***: The use of the new more water-soluble dyes did not have an impact on the particle size distributions. This result was surprising since in the case of styrene we observed the opposite effect, behavior likely related to the higher water solubility and higher k_p value of MMA, as explained above. The amino-modified NHC-BH$_3$ (**21**) represents an interesting alternative that should be tested in the near future.

III. Reactor optimization: new color LED ribbon

The last parameter investigated in emulsion polymerization what the irradiation source. A LED ribbon selectively emitting three primary colors, blue, green and red was used instead of our white LED ribbon (400–800 nm). The aim was to optimize the absorption of the photons by the used dyes according to their maximum wavelength. Moreover, as we already discussed in the preamble (Chapter 1), the shift to higher wavelengths is one option to significantly decrease light scattering phenomena.

The emission spectra corresponding to the three colors were measured by the group of Jacques Lalevée in Mulhouse (Figure 54) and showed that the LEDs only irradiate in the visible region with different surface power densities. It is important to note that for the same LED ribbon, the light intensity of the three different colors is lower than the white light coming from the combination of blue, green and red (*i.e.*, 20 mW cm^{-2} for blue light vs. 26 mW cm^{-2} for white light).

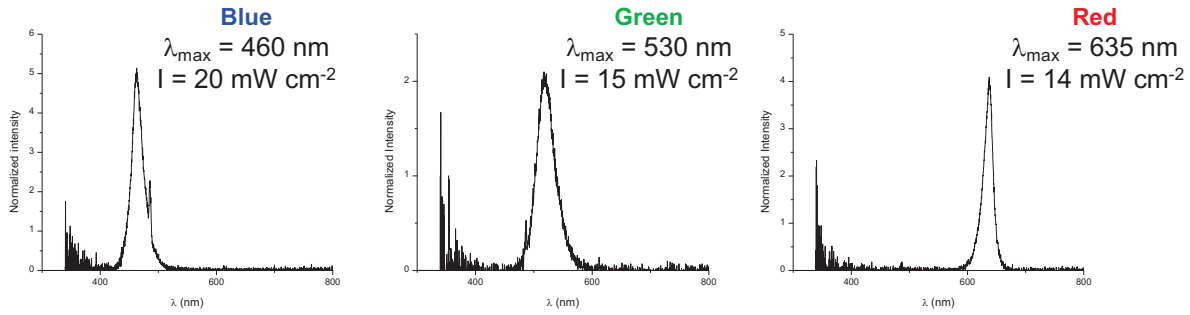

Figure 54. *Characteristic emission spectra of the new color LED ribbon.*

First, we used the disulfide (**4**) alone as a type I photoinitiator for the emulsion polymerization of MMA at 2 CMC of SDS with a solids content of 20 wt.%. As previously mentioned, the disulfide (**4**) alone is capable of photoinitiating the polymerization of MMA in emulsion under white light due to the short absorption of disulfide (**4**) in the higher-energy visible region. The objective was to show that at a higher wavelength, the S–S bond homolytic cleavage of disulfide (**4**) does not occur. For this purpose, we carried out three PMMA latex syntheses under white, blue and green light irradiations, respectively (Figure 55). As expected, the polymerization under green light irradiation did not proceed. On the other hand, the use of the blue LED induced a decrease of the polymerization rate compared with the experiment performed under white light irradiation. This delay may be attributed to a lower radiant flux received by the surface (I

= 20 mW cm^{-2} vs. I = 26 mW cm^{-2} for blue and white light, respectively) that would reduce the generation of thiyl radicals (which is already not very favored).

We next carried out the emulsion photopolymerization of MMA with the three-component PIS in the same conditions (*i.e.,* with the green, blue and white lights, see Figure 55) and we also observed a slight delay in the polymerization when the reaction mixture was irradiated with the blue light in comparison with the white light (92% final conversion after 4.6 h vs. 100% conversion after 3 h for the white light). Under green light irradiation, AO (**1**) has a residual absorption (Figure 43) and photo-reduces the disulfide to generate thiyl radicals. However, the monomer conversion was limited, reaching only 25% after 7.5 h, reflecting the overall inefficiency of the photoinitiation.

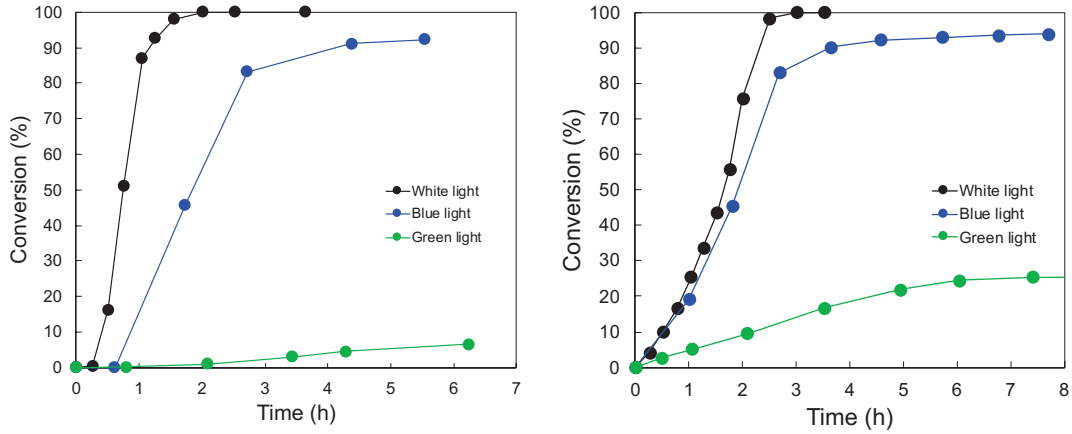

Figure 55. *Conversion profiles of the emulsion photopolymerization of MMA photoinitiated by (left) the disulfide compound only and (right) the three-component system under white, blue and green light irradiations.*

Finally, we attempted to prepare PMMA latexes in emulsion under green light irradiation replacing AO (**1**) by another dye, eosin Y, in the three-component PIS (eosin Y: λ_{max} = 515 nm, ε_{max} = 40 725 L mol^{-1} cm^{-1}). This preliminary study seems very promising since we obtained stable latexes with 70% conversion after 6 h.

General conclusions

We have shown that NHC-boranes are efficient co-initiators for the emulsion photopolymerization of different monomers under visible light irradiation. F. Le Quéméner and D. Subervie have studied two PISs, namely the three-component AO/disulfide (**4**)/NHC-BH_3 (**3**) system which is efficient whatever the monomer composition, and the disulfide (**4**) as type I photoinitiator, able to efficiently initiate the polymerization of various (meth)acrylates, notably MMA or MMA-rich mixtures, but not that of styrene. Both PISs led to highly stable latexes with complete monomer conversions.

The previous theses provided some understanding of the nucleation mechanisms. The authors pointed out a recurrent issue during their work. Especially when the three-component PIS was used to initiate the emulsion polymerization of styrene or MMA, F. Le Quéméner and D. Subervie obtained broad particle size distributions (only above the CMC with styrene and regardless of SDS concentration with MMA), a main difference with the size distributions obtained in analogue systems thermally initiated. The authors argued that it was due to the slow and continuous generation of radicals during the photopolymerizations.

In this work, we found that the different components of the PIS partitioned between the water and monomer phases. For example, the partition coefficients of AO showed that it was mainly located in the styrene or MMA phase. Nevertheless, in conventional emulsion polymerization, the initiation step proceeds in the aqueous phase. The partitioning between the different phases (*i.e.,* water, monomer droplets and monomer-swollen micelles, if present) of the components of the PIS could be at the origin of the production of particles with a broad size distribution. We have thus selected water-soluble dyes and tested them in the emulsion photopolymerization of styrene and MMA. In the case of styrene, narrower size distributions were obtained with the new dyes compared to AO, demonstrating the important role of the dye during the initiation step. However, the size distributions were still broad with MMA. Indeed, MMA is more soluble in water than styrene and its k_p is also higher too. Therefore, the reactions leading to particle nucleation in water are not really impacted by the solubility of the dyes. We have then played with the solubility of another compound of the PIS, by investigating the synthesis of more water-soluble NHC-boranes, especially an amino-functionalized NHC-BH_3. This co-initiator led to a stable PS latex with a very significant improvement of the size dispersity. This positive outcome now needs to be transposed to MMA polymerization.

Finally, we have investigated a color LED ribbon in order to enhance the absorption of photons by the dye according to its absorption maximum wavelength. The first results with Eosin Y seem very promising. Further study on the amino-modified NHC-BH_3 would then be needed to confirm our hypothesis on the solubility effect on the size distributions.

References

[1] W. D. Harkins, *J. Chem. Phys.* **1945**, *13*, 381–382.
[2] W. D. Harkins, *J. Chem. Phys.* **1946**, *14*, 47–48.
[3] W. D. Harkins, *J. Am. Chem. Soc.* **1947**, *69*, 1428–1444.
[4] W. V. Smith, R. H. Ewart, *J. Chem. Phys.* **1948**, *16*, 592–599.
[5] W. V. Smith, *J. Am. Chem. Soc.* **1949**, *71*, 4077–4082.
[6] E. Trommsdorff, H. Kohle, P. Lagally, *Makromol. Chem.* **1948**, *1*, 169–198.
[7] C. P. Roe, *Ind. Eng. Chem.* **1968**, *60*.
[8] R. M. Fitch, C. H. Tsai, in *Polym. Colloids* (Ed.: R.M. Fitch), Springer US, Boston, MA, **1971**, pp. 73–102.
[9] S. C. Thickett, R. G. Gilbert, *Polymer* **2007**, *48*, 6965–6991.
[10] P. J. Feeney, D. H. Napper, R. G. Gilbert, *Macromolecules* **1984**, *17*, 2520–2529.
[11] J.-P. Fouassier, J. Lalevée, *Photoinitiators for Polymer Synthesis: Scope, Reactivity, and Efficiency*, John Wiley & Sons, **2012**.
[12] M. Takeishi, H. Yoshida, S. Niino, S. Hayama, *Makromol. Chem.* **1978**, *179*, 1387–1391.
[13] N. J. Turro, M.-F. Chow, C.-J. Chung, G. C. Weed, B. Kraeutler, *J. Am. Chem. Soc.* **1980**, *102*, 4843–4845.
[14] N. J. Turro, M.-F. Chow, C.-J. Chung, C.-H. Tung, *J. Am. Chem. Soc.* **1980**, *102*, 7391–7393.
[15] N. J. Turro, M. F. Chow, C. J. Chung, C. H. Tung, *J. Am. Chem. Soc.* **1983**, *105*, 1572–1577.
[16] A. L. Buchachenko, *Russ. Chem. Rev.* **1976**, *45*, 375.
[17] N. J. Turro, I. F. Pierola, C.-J. Chung, *J. Polym. Sci. Polym. Chem. Ed.* **1983**, *21*, 1085–1096.
[18] T. Yamamoto, S. Seki, R. Fukae, O. Sangen, M. Kamachi, *Polym. J.* **1990**, *22*, 567–571.
[19] S. Mah, D. Koo, H. Jeon, S. Kwon, *J. Appl. Polym. Sci.* **2002**, *84*, 2425–2431.
[20] S. Mah, D. Lee, D. Koo, S. Kwon, *J. Appl. Polym. Sci.* **2002**, *86*, 2153–2158.
[21] J. Kwak, P. Lacroix-Desmazes, J. J. Robin, B. Boutevin, N. Torres, *Polymer* **2003**, *44*, 5119–5130.
[22] J. F. Quinn, L. Barner, C. Barner-Kowollik, E. Rizzardo, T. P. Davis, *Macromolecules* **2002**, *35*, 7620–7627.
[23] S. E. Shim, Y. Shin, J. W. Jun, K. Lee, H. Jung, S. Choe, *Macromolecules* **2003**, *36*, 7994–8000.
[24] X. Hu, J. Zhang, W. Yang, *Polymer* **2009**, *50*, 141–147.
[25] H. Zhang, L. Zang, J. Luo, J. Guo, *E-Polym.* **2012**, *12*, DOI 10.1515/epoly.2012.12.1.376.
[26] K. Krüger, K. Tauer, Y. Yagci, N. Moszner, *Macromolecules* **2011**, *44*, 9539–9549.
[27] E. D. Günersel, Y. Hepuzer, Y. Yağcı, *Angew. Makromol. Chem.* **1999**, *264*, 88–91.
[28] P. Laurino, H. F. Hernandez, J. Bräuer, K. Krüger, H. Grützmacher, K. Tauer, P. H. Seeberger, *Macromol. Rapid Commun.* **2012**, *33*, 1770–1774.
[29] H. Staudinger, *Berichte Dtsch. Chem. Ges. B Ser.* **1920**, *53*, 1073–1085.
[30] C. H. Bamford, M. J. S. Dewar, A. H. Wilson, *Proc. R. Soc. Lond. Ser. Math. Phys. Sci.* **1948**, *192*, 309–328.
[31] B. H. Zimm, J. K. Bragg, *J. Polym. Sci.* **1952**, *9*, 476–478.
[32] K. E. Russell, A. V. Tobolsky, *J. Am. Chem. Soc.* **1954**, *76*, 395–399.
[33] H. K. Hall, A. Buyle. Padias, Ashish. Pandya, Hitoshi. Tanaka, *Macromolecules* **1987**, *20*, 247–254.

[34] T. Li, T. J. Willis, A. B. Padias, H. K. Hall, *Macromolecules* **1991**, *24*, 2485–2487.
[35] V. Percec, H.-J. Kim, B. Barboiu, *Macromolecules* **1997**, *30*, 6702–6705.
[36] S. K. Ghosh, B. M. Mandal, *Polymer* **1993**, *34*, 4287–4290.
[37] L. Liu, W. Yang, *J. Polym. Sci. Part Polym. Chem.* **2004**, *42*, 846–852.
[38] M. Ratanajanchai, D. Tanwilai, P. Sunintaboon, *J. Colloid Interface Sci.* **2013**, *409*, 25–31.
[39] G. Müller, M. Zalibera, G. Gescheidt, A. Rosenthal, G. Santiso-Quinones, K. Dietliker, H. Grützmacher, *Macromol. Rapid Commun.* **2015**, *36*, 553–557.
[40] K. Shen, Y. Jiang, Z. Liu, D. Qi, H. Wang, Y. Li, *Macromol. Chem. Phys.* **2015**, *216*, 1990–1996.
[41] W. Fan, M. Tosaka, S. Yamago, M. F. Cunningham, *Angew. Chem. Int. Ed.* **2018**, *57*, 962–966.
[42] Y. Nakamura, Y. Kitada, Y. Kobayashi, B. Ray, S. Yamago, *Macromolecules* **2011**, *44*, 8388–8397.
[43] X. Su, Y. Jiang, P. G. Jessop, M. F. Cunningham, Y. Feng, *Macromolecules* **2020**, *53*, 6018–6023.
[44] S. Telitel, S. Schweizer, F. Morlet-Savary, B. Graff, T. Tschamber, N. Blanchard, J. P. Fouassier, M. Lelli, E. Lacôte, J. Lalevée, *Macromolecules* **2013**, *46*, 43–48.
[45] F. Le Quéméner, Utilisation de NHC-Boranes pour la synthèse de nanoparticules et l'amorçage de photopolymérisation en émulsion, phdthesis, Université de Lyon, **2016**.
[46] D. Subervie, NHC-Boranes : amorceurs de photopolymérisation en émulsion et nouveaux matériaux énergétiques, phdthesis, Université de Lyon, **2018**.
[47] F. Le Quéméner, D. Subervie, F. Morlet-Savary, J. Lalevée, M. Lansalot, E. Bourgeat-Lami, E. Lacôte, *Angew. Chem. Int. Ed.* **2018**, *57*, 957–961.
[48] M.-A. Tehfe, M. Makhlouf Brahmi, J.-P. Fouassier, D. P. Curran, M. Malacria, L. Fensterbank, E. Lacôte, J. Lalevée, *Macromolecules* **2010**, *43*, 2261–2267.
[49] M.-A. Tehfe, J. Monot, M. Makhlouf Brahmi, H. Bonin-Dubarle, D. P. Curran, M. Malacria, L. Fensterbank, E. Lacôte, J. Lalevée, J.-P. Fouassier, *Polym. Chem.* **2011**, *2*, 625–631.
[50] D. E. Fast, A. Lauer, J. P. Menzel, A.-M. Kelterer, G. Gescheidt, C. Barner-Kowollik, *Macromolecules* **2017**, *50*, 1815–1823.
[51] O. Ito, *Res. Chem. Intermed.* **1995**, *21*, 69–93.
[52] M. J. Ballard, D. H. Napper, R. G. Gilbert, *J. Polym. Sci. Polym. Chem. Ed.* **1984**, *22*, 3225–3253.
[53] W. H. Lane, *Ind. Eng. Chem. Anal. Ed.* **1946**, *18*, 295–296.
[54] J. Lalevée, S. Telitel, M. A. Tehfe, J. P. Fouassier, D. P. Curran, E. Lacôte, *Angew. Chem. Int. Ed.* **2012**, *51*, 5958–5961.
[55] O. Ito, M. Matsuda, *J. Am. Chem. Soc.* **1979**, *101*, 1815–1819.
[56] L. F. Halnan, D. H. Napper, R. G. Gilbert, *J. Chem. Soc. Faraday Trans. 1 Phys. Chem. Condens. Phases* **1984**, *80*, 2851–2865.
[57] G. H. J. van Doremaele, F. H. J. M. Geerts, L. J. aan de Meulen, A. L. German, *Polymer* **1992**, *33*, 1512–1518.
[58] I. Capek, J. Barton, E. Ordinova, *Chem Zvesti* **1984**, *38*, 803–882.
[59] R. H. Ottewill, R. Satgurunathan, *Colloid Polym. Sci.* **1987**, *265*, 845–853.
[60] R. Brown, B. Stützel, T. Sauer, *Macromol. Chem. Phys.* **1995**, *196*, 2047–2064.
[61] A. M. dos Santos, J. Pohn, M. Lansalot, F. D'Agosto, *Macromol. Rapid Commun.* **2007**, *28*, 1325–1332.
[62] L. Delafresnaye, P.-Y. Dugas, P.-E. Dufils, I. Chaduc, J. Vinas, M. Lansalot, E. Bourgeat-Lami, *Polym. Chem.* **2017**, *8*, 6217–6232.

[63] I. Martín-Fabiani, J. Lesage de la Haye, M. Schulz, Y. Liu, M. Lee, B. Duffy, F. D'Agosto, M. Lansalot, J. L. Keddie, *ACS Appl. Mater. Interfaces* **2018**, *10*, 11221–11232.
[64] K. Ito, K. Tanaka, H. Tanaka, G. Imai, S. Kawaguchi, S. Itsuno, *Macromolecules* **1991**, *24*, 2348–2354.
[65] K. Ito, H. Tsuchida, A. Hayashi, T. Kitano, E. Yamada, T. Matsumoto, *Polym. J.* **1985**, *17*, 827–839.
[66] A. Andrés, M. Rosés, C. Ràfols, E. Bosch, S. Espinosa, V. Segarra, J. M. Huerta, *Eur. J. Pharm. Sci.* **2015**, *76*, 181–191.
[67] V. Michelet, M. Savignac, J.-P. Genêt, in *Encycl. Reag. Org. Synth.*, American Cancer Society, **2004**.
[68] A. Almássy, C. E. Nagy, A. C. Bényei, F. Joó, *Organometallics* **2010**, *29*, 2484–2490.
[69] S. Roy, H. Plenio, *Adv. Synth. Catal.* **2010**, *352*, 1014–1022.
[70] L. B. de Oliveira Freitas, P. Eisenberger, C. M. Crudden, *Organometallics* **2013**, *32*, 6635–6638.
[71] J. Zhang, J.-D. Yang, J.-P. Cheng, *Natl. Sci. Rev.* **n.d.**, DOI 10.1093/nsr/nwaa253.

Chapter 3.

Visible light-induced dispersion polymerization of styrene performed in hydroalcoholic medium

Table of Content

PART 1. STATE-OF-THE-ART 109

I. HISTORICAL CONTEXT 109

II. FORMATION OF PARTICLES BY DISPERSION POLYMERIZATION 110

A. Structure of stabilizer in polar media 112
1. Graft copolymers 112
2. Block copolymers 114
a. Macroinitiators 114
b. Macromolecular chain transfer agents (macro-CTAs) 116
B. Mechanism of particle formation in dispersion polymerization 118
A. Solubility parameters 120
B. Influence of the stabilizer 124
C. Effect of initiator 126
D. Effect of the temperature 129

IV. KINETICS OF DISPERSION POLYMERIZATION 131

A. First theoretical model of dispersion polymerization 131
B. The overall rate of dispersion polymerization 132
C. Determination of the polymerization locus 134
D. Reactivity of macromonomers in copolymerization 136

V. PHOTO-INDUCED DISPERSION POLYMERIZATION: FROM FREE RADICAL PHOTOPOLYMERIZATION TO PHOTO-PISA 138

A. Free radical polymerization in photo-dispersion 139
B. Reversible-deactivation radical polymerization in photo-dispersion 141
C. Polymerization-induced self-assembly in photo-dispersion 144

PART 2. OUR THREE-COMPONENT PHOTOINITIATING SYSTEM APPLIED TO DISPERSION POLYMERIZATION 149

I. DISPERSION PHOTOPOLYMERIZATION OF STYRENE WITH PEGMA 150

A. Transposition from emulsion to dispersion: robustness of our photoinitiating system 150
B. Effect of the photoinitiator concentration 153
C. Effect of stabilizer concentration 156
D. Disulfide vs. three-component photoinitiation system 159
E. Particle size vs. light penetration: reproducibility issue? 162
F. Influence of an organic base 164
1. Effect of TBAH concentration 165
2. Effect of stabilizer concentration in presence of TBAH 169
3. Disulfide as type I photoinitiator in the presence of TBAH 172
G. Conclusions 174

II. DISPERSION PHOTOPOLYMERIZATION OF STYRENE WITH PVP 175

A. Robustness of our photoinitiating system 175
B. Effect of temperature 178
C. Effect of the PVP concentration 181
D. Conclusions 182

GENERAL CONCLUSIONS 183

REFERENCES 185

Despite the successful synthesis of various kinds of latexes by emulsion polymerization (Chapter 2), the upper range of accessible sizes is so far limited to ca. 300 nm. With the aim of preparing larger particles, we focus in this chapter on the preparation of polystyrene latexes through dispersion polymerization using our NHC-based photo-initiating system. Indeed, dispersion polymerization stands out by its capacity to achieve a broad range of particle size (from few hundreds of nm to a few micrometers). In addition, the reaction medium is initially homogeneous, which could help to push the boundaries of light penetration issues.

This chapter is organized in two distinct sections. First, the principle of dispersion polymerization and the influence of key factors on particle size will be discussed as well as the studies that report photoinduced dispersion polymerizations. The second part will focus on the use of our PIS for the preparation of polystyrene latexes through dispersion polymerization by studying the effect of several parameters such as the stabilizer type and concentration, the PIS concentration and its composition and the presence of additives (*i.e.*, an organic base).

Part 1. State-of-the-art

I. Historical context

Dispersion polymerization was developed for the first time in the 1960s by Osmond *et al*.[1] from ICI company for painting applications. Indeed, the preparation of resins in solution was limited by the viscosity increase related to the polymer concentration and molecular weight. The emulsion polymerization process offered an interesting alternative since polymers with high molecular weight and low viscosities could be obtained with a faster polymerization rate compared to solution polymerization. However, despite the green-friendly aspect of water used in emulsion, the latter comes with many disadvantages for painting applications (the use of emulsifiers which deteriorate the film properties, the high latent heat of evaporation of water and the freezing point of water at 0 °C for storage). Therefore, organic continuous medium (hydrocarbon) and acrylic/vinylic monomers were extensively studied and dispersed particles with diameters ranging from 100 nm to 20 µm with a very narrow size distribution were reported.[2] After the first work of ICI, a number of patents were filed on hydrocarbon/acrylic monomer systems that indicated the strong interest that companies had in the perspective of using this technique to make latexes in large amounts. But new environmental issues emerged, notably the limitations on emissions of volatile organic compounds.

Later, in the 1980s, dispersion polymerization was extended to (hydro)alcoholic continuous media to produce monodisperse polystyrene (PS)[3] and poly(methyl methacrylate) (PMMA)[4,5] latexes, by using steric stabilizers such as polyvinylpyrrolidone (PVP)[6,7], polyacrylic acid (PAA)[8,9], poly(2-ethyl-2-oxazoline) (PEOX)[10] or hydroxypropyl cellulose (HPC). The applications flowing from the use of (hydro)alcoholic media involve toner, seed particles to calibration, biomedical diagnostic supports and coatings. El-Aasser, Paine and Ober have contributed to some understanding of the mechanisms involved in particle nucleation and growth, as well as the influence of several parameters on the particle size and the size dispersity.[6,11,12] Subsequently, the partitioning of the monomer between continuous and polymer particle phases was studied by Lacroix-Desmazes and Guillot.[13] Over the years, new techniques of dispersion polymerization have been investigated, especially (photo-) polymerization-induced self-assembly (PISA).[14–19]

Dispersion polymerization has proved to be a robust process for the production of monodisperse particles in various media with sizes ranging from 100 nm to 20 µm, making it a very attractive alternative to emulsion polymerization, for many applications. We will now focus in detail on how dispersion polymerization proceeds.

II. Formation of particles by dispersion polymerization

Before getting into the issue itself, some important definitions must be clarified according to IUPAC Gold Book.

- ***Coagulation*** (or flocculation): when a sol is colloidally unstable (*i.e.*, the rate of aggregation is not negligible), the formation of aggregates is called coagulation or flocculation.
- ***Aggregation***: process whereby dispersed particles form aggregates.
- ***Coalescence***: the disappearance of the boundary between two particles in contact, or between one of these and a bulk phase followed by changes of shape leading to a reduction of the total surface area. The coagulation of an emulsion (the formation of aggregates) may be followed by coalescence.
- ***Sedimentation***: separation of a dispersed system under the action of a gravitational or centrifugal field according to the different densities of the components.
- ***Nucleation***: the process by which precursor particles (*nuclei*) are formed in solution.

- ***Precursor particles*** (*nuclei*): the nucleation is thought to occur by formation of insoluble polymer chains, which collapse and form precursor particles (*nuclei*).
- ***Mature particles***: the surface area required to stabilize the precursor particles is very important. Consequently, the precursor particles are unstable and tend towards reducing the surface area to promote their stability by rapid aggregation, leading to mature particles.

In a typical dispersion polymerization process[20–22], contrary to what happens in emulsion of suspension polymerizations, the reaction medium is initially homogeneous. It contains the monomer, the initiator, the stabilizer, the solvent and sometimes a co-stabilizer. The critical characteristic of dispersion polymerization is that the monomer must be soluble in the dispersion medium, whereas the polymer must be insoluble. The process can be described by a 5-step mechanism as shown in Figure 56.

First the initiator decomposes in the continuous phase to form radicals (1) which react with the monomer to form oligo-radicals (2). At a critical chain length, the oligomers become insoluble in the continuous phase and precipitate to form unstable *nuclei* that rapidly aggregate to mature particles (3) which are stabilized by the (*in situ* or pre-formed) stabilizer. Then, the mature particles can grow either by polymerization of the monomer within the particles or adsorb oligomers from the continuous phase, or by coalescence with other particles (4). The final stabilized latex particles are obtained (5) with diameters ranging from 100 nm to 20 µm.

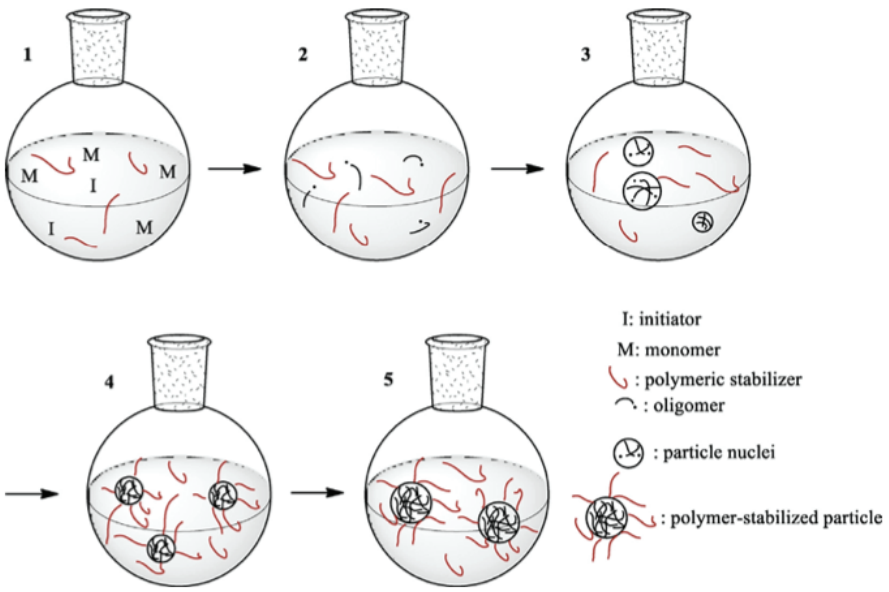

Figure 56. *Typical mechanism of dispersion polymerization: (1) initiation step in the homogeneous phase, (2) formation of oligoradicals (soluble), (3) oligomer precipitation and rapid aggregation of the nuclei, (4) particle stabilization, and (5) particle growth.*[22]

A. Structure of stabilizer in polar media

The stabilizer is initially soluble in the continuous phase and will provide stabilization by attaching onto the particles either directly as a preformed stabilizer or formed *in situ* by chain transfer to polymer or copolymerization. Two categories of stabilizers are commonly used in dispersion polymerization: graft copolymers and block copolymers. It should be noticed that in this case the mechanism of stabilization is highly dependent of the solvent which has to also become a non-solvent for the graft/block copolymer, but a good solvent for the pending stabilizing chains.

1. Graft copolymers

In general, the copolymers are formed *in situ* during dispersion polymerization. A small fraction of polymer chains terminates by chain transfer to the stabilizer and then the monomer goes on polymerizing on the radical sites generated to form graft copolymers. This is the mechanism generally admitted for PVP, a polymer very often used as stabilizer in dispersion polymerization (Figure 57). The resulting graft copolymer becomes insoluble in the continuous phase and adsorbs on the particles. It can also be captured by the growing particles. Once enough graft copolymers have been formed and adsorbed, the particles become sterically stabilized. The main polymers used as stabilizer are PVP, HPC, PAA, PEOX and polyethyleneimine (PEI)[23]. The molecular weight of these stabilizers can vary from 10 000 to 500 000 g mol^{-1}. However, these stabilizers have the drawbacks of being used in a high proportion (from 5 to 80 wt.% based on monomer). Indeed, only a small fraction of the chains is subject to chain transfer reactions.

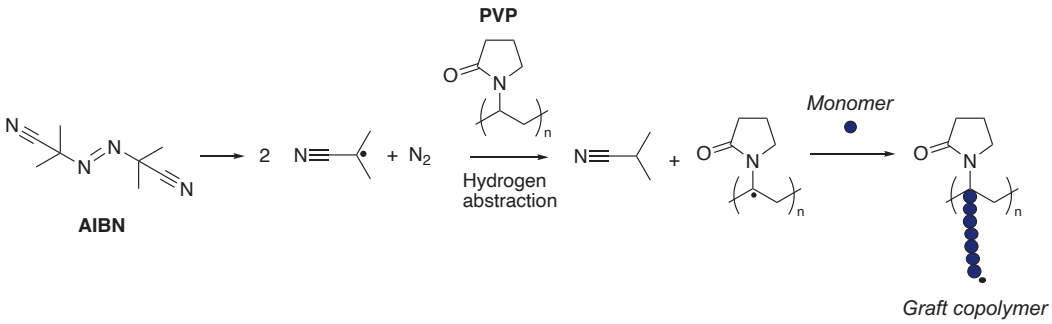

Figure 57. *Mechanism of grafting involving abstraction of hydrogen atoms from the PVP stabilizer to generate a radical site which can add monomer.*

Paine and co-workers showed that in the case of dispersion polymerization of styrene in the presence of HPC, a 10–15 nm surface layer of HPC-containing polystyrene latex was observed by transmission electronic microscopy (TEM). This value was equivalent to an incorporation of HPC on the particle surface of around 1–2 wt.%, corresponding to a maximum incorporation rate of 10–20%.[24,25]

One other technique was thus developed to improve the formation of graft polymers. It consists of using a macromonomer.[26–34] A macromonomer is a polymer chain that includes a polymerizable group at one chain end. It can therefore be included in the main polymer chain to form a comb-like graft copolymer. For example, Pelton *et al.*[26,27] used a macromonomer for the dispersion polymerization of MMA in hexane. It was composed of polydimethylsiloxane (PDMS) chains functionalized by vinylic end groups (Figure 58). This technique of stabilization was also used in alcoholic media[28,29,35] and in both supercritical and liquid CO_2[36–38]. All these studies highlighted that more stable polymer particles were formed by using a macromonomer in comparison with conventional stabilizers such as PVP or HPC.

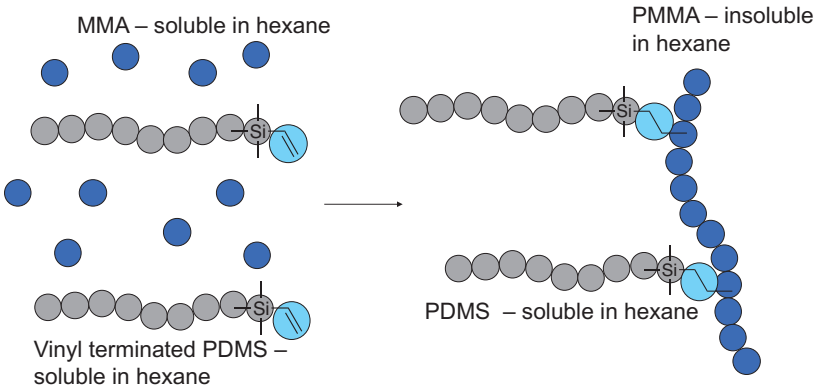

Figure 58. *Formation of PDMS/PMMA graft copolymer in hexane.*[26,27]

For example, Lacroix-Desmazes and co-workers investigated the dispersion polymerization of styrene in ethanol/water mixtures by using different poly(ethylene glycol) (PEG) macromonomers as stabilizer.[39] The aim was to determine the incorporation yield of PEG macromonomers by varying the nature of polymerizable group at the macromonomer chain end (maleate, methacrylate, styrenic and methacryloyl urethane). Indeed, the mechanism of stabilization of the polymer particles is highly dependent on the macromonomer reactivity. Therefore, the authors showed that higher incorporation yield and grafting density were obtained in medium of lower polarity. Moreover, a chain length of the macromonomer of

around 50 ethylene oxide units was required to form stable PS latexes with an incorporation yield around 53% in the case of PEGMA macromonomer.

2. Block copolymers

a. Macroinitiators

Macroinitiators are polymer chains that contain functional groups able to initiate the polymerization. The polymeric unit in the macroinitiator is incorporated in the newly formed polymer as a polymeric segment soluble in the continuous phase, leading to particle stabilization.

Topp *et al.*[40,41] have reported the synthesis of block copolymers composed of poly(ethylene glycol) and poly(N-isopropylacrylamide) (PEG-*b*-PNIPAAm) in water. They used a ceric ion redox system to form radicals at the terminal carbons of PEG. However, their system was not considered to be effective enough in the stabilization of particles because only 10% of the PEG chains led to initiating radicals during the redox reaction with the ceric ions.

Then, Okubo *et al.*[42] reported the synthesis of submicron-sized PMMA particles *via* dispersion polymerization of MMA in $scCO_2$ using a PDMS-based macro-azo-initiator, containing multiple azo groups within the same chain (Figure 59). This led to the formation of stable latexes around 200 nm in diameter. However, the authors demonstrated that only 30% of the azo groups were decomposed. The *inistab* which stabilized the particles thus still features cleavable azo group, which makes it fragile upon heating. Moreover, an important quantity of inistab had to be introduced in the initial system (50 wt.% based on monomer).

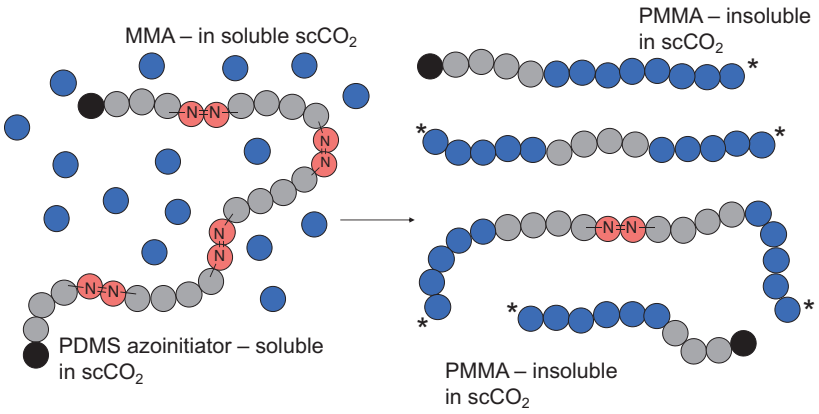

Figure 59. *Formation of block copolymers with a PDMS-based macro-azo-initiator.*[42]

Recently, Yoshinobu *et al.*[43,44] reported the dispersion polymerization of styrene using poly(2-hydroxyethyl methacrylate) (PHEMA) and poly(2-hydroxypropyl methacrylate) (PHPMA)-based hydroxy-functional macro-azo-initiators, and a poly((2-diethylamino)ethyl methacrylate) (PDEA)-based macro-azo-initiator in a hydroalcoholic medium. They obtained a good control of the final particle size (between 100 and 130 nm) in the case of PDEA macro-azo-initiator, and in the sub-micrometer range with the two others macro-azo-initiators. The obtained PS latexes were highly stable, but this stability depends on the nature of the *inistab*. Indeed, PDEA is a pH-sensitive polymer resulting in a flocculation of the PS particles at a high pH (deprotonation of the PDEA chains). In addition, it should be noticed that the synthesis of those macroinitiators is not easy.

Several authors then investigated reversible deactivation radical polymerization (RDRP) in dispersion with the aim to enhance the incorporation yield of the stabilizer and to produce block copolymer nanoobjects.[18,45,46] This technique, known as PISA, takes advantage of the chain-end reactivity of solvophilic macromolecules obtained by RDRP for the polymerization of a second monomer in a suitable solvent.[16,19] The growth of the second block, insoluble in the polymerization medium, leads to the formation of block copolymers that self-assemble into nanoparticles.

Okubo and co-workers reported the dispersion polymerization of MMA in $scCO_2$ with a bromo-terminated PDMS as atom transfer radical polymerization (ATRP) macroinitiator.[47] They demonstrated that all PDMS-Br efficiently initiated the dispersion ATRP. The same authors also studied nitroxide-mediated dispersion polymerizations in $scCO_2$.[48] They used a polymeric alkoxyamine macroinitiator with the expected structure SG1-PS-*b*-PDMS-*b*-PS-SG1 (SG1: *N*-tert-butyl-*N*-(1-diethylphosphono-2,2-dimethylpropyl) nitroxide), to serve as initiator and stabilizer. However, the authors obtained broad molecular weight distributions, which was attributed to the simultaneous presence of species that were able to grow from one or both ends and with some contribution from bimolecular termination by combination of difunctional chains.

Delaittre *et al.*[49] reported the elaboration of temperature-responsive hydrogel nanoparticles using a poly(sodium acrylate) SG1-based macro-alkoxyamine as a macroinitiator for the nitroxide-mediated dispersion polymerization of *N*,*N*-diethylacrylamide in water. Stable monodisperse particles with diameter ranging from 49 to 118 nm at high temperature (50 °C) were successfully obtained by this approach, showing that the macro-alkoxyamine was an effective stabilizer precursor.

b. Macromolecular chain transfer agents (macro-CTAs)

Bourgeat-Lami and Guyot have used a thiol-ended polyethylene oxide macro-thiol (PEO-SH) to form PS latexes in ethanol as illustrated in Figure 60.[50] They obtained stable monodisperse particles with diameters ranging from 200 nm to 2 µm, depending on the initial PEO-SH concentration. They showed that the high stabilizing efficiency of the PEO-SH was due to a higher chain transfer rate constant of the macro-thiol when compared to PVP (10 000 times higher), making PEO-SH a highly efficient chain transfer agent. Also, a low amount of PEO-SH was enough to produce stable PS particles. But only 15% of the PEO-SH was grafted on the particle surface. According to the authors, the poor incorporation yield of PEO might be due to the high transfer reaction rate. Indeed, the PS chains formed onto the initial PEO-SH are too short to lead to amphiphilic block copolymers, preventing their anchoring to the particles, and accumulating consequently in the continuous phase.

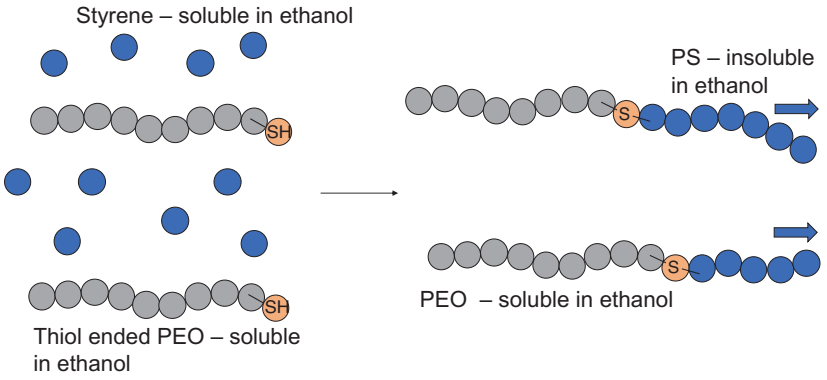

Figure 60. *Formation of block copolymers with a reactive stabilizer PEO-SH.*[50]

Okubo *et al.*[51] described the formation of PMMA particles by dispersion polymerization of MMA in $scCO_2$ in the presence of mercaptopropyl terminated PDMS as stabilizer. They obtained stable spherical particles but again only 20% of mercaptopropyl terminated PDMS was involved in the stabilization of the particles.

Zheng and Pan reported the reversible addition-fragmentation chain transfer (RAFT) copolymerization of 4-vinylpyridine (4-VP) and divinylbenzene (DVB) in tetrahydrofuran (THF) and cyclohexane using dithiobenzoate-terminated PS as macro-CTA.[52] In cyclohexane, micelles with diameter less than 50 nm were formed after 5 h with PS as the shell and poly(4VP-*co*-DVB) as the core. However, the polymerization was very low due to the restriction of monomer diffusion in the micelle cores.

Bathfield *et al.*[53] reported the dispersion polymerization of *n*-butyl acrylate (*n*-BA) in ethanol/water mixture in the presence of poly(*N*-acryloylmorpholine)-CTA (PNAM-CTA) (Figure 61). Stable and monodisperse particles with diameters comprised between 100 and 300 nm were successfully obtained. The authors determined that around 55% of the introduced PNAM-CTA chains were involved in particle formation.

Finally, He *et al.*[54] studied RAFT dispersion polymerization of styrene with trithiocarbonate-capped poly(acrylic acid) (PAA) as macro-RAFT in methanol to form various nano- and micro-object morphologies of PAA-*b*-PS. They demonstrated the importance of the core-forming block length to the corona-forming block length ratio on the control of the morphology.

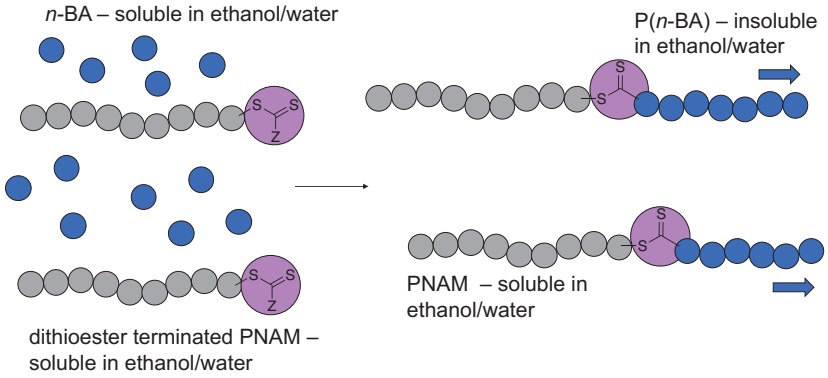

Figure 61. *Formation of block copolymers with a macro-RAFT agent.*[53]

3. Conclusion

The stabilizers that are synthesized *in situ* by chain transfer to polymer of copolymerization present the advantage to be efficiently adsorbed on the particles since their composition is near the one of dispersed polymers. Reactive macromolecules used as precursors of stabilizers in dispersion polymerization are generally more efficient than conventional homopolymers for the stabilization of the particles and lead to relatively high incorporation yield at low reactive macromolecule concentration. Two types of stabilizers are usually added to the dispersion formulations: graft copolymers and block copolymers. The following section will discuss the mechanism of particle formation in dispersion polymerization in the presence of polymeric stabilizer.

B. Mechanism of particle formation in dispersion polymerization

The different events occurring in a dispersion polymerization process (Figure 56) are actually quite complex. Indeed, the complexity comes with the fate of free radicals generated continuously in the continuous phase since many physical and chemical processes may occur simultaneously (Figure 62).[55] The free radicals can either react with the monomer or the stabilizer or can be absorbed by precursor particles or particles in growth, which typically continues until the end of the polymerization.

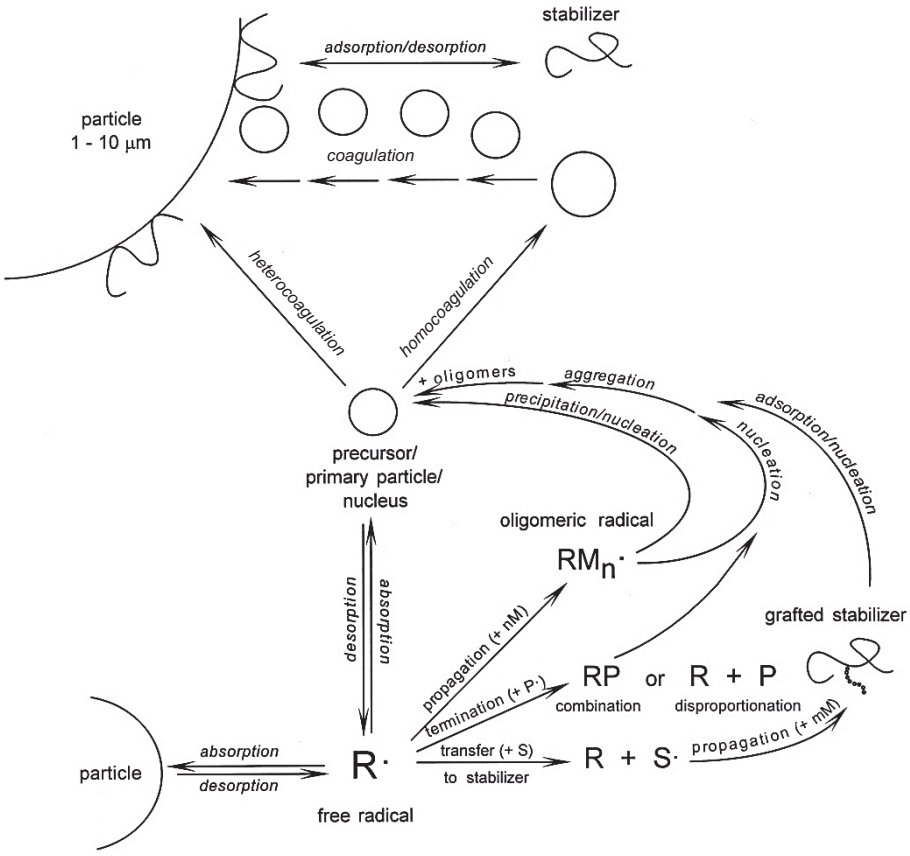

Figure 62. *Schematic representation of mechanisms involved in free radical dispersion polymerizations – words in italics represent physical processes.*[55]

Moreover, the chemical reactions (decomposition of the initiator, initiation, propagation, termination and transfer), which occur during the polymerization, initially take place in the continuous phase. But, with the formation of the polymer particles, a second phase appears which leads to a partitioning of the initial species (monomer and initiator), depending largely on the nature of the continuous phase.

One of the most important steps during the polymerization in dispersion is the nucleation because the particle number of the final latex is fixed at an early stage of the reaction, leading to monodisperse particles, which ideally happens when the phenomena of secondary nucleation or coalescence are not present. Nucleation can occur by a number of mechanisms including self-nucleation, aggregative nucleation and coagulative nucleation.[2]

A simple mechanistic model for the formation of particles was developed by Paine[11], on the basis of the previous works of Fitch and Tsai[56], and Gilbert and co-workers[57]. It is postulated that first the oligomer chains are formed and reach a critical chain length where they are insoluble in the continuous phase, collapse and form unstable precursor particles. At this point, several ways to form stable nuclei are expected: (1) the unstable *nuclei* coagulate followed by coalescence with each other (homocoagulation), (2) the collision with a stabilizer or alternatively (3) the growth by propagation of the polymer chain can occur (Figure 63).[58]

According to Paine, in the presence of stabilizer (*in situ* formed), the coagulation stops when the particle surface is entirely covered by the stabilizer. Then, the oligomers in growth from the continuous phase could be either captured by the particles or nucleated to form unstable precursor particles which will be captured by the existing mature particles. However, Paine neglected the influence of the solvent polarity on the particle formation. We will discuss later the fact that the solvent polarity has an impact on the critical chain length for precipitation of the oligomer, the specie partition and the stabilizer efficiency so that its effect on the dispersion polymerization cannot be easily quantified. The mechanism of particle formation is mostly only qualitatively grasped because it is largely extrapolated from precipitation, emulsion or solution polymerizations.

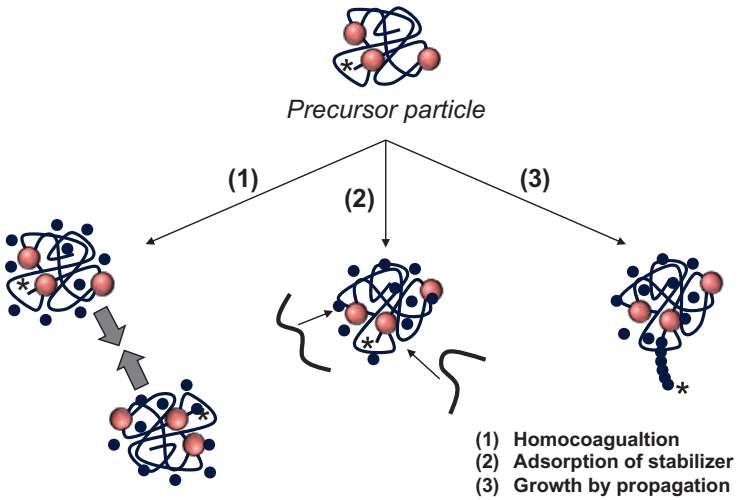

Figure 63. *Schematic diagram of the events in coagulative nucleation.*

Once the particles are formed, the system becomes biphasic and the different species such as monomer, initiator and oligomers partition between the continuous phase and the particle phase. Therefore, two mechanisms can be involved in the particle growth step: (1) the monomer in the continuous phase forms oligomer which precipitates and is captured by the existing particles or (2) the polymerization proceeds in the monomer-swollen particles. Here again, the solvent polarity will have a significant impact on the polymerization locus.

The various studies available in the literature clearly show that the particle size and its distribution are impacted by the type of monomer and its concentration, the composition of the continuous phase, the concentration and the type of stabilizer, the initiator and its concentration, and the temperature of the polymerization. All of these parameters are related to the solvency of the continuous phase which is considered to be one of the most important factors influencing the mechanism of particle formation in dispersion polymerization.

III. Influence of several parameters on the particle size and size distribution

A. Solubility parameters

As a rule of thumb, the particle size increases with increasing solvency of the continuous phase for the polymer. Several authors have tried to correlate the particle size and the solubility parameters of the solvents and the polymer with varying levels of success.

Lok and Ober concluded that the composition of the initial continuous phase was important to control the final particle size of polystyrene since the formation of stable particles is restricted to the early stages of the polymerization.[12] They have based their work on Hansen solubility parameters (HSP) of selected solvents, as reported in Table 16.[59] Each solvent can be described by three HSP. The first is the dispersion parameter, δ_D, which is related to the electric polarizability of the atom or molecule. For example, styrene has more polarizable electrons than water, and so δ_D is higher (9.1 and 6.0, respectively). The second parameter is the polar term δ_P and is related to the permanent dipoles (Van der Waals forces). Finally, the third parameter is the hydrogen bond term δ_H. δ_t represent the total solubility parameter resulting from the contribution of each of the three HSP.

$$\delta_t = \sqrt{\delta_D^2 + \delta_P^2 + \delta_H^2} \quad (Eq. 3.1)$$

Thus, the more similar the solubility parameters of the polymer and solvent, the more soluble the polymer will be in the solvent.

Table 16. *Solubility parameters of different solvents used for the starting continuous phase in dispersion polymerization. All δ values reported here are in units of* $cal^{1/2}\ cm^{-3/2}$.

Solvent	Dielectric constant	Dipole moment (D)	δ_t	δ_D	δ_P	δ_H
Dimethoxyethane	-	-	8.6	-	-	-
THF	7.32	1.63	9.1	8.2	2.8	3.9
Styrene	-	-	9.3	9.1	0.5	2.0
2-Ethoxyethanol	-	2.08	10.5	7.8	4.5	7.0
t-Butanol	10.9	1.66	10.6	-	-	-
2-Methoxyethanol	16	2.2	11.4	7.9	4.5	8.0
Isopropyl alcohol	18.3	1.66	11.5	-	-	-
Ethanol	24.3	1.69	12.7	7.7	4.3	9.5
Methanol	32.6	1.70	14.5	7.4	6.0	10.9
Water	78.5	1.84	23.4	6.0	15.3	16.7
Polystyrene	2.5	-	8.9	-	-	-

The contributions of HPC as stabilizer and benzoyl peroxide (BPO) as initiator were neglected because they are present in very low amounts with respect to the other compounds. The authors observed that the particle size decreased when the solvent polarity increased. For example, when 2-methoxyethanol (δ_t = 11.4) was used alone, particles were swollen with solvent and reached size from 5 to 50 μm, while ethanol (δ_t = 12.7) alone produced smaller particles (from 0.5 to 3 μm). Indeed, ethanol is a stronger non-solvent for polystyrene. An appropriate ratio between ethanol and 2-methoxyethanol enabled the preparation of particles from 5 to 10 μm in diameter. However, the authors noticed that different solvent systems led to particles of comparable sizes. In this study, the chain transfer properties of the solvent and the solubility of the stabilizer were neglected. Their approach pointed at the solubility parameters, but it is important to consider the full system.

Almog *et al.*[3] also studied the effect of the solvency on the dispersion polymerization of styrene in alcoholic medium with vinyl alcohol/vinyl acetate copolymer (PVAc-A1) (82 wt.% VAc content) and methyl tricaprylyl ammonium chloride (Aliquat 366) as stabilizers. The authors observed that by changing the solvent from methanol to *t*-butanol, the diameter of the

resulting particles increased (Figure 64). This was attributed to the swelling capacity of the alcohol with the lower total solubility parameter δ_t. The authors did not stop their study there and evidenced two other effects of the solvency: on the one hand, the increase in the critical chain length at which point the oligomers nucleate, resulting in delay in particle formation (therefore fewer and larger particles were obtained), and one the other hand, the impact on the mechanism of stabilization. Indeed, at a high solvency of the continuous phase, the stabilizer may not provide efficient stabilization from the formation *in situ* by chain transfer to polymer of the graft copolymer, which is adsorbed onto the polymer particle.

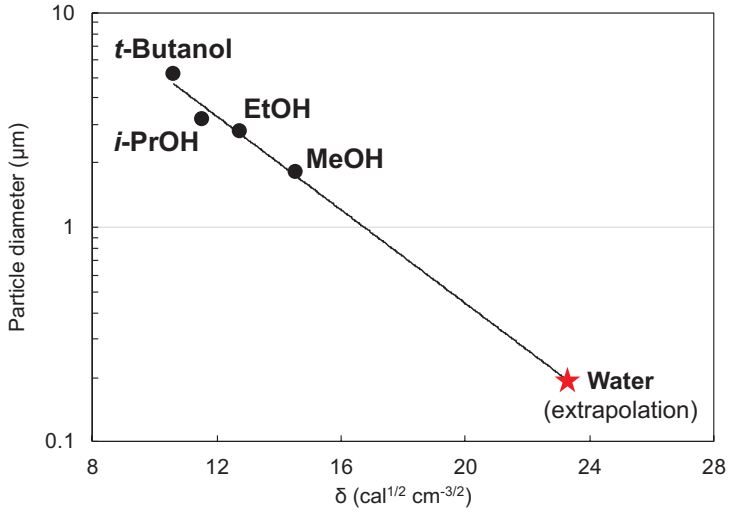

Figure 64. *Effect of the solubility parameter of the alcohols on the diameter of the polystyrene particles obtained.*[3]

Paine *et al.*[60] tried to develop a predictive tool for the effect of solvency on particle size according to the three-dimensional HSP. They worked on the dispersion polymerization of styrene in ether alcohol mixtures or *n*-alcohols, using HPC as stabilizer. Contrary to the method used by Ober and Lok to determine the total solubility parameter, Paine and co-workers have noticed the relatively constant value of the dispersion term δ_D and decided to ignore it for their study. Thus, they elaborated a solvent parameter space for mechanistic consideration based on δ_H and δ_P (Figure 65).

For example, alkanes (usual solvents for non-aqueous dispersion polymerizations at the origin), toluene and styrene have low δ_H and δ_P. Conversely, alcohols cover a wide range on the solvent parameter space (purple). The solvents usually used for solution polymerization of styrene are found in a region bounded by $2 < \delta_H < 6$ and $1 < \delta_P < 6$, i.e., the solvents with Hansen solubility parameters near those of polystyrene ($\delta_H = 2$ and $\delta_P = 2.8$)[61]. Mixtures of solvents have intermediate solvency properties calculated from the volume weighted average of the values

for the pure solvents. The solvents with higher hydrogen bonding terms such as ethanol in which the polystyrene is insoluble lead to two phase polymerization (dispersion).

According to the authors, 2-methoxyethanol and ethanol were the upper limits of δ_P and δ_H for dispersion polymerization of styrene (in their experimental conditions). It is important to note that the largest particles were obtained when the polarity and hydrogen bonding terms were the nearest to those of the stabilizer HPC. The conclusion from this work was that the solvency criterion is not enough to determine the particle size. The solubility of the graft copolymer formed *in situ* to stabilize the polymer particles must be taken into account.

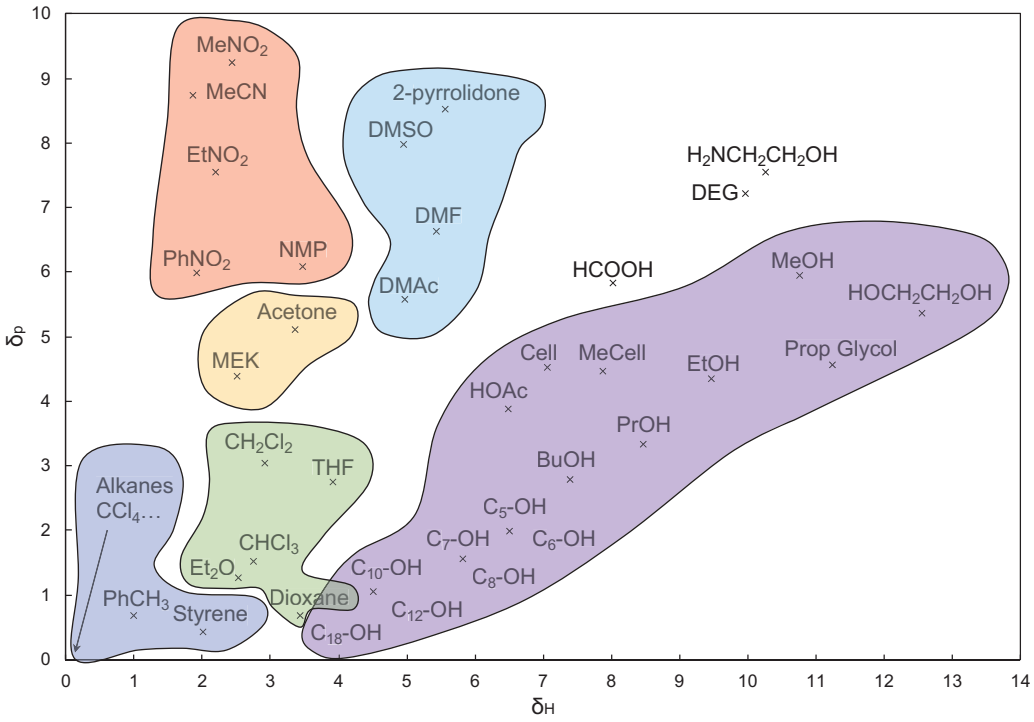

Figure 65. *Hansen solvency map showing the location of the solvents useful for dispersion polymerization reactions.*[60]

In summary, the particle size increases with increasing solvency of the continuous phase for the polymer. Indeed, the higher the solvency for the polymer, the more the critical chain length of the oligomers. Several authors tried to correlate the particle size and the solubility parameters of the solvents and the polymer based on HSP. It was shown that the solubility of the graft copolymer formed in situ to stabilize the polymer particles must be taken into account.

B. Influence of the stabilizer

The stabilizer plays a crucial role in the particle formation and the control of their size. We have already barely mentioned the influence of solvency on the solubility of the graft copolymer. We will now discuss the mechanism of stabilization and the major effects of solubility parameter of the continuous phase.

The precursor particles undergo homocoagulation as long as the surface area and/or the number of these coagulated species is small enough to be stabilized by the stabilizer. The point at which the homocoagulation stops and the number of particles is fixed is called the stabilization point. Furthermore, an increase in solvency leads to oligoradicals with longer critical chain lengths (and higher molecular weight) which are formed before particle nucleation causing the generation of larger particles.

According to Paine and co-workers, the solubility of the HPC-*g*-PS graft copolymer formed during the dispersion polymerization has an impact on the initial particle number and the molecular weight.[24,25] Indeed, the PS fragment is preferentially adsorbed onto the particle surface and the HPC chains are very soluble in the continuous phase. For example, if the PS fragment of the graft copolymer has a very low molecular weight compared to that of the HPC chain, then HPC-*g*-PS may be too soluble in good solvents for the stabilizer and may not adsorb onto the particle surface to play the role of a steric stabilizer, resulting in the formation of an unstable dispersion. This is why it is important to consider the solubility properties of the graft and block copolymers with regards to the initial medium solvency.

Among all the steric stabilizers, PVP has been shown to provide the best stabilization in hydroalcoholic media leading to narrow size distributions.[3,6,62–65] El-Aasser and co-workers reported the dispersion polymerization of MMA in methanol and *n*-BA in methanol-water mixtures and studied the effect of the concentration and molecular weight of PVP on the particle size (Figure 66).[63,66] The final latexes showed narrow size distributions in each case and their sizes ranged from 1 to 7 µm. The latter decreased with increasing PVP molecular weight for a given PVP concentration. The particle size also decreased with increasing PVP concentration. For the five systems considered, the slopes of the particle size evolution vs. PVP concentration were quite similar. The power dependence of the particle size on the PVPK-90 concentration was –0.25, in the case of PMMA. For the other curves, the slope was around –0.4. According to the authors, the PVP concentration has an impact on the extent of nuclei aggregation by changing the adsorption rate of the graft copolymer. If the PVP/polymer ratio is too high, the

graft copolymer containing longer PVP chains will be more soluble in the continuous phase, resulting in a low adsorption on the precursor particles and thus, larger polymer particles are formed.

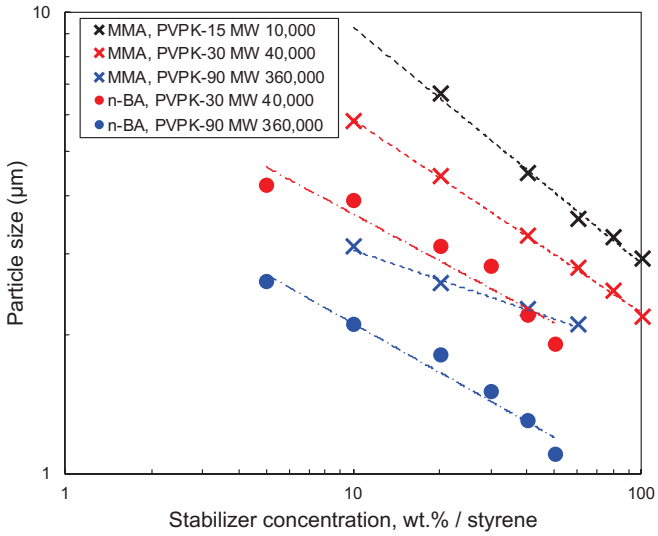

Figure 66. *Effect of PVP concentration and molecular weight on PMMA and P(n-BA) particle sizes.*[63,66]

Similar results were reported for the dispersion polymerization of styrene.[6] Paine and co-workers studied the effect of PVP concentration and molecular weight on particle size in ethanol with Triton N-57 as a co-stabilizer.[67] They obtained stable PS particles with sizes ranging from 3 to 10 µm and narrow size distributions. In certain experimental conditions, i.e., at low stabilizer concentration and molecular weight, a co-stabilizer is required to obtain narrow particle size distributions. Figure 67 shows the influence of PVP concentration for three different molecular weights on the particle size. For the three curves, the slope of the particle size *vs.* PVP concentration was about –0.3. But, according to the authors, these slopes are lower than predicted for the simplest adsorption mechanism of stabilization by PVP, where the amount of surface area stabilized would be proportional to the stabilizer concentration, predicting a slope of -1.

Surprisingly, Almog *et al.*[3] reported no such effect of PVP concentration on PS particle sizes, which remain around 2 µm for concentrations ranging from 15 to 30 wt.% (based on styrene) in ethanol. However, they did not mention the molecular weight of the PVP and, an important difference with the study of Paine was that a cationic co-stabilizer (Aliquat 336) was also present (2/7 of PVP amount).

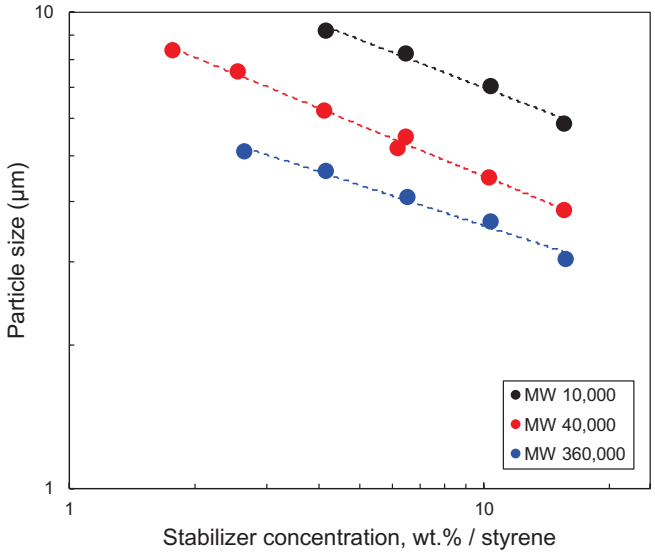

Figure 67. *Effect of PVP concentration and molecular weight on particle size in ethanol with 26.3% volume of styrene, Triton N-57 (6.3 wt.% based on styrene) and AIBN (1 wt.% based on styrene).*[67]

To conclude, the particle size seems to decrease when the stabilizer concentration and/or its molecular weight increase. However, some studies show no effect of the stabilizer concentration on the particle size, indicating the complexity of dispersion polymerization. Further comparisons are difficult since slight differences in the initial experimental conditions might impact the global dispersion polymerization process.

C. Effect of initiator

One general observation is that an increase in the initiator concentration produces fewer and larger particles. Since the nucleation in dispersion polymerization is the point at which particles are formed in the continuous phase, it is thus expected to be affected by the production rate of free radicals. This rate depends on the concentration and the type of the initiator as well as the reaction temperature which affects the dissociation rate of the initiator.

For instance, Tseng *et al.*[6] studied the influence of different types of initiators by taking into account their half-lives ($t_{1/2}$) and concentrations. The resulting particle sizes and size distributions are reported in Table 17. Dispersion polymerization of styrene at 70 °C with initiator 2,2'-azobis(2,4-dimethyl)valeronitrile (ADVN) which decomposes fast ($t_{1/2}$ = 58 min) produced bimodal or broad particle size distributions. The same trend was observed with BPO ($t_{1/2}$ = 1049 min). Dispersion polymerizations of styrene using AIBN, 4,4'-azobis(4-

cyanopentanoic acid) (ACPA) or 2,2′-azobis(2-methylbutyronitrile) (AMBN) initiators resulted in stable particles and narrow particle size distributions.

The authors found that the particle size was proportional to [AIBN] and [AMBN] with, in both cases, a slope of 0.4. An increase in initiator concentration led to larger particle sizes. This was attributed to a higher instantaneous oligoradicals concentration which should probably aggregate and form larger precursor particles before enough stabilizer would adsorbs onto them to provide stability.

In addition, in the case of a fast decomposition of the initiator (ADVN), a secondary nucleation during the growth step may occur since the adsorption speed of the stabilizer could not catch up with the nucleation rate. In contrast, a slow decomposition of the initiator (BPO) generates oligoradicals at a much slower rate. In this case, the nucleation step will last longer, which may result in various final sizes. A moderate rate of radical generation ensures a balance between a short nucleation step and adsorption of stabilizer so that all precursor particles grow to uniform final particle sizes.

Table 17. *Effect of initiator type and concentration on particle size and size distribution of PS latexes prepared by dispersion polymerization in ethanol with PVP as stabilizer and Aerosol OT as co-stabilizer.*[6]

Initiator (wt.%/ styrene)	**AIBN** $t_{1/2}$ = 289 min	**ACPA** $t_{1/2}$ = 293 min	**AMBN** $t_{1/2}$ = 500 min	**BPO** $t_{1/2}$ = 1049 min	**ADVN** $t_{1/2}$ = 58 min
0.5	2.2 µm	2.1 µm	2 µm	0.3 – 1.3 µm (broad)	4 µm + 0.4 – 2.3 µm (bimodal)
1	3 µm	2.7 µm	2.4 µm	0.3 – 1.6 µm (broad)	4.6 µm + 0.4 – 2.7 µm (bimodal)
2	3.6 µm	3.5 µm	3.2 µm	2 µm + 0.4 – 1.3 µm (bimodal)	0.4 – 6 µm (broad)
4	5 µm	5 µm	4.5 µm	2.7 µm + 0.4 – 2 µm (bimodal)	0.4 – 7.4 µm (broad)

Kobayashi *et al.*[23] reported the influence of the initiator concentration on the size and size distribution of PMMA particles synthesized at 56 °C in methanol-water mixtures using PEOX as stabilizer and ADVN as initiator. They also observed that the particle size increased with the initiator concentration. The authors obtained a similar behavior during dispersion polymerization of styrene in ethanol-water mixtures under the same experimental conditions[10].

Tuncel *et al.*[9] investigated the dispersion polymerization of styrene initiated by AIBN with PAA as stabilizer in three dispersion media (isopropanol/water, 1-butanol/water and 2-butanol/water). For each medium, the authors determined the solubility parameter for two alcohol/water ratios of 70/30 and 90/10 in volume. They again observed the same trend that the particle size increased with the initiator concentration (Figure 68). The polymerization started with a high number of radicals per unit volume in the case of high initiator concentration. The authors argued that this high number of radicals could lead to the formation of a high instantaneous oligoradical concentration, which will favor termination reactions and lead to shorter polymer chains. The nucleation occurs when the polymer chains reach a critical molecular weight at which they precipitate. This precipitation will thus occur later in the reaction when the initiator concentration is high. Accordingly, the graft copolymers formed from these first oligomers should be more soluble in the continuous phase and not able to efficiently stabilize the precursor particles. Therefore, the unstabilized *nuclei* coalesce with each other and few numbers of mature particles are formed but with larger size.

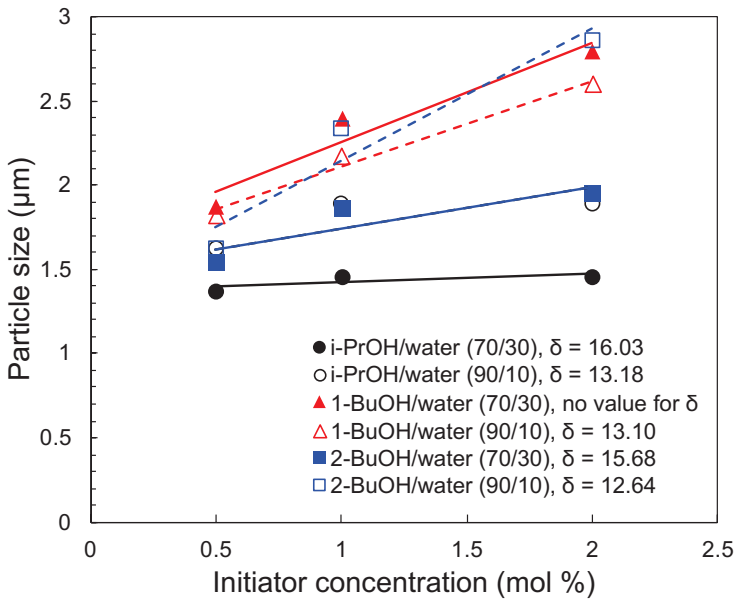

Figure 68. *Effect of initiator concentration on particle size in different dispersion media.*[9]

Paine *et al.*[67] found, in agreement with the work of Vanderhoff and El-Aasser (who obtained a slope of 0.4 under similar conditions), that the particle size was proportional to [AIBN] to the 0.39 power. According to the authors, larger particles were obtained at higher initiator concentrations because lower molecular weight PS was formed, making the PVP-*g*-PS graft copolymer more soluble and thus, the particles were less well stabilized.

However, Wang *et al.*[66] observed a slight decrease of the P(*n*-BA) particle size at higher concentration for both AIBN and ACPA in methanol-water mixture with PVP K90 (molecular weight of 360 000 g mol^{-1}) as stabilizer. In this particular case, the efficient adsorption of the graft copolymer depends on the nature of the stabilizer and the monomer (and then the polymer formed). Moreover, it is also possible that the PVP can adsorb onto precursor particles without grafting from the oligoradicals in growth (transfer reactions), even at a relatively small fraction, depending on the affinity with the monomer used.

To sum up, in dispersion polymerization an increase of initiator concentration mainly leads to an increase of particle size and thus to a smaller number of particles. This observation is largely due to a faster generation of radicals, which in turn increased the instantaneous oligoradical concentration resulting in aggregation and the formation of larger precursor particles before enough stabilizer would adsorbs onto them to provide stability. The type of the stabilizer thus may influence the adsorption of the graft copolymer onto the primary particles.

D. Effect of the temperature

The variation of the temperature in dispersion polymerization can have an impact on the following factors:

- The critical chain length for precipitation due to the change in the solvency of the continuous phase.
- The concentration of the precipitated oligomer chains, which is related to both the decomposition rate of the initiator (more radicals formed) and the propagation rate of the oligomeric radicals.
- The adsorption rate of the stabilizer because of a change in the stabilizer solubility in the reaction medium.
- The viscosity of the continuous phase.

According to the literature, a higher polymerization temperature leads to an increase in particle size. For example, Chen and Yang[68] reported that PS particle size increased from 2 to 7.8 µm when the temperature was raised from 60 to 80 °C (Figure 69). Smaller particles were obtained at lower temperature because the HPC-*g*-PS graft copolymer is less soluble and will rapidly adsorbed onto the precursor particles to stabilize them.

Bamnolker and Margel[69] studied the effect of temperature on the particle size for the dispersion polymerization of styrene in the presence of PVP and P(vinyl pyridine-*co*-VAc) as stabilizer and BPO and AIBN as initiators in a mixture of ethanol and 2-methoxy ethanol. The increase in the particle size at higher temperature indicates that the aggregative nucleation is controlled by the adsorption rate of the stabilizer. If the generation rate of the oligoradicals is much faster than the adsorption rate of the stabilizer, the oligomers will tend to aggregate and form larger particles before enough stabilizer adsorbs to stabilize them, especially since the stabilizer is also more soluble in the continuous phase.

However, Šušoliak and Bartoň[70] reported no effect of temperature on the particle size for the dispersion polymerization of MMA in heptane at 50 and 90 °C in the presence of a three-block isoprene-styrene-isoprene copolymer as stabilizer. Once again, it must be good to remain cautious in these results and not generalize since each system is different.

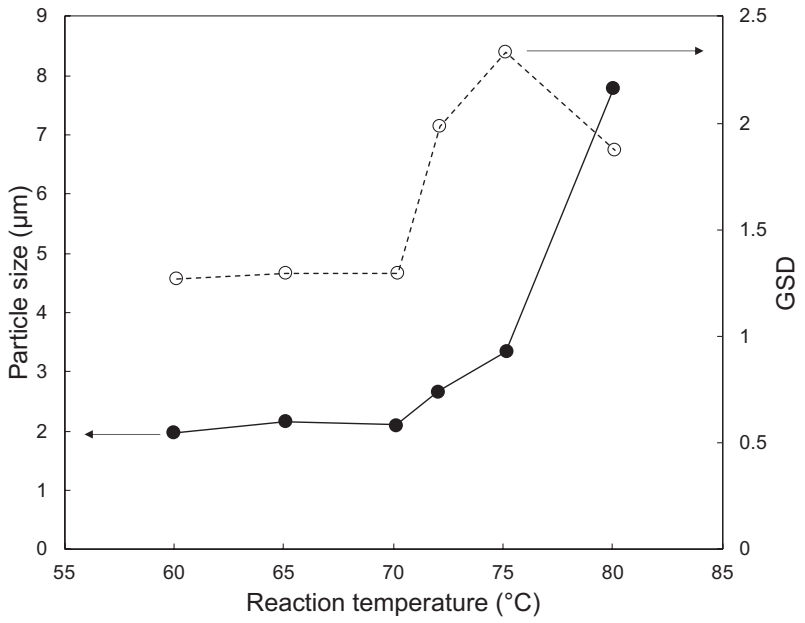

Figure 69. *Effect of reaction temperature on size and geometric standard deviation (GSD) of PS particles synthesized in an ethanol-2-methoxy ethanol mixture. Experimental conditions: [styrene] = 150 g L^{-1}, [BPO] = 6 g L^{-1} and [HPC] = 15 g L^{-1}.[68]*

The temperature is an important parameter that impacts directly the solubility of each components in the continuous phase and thereby the formation of particles. In general, it is considered that the particle size increases with increasing polymerization temperature.

IV. Kinetics of dispersion polymerization

In a typical dispersion polymerization, the decomposition of the initiator occurs in the continuous phase and generates primary radicals. However, when the first polymer particles are formed, the polymerization takes place in both the continuous phase and the particle phase. At this point, partitioning behaviors of the monomer and initiator between these phases must be considered. This obviously depends on many factors, but mainly the solvency of the reaction medium and the nature of the monomer/polymer system. The reaction rate thus results from a combination of polymerization in the continuous phase and polymerization inside the swollen polymer particles.

A. First theoretical model of dispersion polymerization

In 1969, Barrett and Thomas developed a theoretical model for interpreting the dispersion polymerization of MMA in *n*-dodecane with AIBN as initiator and an amphipathic copolymer as stabilizer that contains the pentamer of 12-hydroxystearic acid and PMMA.[71] The authors proposed a model based on polymerization within the monomer-swollen particles according to laws of bulk polymerization kinetics. A theoretical expression was obtained assuming that the radicals generated in the continuous phase are immediately captured by the polymer particles (*i.e.*, all radicals are located in the particle phase) and the monomer is in equilibrium between the particle phase and the continuous phase.

In those conditions, the radicals inside the particles can be subject to the high viscosity of these monomer-swollen particles hindering radical termination. This results in a higher concentration of radicals which can lead to an increase of the polymerization rate. This is the Trommsdorff effect (gel effect) which is indeed experimentally observed (Figure 70). The overall rate of polymerization can be thus expressed as follows:

$$R_p = \alpha k_p [M] \left(\frac{\nu R_i}{k_t}\right)^{0.5} \quad (Eq.\,3.2)$$

where α is a monomer partition coefficient, k_p and k_t the propagation and termination rate constants, [M] the overall monomer concentration in the dispersion, ν the volume fraction and R_i the rate of initiation.

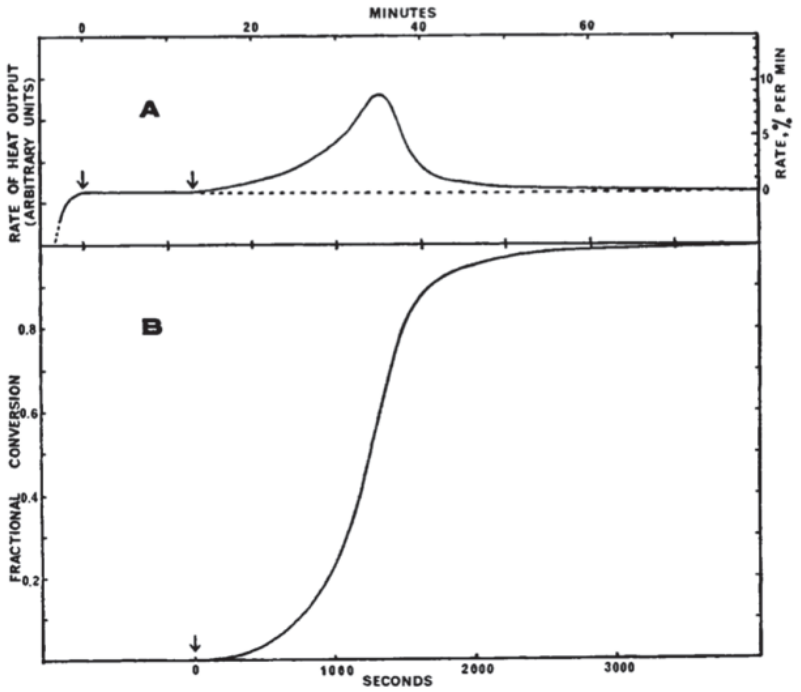

Figure 70. *Dispersion polymerization of MMA – (A) differential thermal analysis curve of rate of heat output against time and (B) corresponding time-conversion curve obtained by integration of (A). MMA 50 wt.%, AIBN 0.2 wt.% and amphipathic copolymer as stabilizer 2.5 wt.% in n-dodecane at 80 °C.*[71]

The model proposed by Barrett and Thomas is very similar to the pseudo-bulk kinetics for emulsion polymerization, *i.e.*, two radicals (or more) can coexist within the same particle without instantaneously terminating (see Chapter 2). In agreement with their proposed model, the authors obtained a sigmoidal shape of the time-conversion curve (namely S-curve – see Figure 70). However, they did not take into account the number of particles in their approximation. Besides, in bulk polymerization, the initiator efficiency might be reduced at high conversion due to the cage effect.

In the case of the dispersion polymerization of styrene in hydroalcoholic mixtures, it was found that the conversion displays characteristics similar to those of MMA in hydrocarbon-based liquids. It can be seen that in the ethanol/water system the reaction proceeds rapidly indicating a pronounced gel effect.[72]

B. The overall rate of dispersion polymerization

Before the formation of the precursor particles, the reaction proceeds as in a solution polymerization. The rate of polymerization depends on the number of radicals, the monomer concentration and the initial temperature. Liu *et al.*[72] studied those effects on the rate of

dispersion polymerization of styrene at 65 °C in ethanol-water mixture (90/10 vol%) initiated by AIBN and stabilized using a PEO_{40}-$(CH_2)_{11}$-MA macromonomer. Assuming the very low concentration of the stabilizer used compared to styrene, the rate of styrene polymerization may be approximated as the overall rate of polymerization for this system, *i.e.*, before the nucleation step:

$$R_p = k_p[styrene^{\circ}][styrene] \quad (Eq.\,3.3)$$

where k_p is the propagation rate constant for the styrene polymerization.

According to the steady state assumption, the growing oligoradical concentration is constant which means that the rate of initiation is equal to the rate of termination. The authors supposed that the termination was carried out mainly by chain transfer reactions.

$$2fk_d[AIBN] = k_{tr}[styrene^{\circ}][X] \quad (Eq.\,3.4)$$

where X could be monomer, polymer, initiator and other species, f the AIBN efficiency, k_d the rate constant for AIBN decomposition and k_{tr} the termination of styrene polymerization. Further, equation 3.5 was obtained by combining equations 3.3 and 3.4 as follows:

$$R_p = 2fk_p \frac{k_d}{k_{tr}} \frac{[AIBN][styrene]}{[X]} \quad (Eq.\,3.5)$$

The authors observed a linear correlation between the increase of the initial concentration of styrene and AIBN respectively and the increase of the initial rate of polymerization R_p. The following relationship was obtained:

$$R_P = K[styrene]_{ini}^{0.92}[AIBN]_{ini}^{0.90} \quad (Eq.\,3.6)$$

The exponent values were very closed to the ones expected from *Eq*. 3.5. This result means that the dispersion polymerization of styrene in the early stage (< 10% conversion in their conditions) is similar to a solution polymerization. However, the authors did not consider the polymerization rate in the presence of polymer particles.

Riza *et al*.[73] studied the rate of dispersion polymerization of styrene in the presence of a MMA group-terminated PEG macromonomer (M_n = 1 000 g mol^{-1}) as stabilizer and 2,2'-azobis(2-(2-imidazolin-2-yl)propane) as initiator in an ethanol-water mixture (80/20 vol%). As particles are formed, the partitioning of monomer and initiator determines the rates of polymerization in the two phases. The overall rate of dispersion polymerization should be written as follows:

$$R_P = R_{P\ in\ particles} + R_{P\ in\ continuous\ phase} = k_p[M]_{eq}\frac{\tilde{n}N}{N_A} + 2fk_dk_P[M]\left(\frac{[I]}{k_t}\right)^{0.5} \quad (Eq.3.7)$$

with k_p the rate constant for propagation, k_t the rate constant for termination, k_d the rate constant for decomposition of initiator, f the initiator efficiency, [I] the concentration of initiator, $[M]_{eq}$ the equilibrium monomer concentration in particles, [M] the monomer concentration in the continuous phase, ñ the number of radicals per particle, N the number of particles per unit volume and N_A the Avogadro's number.

C. Determination of the polymerization locus

The partitioning behaviors of the monomer, initiator, radicals and, to a lesser extent, solvent are determined by thermodynamics. Lu *et al.*[74] proposed a thermodynamic model for the simulation of monomer partitioning behavior based on Flory-Huggins theory[75] as extended by Morton *et al.*[76] in the dispersion polymerization of styrene in ethanol initiated by ACPA or AIBN and stabilized with PVPK-30 and AOT 100 at 70 °C. This simulation showed that the monomer concentration in the two phases decreased during the polymerization and also that it was relatively low in the particles, as shown in Figure 71.

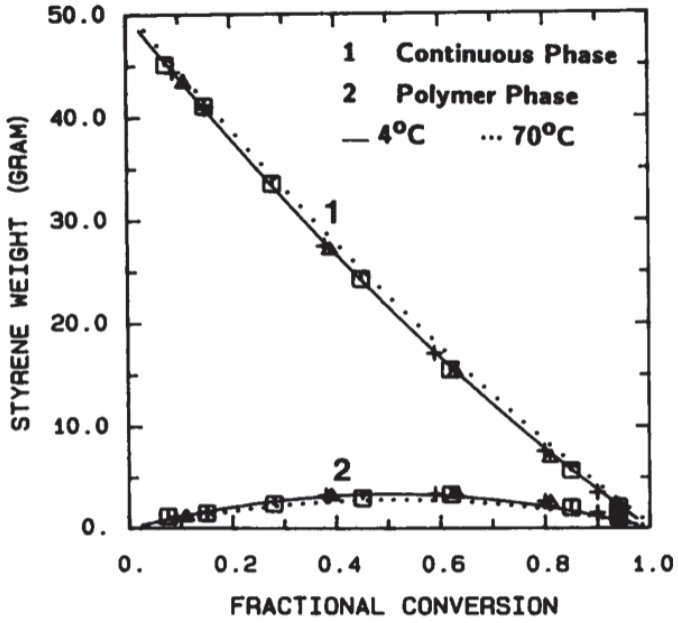

Figure 71. *Simulation of styrene partitioning in continuous phase (lines 1) and particle phase (lines 2) versus conversion at 4 °C and 70 °C with the calculated data (spots) based on the experimental results.*[74]

It is also independent of the stabilizer concentration but strongly dependent on the initial monomer concentration. The partition coefficient of styrene, defined as the ratio of the concentration of styrene in the particle phase to that in the continuous phase, increased slightly from 0.8 at 5% conversion to 1.1 at 95% conversion. At the early stage of polymerization (< 5% conversion), the precursor particles already contained a volume fraction of PS of about 0.7. It increased with conversion. It should be noted that a small amount of ethanol is absorbed in the polymer particles (0.1–1% of the total ethanol). Based on their simulation of partitioning behavior, the authors determined that the styrene and the initiator were mainly located in the continuous phase where the polymerization should occur similarly to solution polymerization.[74] However, as shown in Figure 72, under the same reaction conditions, the kinetic study showed significant differences between dispersion and solution polymerization, suggesting that the polymerization also occurred in the polymer particles in the case of a dispersion process, with a relatively marked gel effect. The authors also noticed that the rate of polymerization was dependent on initial monomer concentration and independent of initiator concentration at higher conversion (> 50% conversion).

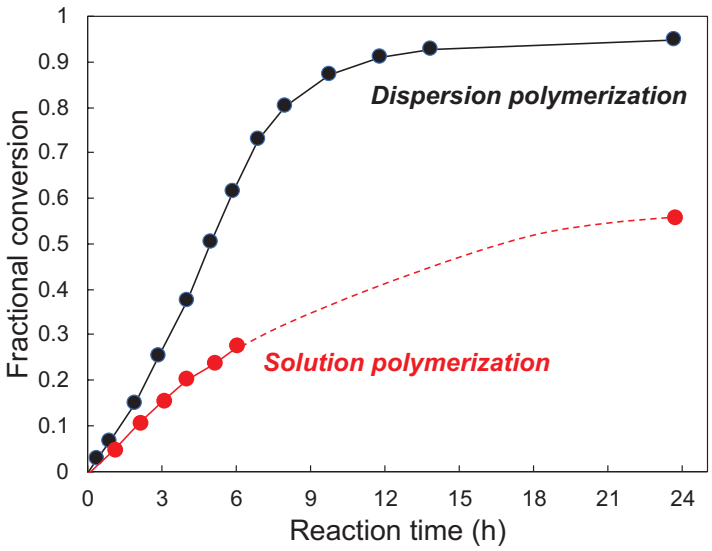

Figure 72. *Conversion-time curves of dispersion (dark line) and solution (red line) polymerization of styrene under the same reaction conditions but without stabilizer in the latter case. Experimental conditions: styrene 25 wt.%, AIBN 1 wt.% based on styrene, PVPK-30 2.33 wt.% based on ethanol and Aerosol OT 0.67 wt.% based on ethanol.*[74]

However, their study did not include the more general case where water is also present in the system. Indeed, the addition of water has a strong effect on the partitioning of the monomer, resulting in a even more significant gel effect. Lacroix-Desmazes and Guillot[13] studied the partitioning behavior of styrene in dispersion polymerization in ethanol/water mixture initiated

by AIBN and stabilized with PVPK-30. They observed a considerable increase of the styrene partitioning in favor of the particles when water was added to the system. In comparison with the case of pure ethanol, the concentration of styrene in the particles was about 4.8 times higher in the ethanol/water mixture (70/30 vol%), but the partition coefficient was constant during the polymerization. In agreement with the observations of Lu *et al.*[74], the authors found significant effects on styrene partitioning with variation of initial styrene concentration and temperature, but the partitioning was not related to the final particle size. The presence of water led to a high capture efficiency of the oligoradicals from the continuous phase by existing particles due to the initial medium solvency and the high concentration of styrene in the particles. The authors showed that the average number of radicals per particle can reach very high values (up to several thousands) resulting in a large gel effect.

More recently, Jiang *et al.*[77] studied the kinetics of dispersion polymerization of MMA at 70 °C in methanol-water mixtures using AIBN as initiator and PVPK-30 as stabilizer. They also found that the MMA concentration decreased with time in both the continuous and the particle phase whereas the partition coefficient of MMA was constant at 0.47. This value is smaller than that reported in the styrene/ethanol system (the partition coefficient varied from 0.8 to 1.1) and in the styrene/ethanol/water system (4.8 for ethanol/water = 70/30 vol%). The authors calculated an average number of free radicals per particle of around 5 000 and thus considered that the dispersion polymerization of MMA followed pseudo-bulk kinetics.

D. Reactivity of macromonomers in copolymerization

Another important feature of dispersion polymerization reactions is the reactivity of the macromonomers used to stabilize the latex particles. Indeed, homopolymerization of the macromonomer can occur when high local concentrations are present. Capek *et al.*[78] reported that in ethanol-water mixture (80/20 vol%) and in the presence of methacryloyl-terminated poly(ethylene oxide) (MMA-PEO, M_n = 1 000 g mol^{-1}), the macromonomer MMA-PEO was found to polymerize more slowly than styrene. The authors attributed this observation to the enhanced diffusion control of the propagating steps and the low reactivity of the propagating radicals with the macromonomer. According to their experimental conditions, the styrene concentration is higher than the macromonomer concentration (3 mol% based on monomer). The Jaacks method was applied to determine the styrene reactivity ratio ($r_{styrene}$).[79] Capek and co-workers found $r_{styrene}$ = 1.30 (below 10% conversion). This value suggested that styryl

radical preferentially added to a styrene unit under the experimental conditions mention above ($k_{styren\text{-}styrene} > k_{styrene\text{-}MMAPEO}$).

Ito *et al*.[80] reported the monomer reactivity ratios for copolymerizations of styrene with PEO methyl ether methacrylate, with different molecular weights (n = 1, 2, 3, 25, 35 and 62 EO units). The authors determined the monomer reactivity ratios by using the method ok Kelen and Tüdös (Table 18).[81] The monomer reactivity ratios indicated that the copolymers obtained were clearly random in sequence distribution. However, beyond 3 units of EO, there is a widening gap between the molar composition of the copolymer. Then, the authors also applied the method of Jaacks and showed that the reactivity of the macromonomer decreased with increasing the molecular weight of the latter.

Table 18. *Monomer reactivity ratios for copolymerizations of styrene and PEO-MMA.*[81]

n (EO unit)	$r_{styrene}$	$r_{PEO\text{-}MMA}$
1	0.37 ±0.13	0.43 ±0.05
2	0.38 ±0.08	0.52 ±0.09
3	0.49 ±0.09	0.44 ±0.08

Lacroix-Desmazes and Guyot[39,82] determined the conversion of the $(PEO)_{51}$-MA macromonomer during the dispersion polymerization of styrene at 70 °C in ethanol-water mixture (95/5 vol%), a fixed solids content at 11 wt.% and 1 wt.% of $(PEO)_{51}$-MA based on styrene. Figure 73 shows that at the beginning of the polymerization, the macromonomer was moderately consumed to form just enough graft copolymers which adsorbed on the primary particle surface to prevent them from coagulation. At the end of the polymerization, more consumption of the macromonomer occurred with an increase of the incorporation yield. The authors believed that the residual styrene in the continuous phase and the macromonomer formed graft copolymers that were probably not so strongly anchored on the particle surface, due to small amount of styrene units contained in the graft copolymer.

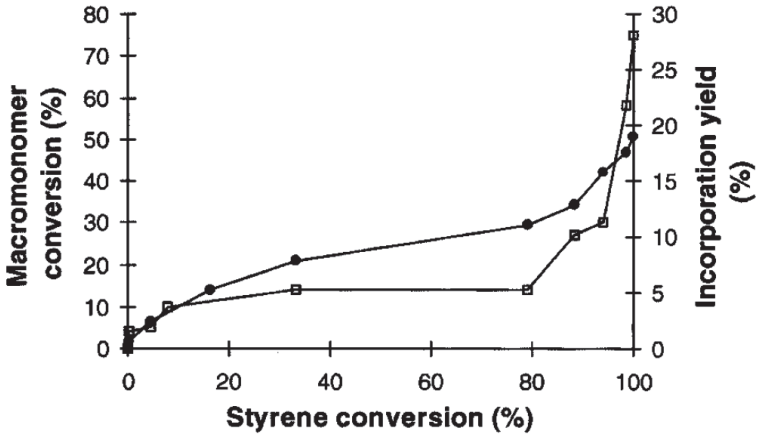

Figure 73. *Conversion of the $(PEO)_{51}$-MA macromonomer (sphere) and incorporation yield (square) vs. styrene conversion.*[39,82]

To conclude, in a dispersion polymerization process there are two polymerization loci: the polymer phase and the continuous phase. The monomer partitioning conditions the kinetics of polymerization. However, it is difficult to generalize the kinetics of dispersion polymerization since it is strongly dependent on the choice of system components and in particular on the solvency of the reaction medium and the particle size.

V. Photo-induced dispersion polymerization: from free radical photopolymerization to photo-PISA

The interest for photoinitiation in dispersion polymerization results from the transparency of the reaction medium in the early stages of the polymerization. However, the photopolymerization in dispersion has barely been reported. Indeed, in a photopolymerization process, the decomposition rate of the photoinitiator is very fast, especially under UV light irradiation compared to thermally activated initiator, which leads to the generation of a large number of radicals. These radicals then produce instantaneously a high concentration of oligoradicals that aggregate rapidly to form precursor particles. Therefore, the stabilization is crucial since the collision between these precursor particles should be more frequent resulting in the formation of very large particles before enough stabilizer would adsorb onto them to provide stability. Consequently, the formation of large particles causes light scattering effects and thus, a reduction of the light penetration. Nevertheless, a few studies have demonstrated the possibility to prepare synthetic latexes by UV irradiation in free radical dispersion polymerization. Over the past five years, a renewed interest has been emerging in the

development of new polymerization technique such as (PISA). The following sections will present different studies carried out in photo-dispersion using three methods: (1) free radical polymerization, (2) reversible-deactivation radical polymerization and (3) PISA.

A. Free radical polymerization in photo-dispersion

Chen *et al*.[83] reported in 2008 the photoinitiated free-radical polymerization of MMA in ethanol/water mixture in the presence of PVPK-10 as stabilizer and Darocur 1173 as photoinitiator (Figure 74). Within 30 min of UV irradiation at room temperature, they obtained uniform latex particles with a monomer conversion over 90% and particle diameters around 1 µm under optimum conditions. The authors studied several parameters which have an impact on particle size and size distributions (concentration of stabilizer, monomer and photoinitiator, and the solvency). The particle size decreased with increasing the stabilizer concentration, as observed in the case of conventional thermal initiated dispersion polymerization. They also found a linear relationship between the particle size and the PVP concentration with a slope of – 0.44, again in agreement with thermal initiation.[63,66] Likewise, the particle size increased with increasing the photoinitiator concentration.

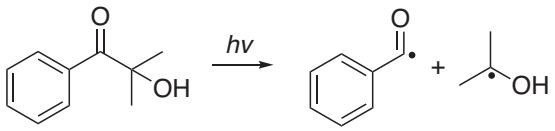

Darocur 1173

Figure 74. *UV irradiation of the photoinitiator Darocur 1173 for the dispersion photopolymerization of MMA.*

The authors observed that at high solvency of the medium (obtained for high ethanol contents), the stabilization became inefficient resulting in non-spherical particles (Figure 75d). Indeed, by increasing the solvency of the medium (i.e., a good solvent for the PVP stabilizer), larger and fewer particles were obtained as predicted by Paine, due to very low adsorption of the PVP-*g*-PMMA graft copolymer onto the primary particles, intensifying the coalescence among these nuclei. Moreover, it should be noticed that photoinitiation brings another complexity to the mechanistic comprehension of dispersion polymerization because of the resulting high decomposition rate constant.

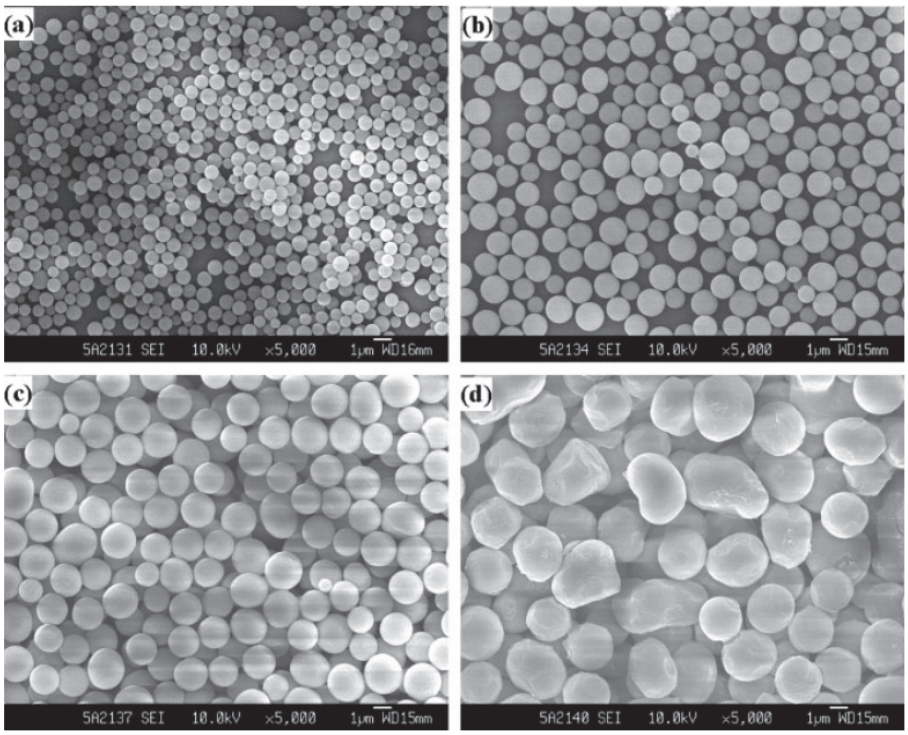

Figure 75. *SEM images of PMMA latexes obtained by photoinitiated dispersion polymerization of MMA with different ethanol/water ratios (wt./wt.): (a) 35/65; (b) 45/55; (c) 50/50; (d) 55/45.*[83]

A study on parameters influencing the particle size and the particle size distribution, such as initiator, stabilizer and monomer concentrations, the solvency of the reaction medium and the UV light intensity was reported by Huang *et al.* in 2010.[84] The authors prepared poly(MMA-*co*-methacrylic acid) microspheres with carboxyl groups on their surface under UV irradiation at 20 °C in ethanol/water mixtures with AIBN as photoinitiator and PVP (molecular weight not mentioned) as stabilizer. A complete conversion was reached after 24 h. The authors studied the effect of UV light intensity (from 0.15 to 0.5 mW cm^{-2}) on the particle size and size distribution (Figure 76). A decrease in UV light intensity led to larger particles with wider size distributions. The decomposition rate of AIBN decreased due to the lower photon flux transmitted. Consequently, the nucleation stage should be extended with a possible secondary nucleation which widened the size distributions.

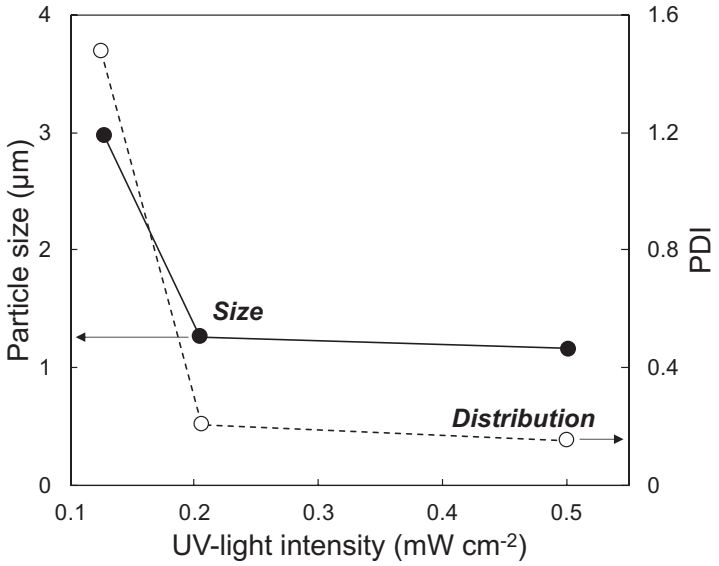

Figure 76. *Effect of UV light intensity on the size and size distribution of poly(MMA-co-MAA) microspheres synthesized by photo-dispersion polymerization in a water/ethanol mixture (60/40 in volume) using AIBN at 4 wt.% and PVP at 20 wt.% based on monomers.*[84]

Another study under very similar conditions was reported by Zhu and co-workers.[85] Poly(styrene-*co*-maleic anhydride) microspheres were prepared at higher UV light intensity (0.7 mW cm^{-2}). A secondary nucleation was also observed.

B. Reversible-deactivation radical polymerization in photo-dispersion

RDRP techniques have also been developed in dispersion photopolymerization. Among them, reversible addition-fragmentation chain transfer (RAFT)[86] is very popular because of its mild reaction conditions (absence of heavy metals, compatibility with a large range of monomers and solvents). This technique also leads, via different strategies, to latex particles with controlled molecular weights, well-defined surface functionalities and narrow size distributions.[46]

In 2003, Shim *et al.*[87] described the dispersion photopolymerization of styrene via RAFT at 50–70 °C in ethanol in the presence of PVP (M_n = 40 000 g mol^{-1}) as stabilizer and AIBN as photoinitiator. They synthesized and used the 4-thiobenzoyl sulfanylmethyl-benzoic acid RAFT agent (Figure 77a). A 365 nm UV lamp was used to initiate the polymerization. The number average particle size was comprised between 0.68 and 0.99 µm, and the polydispersity index (D_w/D_n value determined by microscopy) ranged from 1.26 to 2.51, which corresponds

to relatively broad particle size distributions. This also indirectly means a lack of molecular weight control. Moreover, AIBN should be also thermally activated (50–70 °C) and the authors did not mention its contributions as photoinitiator. Shim and co-workers also indicated that the increase in D_w/D_n was due to the photo-degradation of PVP during polymerization.[88] Ki *et al*.[89] also reported the dispersion photopolymerization of styrene under similar conditions with a P4VP-based macro-RAFT agent (Figure 77b) as both macro-initiator and stabilizer (but not enough to control the growth of the polymer chains like in PISA – see below); however the authors did not find a significant improvement in the size distributions.

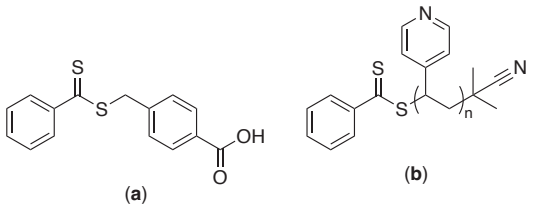

Figure 77*. Chemical structure of* ***(a)*** *4-thiobenzoyl sulfanylmethyl-benzoic acid RAFT agent and* ***(b)*** *P4VP macro-RAFT agent.*

Then, in 2012, Tan *et al.*[90] obtained for the first time highly monodisperse particles by RAFT dispersion photopolymerization of MMA in the presence of PVPK-30 with Darocur 1173 as photoinitiator under visible light (LED light intensity = 0.8 mW cm^{-2}). Three kinds of trithiocarbonates were employed as RAFT agents and the final conversion reached 90% after 3 h. The combination of photoinitiation and a RAFT process overcomes the problems related to the high rate of photoinitiated polymerization which induces a nucleation too rapid for the stabilizer to have enough time to stabilize the nuclei effectively. The photoinitiated RAFT dispersion polymerization process is illustrated in Figure 78.

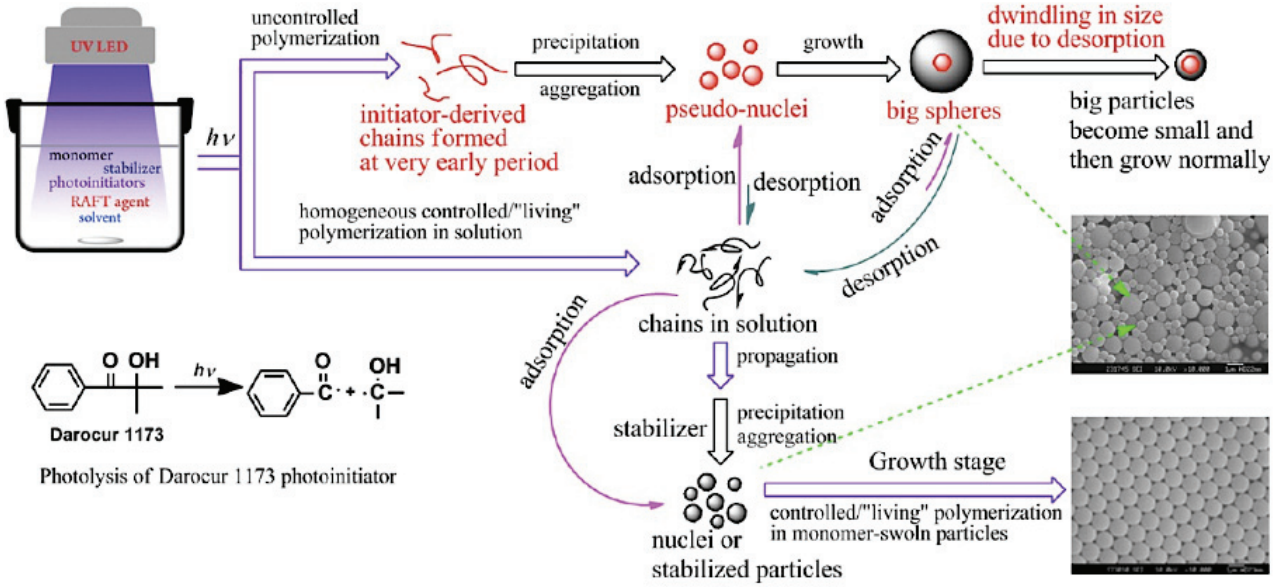

Figure 78. *Illustration of the photoinitiated RAFT dispersion polymerization reported by Tan et al.*[90]

According to the SEM images of the particles formed at different times when the RAFT agent was added initially, a lot of particles with small and large sizes were formed at the beginning of the reaction, but the larger ones disappeared at the end of the nucleation stage. The presence of large particles was only observed in the case of RAFT process. On the one hand, the use of RAFT agent led to a large amount of controlled polymer chains that propagated gradually and then precipitated to form precursor particles. But, on the other hand, at the same time, uncontrolled polymer chains generated from the photoinitiator decomposition should propagate rapidly and then precipitate to form what the authors called "pseudo-nuclei". According to them, the formation of large particles was due to the absorption of a fraction of controlled polymer chains before they precipitated. The disappearance of the large particles was related to the equilibrium between the adsorption/desorption of the short polymer chains to the particles. Indeed, at the early stage of the reaction, the controlled polymerization generated soluble short polymer chains absorbed by the "pseudo-nuclei" from the solution. Then, the temporary large particles must act as a reservoir for the short polymer chains.

Tan and co-workers are clearly the pioneers of RAFT dispersion photopolymerization. They investigated the use of a macro-RAFT agent as stabilizer for RAFT dispersion photopolymerization of PMMA.[91] The *in situ* formation of block copolymers led to the preparation of PMMA microspheres stabilized by poly(methoxy poly(ethylene glycol) acrylate) chains. They also introduced the macromonomer methoxy-poly(ethylene glycol) methacrylate (M_n = 2 000 g mol^{-1}) as the hydrophilic steric stabilizer of PMMA microspheres[92], they studied the influence of the structure of the RAFT agent on the particle morphology[93], they evidenced

the encapsulation of lanthanide nanoparticles[94], and reported the formation of monodisperse cross-linked PMMA microspheres as welle as the preparation of amine-functionalized poly(glycidyl methacrylate) microspheres for various applications.[95]

C. Polymerization-induced self-assembly in photo-dispersion

Dispersion photopolymerization has witnessed a renewed interest since 2015 with the extension of PISA to photopolymerization.[15,16] In PISA formulations in dispersion polymerization, a solvophilic macro-CTA or a macroinitiator is used to polymerize a soluble monomer. The chain extension of the first block by a solvophobic segment leads to the formation of diblock copolymers that self-assemble *in situ* to generate a diverse set of nano-objects with various morphologies (micelles, vesicles, worms…). It should be noticed that the mechanism of particle formation is different from that of conventional dispersion polymerization, even if the reaction starts in a homogeneous solution in both cases.

The first example of photo-PISA was reported by Cai and co-worker in 2015 with the polymerization of diacetone acrylamide (DAAm) using a water-soluble poly(2-hydropropylmethacrylamide) ($PHPMA_{166}$) macro-RAFT and sodium phenyl-2,4,6-trimethylbenzoylphosphinate (SPTP) as photoinitiator under visible light irradiation at 25 °C (Figure 79).[96] The insolubility of the P(DAAm) block led to the *in situ* formation of broadly defined spherical nanoparticles with fast polymerization rates reaching high monomer conversions after one hour of irradiation. The authors extended their system to original approaches to conduct photo-PISA: the use of polyion complexation (PIC-PISA) in the presence of anionic poly(sodium 2-acrylamido-2-methylpropanesulfonate) as PIC-template[97] and the synthesis of nanotubes via hydrogen bonding-driven polymerization-induced self-assembly (HB-PISA).[98]

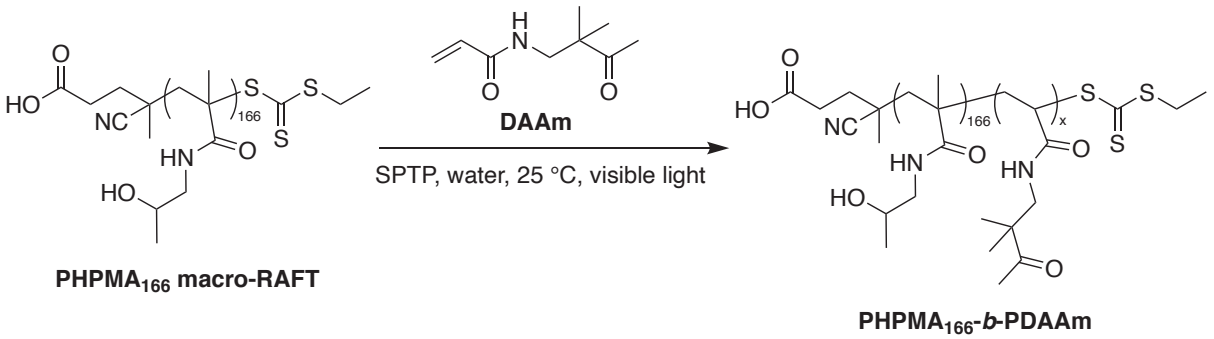

Figure 79. *PISA via RAFT aqueous dispersion polymerization using a PHPMA macro-RAFT.*[96]

A growing number of studies have since been conducted to extend the photo-PISA technique to other monomers and macro-CTAs, varying the type of the photoinitiators and the wavelength employed. These researches on photo-PISA have been reviewed by Yeow and Boyer and categorized according to the mechanism of radical production (Figure 80).[14] The Boyer group developed a photoinduced electron transfer-reversible addition-fragmentation chain transfer (PET-RAFT) polymerization to form nanoparticles with various morphologies, such as spherical micelles, worm-like micelles and vesicles, at room temperature.[99,100] They used a ruthenium-based photo-redox catalyst, $Ru(bpy)_3Cl_2$, to regulate the dispersion polymerization of benzyl methacrylate in ethanol in the presence of poly(oligo(ethylene glycol) methyl ether methacrylate) macro-CTA under blue light irradiation. However, the polymerization rates were rather low. The final monomer conversion reached 73% after 24 h. The same group worked on another photo-redox initiating system based on 5,10,15,20-tetraphenyl-21*H*,23*H* zinc porphyrin (ZnTPP) used as catalyst under low energy red or yellow light.[101] Indeed, as discussed in Chapter 1, an increase in wavelength leads to a reduction of light scattering and thus an improvement of the light penetration. Different morphologies were obtained at high monomer conversions (>98%) after 48 h.

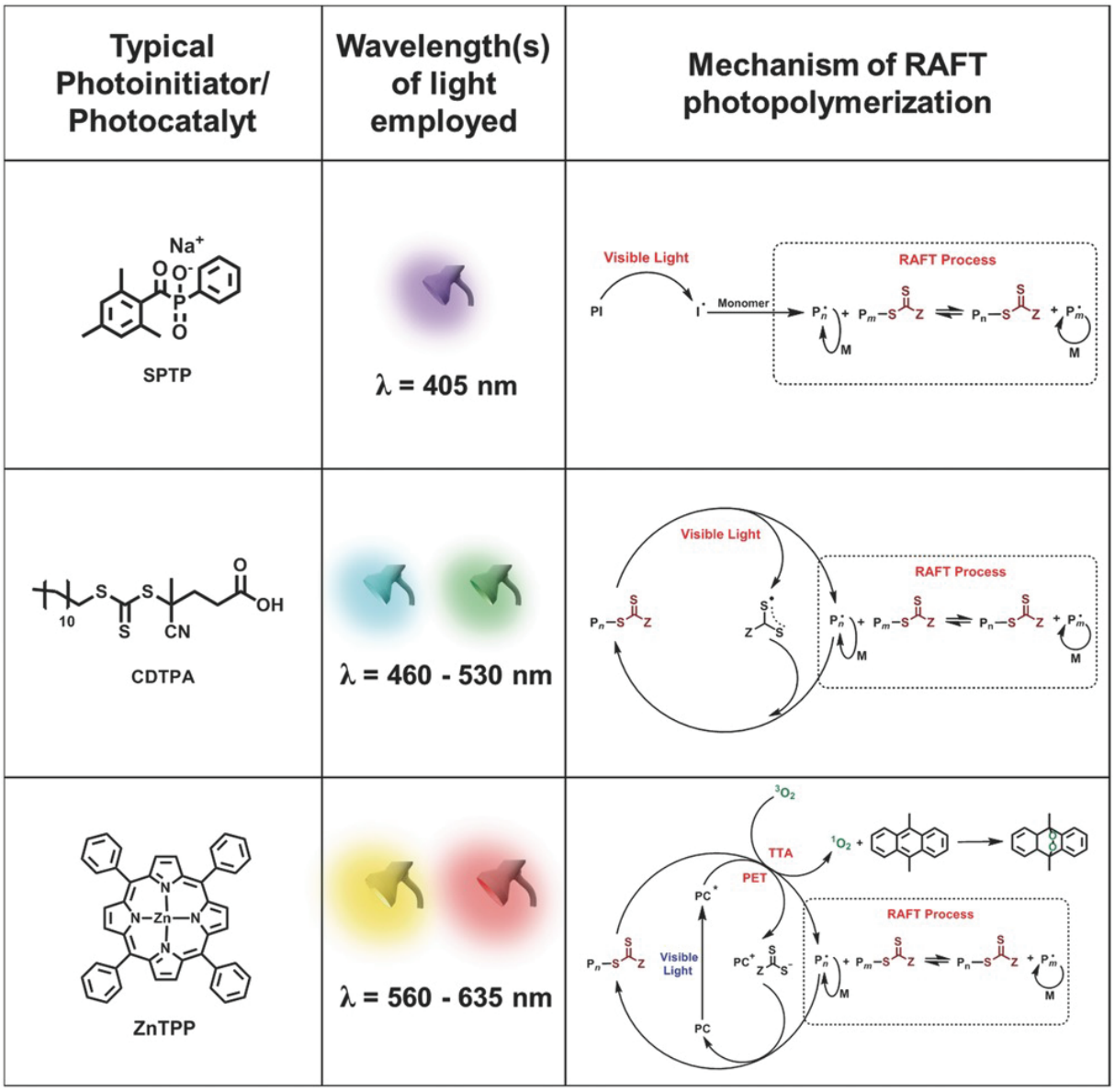

Figure 80. *Different mechanisms for initiating PISA polymerizations under visible light: photoinitiator (PI) (top row), photoiniferter (middle row) and photocatalyst (PC) (bottom row) approaches.*[14]

Zhang and coworkers reported dispersion photo-PISA by employing purple LED (λ_{max} = 405 nm, 0.46 mW cm^{-2}) with SPTP as photoinitiator to polymerize 2-hydroxypropyl methacrylate in water with the presence of mPEG$_{113}$-4-cyano-4-(ethylthiocarbonothioylthio) pentanoic acid (CEPA) as macro-RAFT agent as illustrated in Figure 81.[102–104] The same group also described the dispersion photo-PISA of isobornyl acrylate in hydroalcoholic mixtures.[105,106] The authors showed that the photo-PISA process has considerable potential for the formation of bio-related stimuli-responsive nano-objects in comparison to conventional thermally initiated PISA. Furthermore, the low polymerization temperature made the encapsulation of sensitive proteins easier.[107]

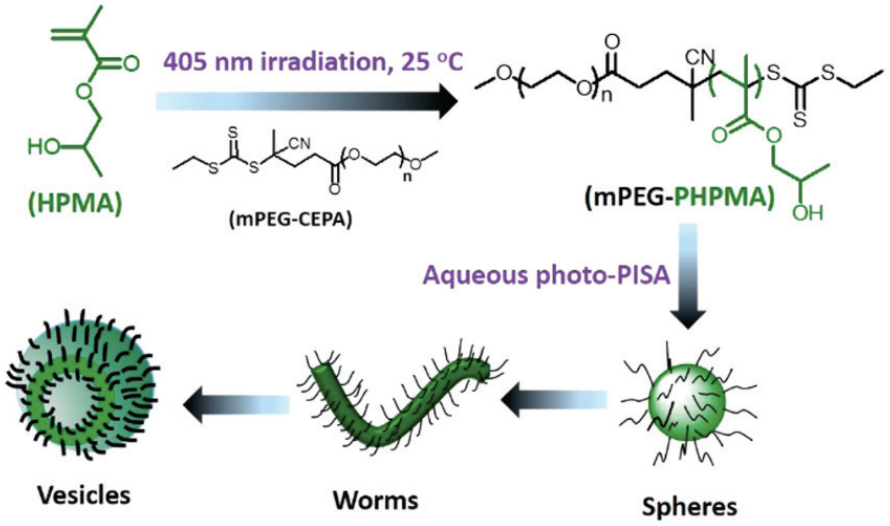

Figure 81. *Scheme for preparation of various nanoobjects via aqueous photo-PISA.*[102]

Very recently, Tkachenko *et al.*[108] prepared diblock copolymer nanoparticles by photo-PISA in dispersion. First, the solvophilic poly(hydroxyethyl acrylate) ($PHEA_{25}$) block was synthesized by using a S-cyanomethyl-S-dodecyltrithiocarbonate (TTC) macro-RAFT agent that undergoes a reversible β-fragmentation under blue light irradiation. Subsequently, styrene (20 wt.% solids content) was added to the $PHEA_{25}$-TTC macro-RAFT agent in a methanol-water mixture (95/5 wt.%) at 35 and 55 °C under blue light irradiation. Very small particles (20–40 nm) with narrow size distributions were obtained. The authors then considered the issue of optical properties during the polymerization. In the 500–800 nm range, no absorption was observed, meaning that only scattering could be taken into account. Indeed, as very small particles were formed, the experimental values of scattering coefficient S_λ were in agreement with the Rayleigh scattering, *i.e.*, S_λ proportional to the inverse of the wavelength to the power four. In the 280–500 nm range, the $PHEA_{25}$-TTC macro-RAFT agent absorbs (K_λ^{TTC}) with a maximum absorption at 310 nm. The authors showed a diminution of the K_λ^{TTC} during the dispersion photopolymerization. The same trend was obtained in the case of solution polymerization (i.e., without the particle formation), suggesting that the microenvironment variation of the $PHEA_{25}$-TTC macro-RAFT agent was not accountable and thus a photodegradation of the latter may occur.

In summary, despite the transparency of the reaction mixture in early stages offered by the dispersion polymerization process, the number of studies on the use of UV-visible light to initiate polymerization remains rather limited, certainly due to the intrinsic complexity of this technique. To overcome this limitation, dispersion photo-PISA process was investigated at longer wavelengths of light (red region) to control the polymerization. However, this recent technique remains so far dedicated to the synthesis of block copolymers nanoparticles.

In the follow part, we will introduce our PIS developed in emulsion polymerization (Chapter 2) to the dispersion polymerization of styrene under visible light irradiation. The aim was to take advantage of the dispersion process, i.e., the initially homogeneous medium and its transparency, and to reach much larger particles than those obtained in emulsion (max. 300 nm).

Part 2. Our three-component photoinitiating system applied to dispersion polymerization

We have introduced in Chapter 2 a water-soluble PIS that can deliver, under visible light, very stable latexes by aqueous emulsion polymerization. As a reminder, it consists of a Boron-based co-initiator that can be activated upon H transfer to a photogenerated thiyl radical.[109] We have shown that our photoinitiating system is capable of initiating the emulsion photopolymerization of styrene and acrylic monomers, and leads to particles with diameters ranging from 50 to 300 nm and solids contents up to 30%.

However, we showed that the different species of the photoinitiating system can partition between the different phases of the system (water, monomer droplets and particles) resulting in some cases in broad particle size distributions. Also, due to the presence of the monomer droplets and/or micelles at the beginning of the reaction and of growing particles afterward, the light might be subject to scattering effects limiting the penetration within the reactor and thus limiting the generation of radicals.

Our objective in this chapter was to focus on the dispersion photopolymerization process because we thought that the transparency of the reaction medium to the visible-light irradiation before polymerization would be beneficial. That is why we wanted to evaluate the potential of dispersion photopolymerization of styrene with our PIS. The aim was to obtain particles larger than emulsion polymerization allows so far (*i.e.*, 300 nm). Indeed, as discussed in Chapter 1, the scattering efficiency reached a maximal value for a particle size near the selected wavelength and decreases until it reaches a plateau with increasing particles size. In this way, the light should be less subjects to scattering and better penetrates within the reaction medium.

As a reminder, the PIS is composed of acridine orange (**1**), a dicarboxylic acid aryl disulfide (**4**) and NHC-BH_3 (**3**) (Figure 82). All the experiments have been performed in water/ethanol mixtures. As mentioned in Part 1, dispersion polymerization requires the use of a stabilizer. In our study, two macromolecules have been investigated: a PEG macromonomer (*i.e.*, poly(ethylene glycol) methyl ether methacrylate, PEGMA, M_n = 2 080 g mol^{-1}) and PVP-K30 (M_n = 40 000 g mol^{-1}).

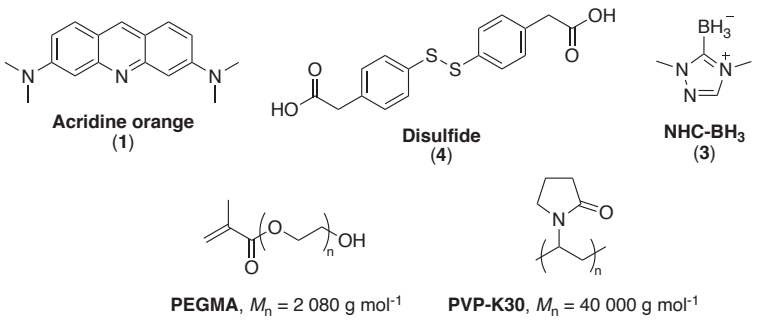

***Figure 82**. Chemical structure of the PIS and the two stabilizers, PEGMA and PVP-K30, used for the dispersion photopolymerization of styrene under visible light irradiation.*

I. Dispersion photopolymerization of styrene with PEGMA

A. Transposition from emulsion to dispersion: robustness of our photoinitiating system

The first series of experiments was run with PEGMA, a macromonomer commonly used in dispersion polymerization leading to graft copolymers strongly adsorbed onto the particle surface.[39,110] As a first step, the reproducibility of the synthesis was investigated (Table 19).

***Table 19.** Reproducibility of dispersion polymerizations of styrene stabilized with PEGMA (18 wt.% based on styrene) under visible light. [a]*

Run	Time (h)	Conv. (%)	D_h[b] (nm)	PDI[b]	D_n[c] (nm)	D_w/D_n[c]	N_p (x10^{15} cm^{-3})	M_n[d] (g mol^{-1})	$Đ$[d]
1	22.3	82	129	0.07	118	1.10	8.9	78 000	6.2
2	24.6	90	143	0.01	143	1.10	5.6	87 000	4.9
3	23.7	92	144	0.04	152	1.09	5.2	91 000	5.1

[a] Experimental conditions: reaction temperature fixed at 40 °C, ethanol/water = 70/30 (wt.%). The solids content was fixed at 10 wt.%, PEGMA at 18 wt.% relative to styrene. [AO] = 1.3 10^{-5} mol L^{-1} (1 mol% with regard to NHC-BH_3), [disulfide] = 6.3 10^{-4} mol L^{-1} (50 mol% with regard to NHC-BH_3) and [NHC-BH_3] = 1.3 10^{-3} mol L^{-1}.
[b] Determined by dynamic light scattering (DLS).
[c] Determined by transmission electronic microscopy (TEM).
[d] Determined by size-exclusion chromatography in THF (SEC–THF).

The three conversion curves of styrene as a function of reaction time with 18 wt.% of PEGMA (based on styrene) are plotted in Figure 83 and show the reproducibility of the dispersion photopolymerization of styrene. Conversion reached approximately 90% after 24 h of

irradiation (temperature controlled at 40 °C) and the latexes obtained were stable without any presence of coagulum. The reaction started from a homogeneous solution containing our three-component PIS, styrene, PEGMA and the ethanol/water mixture. The radicals generated from the PIS add to styrene units and form oligomers that precipitate when they reach a critical chain length. Enough graft copolymer chains are likely formed at the same time to stabilize the primary particles, even if as mentioned in Part 1.IV.D, the macromonomer PEGMA was found to polymerize more slowly than styrene.[30,80]

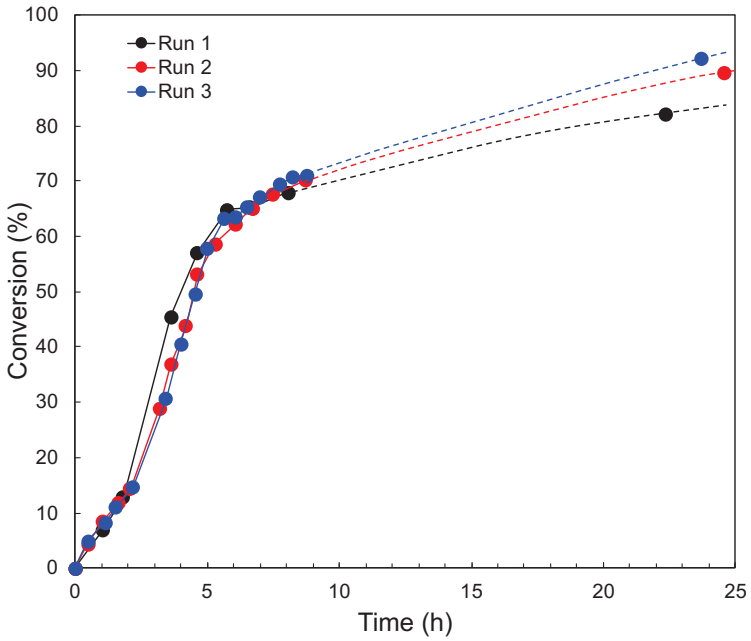

Figure 83. *Reproducibility – Evolution of conversion with time for dispersion photopolymerization of styrene with the stabilizer PEGMA, 18 wt.% based on styrene (experimental conditions are mentioned in Table 19).*

The average hydrodynamic particle diameters (D_h) of the final latexes measured by DLS were similar with respectively 129 nm, 143 nm and 144 nm, and low polydispersity indexes (PDI ≤ 0.07) were obtained in all cases. The slightly lower particle size reached in run 1 could be related to the lower conversion attained (the reaction was stopped before reaching 90 % conversion). The number average TEM particle diameters (D_n) follow the same trend. Contrary to DLS measurements, TEM images and the corresponding size histograms in Figure 84 show broad particle size distributions. This is attributable to the fact that DLS emphasizes larger objects at the expense of smaller ones. It is worth mentioning here that size distributions are usually narrow in thermally initiated dispersion polymerization, as will be discussed later (see Table 23, run 13). Finally, the similar molar masses obtained at the end of the polymerizations further confirm the good reproducbility of these experiments (Table 19).

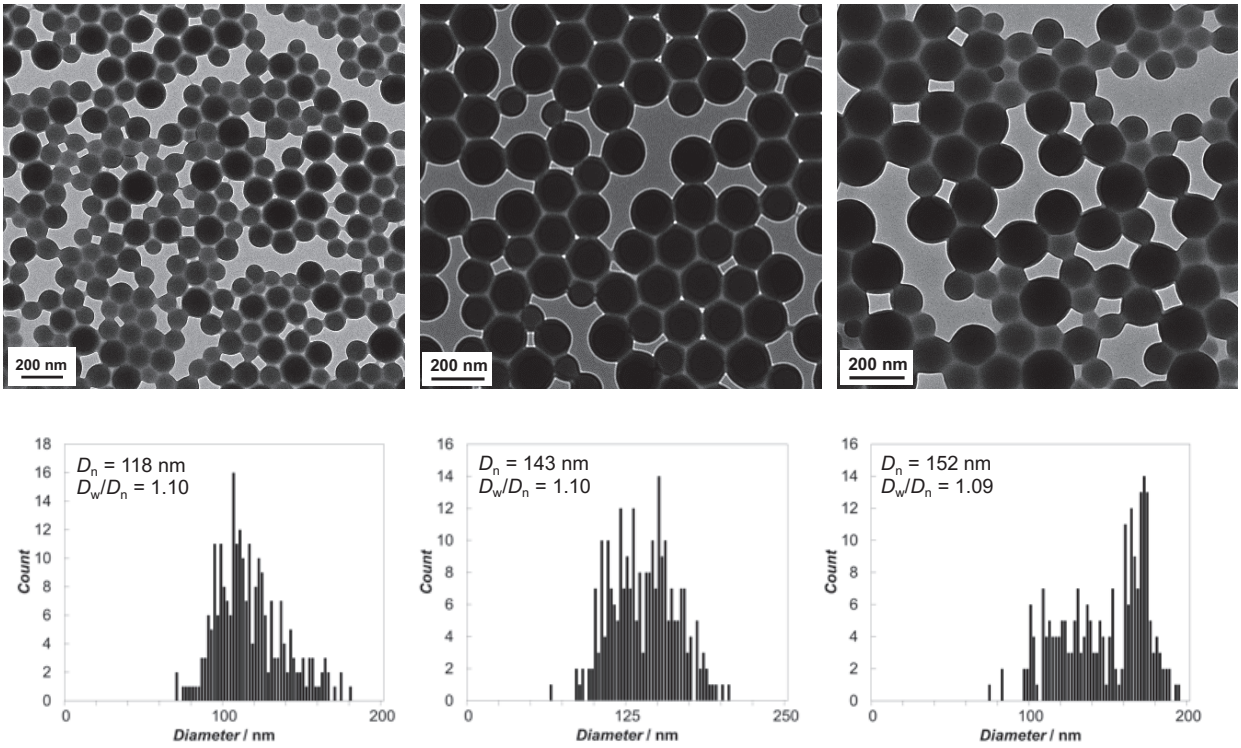

Figure 84. *TEM images and particle size distributions of the latexes obtained in the conditions described in Table 3, entries 1 (left) 2 (middle) and 3 (right). See Table 19 for more experimental details.*

As mentioned above, the experiments are reproducible, and the conversion profiles all exhibit a sigmoidal shape, commonly observed in dispersion polymerization. Barrett and Thomas suggest that a sigmoidal shape of the time-conversion curve is characteristic of an auto-acceleration (gel effect) in the polymerization rate.[71] It corresponds to an increase in the viscosity inside the particles where a large number of radicals coexist. These authors worked on MMA polymerization in *n*-dodecane, but further studies indicate that the dispersion polymerization of styrene in ethanol/water proceeds similarly.[30,72,78] In our study, we observe a gel effect which indicates that despite the small particles size, radicals can coexist in the same particle, probably due to high viscosity. The main locus of the polymerization being the particles once they are present, we believe that the accelerations can also be attributed to the rapid capture of the radicals by the small particles that are produced (for a similar solids content, the total area available for the capture of the radicals is much higher for small particles).[82] According to this, the observed auto-acceleration could be thus the result of two combined effects: i) a higher radical capture and ii) a relatively low monomer concentration in the particles resulting in a high internal viscosity, and hence a lower probability of radical termination.

In addition, the three-component PIS may partition between the continuous phase and the monomer-swollen particles, and therefore, it is also possible that the generation of radicals not only occur in the continuous phase but also directly in the polymer particles. As the monomer-

swollen PS particles do not absorb the visible light, the PIS potentially located in the polymer particles can also be activated by irradiation. Scattering effects would still occur, which would lead to a local attenuation of the energy, but undoubtedly sufficient to activate the PIS. There could be also reflection phenomena but that would just deviate the incident radiation without a loss of energy. Therefore, the presence of PIS in the monomer-swollen particles may also accelerate the polymerization.

As reported in the litterature[29,39], compared to the use of a stabilizer such as PVP, the use of the macromonomer should enhance the stabilization of the particles and thus rapidly fix the number of particles. However, we observed relatively broad particles size distributions. We believe that the photoinduced initiation step produces radicals rather slowly and continuously, leading to a slow and continuous nucleation, which would contribute to broaden the particle size distribution. In comparison, when AIBN is used as initiator, the nucleation is considered to be very fast which consequently leads to the rapid formation of precursor particles. The oligomers that are generated in the continuous phase enter in the precursor particles before they precipitate, leading therefore to a narrow size distribution unlike the case of the photopolymerization process.[111]

We systematically observed a slowing down of the polymerization after 60 % conversion. This may due to the reduced styrene concentration both in the polymer particles and in the continuous phase. Moreover, as the reaction progresses, the medium became turbid, limiting the light penetration within the reaction due to scattering effects. This could reduce the efficiency of our PIS, explaining the decrease in polymerization rate at high conversions.

B. Effect of the photoinitiator concentration

We then studied the influence of the photoinitiator concentration on the particle size and the polymerization kinetics. The results are reported in Table 20. The concentration of each component of the PIS was varied at the same time (run 4) or only that of NHC-BH_3 and disulfide (run 5).

***Table 20**. Effect of photoinitiator concentration on the dispersion polymerization of styrene under visible light.[a]*

Run	*c*(AO) (mmol L^{-1})	*c*(NHC-BH_3) (mmol L^{-1})	Time (h)	Conv. (%)	D_h[b] (nm)	PDI[b]	D_n[c] (nm)	D_w/D_n[c]	N_p(x10^{15} cm^{-3})	M_n[d] (g mol^{-1})	$Đ$[d]
3	0.013	1.3	23.7	92	144	0.04	152	1.09	5.2	91 000	5.1
4	0.026	2.6	30.3	78	168	0.01	165	1.05	3.2	75 000	3.6
5	0.013	2.6	30.1	75	157	0.04	167	1.05	2.9	70 000	3.4

[a] Experimental conditions: reaction temperature fixed at 40 °C, ethanol/water = 70/30 (wt.%). The solids content was fixed at 10 wt.%, PEGMA at 18 wt.% relative to styrene and disulfide at 50 mol% with regard to NHC-BH_3.
[b] Determined by DLS.
[c] Determined by TEM.
[d] Determined by SEC–THF.

By increasing twice the concentration of all the reagents of our PIS (Run 4), the polymerization rate decreased as illustrated in Figure 85, and the final conversion reached 78% after 30.3 h *vs.* 92% after 23.7 h at lower photoinitiator concentration (run 3). Likewise, we observed a decrease of the polymerization rate when only NHC-BH_3 and disulfide concentrations were doubled (run 5). Moreover, the particle size increased slightly when the photoinitiator concentration increased and the size dispersity was improved from D_w/D_n = 1.09 for run 3 to D_w/D_n = 1.05 for runs 4 and 5 (Figure 86).

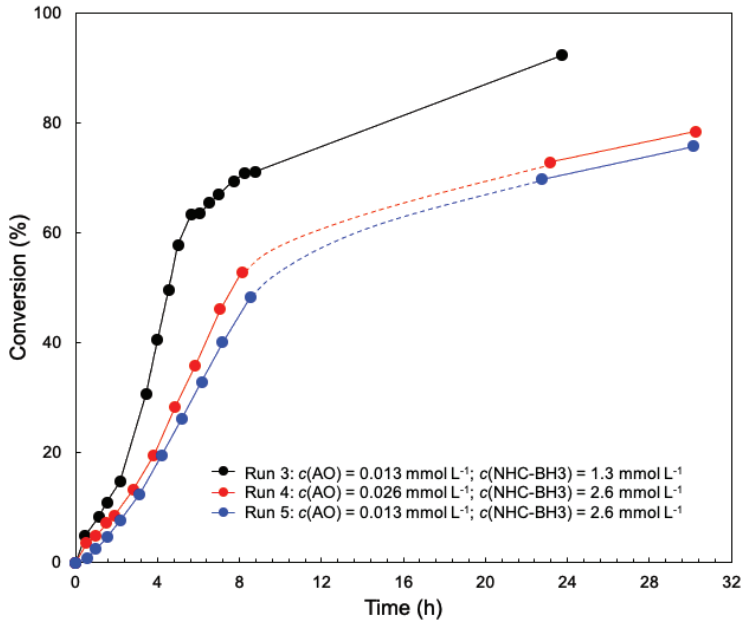

***Figure 85**. Evolution of conversion with time for dispersion photopolymerization of styrene for different photoinitiator concentration (experimental conditions are detailed in Table 20).*

We surprisingly observed a lower polymerization rate when the concentration of the reagents of our PIS was increased. Lacroix-Desmazes and Guyot[82] highly increased the AIBN concentration (multiplied by a factor of 10) for the dispersion polymerization of styrene in ethanol-water mixture (70/30 vol%) at 1.5 wt.% of a similar PEGMA macromonomer (51 EO units) and observed a strong acceleration of the polymerization at high AIBN concentration. Some other authors also showed that at high initiator concentration, the rate of radical formation became greater.[112,113] As initially the polymerization is mostly taking place in the continuous phase, the rate of polymerization is directly related to the initial initiator concentration. We believe that the high concentration of AO used in our experimental conditions (run 4) may induce an inner filter effect[114] impacting the generation of radicals. This explanation can however not be put forward when the AO concentration was unchanged, and a lower polymerization rate was also observed (run 5). It is possible that by increasing the disulfide and NHC-BH_3 concentrations and thus the number of radicals produced, termination reactions would occur more frequently, reducing *in fine* the number of available radicals.

The molar masses obtained in runs 4 and 5 are smaller than that of the reference experiment. This might be related to the slight increase of the particle size but remains difficult to fully rationalize at this stage.

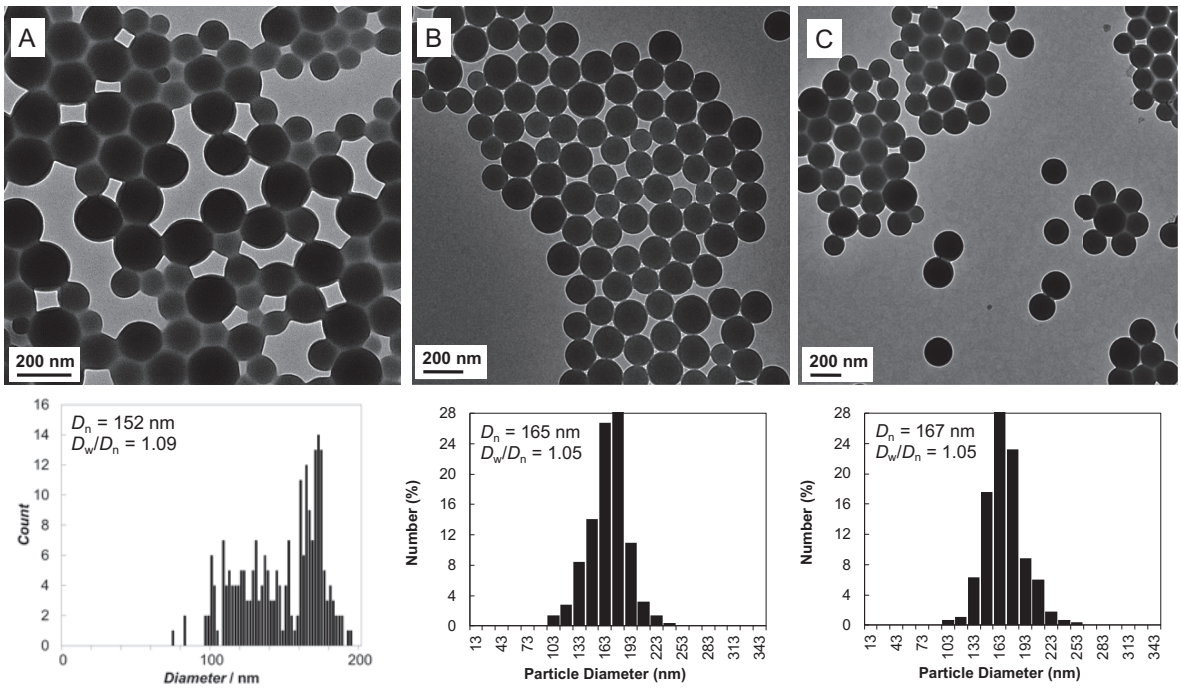

Figure 86. *TEM images and particle size distributions of the latexes obtained by in the conditions described in Table 20, for different concentrations of the reagent of our PIS: (A) Run 3, (B) Run 4 and (C) Run 5.*

C. Effect of stabilizer concentration

The influence of PEGMA concentration was next investigated. The photopolymerizations were thus conducted in the presence of different amounts of PEGMA, from 2.5 to 25 wt.% relative to styrene. The results are presented in Table 21.

Table 21. *Effect of PEGMA concentration on the dispersion polymerization of styrene under visible light.* [a]

Run	PEGMA (wt.%)	Time (h)	Conv. (%)	D_h[b] (nm)	PDI[b]	D_n[c] (nm)	D_w/D_n[c]	N_p (x10^{15} cm^{-3})	M_n[d] (g mol^{-1})	$Đ$[d]
6	25	22.3	97	131	0.01	97	1.12	19.3	104 000	3.8
3	18	23.7	92	144	0.04	152	1.09	5.2	91 000	5.1
7	10	21.8	88	176	0.06	207	1.19	1.8	58 000	5.9
8	5	23.7	98	363	0.03	345	1.23	0.44	40 000	9.3
9	2.5	23.5	100	505	0.19	340	1.15	0.46	32 000	7.7

[a] Experimental conditions: reaction temperature fixed at 40 °C, ethanol/water = 70/30 (wt.%). The solids content was fixed at 10 wt.%. [AO] = 1.3 10^{-5} mol L^{-1} (1 mol% with regard to NHC-BH_3), [disulfide] = 6.3 10^{-4} mol L^{-1} (50 mol% with regard to NHC-BH_3) and [NHC-BH_3] = 1.3 10^{-3} mol L^{-1}.
[b] Determined by DLS.
[c] Determined by TEM.
[d] Determined by SEC–THF.

Whatever PEGMA concentration, the final conversion after *ca*. 24 h of polymerization was at least 88%, and almost complete in most cases (Table 21). Kinetic studies showed a drastic decrease of the reaction rate at the beginning of the polymerization as the PEGMA concentration decreased (Figure 87). Capek *et al.*[30] also observed a decrease in the initial rate of polymerization (*ca*. at 20% conversion) with decreasing PEGMA concentration (M_n = 1 000 g mol^{-1}). For the experiment performed with 25 wt.% of PEGMA, the monomer conversion reached 65% after 7 h, whereas it was only 25% for 2.5 wt.% of PEGMA in the same conditions. Nevertheless, the final conversions still reached 100% after 24 h for 5 and 2.5 wt.% of PEGMA. This showed that even if the polymerization rates were low, radicals were still generated over a long period.

As expected, a decrease in PEGMA concentration led to an increase of particle size from 97 nm for 25 wt.% to 340 nm for 2.5 wt.%. Accordingly, the particle number decreased with decreasing the PEGMA concentration (Table 21). It should be noticed that the particle size did not however exceed 345 nm. In addition, the decrease of PEGMA concentration had a negative impact on the particle size distributions, with for example D_w/D_n = 1.09 at 18 wt.% of PEGMA while at 5 wt.% of PEGMA, D_w/D_n = 1.23. The increase in particle size observed as PEGMA

concentration decreases is due to the fact that a lower amount of stabilizer was available to stabilize the particles, and thus larger and fewer particles were obtained. Moreover, a decrease in PEGMA concentration also led to a significant decrease of the molar masses from 104 000 g mol^{-1} for 25 wt.% to 32 000 g mol^{-1} for 2.5 wt.%. This trend could indicate that the number of radicals per particle would increase, and so the termination rate, as the particle increases. More termination reactions could also explain why the polymerization rate is lower for the bigger particles. In most cases of dispersion polymerization, an inverse correlation between particle size and molar mass is observed: the larger particles have the lowest molar masses.[67]

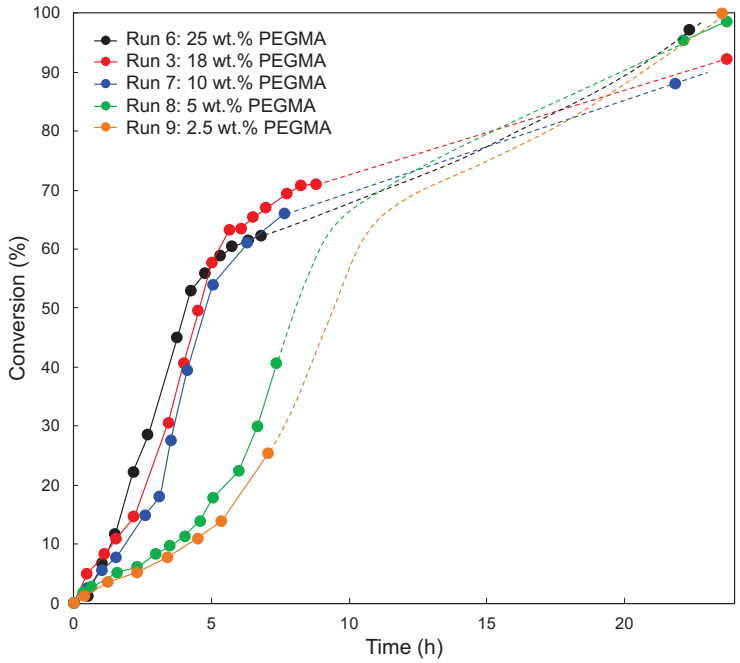

Figure 87. *Evolution of conversion with time for dispersion photopolymerization of styrene for different amounts of stabilizer: 25 (black curve), 18 (red curve), 10 (blue curve), 5 (green curve) and 2.5 (orange curve) wt.% of PEGMA. See Table 21 for experimental details.*

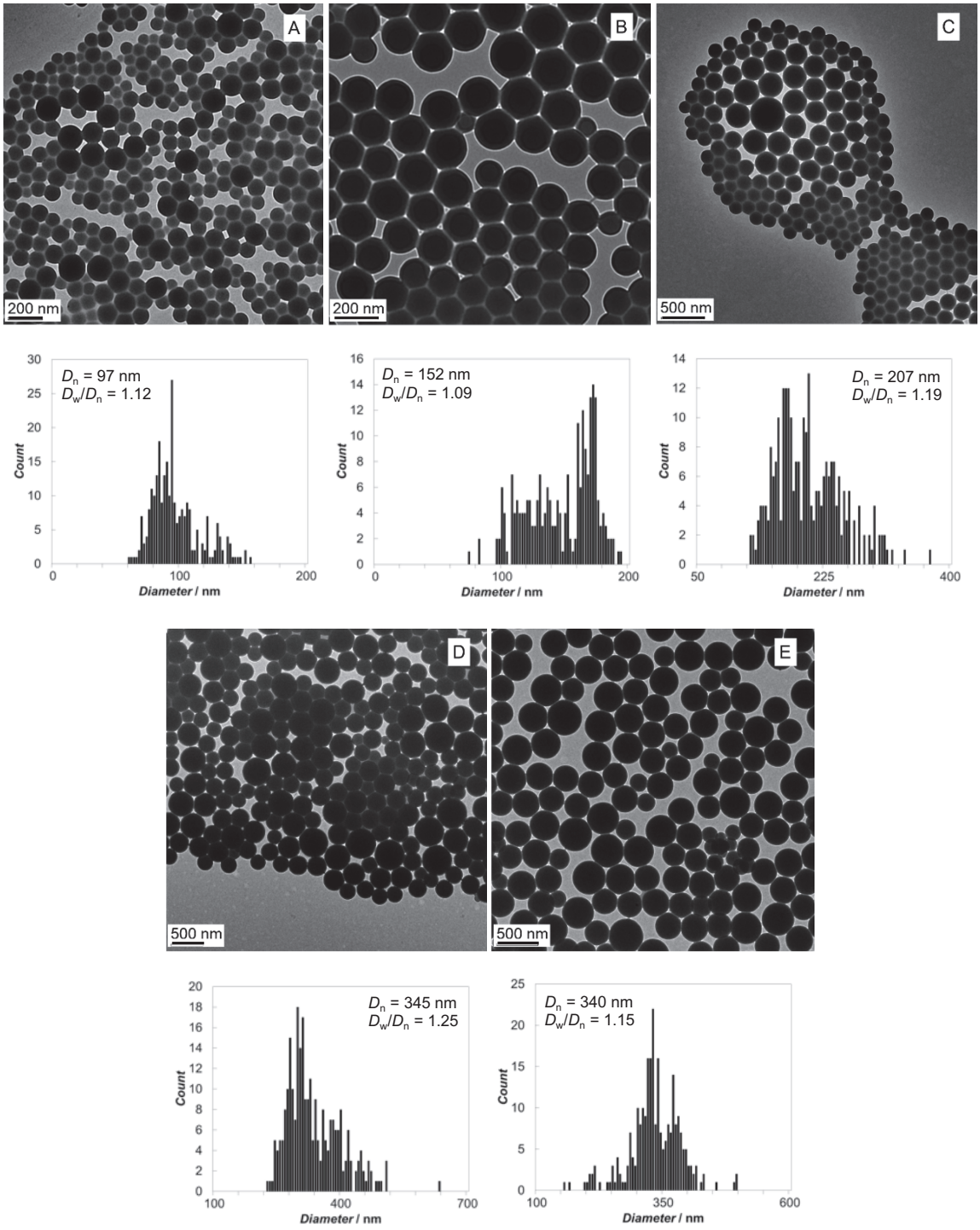

Figure 88. *TEM images and particle size distributions of the latexes obtained in the conditions described in Table 21, for different PEGMA concentration; (A) 25, (B) 18, (C) 10, (D) 5 and (E) 2.5 wt.% relative to styrene.*

As mentioned above, the obtention of broad particle size distributions for all samples may be due to the rather slow generation of radicals from our PIS resulting in a low and continuous nucleation. Indeed, the slow and continuous production of new radicals (as already observed in emulsion polymerization[109]) even after several hours likely favors the continuous production of new particles, which might also be favored by slow consumption of PEGMA (these

macromonomers are reported to exhibit lower reactivity than styrene, especially at low PEGMA concentration).[78] Reaction monitoring by NMR and gas chromatography could provide the relative consumption of styrene and PEGMA macromonomer to gather more information on the implication of PEGMA in particle stabilization.

D. Disulfide vs. three-component photoinitiation system

As already discussed in Chapter 2, F. Le Quéméner and D. Subervie showed that the thiyl radicals generated from the homolytic cleavage of the S–S bond under visible light led to efficient emulsion polymerization of MMA but not styrene. They assumed that it was due to the combination of a greater MMA solubility in water and a k_p value higher than for styrene. With the aim of confirming the first hypothesis, an experiment was performed using the disulfide alone as photoinitiator for the dispersion photopolymerization of styrene using 18 wt% of PEGMA. The results are reported in Table 22.

Table 22. *Effect of the composition of the photoinitiating system for the dispersion photopolymerization of styrene.*[a]

Run	PIS	Time (h)	Conv. (%)	D_h[b] (nm)	PDI[b]	D_n[c] (nm)	D_w/D_n[c]	N_p (x10^{15} cm^{-3})	M_n[d] (g mol^{-1})	$Đ$[d]
3	Full system	23.7	92	144	0.04	152	1.09	5.16	91 000	5.1
10	Disulfide	8.1	82	335	0.02	337	1.02	0.39	200 000	4.1

[a] Experimental conditions: reaction temperature fixed at 40 °C, ethanol/water = 70/30 (wt.%). The solids content was fixed at 10 wt.%, PEGMA at 18 wt.% relative to styrene. [AO] = 1.3 10^{-5} mol L^{-1} (1 mol% with regard to NHC-BH_3), [disulfide] = 6.3 10^{-4} mol L^{-1} (50 mol% with regard to NHC-BH_3) and [NHC-BH_3] = 1.3 10^{-3} mol L^{-1}.
[b] Determined by DLS.
[c] Determined by TEM.
[d] Determined by SEC–THF.

The results of Table 7 clearly show that the disulfide used alone was capable of photoinitiating the polymerization of styrene in dispersion. Indeed, in these conditions, styrene is soluble in the ethanol/water mixture and the thiyl radicals can easily add to the monomer. Moreover, when the disulfide is used alone, the polymerization needs more time to start. The retardation observed at the beginning of the reaction for the disulfide alone may be attributed to the fact that the disulfide poorly absorbs visible light (unefficient homolytic S–S bond cleavage and/or reversible addition to styrene), resulting in low generation of radicals in comparison with the full PIS. However, the rate was significantly faster after 4 h of reaction (Figure 89), and the monomer conversion reached 82% in 8 h, whereas for the same time it reached only 70% with

the full system. We observed a significant gel effect with disulfide alone (red curve in Figure 89). This observation was confirmed by the higher molar mass obtained for the disulfide alone (M_n = 200 000 g mol^{-1}) than for the full PIS (M_n = 91 000 g mol^{-1}).

PS particles were obtained with a diameter of 337 nm for disulfide alone as photoinitiator vs. 152 nm for the full system (Figure 90). Moreover, when the disulfide was used alone, we obtained a narrower particle size distribution (D_w/D_n = 1.02) than with the full PIS (D_w/D_n = 1.09).

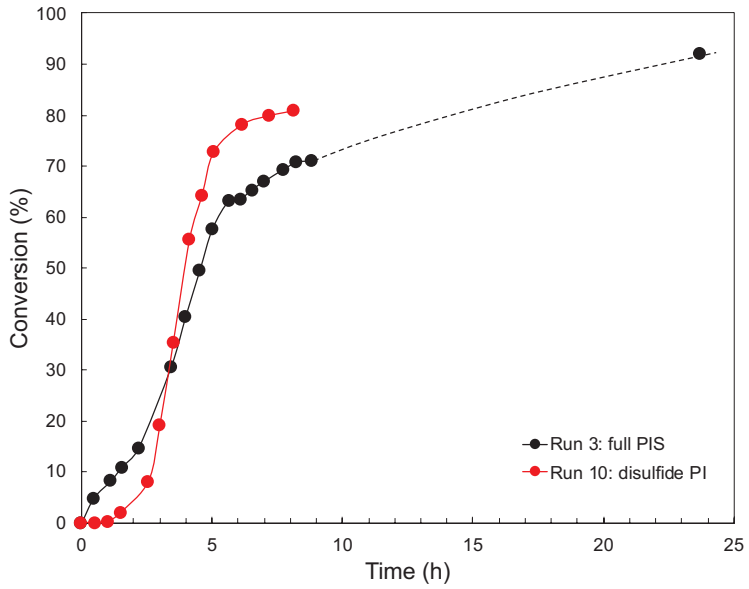

Figure 89. *Evolution of conversion with time for dispersion photopolymerization of styrene for different PIS: our three-component PIS (dark curve) vs. disulfide alone (red curve). See Table 22 for experimental details.*

The use of disulfide alone as photoinitiator leads to the formation of few precursor particles because there are fewer radicals initially generated (retardation observed at the beginning of the reaction). These *nuclei* are not immediately stabilized because the generation of graft copolymer of P(PEGMA-*co*-Styrene) should be reduced compared to the propagation of the oligoradicals. Therefore, the particles are larger than with the full PIS, but they remain small enough to effectively capture radicals from the continuous phase. The thiyl radicals slowly generated in the continuous phase (and in the monomer-swollen particles if we admit that the disulfide partitions), can accumulate before recombining due to the low radical diffusion. The high radical concentration within polymer particles results in an important gel effect and thus to higher molar mass.

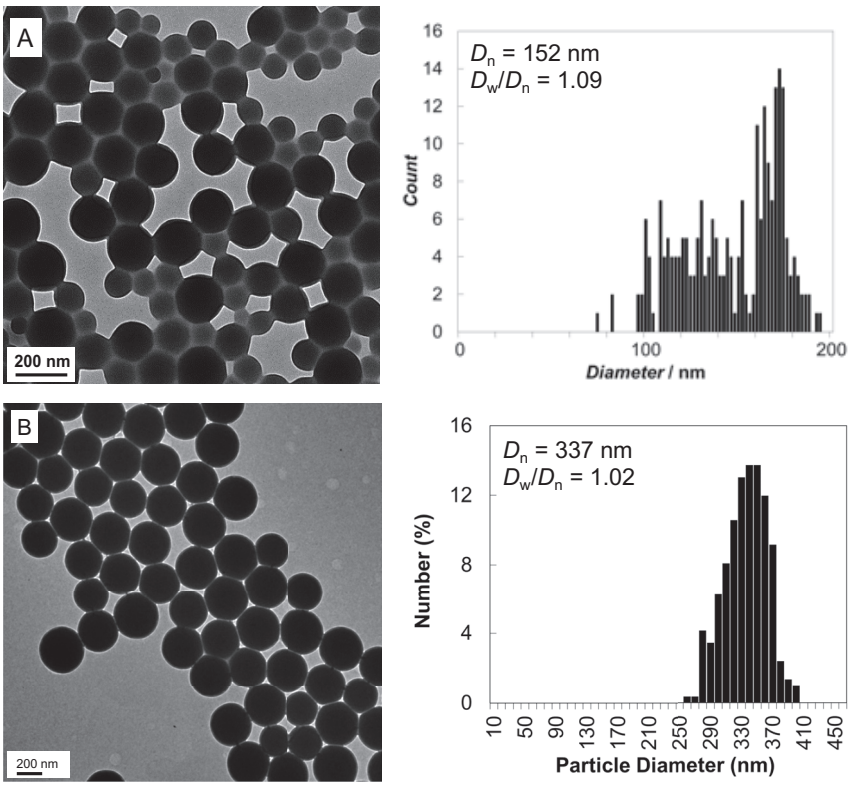

Figure 90. *TEM images and particle size distributions of the latexes obtained in the conditions described in Table 22, for different PIS: (A) with our three-component PIS and (B) with disulfide alone.*

The narrow particle size distribution observed when the disulfide was used alone indicates that PEGMA macromonomer efficiently stabilized the particles. We believe that we are in the case of a moderate rate of radical generation that ensures a good balance between an efficient nucleation step and adsorption of graft copolymers. All *nuclei* thereby grew to uniform final particle sizes. In addition, the narrow size distribution may ensure a better light penetration and allow us to reach larger particle sizes.

We demonstrated that the disulfide alone can indeed successfully photoinitiate the dispersion polymerization of styrene contrary to what we observed in emulsion polymerization. The solubility of styrene in the continuous phase seems to be the key factor. Moreover, the use of the sole disulfide as photoinitiator led to larger particles with a narrow size distribution in comparison with the full PIS. This result is thus surprising since in this range of particles size (200–500 nm), we have to deal with an attenuation of the light through the reactor. Indeed, in Chapter 1, we have shown that the scattering efficiency reaches its maximum value around the wavelength of the incident source. The following paragraph concerns the reproducibility issues of our experiments where we attempted to relate the particle sizes and the light penetration.

E. Particle size vs. light penetration: reproducibility issue?

We have shown in the previous section concerning the influence of the PEGMA concentration that at 10 wt.% of PEGMA, the conversion curve was very similar to the one at 18 wt.%, whereas between 10 and 5 wt.% the difference was quite significant (Figure 87). We thereby decided to repeat some of these syntheses. The following experiments were performed using 10 wt.% of PEGMA relative to styrene (Table 23, runs 11 and 12).

Table 23. *Reproducibility of dispersion polymerizations of styrene stabilized with PEGMA 10 wt.% under visible light and thermally induced.*[a]

Run	Time (h)	Conv. (%)	D_h[c] (nm)	PDI[c]	D_n[d] (nm)	D_w/D_n[d]	N_p (x10^{15} cm^{-3})	M_n[e] (g mol^{-1})	$Đ$[e]
7	21.8	88	176	0.06	207	1.19	1.8	58 000	5.9
11	22.7	56	178	0.10	269	1.15	0.5	52 000	7.0
12	28	88	186	0.01	202	1.06	2.0	60 000	5.4
13[b]	6	96	324	0.02	346	1.02	0.4	116 000	4.7

[a] Experimental conditions: reaction temperature fixed at 40 °C, ethanol/water = 70/30 (wt.%). The solids content was fixed at 10 wt.%, PEGMA at 10 wt.% relative to styrene. [AO] = 1.3 10^{-5} mol L^{-1} (1 mol% with regard to NHC-BH_3), [disulfide] = 6.3 10^{-4} mol L^{-1} (50 mol% with regard to NHC-BH_3) and [NHC-BH_3] = 1.3 10^{-3} mol L^{-1}.
[b] Similar conditions concerning [a] except for the reaction temperature fixed at 70 °C and the use of AIBN as initiator at 1 wt.% relative to styrene.
[c] Determined by DLS.
[d] Determined by TEM.
[e] Determined by SEC–THF.

The conversion – time curves of the three syntheses realized under the same experimental conditions are plotted in Figure 91 (runs 7, 11 and 12) and compared with the thermally induced experiment (run 13, green line). In terms of kinetics, the experiments under photoinduced conditions were definitively not reproducible. Only the curve from run 7 (dark line) displayed a sigmoidal shape with an auto-acceleration. This reaction was stopped after 22 h at 90 % conversion. For the two other syntheses, the auto-acceleration may occur later (dashed lines which represent the hypothetic conversions as a function of time). However, upon a closer look, one can notice that for the first two hours of the synthesis the three curves show a similar trend. After that point, they develop randomly. We think that the stochastic behavior after 2 h may be due to the growth of particles which reach a critical size attenuating the light penetration within the reaction medium.

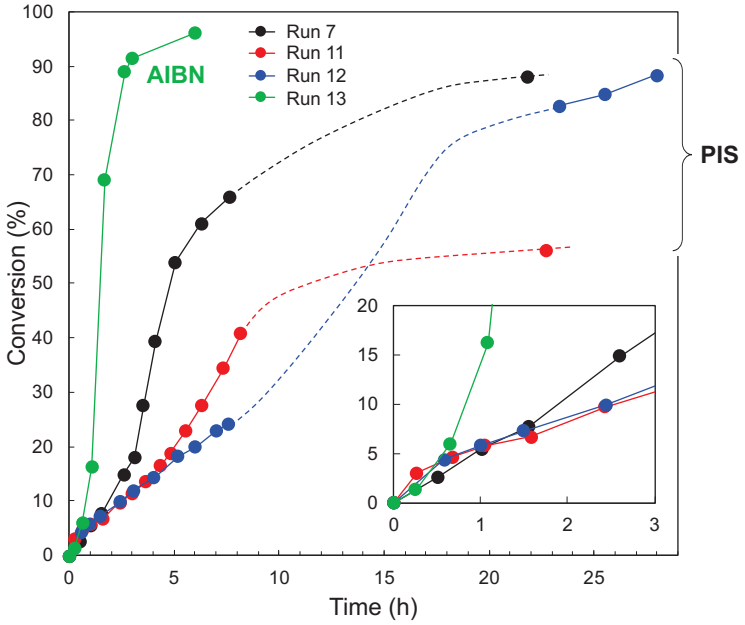

Figure 91. *Reproducibility – Evolution of conversion with time for dispersion polymerization of styrene with the stabilizer PEGMA (10 wt.% with respect to styrene) under visible light (runs 7, 11 and 12) and thermally induced (run 12).*

Moreover, we obtained identical particle sizes for runs 7 and 12 (D_n = 207 and 202 nm, respectively), where the monomer conversions are the most advanced (88%) in comparison with run 11 (D_n = 269 nm with a final conversion reaching 56% after 23 h). The molar masses were very similar with very broad size distributions.

In our case, another factor must have an impact on the kinetic but not on the final particle size at similar final conversions (for runs 7 and 12). In other words, even if the final destination (*i.e.*, the final conversion) is exactly the same, the path to reach it is very different. Besides, we showed that at 18 wt.% of PEGMA, the conversion curves were reproducible (see Table 19 runs 1, 2 and 3). The only difference was the higher PEGMA concentration which led to smaller particle sizes (*ca.* 150-170 nm). We thus believe that at relatively low conversions (between 0 and 20%), a critical size must be reached for the particles, that attenuates the light penetration within the reaction medium *via* scattering effects (which would also be enhanced with broad particle size distribution).

Chemtob and co-workers observed that the light was attenuated as soon as the polymer particles reach about 50 nm, even in the visible domain.[115] The scattering efficiency is increased when the particle size increases at a selected wavelength (see Chapter 1). The particle sizes measured by DLS for the three experiments (runs 7, 11 and 12) at 2.5 h (approximately 10% conversion) were between 150 and 170 nm, which corresponds to a size parameter around 0.8 (considering λ_{max} = 430 nm of AO). This value corresponds to the Mie scattering regime. We believe that

during the dispersion photopolymerizations, the light is attenuated by scattering, resulting in a diminution of the production of radicals. Nevertheless, the photopolymerization proceeds since the stirring ensures the diffusion of these radicals through the reaction medium.

The experiments were compared to a conventional dispersion polymerization thermally initiated by AIBN at 70 °C. It is important to mention that the concentration of AIBN was about 4 times higher than that of the NHC-borane ($5.7\ 10^{-3}$ M vs. $1.3\ 10^{-3}$ M, respectively). Even if a straightforward comparison of the radical flux generated by both types of initiation remains difficult, the polymerization initiated by AIBN was much faster than the ones initiated by the photoinitiating system. The rate of thermal initiation was similar initially (see "zoom" in Figure 91), but after 1 h, the polymerization was much faster (also related to a higher rate constant of propagation at 70 °C). The particle size was also higher and the particle size distribution narrower (D_n = 346 nm and D_w/D_n = 1.02). Finally, we obtained a higher molar mass with the use of AIBN (M_n = 116 000 g mol^{-1}) than with our PIS (around 60 000 g mol^{-1}). It is however difficult to compare these two values since the initiators were not introduced at similar concentrations and the reaction temperature was not the same.

The generation of radicals and the formation of particles with high scattering efficiency (*i.e.*, with diameters larger than around 200 nm) seem to be key factors at the origin of the poor reproducibility observed for the photopolymerization reactions in dispersion. Indeed, a slow and continuous generation of radicals like it seems to be the case in the photoinitiated systems would not only lead to broad particle size distribution but also bring scattering issues. The stochastic behavior after 2 h occurs at very low conversions (10-15%) for particle sizes around 150–170 nm. In the following sections, we introduced an organic base to our system in order to investigate its influence on the nucleation rate.

F. Influence of an organic base

One factor that could explain why radical generation is slow in the photoinitiated systems could be a partial solubility of dicarboxylic acid diphenyl disulfide in the hydroalcoholic mixture. Indeed, in presence of carboxylic acid groups, disulfide can likely partition between the continuous phase and the monomer-swollen particles, leading to a less efficient photoinitiation. By analogy with the experimental conditions in emulsion (basic pH, see Chapter 2), we thus decided to use a quaternary ammonium salt, tetrabutylammonium

hydroxide (TBAH) acting as an organic base to favor partitioning of the disulfide towards the continuous phase and thus improving the photoinitiation in the continuous phase.

1. Effect of TBAH concentration

The concentration of TBAH was first investigated. All the syntheses were carried out at PEGMA 18 wt.% with a solids content of 10 wt.%, and a constant concentration of the three-component photoinitiating system. The results are reported in Table 24.

Table 24. *Dispersion polymerization of styrene stabilized with PEGMA under visible light at different concentration of TBAH.*[a]

Run	*c*(TBAH) (mmol L^{-1})	Time (h)	Conv. (%)	D_n[b] (nm)	D_w/D_n[b]	N_p (x10^{15} cm^{-3})	M_n[c] (g mol^{-1})	$Đ$[c]
3	0	23.7	92	152	1.09	5.2	91 000	5.1
14	1.25	24.1	84	130	1.07	6.9	144 000	5.9
15	2.5	30	98	171	1.02	3.5	127 000	3.4
16	5.0	30	89	196	1.02	2.0	129 000	4.5
17	2.5	31	98	183	1.03	2.9	126 000	4.0

[a] Experimental conditions: reaction temperature fixed at 40 °C, ethanol/water = 70/30 (wt.%). The solids content was fixed at 10 wt.%, PEGMA at 18 wt.% relative to styrene. [AO] = 1.3 10^{-5} mol L^{-1} (1 mol% with regard to NHC-BH_3), [disulfide] = 6.3 10^{-4} mol L^{-1} (50 mol% with regard to NHC-BH_3) and [NHC-BH_3] = 1.3 10^{-3} mol L^{-1}.
[b] Determined by TEM.
[c] Determined by SEC–THF.

For all TBAH concentrations, the conversion – time curves exhibit a sigmoidal shape (Figure 92) and the final conversion was high in each case. The addition of TBAH led to faster reactions and the polymerization rate was the highest for TBAH concentration of 2.5 mM. This observation may be explained by the fact that TBAH can deprotonate the disulfide, which should increase its solubility in the hydroalcoholic solution instead of migrating toward the monomer-swollen particles, thus enhancing its availability and allowing a more efficient production of radicals in the continuous phase. The addition of more TBAH, *c*(TBAH) = 5 mM, led to a decrease of the polymerization rate. This can be attributed to the reduction of the acridine orange reactivity under basic pH conditions (at pH > 9, the molar exctintion coefficient rapidly decreases upon light exposure).

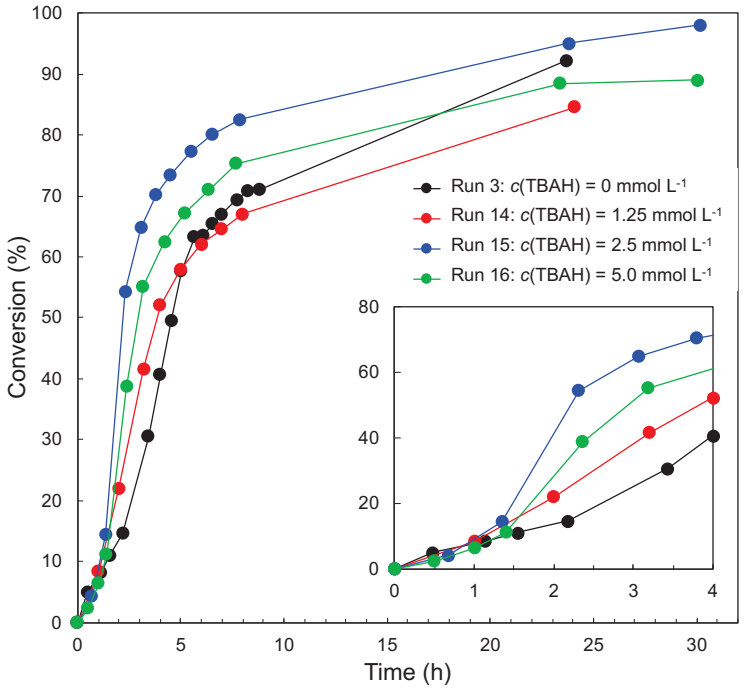

***Figure 92**. Evolution of conversion with time for dispersion photopolymerization of styrene for different concentration of TBAH: 0 (Run 3), 1.25 (Run 14), 2.5 (Run 15) and 5 mol L^{-1} (Run 16).*

Moreover, an increase in TBAH concentration led to an increase of particle size from 130 nm at 1.25 mM to 196 nm at 5 mM (Figure 93). Very interestingly, we also observed an improvement of the size dispersity when the TBAH concentration increased (from D_w/D_n = 1.09 to 1.02 for 0 and 5 mM, respectively). Moreover, the molar masses were higher when TBAH was used than without (Table 24).

The polymerization rates are all similar within the first hours of the polymerization as shown in Figure 92, which likely corresponds to the nucleation stage, indicating that TBAH would not impact the nucleation itself. However, once the particles formed, the higher polymerization rate observed when TBAH is used can likely be attributed to a higher availability of the disulfure in the continuous phase leading to a higher production of oligoradicals, which can enter into the particles, despite the fact that larger particles were formed. We thus believe that the adsorption speed of the stabilizer could not catch up with the nucleation rate, but this has no impact on its efficiency. Nevertheless, we cannot rule out at this stage a possible impact of TBAH on the PIS efficiency.

In addition, the particles size increased, and thus the number of particles decreased when the TBAH concentration increased. One possible explanation may lie in the solubility of the PEG chains with respect to TBAH concentration. Indeed, the presence of salts could negatively affect PEG solubility in the continuous phase (*via* a salting out effect[116–118]) and consequently, the

resulting graft copolymer would be less efficient for particle stabilization resulting in larger particles, with nevertheless narrow size distribution.

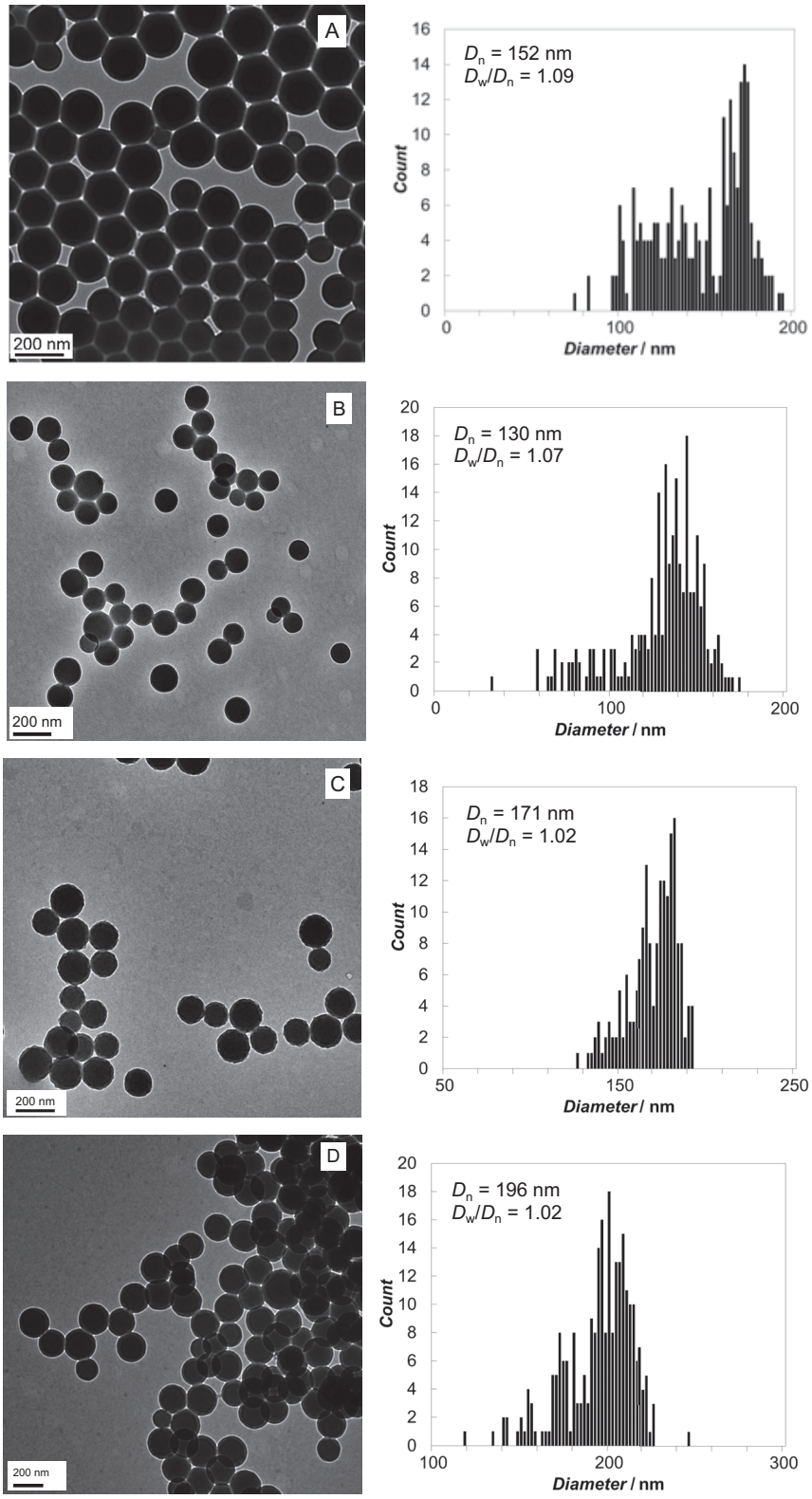

Figure 93. *TEM images and corresponding histograms of PS latexes obtained at different TBAH concentrations: (A) 0, (B) 1.25, (C) 2.5 and (D) 5.0 mol L^{-1}. See Table 24 for experimental details.*

We decided to use TBAH at a concentration of 2.5 mM to reproduce the synthesis (see Table 24 run 17). The conversion curves in Figure 94 indicate that the syntheses were indeed reproducible. We obtained similar results in terms of kinetics and particle size (run 15: D_n = 171 nm with D_w/D_n = 1.02 vs. run 17: D_n = 183 nm with D_w/D_n = 1.03). The particle sizes obtained in this case are slightly smaller than the ones observed for the experiments carried out at 10 wt.% of PEGMA without TBAH (runs 7 and 12, see Table 23), for which we faced reproducibility issues. The main difference between these experiments is that the presence of TBAH leads to much faster photopolymerization, especially higher nucleation rates. But also, narrower particle size distributions are obtained, which probably reduces scattering issues.

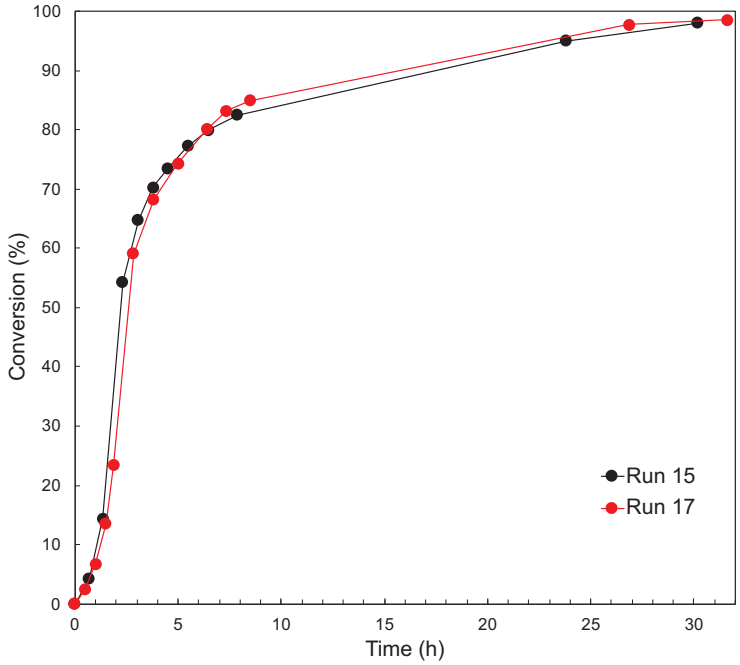

Figure 94. *Reproducibility – Evolution of conversion with time for dispersion photopolymerization of styrene with the stabilizer PEGMA (18 wt.% based on styrene) and [TBAH] = 2.5 10^{-3} M.*

To sum up, despite the intrinsic problems related to the interaction between light and particles, we were able to reach sizes similar to those where reproducibility issues were previously observed by improving the photoinitiation efficiency in the presence of TBAH, leading to faster polymerizations and producing particles with narrower particle size distribution, and therefore a less impact of light scattering.

2. Effect of stabilizer concentration in presence of TBAH

The photopolymerizations were then conducted in the presence of a decreasing amount of PEGMA in the presence of TBAH, from 18 to 5 wt.% relative to styrene. The results are presented in Table 25.

Table 25. *Effect of PEGMA concentration on the dispersion polymerization of styrene under visible light in the presence of TBAH at 2.5 10^{-3} mol L^{-1}.* [a]

Run	PEGMA (wt.%)	Time (h)	Conv. (%)	D_n[b] (nm)	D_w/D_n[b]	N_p (x10^{15} cm^{-3})	M_n[c] (g mol^{-1})	$Đ$[c]
15	18	30	98	171	1.02	3.53	127 000	3.4
18	15	31.1	92	207	1.01	1.86	117 000	5.5
19	10	30.1	92	253	1.03	0.98	97 000	6.3
20	5	30.2	81	358	1.02	0.32	101 000	6.7

[a] Experimental conditions: reaction temperature fixed at 40 °C, ethanol/water = 70/30 (wt.%). The solids content was fixed at 10 wt.%, PEGMA at 18 wt.% relative to styrene. [AO] = 1.3 10^{-5} mol L^{-1} (1 mol% with regard to NHC-BH_3), [disulfide] = 6.3 10^{-4} mol L^{-1} (50 mol% with regard to NHC-BH_3), [NHC-BH_3] = 1.3 10^{-3} mol L^{-1} and [TBAH] = 2.5 10^{-3} mol L^{-1}.
[b] Determined by DLS.
[c] Determined by SEC-THF.

Kinetic studies showed a decrease of the polymerization rate with decreasing the PEGMA concentration (Figure 95). In the case of PEGMA 18 wt.%, the monomer conversion reached 98% after 30 h whereas at PEGMA 5 wt.%, after 30 h the monomer conversion was 81% (with a slight inhibition of a few hours). Note that the initiation rates at low PEGMA concentration were faster than the ones carried out under the same conditions without TBAH (run 20 of Table 25 vs. run 8 of Table 21).

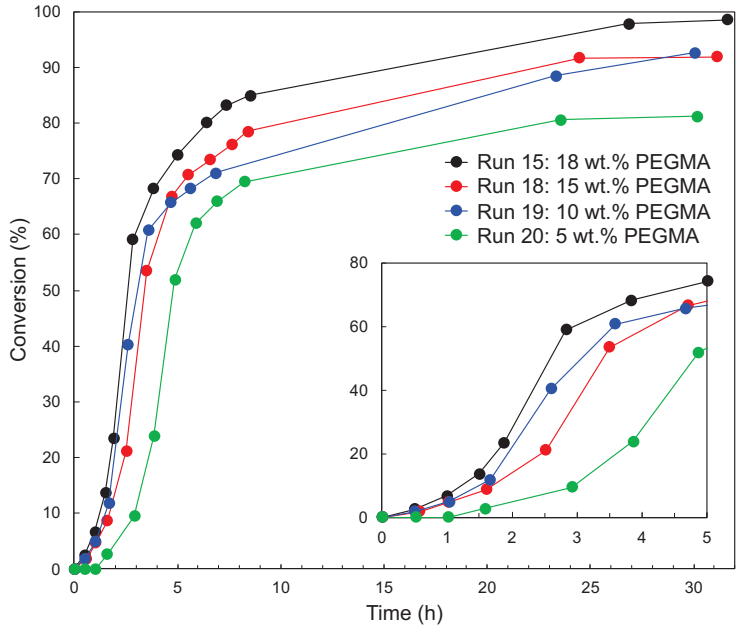

Figure 95. *Evolution of conversion with time for dispersion photopolymerization of styrene for different amounts of PEGMA in the presence of TBAH at 2.5 10^{-3} mol L^{-1} (18 (run 15), 15 (run 18), 10 (run 19) and 5 (run 20) wt.% relative to styrene (see Table 25 for experimental details).*

Decreasing the PEGMA concentration led to an increase of particle size from 171 nm at 18 wt.% to 358 nm at 5 wt.% (Figure 96). During the nucleation step, the precursor particles aggregated to reduce the surface to be covered since a lower graft copolymer amount was available to stabilize them. This results in the formation of larger and fewer particles. Moreover, we obtained narrow particle size distributions for all PEGMA concentrations, which was not the case without TBAH. Moreover, in comparison with the previous study on the variation of PEGMA concentration in the absence of TBAH (see Table 21), we observed only a slight difference of the molar masses that varied from 101 000 to 127 000 g mol^{-1} with increasing the PEGMA concentration from 5 to 18 wt.%. These molar masses were higher than in the absence of TBAH (Table 21), especially for the low PEGMA cocnentration (101 000 g mol^{-1} vs. 40 000 g mol^{-1} at 5 wt.% of PEGMA with and without TBAH, respectively). We believe that in the presence of TBAH, a high number of radicals is generated (because the disulfide remains in the continuous phase on the particles are formed), which leads to faster polymerization rates and subsequently a gel effect that occurs at an early stage.

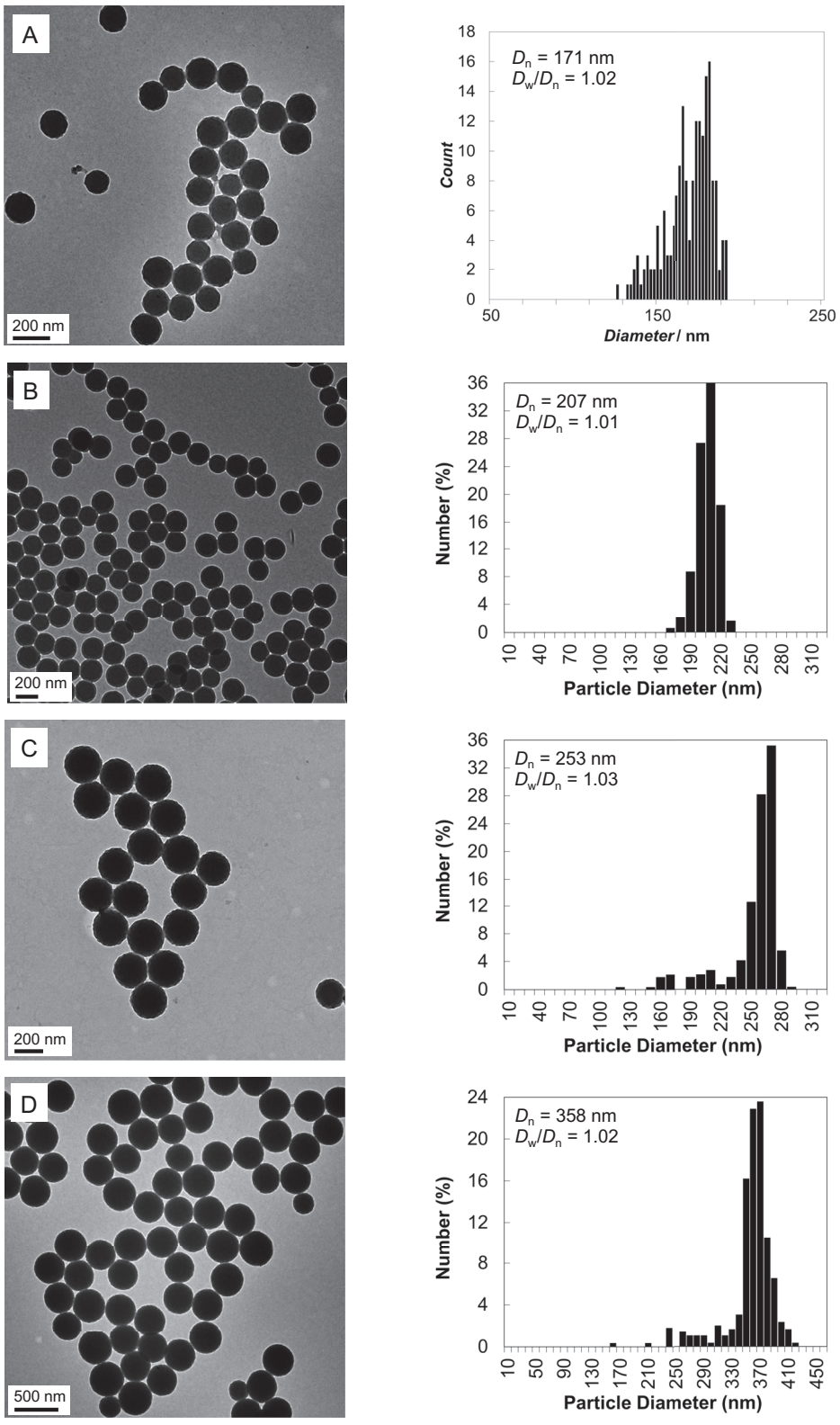

***Figure 96**. TEM images and particle size distributions of the PS latexes obtained, for different PEGMA concentration in the presence of TBAH at 2.5 10^{-3} mol L^{-1}: (A) 18, (B) 15, (C) 10 and (D) 5 wt.% relative to styrene (see Table 25 for experimental details).*

3. Disulfide as type I photoinitiator in the presence of TBAH

Next, we studied the influence of TBAH when disulfide was used alone to photoinitiate the dispersion polymerization of styrene. The results are reported in Table 26.

Table 26. *Effect of the composition of the photoinitiating system for the dispersion photopolymerization of styrene in the presence of TBAH at PEGMA 18 wt.%.* [a]

Run	PIS	Presence of TBAH	Time (h)	Conv. (%)	D_n[b] (nm)	D_w/D_n[b]	N_p (x10^{15} cm^{-3})	M_n[c] (g mol^{-1})	$Đ$[c]
15	Full system	yes	30	98	171	1.02	3.53	127 000	3.4
21	Disulfide	yes	30.1	90	250	1.01	1.03	260 000	4.7
3	Full system	no	23.7	92	152	1.09	5.16	91 000	5.1
10	Disulfide	no	8.1	82	337	1.02	0.39	200 000	4.1

[a] Experimental conditions: reaction temperature fixed at 40 °C, ethanol/water = 70/30 (wt.%). The solids content was fixed at 10 wt.%, PEGMA at 18 wt.% relative to styrene. [AO] = 1.3 10^{-5} mol L^{-1} (1 mol% with regard to NHC-BH_3), [disulfide] = 6.3 10^{-4} mol L^{-1} (50 mol% with regard to NHC-BH_3), [NHC-BH_3] = 1.3 10^{-3} mol L^{-1} and [TBAH] = 2.5 10^{-3} mol L^{-1}.
[b] Determined by DLS.
[c] Determined by SEC-THF.

Once again, a highly stable PS latex was successfully obtained with the sole use of the disulfide as photoinitiatior. When the full system was used, the initial polymerization rate was slightly higher than with the disulfide alone, plus the final conversion was limited to 90% in the latter case (see runs 15 and 21 in Figure 97). This retardation at the beginning of the polymerization was attributed to the few thiyl radicals generated by the decomposition of the disulfide under visible light radiation (the latter poorly absorbs in the visible range). This results in the formation of fewer and larger particles (D_n = 250 nm vs. D_n = 171 nm for the full system). The size distributions were narrow in both cases. We also observed a significant gel effect with both the full PIS and disulfide alone (blue and green curves in Figure 97). This observation was confirmed by the high molar masses obtained for the disulfide alone (M_n = 260 000 g mol^{-1}) and for the full PIS (M_n = 127 000 g mol^{-1}). Note that the molar mass was much higher with disulfide alone than for the full PIS.

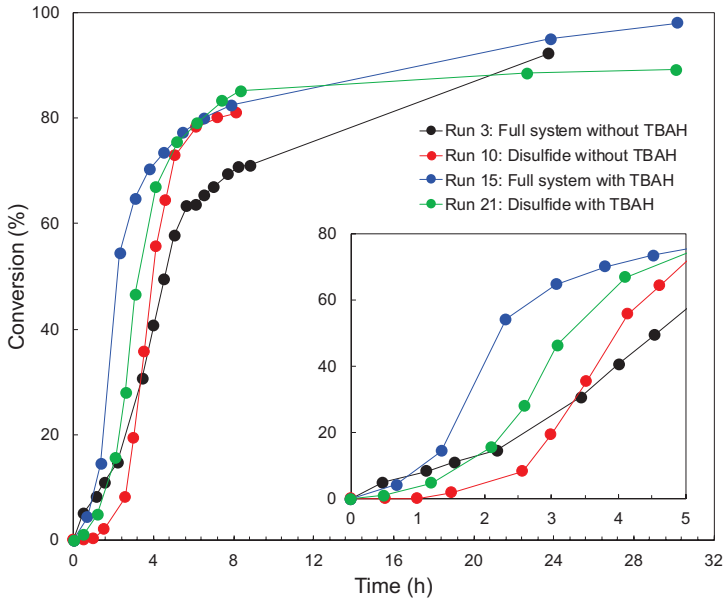

Figure 97*. Conversion curves as a function of time for the full photoinitiating system vs. disulfide alone with or without the presence of TBAH (2.5 mM) at 18 wt.% of PEGMA based on styrene (see Table 22 and Table 26 for experimental conditions).*

Moreover, in the absence of TBAH, we obtained with the disulfide alone slower photopolymerization and a lower molar mass of 200 000 g mol^{-1} (run 10) than in the presence of TBAH. This was due to the efficiency of the disulfide mostly located in the continuous phase in the presence of TBAH. In the same way, the particles formed in the presence of TBAH were smaller than without TBAH (D_n = 250 nm vs. D_n = 337 nm). This suggested that the precursor particles were more stabilized in the presence of TBAH probably because of the higher number of thiyl radicals initially generated that could increase the chances of addition with PEGMA to form graft copolymers. It is also possible that the carboxylate groups participate to the stabilization of the particles. It should be noticed that generally we obtained narrow size distributions for the large particles. We thus assumed that the size distribution has a significant impact on the light penetration since we were not able to reproduce experiments with final particle sizes around 200 nm and broad size distributions.

In addition, according to Figure 97, as previously disccused before, we observed a significant gel effect when the disulfide was used alone without TBAH (run 10), which was not the case in the presence of TBAH (run 21), even if a high molar mass was obtained. The obtention of the high molar mass with TBAH can be attributed to a radical compartmentalization effect. Indeed, a greater number of particles was formed resulting in fewer radicals per particles, and

therefore the probably that termination reactions occur are reduced (which are generally favored when the particle size is small).

G. Conclusions

In summary, dispersion photopolymerization of styrene carried out in the presence of PEGMA macromonomer as a reactive stabilizer exhibited some reproducibility issues and the final particles were obtained with broad size distributions. This is probably due to a slow and continuous generation of radicals (the disulfide in our case which may partitions between the continuous phase and the polymer particles), resulting in a slow polymerization. The broad size distributions might attenuate the light irradiation. This was partially solved by the addition of an organic base (TBAH) which probably leads to a faster generation of radicals in the continuous phase and thus a faster overall polymerization.

In comparison with our previous work on emulsion polymerization of styrene, where the largest particle size we obtained was around 300 nm, the diameter of the obtained PS latexes is around 360 nm, with narrow size distributions when TBAH was used. Indeed, we assumed that the disulfide was mostly localized in the continuous phase in the presence of TBAH, leading to a more efficient generation of radicals and a fast polymerization. We also confirmed that dispersion photopolymerization of styrene was successful when the disulfide was used as sole photoinitiator. Due to the poor absorption of the disulfide in the visible range, we observed a retardation of the nucleation which led to fewer and larger particles than with the full PIS, but they remain small enough to effectively capture oligoradicals from the continuous phase. We also observed an important gel effect when the disulfide was used alone, since a high number of radicals can accumulate within polymer particles before recombining. This gel effect was confirmed by the obtention of high molar mass.

The reproducibility issues were then solved by increasing the nucleation rate (efficient photoinitiation in the presence of TBAH). Moreover, the size distribution was found to be a crucial parameter to form large particles while limiting the possible multiple scattering effects.

In the following part, with the aim of increasing further the final particle size, we have evaluated a classical steric stabilizer for dispersion polymerization: poly(*N*-vinylpyrrolidone).

II. Dispersion photopolymerization of styrene with PVP

A. Robustness of our photoinitiating system

We investigated first the reproducibility of experiments when using the three-component PIS. Dispersion photopolymerization of styrene in the presence of PVPK-30 (M_n = 40 000 g mol^{-1}) was carried out under the same conditions as for PEGMA, *i.e.,* introducing similar weight content (which obviously implies a different number of polymer chains). Besides, no TBAH was used. All the results are reported in Table 27. It is worth stressing that PVP participates to particle stabilization *via* chain transfer reactions occurring along the PVP chains, while PEGMA is involved in the propagation step. It is thus difficult to strictly compare the stabilization mode of these two macromolecules. Nevertheless, in the literature, a lower concentration of macromonomer is usually needed compared to more conventional stabilizers such as PVP, indicating that the former is more efficient.[111]

The conversion curves of styrene as a function of reaction time with 10 wt.% of PVPK-30 are plotted in Figure 98. Only two conversion curves over three are identical. For the two reproducible syntheses, the conversion of styrene reached approximately 70% after 24h of irradiation at 40 °C (dark and red lines) and for the third one, the conversion reached 83% after 23 h (blue line). The latexes were stable without any coagulum.

Table 27. *Dispersion polymerization of styrene stabilized with PVPK-30 thermally and photo-induced.* [a]

Run	Time (h)	Conv. (%)	D_n[c] (nm)	D_w/D_n[c]	N_p (x10^{13} cm^{-3})
22	30.4	71	859	1.001	2.1
23	24.3	69	794	1.006	2.6
24	23.2	83	766	1.002	3.4
25[b]	6.4	100	931	1.005	2.2

[a] Experimental conditions: reaction temperature fixed at 40 °C, ethanol/water = 70/30 (wt.%). The solids content was fixed at 10 wt.%, PVPK-30 at 10 wt.% relative to styrene. [AO] = 1.3 10^{-5} mol L^{-1} (1 mol% with regard to NHC-BH$_3$), [disulfide] = 6.3 10^{-4} mol L^{-1} (50 mol% with regard to NHC-BH$_3$) and [NHC-BH$_3$] = 1.3 10^{-3} mol L^{-1}.
[b] Similar conditions concerning [a] except for the reaction temperature fixed at 70 °C and the use of AIBN as initiator at 1 wt.% relative to styrene.
[c] Determined by TEM.

At the beginning of the polymerization, the three reaction mixtures were totally homogeneous and transparent. The conversion curves started to deviate after *ca.* 5 h. Experimentally, we

noticed that after this time (which must correspond to a critical particle size), the reaction medium became very turbid (the milky aspect was more pronounced than with PEGMA) as precursor particles are formed and grow, causing scattering of light and thus its attenuation within the reaction mixture. We believe that the stochastic behavior of the medium after a certain period when we tried to reproduce the experiments with 10 wt.% of PVP may be due to the growth of particles which reached a critical size around 380 nm (measured by DLS), therefore negatively impacting the light penetration within the reaction medium, and the generation of radicals should thus be hindered.

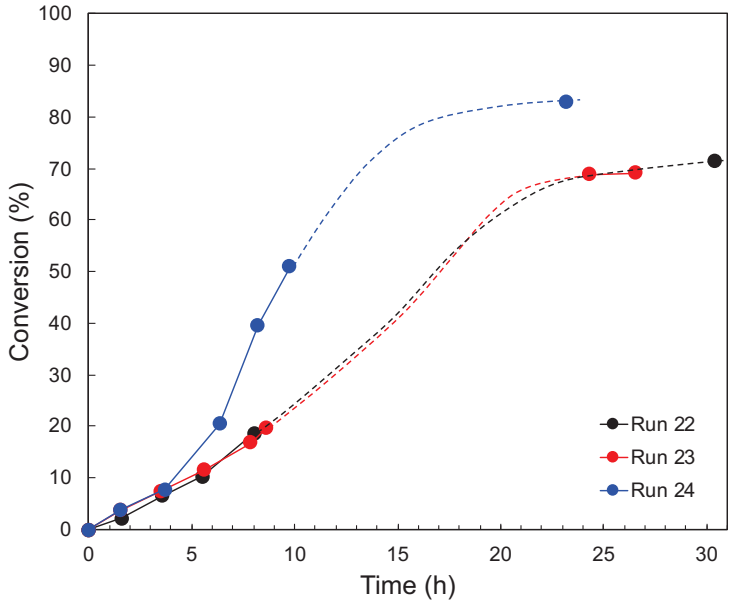

Figure 98. *Reproducibility – Evolution of conversion with time for dispersion photopolymerization of styrene with the stabilizer PVP 10 wt.% based on styrene (see Table 27 experimental conditions).*

Moreover, we observed that at conversion around 70–80%, the conversions reached a plateau. This can be attributed to the low styrene concentration in the polymer particles and the weak generation of radicals at the end of the polymerization.

In comparison with PEGMA macromonomer as a reactive stabilizer where the final particle size reached 360 nm, here we formed much larger particles (766–859 nm). Interestingly, we also obtained very narrow particle size distributions, without using TBAH (Figure 99 and Table 27).

Moreover, we carried out a "blank" experiment using thermal initiation (Table 27, run 25). Dispersion polymerization of styrene was carried out with AIBN at 70 °C, using 10 wt.% of PVP. Complete conversion was achieved after 6.4 h. Again, the particles were much larger with PVP (D_n = 931 nm, run 25) than with PEGMA (D_n = 346 nm, run 13). Besides, the size obtained

from photoinduced polymerization of styrene (D_n = 859, 794 and 766 nm for respectively runs 22, 23 and 24) was a bit smaller to what was obtained in heating conditions (D_n = 931 nm, Run 25).

The preparation of very large particles with very narrow size distributions in photoinduced dispersion polymerization was surprising and gratifying since we argued that as the particles grow, they reach a critical size at which point the light is subject to scattering limiting the generation of radicals, resulting in a stochastic behavior and a limitation in size. The nucleation should be fast enough before perturbation related to scattering occur. Only the growth step in this case could be affected when the particles reach a critical size around 380 nm which corresponds approximately to the irradiation wavelength (maximal scattering efficiency). As mentioned in Chapter 1, for a specific wavelength of light (λ_{max} = 430 nm in our case relative to the maximum absorbance of AO), there is an optimum scattering efficiency with respect to particle size. In the Mie theory, this optimum is found when the particle size corresponds to the irradiation wavelength. When this value is exceeded, the scattering efficiency decreases to reach a plateau. We thus believe that after reaching this critical size, the generation of radicals is less impacted, and the particles can continue to grow to reach micron sizes (regardless of the reproducibility issues).

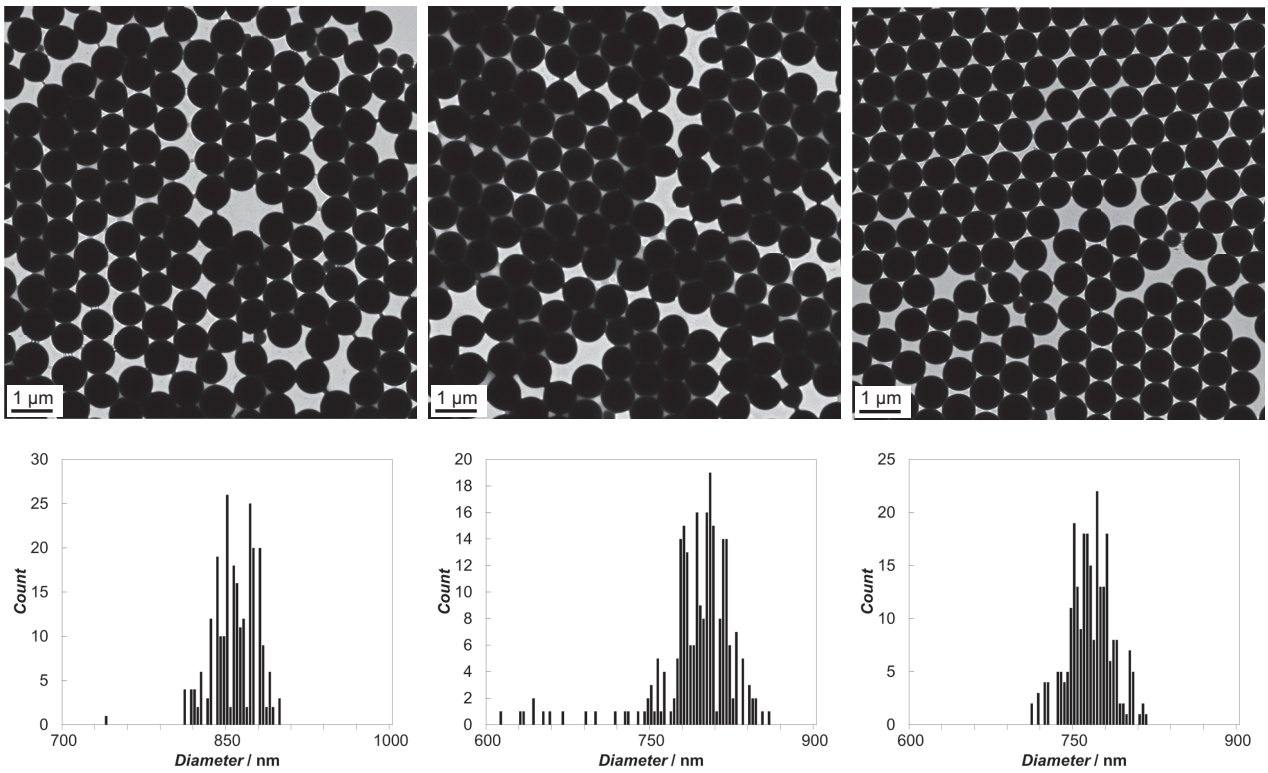

Figure 99. *TEM images and particle size distributions of the latexes obtained in the conditions described in Table 27, runs 22 (left) 23 (middle) and 24 (right).*

We believe that the formation of very large particles was intrinsically due to the stabilization by the PVP. Indeed, NHC-boryl is a nucleophilic radical that will not easily undergo hydrogen-atom abstraction from PVP. A small fraction of oligoradicals should terminate by chain transfer to PVP, thus generating radical sites on PVP from which PS segments can grow. The resulting graft copolymer becomes insoluble in the continuous phase and adsorbs on the particles. During the nucleation step, not enough graft copolymers are generated to stabilize the precursor particles and the latter likely aggregates to form larger particles stabilized by the few amounts of the graft copolymer. PVP has the drawbacks of being used in a relatively high proportion and only a very small fraction of the chains is subject to chain transfer reactions. But this stabilizer is very efficient since we obtained a very narrow size distribution.

As mentioned in the previous section, the size distribution seems to be a key factor for the obtention of large particles. We were thus able to exceed the critical size for which the light is scattered to its maximum and reach very large particle sizes with extremely narrow size distributions.

B. Effect of temperature

In the following experiments, the temperature was not controlled at 40 °C. The temperature profiles are represented in Figure 100. They exhibited very similar trend for both experiments (and for the upcoming experiments). The temperature started at 24 °C and reached 48–50°C after 3 h due to the heat released by the LED. The results are reported in Table 28. Note that the latexes were stable without any coagulum.

***Table 28**. Dispersion polymerization of styrene stabilized with PVPK- photo-induced under visible light without temperature controlled.* [a]

Run	Time (h)	Conv. (%)	D_n[b] (nm)	D_w/D_n[b]	N_p (x10^{13} cm^{-3})
26	25.4	72	1 006	1.014	1.23
27	28.9	72	925	1.008	1.66

[a] Experimental conditions: ethanol/water = 70/30 (wt.%). The solids content was fixed at 10 wt.%, PVPK-30 at 10 wt.% relative to styrene. [AO] = 1.3 10^{-5} mol L^{-1} (1 mol% with regard to NHC-BH_3), [disulfide] = 6.3 10^{-4} mol L^{-1} (50 mol% with regard to NHC-BH_3) and [NHC-BH_3] = 1.3 10^{-3} mol L^{-1}.
[b] Determined by TEM.

The conversion curves of styrene as a function of reaction time with 10 wt.% of PVP are plotted in Figure 100. Here again, the two conversion curves deviate at 3.5 h (< 10% monomer conversion), but they reach the same final conversion, approximately 72% after 25 h of irradiation. Even if the final destination (final conversion) was exactly the same, the path to reach it was very different. The stochastic behavior after 3.5 h once again supports that at a critical size of particles formed early in the polymerization, the light penetration within the reaction medium was stopped, which may cause locally a reduction in the rate of radical generation.

The DLS measurements indicated a particle size of around 250 nm at 10% styrene conversion, which corresponded to the critical size deducted previously when reproducibility issues occurred. Nevertheless, we formed very large particles (1 µm and 925 nm) with narrow particle size distributions (Table 28 and Figure 101).

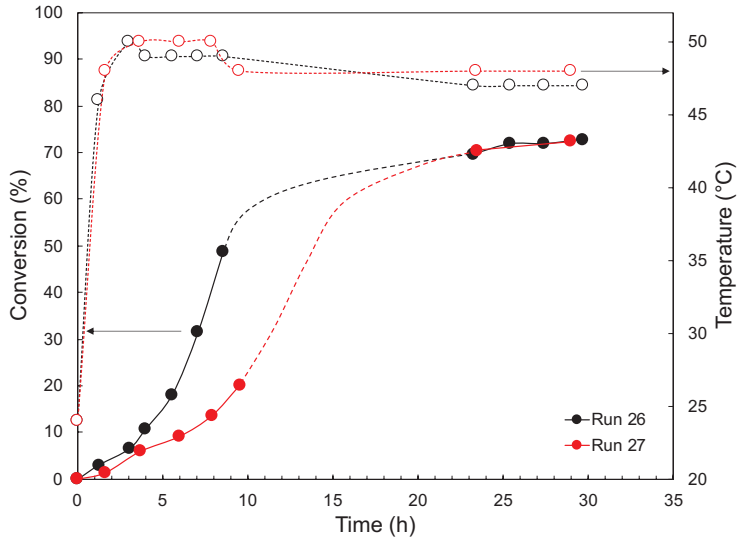

Figure 100. *Reproducibility – Evolution of conversion with time for dispersion photopolymerization of styrene with the stabilizer PVP 10 wt.% based on styrene and uncontrolled temperature (see Table 28 experimental conditions).*

In comparison with the experiments carried out at 40 °C (see Table 27), the particles were larger when the polymerization temperature reached 48–50 °C, for exactly the same experimental conditions (D_n = 859, 794 and 766, runs 22, 23 and 24 – see Table 27 vs. D_n = 1 006 and 925 nm, runs 26 and 27 – see Table 28). This observation was in agreement with what was found in the literature (*i.e.*, the increase of the temperature leads to an increase of the particle size).[68,69] At higher temperature, PVP-*g*-PS graft copolymer should be more soluble in the medium and therefore would adsorb more slowly onto the precursor particles to stabilize them, resulting in larger particles.

Despite the fact that these two experiments were not reproducible, we have been able to increase even more the particle size up to 1 □m. That is why in the following sections, we will discuss our results mainly in terms of particle size and not their kinetic behavior.

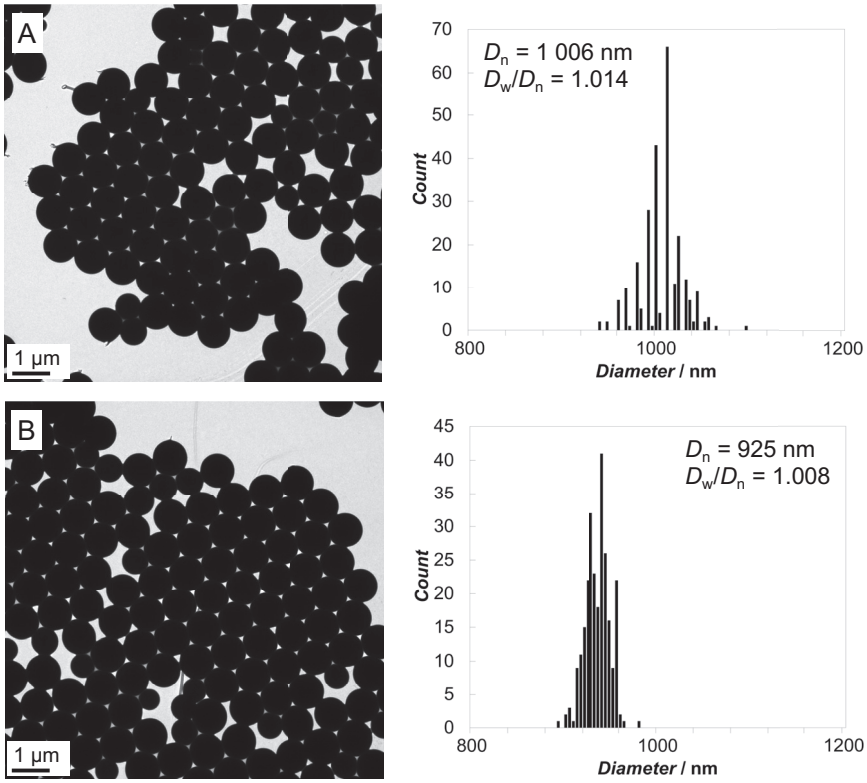

Figure 101. *TEM images and particle size distributions of the latexes obtained in the conditions described in Table 28, runs 30 (A) and 31 (B).*

C. Effect of the PVP concentration

In this section, the photopolymerizations were then conducted in the presence of a decreasing amount of PVP from 15 to 5 wt.% relative to styrene. The aim was to push our system to its limits and further increase particle size. The results are presented in Table 29.

Table 29. *Effect of PVP concentration on the dispersion polymerization of styrene under visible.* [a]

Run	PVP (wt.%)	Time (h)	Conv. (%)	D_n[b] (nm)	D_w/D_n[b]	N_p (x10^{13} cm^{-3})
28	15	23.5	58	775	1.038	1.01
29	10	25.4	72	1 006	1.014	1.23
30	5	23.7	58	1 212	1.063	0.57

[a] Experimental conditions: ethanol/water = 70/30 (wt.%). The solids content was fixed at 10 wt.%, PVPK-30 at 10 wt.% relative to styrene. [AO] = 1.3 10^{-5} mol L^{-1} (1 mol% with regard to NHC-BH_3), [disulfide] = 6.3 10^{-4} mol L^{-1} (50 mol% with regard to NHC-BH_3) and [NHC-BH_3] = 1.3 10^{-3} mol L^{-1}.
[b] Determined by TEM.

As expected, a decrease in PVP concentration led to an increase of particle size from 775 nm for 15 wt.% to 1.2 µm for 5 wt.% (Figure 102). The decrease in particle size is due to the fact that a lower amount of stabilizer was available to stabilize the particles, and thus larger particles were obtained. The obtention of a broader particle size distribution in the case of 5 wt.% of PVP may be due to the rather slow generation of radicals from our PIS resulting in a low and continuous nucleation (particularly at low stabilizer concentration). The reactions leading to particle stabilization when PVP is used has been delailed above. When PVP concentration was low, the formation of graft copolymer is thus less favored, which may explain the broader size dispersity. Nevertheless, we were able to increase even more the particle size by decreasing the PVP concentration at 5 wt.%, reaching *ca.* 1.2 µm.

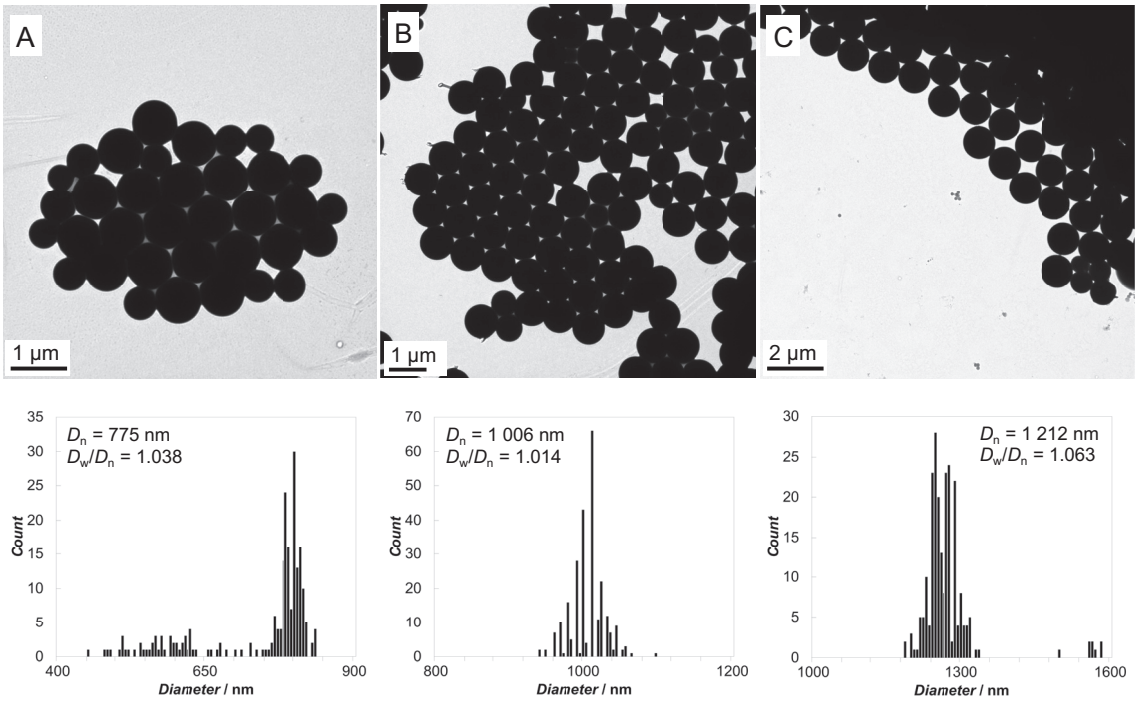

***Figure 102**. TEM images and particle size distributions of the PS latexes obtained, for different PVP: (A) 15, (B) 10 and (C) 5 wt.% relative to styrene (see Table 29 for experimental details).*

D. Conclusions

In summary, dispersion photopolymerization of styrene carried out in the presence of PVP as stabilizer exhibited reproducibility issues but the final particles were very large compared to the PS particles prepared in the presence of PEGMA, and with very narrow size distributions. Moreover, to our knowledge, this is the first example of dispersion photopolymerization under visible light irradiation where the PS particle sizes exceed one micron. The reproducibility issues are probably due to a combination of a slow and continuous generation of radicals and the maximum scattering efficiency occurring when the particles grow and reach a critical size around 380 nm. In addition, the fact that extremely broad size distributions were obtained could reduce scattering effect.

To sum up, we have succeeded in producing particles larger than 1 µm in diameter. Even if the kinetics are not reproducible, the final properties of the latexes are quite robust (size distributions, conversions).

General conclusions

In this chapter, we synthesized stable PS latexes without the presence of any coagulum with our three-component photoinitiating system based on NHC-Borane in hydro-alcoholic media under dispersion polymerization conditions using visible light irradiation. We also demonstrated that under those conditions, where all the compounds are initially soluble in the reaction mixture, dispersion photopolymerization of styrene was successful with the use of the disulfide alone. This supports one of the hypotheses made in the case of emulsion photopolymerization that the solubility of styrene is a key factor. We obtained here narrower particle size distributions, with both PVP and PEGMA (under optimal conditions).

First, the study with PEGMA macromonomer as a reactive stabilizer led to broad size distributions in comparison with thermally activated dispersion polymerizations, and to reproducibility issues. We believe that the generation of radicals was slow, resulting in a slow polymerization. This can be attributed by analogy with the emulsion conditions (basic pH) to the partition of the disulfide between the continuous phase and the polymer particles. We assumed that the stochastic behavior of the medium after a certain period of time might be related to a critical size (between 150 – 200 nm), from which the light penetration within the reaction medium could be negatively impacted. The addition of an organic base (TBAH) provided faster photopolymerizations with an excellent reproducibility and narrow size distributions. We believe that TBAH improves the disulfide solubility in the hydroalcoholic medium, leading to a higher generation of radicals. In addition, in the presence of TBAH, we observed an increase in the particle sizes. With the full PIS, TBAH could negatively affect PEG solubility in the continuous phase (salting out effect) resulting in a less efficient stabilization of the particles by the graft copolymer. When the disulfide was used alone as photoinitaitor, the poor decomposition of the disulfide in the visible range led to a retardation of the nucleation and thus, a weak probability to generate graft copolymer resulting in the production of fewer and larger particles. In addition, we demonstrated a more significant auto-acceleration with the disulfide alone than the full PIS (with or without TBAH), confirmed by the higher molar masses obtained.

Then, we used PVP and obtained very large particles up to 1.2 µm in diameter and very narrow particle size distributions proving the effectiveness of this stabilizer for the dispersion photopolymerization of styrene. To our knowledge, the production of such large latex particles by photoinitiated polymerization under visible light irradiation, has never been reported before

in the literature. However, as very large particles were formed, the polymerization kinetics was again not reproducible. We found in this case a larger critical size (380 nm) for which the stochastic behavior was observed. This difference of critical sizes might be due to the nucleation step (it should be faster enough in the case of PVP before perturbation related to scattering occurs). The formation of extremely narrow size distributions suggests that the latter is a key factor for the obtention of large particles. We were indeed able in those conditions to exceed the critical size which corresponds to an optimum scattering efficiency and continue the growth of particles.

To avoid the nucleation step, the use of seed particles of different sizes (from 50 nm to 1 µm) with very narrow size distributions could bring some interesting information on the impact of particle size and light penetration on the initiation efficiency. To go further, it should be also interesting to design a continuous flow photoreactor with very low optical path length in order to get rid of the light penetration issue.[119] It would also be interesting to match the refractive indices between the reaction medium and the polymer particles to reduce the light scattering. This could validate our hypothesis on the reproducibility issues related to a critical size.

References

[1] D. W. J. Osmond, H. H. Thompson, *Dispersion Polymerisation*, **1962**, GB893429 (A).
[2] K. E. J. Barrett, *Dispersion Polymerization in Organic Media*, Wiley, **1975**.
[3] Y. Almog, S. Reich, M. Levy, *Br. Polym. J.* **1982**, *14*, 131–136.
[4] S. Shen, E. D. Sudol, M. S. El-Aasser, *J. Polym. Sci. Part Polym. Chem.* **1994**, *32*, 1087–1100.
[5] S. Kobayashi, H. Uyama, Y. Matsumoto, I. Yamamoto, *Makromol. Chem.* **1992**, *193*, 2355–2362.
[6] C. M. Tseng, Y. Y. Lu, M. S. El-Aasser, J. W. Vanderhoff, *J. Polym. Sci. Part Polym. Chem.* **1986**, *24*, 2995–3007.
[7] B. Thomson, A. Rudin, G. Lajoie, *J. Polym. Sci. Part Polym. Chem.* **1995**, *33*, 345–357.
[8] T. Corner, *Colloids Surf.* **1981**, *3*, 119–129.
[9] A. Tuncel, R. Kahraman, E. Pişkin, *J. Appl. Polym. Sci.* **1993**, *50*, 303–319.
[10] H. Uyama, S. Kobayashi, *Polym. Int.* **1994**, *34*, 339–344.
[11] A. J. Paine, *Macromolecules* **1990**, *23*, 3109–3117.
[12] K. P. Lok, C. K. Ober, *Can. J. Chem.* **1985**, *63*, 209–216.
[13] P. Lacroix-Desmazes, J. Guillot, *J. Polym. Sci. Part B Polym. Phys.* **1998**, *36*, 325–335.
[14] J. Yeow, C. Boyer, *Adv. Sci.* **2017**, *4*, 1700137.
[15] F. D'Agosto, J. Rieger, M. Lansalot, *Angew. Chem. Int. Ed.* **2020**, *59*, 8368–8392.
[16] J. Rieger, *Macromol. Rapid Commun.* **2015**, *36*, 1458–1471.
[17] M. J. Derry, L. A. Fielding, S. P. Armes, *Prog. Polym. Sci.* **2016**, *52*, 1–18.
[18] X. Wang, L. Shen, Z. An, *Prog. Polym. Sci.* **2018**, *83*, 1–27.
[19] N. J. W. Penfold, J. Yeow, C. Boyer, S. P. Armes, *ACS Macro Lett.* **2019**, *8*, 1029–1054.
[20] P. Lacroix-Desmazes, in *Latex Synthétiques - Élabor. Propr. Appl.*, Lavoisier, **2006**, pp. 259–279.
[21] S. Kawaguchi, K. Ito, in *Polym. Part.* -- (Ed.: M. Okubo), Springer, Berlin, Heidelberg, **2005**, pp. 299–328.
[22] A. P. Richez, H. N. Yow, S. Biggs, O. J. Cayre, *Prog. Polym. Sci.* **2013**, *38*, 897–931.
[23] S. Kobayashi, H. Uyama, I. Yamamoto, Y. Matsumoto, *Polym. J.* **1990**, *22*, 759–761.
[24] A. J. Paine, *J. Colloid Interface Sci.* **1990**, *138*, 157–169.
[25] A. J. Paine, Y. Deslandes, P. Gerroir, B. Henrissat, *J. Colloid Interface Sci.* **1990**, *138*, 170–181.
[26] R. H. Pelton, A. Osterroth, M. A. Brook, *J. Colloid Interface Sci.* **1990**, *137*, 120–127.
[27] R. Pelton, A. Osterroth, M. A. Brook, *J. Colloid Interface Sci.* **1991**, *147*, 523–530.
[28] S. Kobayashi, H. Uyama, J. H. Choi, Y. Matsumoto, *Polym. Int.* **1993**, *30*, 265–270.
[29] P. Lacroix-Desmazes, A. Guyot, *Macromolecules* **1996**, *29*, 4508–4515.
[30] I. Capek, M. Riza, M. Akashi, *J. Polym. Sci. Part Polym. Chem.* **1997**, *35*, 3131–3139.
[31] S. M. Klein, V. N. Manoharan, D. J. Pine, F. F. Lange, *Colloid Polym. Sci.* **2003**, *282*, 7–13.
[32] S. E. Shim, H. Jung, K. Lee, J. M. Lee, S. Choe, *J. Colloid Interface Sci.* **2004**, *279*, 464–470.
[33] H. Jung, S. Y. Kim, K. Lee, B. H. Lee, S. E. Shim, S. Choe, *J. Polym. Sci. Part Polym. Chem.* **2005**, *43*, 3566–3573.
[34] H. Jung, K. Song, K. Lee, B. H. Lee, S. Choe, *J. Colloid Interface Sci.* **2007**, *308*, 130–141.
[35] W. Li, K. Matyjaszewski, *Macromol. Chem. Phys.* **2011**, *212*, 1582–1589.
[36] K. A. Shaffer, T. A. Jones, D. A. Canelas, J. M. DeSimone, S. P. Wilkinson, *Macromolecules* **1996**, *29*, 2704–2706.

[37] M. L. O'Neill, M. Z. Yates, K. P. Johnston, C. D. Smith, S. P. Wilkinson, *Macromolecules* **1998**, *31*, 2838–2847.
[38] M. Z. Yates, P. S. Shah, K. P. Johnston, K. T. Lim, S. Webber, *J. Colloid Interface Sci.* **2000**, *227*, 176–184.
[39] P. Lacroix-Desmazes, A. Guyot, *Polym. Adv. Technol.* **1997**, *8*, 608–615.
[40] M. D. C. Topp, P. J. Dijkstra, H. Talsma, J. Feijen, *Macromolecules* **1997**, *30*, 8518–8520.
[41] M. D. C. Topp, I. H. Leunen, P. J. Dijkstra, K. Tauer, C. Schellenberg, J. Feijen, *Macromolecules* **2000**, *33*, 4986–4988.
[42] M. Okubo, S. Fujii, H. Maenaka, H. Minami, *Colloid Polym. Sci.* **2002**, *280*, 183–187.
[43] S. Fujii, M. Suzaki, Y. Kakigi, K. Aono, S.-I. Yusa, Y. Nakamura, *J. Polym. Sci. Part Polym. Chem.* **2011**, *49*, 1633–1643.
[44] S. Fujii, K. Aono, M. Suzaki, S. Hamasaki, S. Yusa, Y. Nakamura, *Macromolecules* **2012**, *45*, 2863–2873.
[45] J. Jennings, G. He, S. M. Howdle, P. B. Zetterlund, *Chem. Soc. Rev.* **2016**, *45*, 5055–5084.
[46] P. B. Zetterlund, S. C. Thickett, S. Perrier, E. Bourgeat-Lami, M. Lansalot, *Chem. Rev.* **2015**, *115*, 9745–9800.
[47] H. Minami, Y. Kagawa, S. Kuwahara, J. Shigematsu, S. Fujii, M. Okubo, *Des. Monomers Polym.* **2004**, *7*, 553–562.
[48] J. Ryan, F. Aldabbagh, P. B. Zetterlund, M. Okubo, *Polymer* **2005**, *46*, 9769–9777.
[49] G. Delaittre, M. Save, B. Charleux, *Macromol. Rapid Commun.* **2007**, *28*, 1528–1533.
[50] E. Bourgeat-Lami, A. Guyot, *Colloid Polym. Sci.* **1997**, *275*, 716.
[51] S. Fujii, H. Minami, M. Okubo, *Colloid Polym. Sci.* **2004**, *282*, 569–574.
[52] G. Zheng, C. Pan, *Macromolecules* **2006**, *39*, 95–102.
[53] M. Bathfield, F. D'Agosto, R. Spitz, C. Ladavière, M.-T. Charreyre, T. Delair, *Macromol. Rapid Commun.* **2007**, *28*, 856–862.
[54] W.-D. He, X.-L. Sun, W.-M. Wan, C.-Y. Pan, *Macromolecules* **2011**, *44*, 3358–3365.
[55] E. D. Sudol, in *Polym. Dispers. Princ. Appl.* (Ed.: J.M. Asua), Springer Netherlands, Dordrecht, **1997**, pp. 141–153.
[56] R. M. Fitch, C. H. Tsai, in *Polym. Colloids* (Ed.: R.M. Fitch), Springer US, Boston, MA, **1971**, pp. 73–102.
[57] P. J. Feeney, D. H. Napper, R. G. Gilbert, *Macromolecules* **1984**, *17*, 2520–2529.
[58] M. D. Croucher, M. A. Winnik, in *Introd. Polym. Colloids* (Eds.: F. Candau, R.H. Ottewill), Springer Netherlands, Dordrecht, **1990**, pp. 35–72.
[59] C. M. Hansen, *The Three-Dimensional Solubility Parameter and Solvent Diffusion Coefficient: Their Importance in Surface Coating Formulation*, Danish Technical Press, **1967**.
[60] A. J. Paine, *J. Polym. Sci. Part Polym. Chem.* **1990**, *28*, 2485–2500.
[61] J. Brandrup, E. H. Immergut, *Polymer Handbook*, Wiley, New York, **1975**.
[62] J. W. Vanderhoff, M. S. El-Aasser, F. J. Micale, E. D. Sudol, C. Tseng, A. Silwanowicz, D. M. Kornfeld, F. A. Vicente, *J. Dispers. Sci. Technol.* **1984**, *5*, 231–246.
[63] S. Shen, E. D. Sudol, M. S. El-Aasser, *J. Polym. Sci. Part Polym. Chem.* **1993**, *31*, 1393–1402.
[64] M. Hattori, E. D. Sudol, M. S. El-Aasser, *J. Appl. Polym. Sci.* **1993**, *50*, 2027–2034.
[65] R. Hu, V. L. Dimonie, E. D. Sudol, M. S. El-Aasser, *J. Appl. Polym. Sci.* **1995**, *55*, 1411–1415.
[66] D. Wang, V. L. Dimonie, E. D. Sudol, M. S. El-Aasser, *J. Appl. Polym. Sci.* **2002**, *84*, 2692–2709.
[67] A. J. Paine, W. Luymes, J. McNulty, *Macromolecules* **1990**, *23*, 3104–3109.

[68] Y. Chen, H.-W. Yang, *J. Polym. Sci. Part Polym. Chem.* **1992**, *30*, 2765–2772.
[69] H. Bamnolker, S. Margel, *J. Polym. Sci. Part Polym. Chem.* **1996**, *34*, 1857–1871.
[70] O. Šušoliak, J. Bartoň, *Chem. Pap.* **1985**, 12.
[71] K. E. J. Barrett, H. R. Thomas, *J. Polym. Sci. [A1]* **1969**, *7*, 2621–2650.
[72] J. Liu, C. H. Chew, S. Y. Wong, L. M. Gan, J. Lin, K. L. Tan, *Polymer* **1998**, *39*, 283–289.
[73] M. Riza, I. Capek, A. Kishida, M. Akashi, *Angew. Makromol. Chem.* **1993**, *206*, 69–75.
[74] Y. Y. Lu, M. S. El-Aasser, J. W. Vanderhoff, *J. Polym. Sci. Part B Polym. Phys.* **1988**, *26*, 1187–1203.
[75] P. J. Flory, *Principles of Polymer Chemistry*, Cornell University Press, **1953**.
[76] M. Morton, S. Kaizerman, M. W. Altier, *J. Colloid Sci.* **1954**, *9*, 300–312.
[77] S. Jiang, E. D. Sudol, V. L. Dimonie, M. S. El-Aasser, *J. Polym. Sci. Part Polym. Chem.* **2008**, *46*, 3638–3647.
[78] I. Capek, M. Riza, M. Akashi, *Makromol. Chem.* **1992**, *193*, 2843–2860.
[79] V. Jaacks, *Makromol. Chem.* **1972**, *161*, 161–172.
[80] K. Ito, H. Tsuchida, A. Hayashi, T. Kitano, E. Yamada, T. Matsumoto, *Polym. J.* **1985**, *17*, 827–839.
[81] T. Kelen, F. Tüdös, B. Turcsányi, *Polym. Bull.* **1980**, *2*, 71–76.
[82] P. Lacroix-Desmazes, A. Guyot, *Polym. Adv. Technol.* **1997**, *8*, 601–607.
[83] J. Chen, Z. Zeng, J. Yang, Y. Chen, *J. Polym. Sci. Part Polym. Chem.* **2008**, *46*, 1329–1338.
[84] Z. Huang, F. Sun, S. Liang, H. Wang, G. Shi, L. Tao, J. Tan, *Macromol. Chem. Phys.* **2010**, *211*, 1868–1878.
[85] Z. Zhu, F. Sun, L. Yang, K. Gu, W. Li, *Chem. Eng. J.* **2013**, *223*, 395–401.
[86] S. Perrier, *Macromolecules* **2017**, *50*, 7433–7447.
[87] S. E. Shim, H. Jung, H. Lee, J. Biswas, S. Choe, *Polymer* **2003**, *44*, 5563–5572.
[88] H. Kaczmarek, A. Kamińska, M. Świątek, J. F. Rabek, *Angew. Makromol. Chem.* **1998**, *261–262*, 109–121.
[89] B. Ki, Y. C. Yu, H. J. Jeon, W.-R. Yu, H. W. Ryu, J. H. Youk, *Fibers Polym.* **2012**, *13*, 135–138.
[90] J. Tan, X. Rao, X. Wu, H. Deng, J. Yang, Z. Zeng, *Macromolecules* **2012**, *45*, 8790–8795.
[91] J. Tan, X. Rao, J. Yang, Z. Zeng, *Macromolecules* **2013**, *46*, 8441–8448.
[92] J. Tan, G. Zhao, Y. Lu, Z. Zeng, M. A. Winnik, *Macromolecules* **2014**, *47*, 6856–6866.
[93] J. Tan, X. Rao, D. Jiang, J. Yang, Z. Zeng, *Polymer* **2014**, *55*, 2380–2388.
[94] J. Tan, G. Zhao, Z. Zeng, M. A. Winnik, *Macromolecules* **2015**, *48*, 3629–3640.
[95] J. Tan, L. Fu, X. Zhang, Y. Bai, L. Zhang, *J. Mater. Sci.* **2016**, *51*, 9455–9471.
[96] Y. Jiang, N. Xu, J. Han, Q. Yu, L. Guo, P. Gao, X. Lu, Y. Cai, *Polym. Chem.* **2015**, *6*, 4955–4965.
[97] Q. Yu, Y. Ding, H. Cao, X. Lu, Y. Cai, *ACS Macro Lett.* **2015**, *4*, 1293–1296.
[98] P. Gao, H. Cao, Y. Ding, M. Cai, Z. Cui, X. Lu, Y. Cai, *ACS Macro Lett.* **2016**, *5*, 1327–1331.
[99] J. Yeow, J. Xu, C. Boyer, *ACS Macro Lett.* **2015**, *4*, 984–990.
[100] J. Yeow, J. Xu, C. Boyer, *J. Vis. Exp. JoVE* **2016**, DOI 10.3791/54269.
[101] J. Yeow, S. Shanmugam, N. Corrigan, R. P. Kuchel, J. Xu, C. Boyer, *Macromolecules* **2016**, *49*, 7277–7285.
[102] J. Tan, H. Sun, M. Yu, B. S. Sumerlin, L. Zhang, *ACS Macro Lett.* **2015**, *4*, 1249–1253.
[103] J. Tan, Y. Bai, X. Zhang, C. Huang, D. Liu, L. Zhang, *Macromol. Rapid Commun.* **2016**, *37*, 1434–1440.
[104] J. Tan, Y. Bai, X. Zhang, L. Zhang, *Polym. Chem.* **2016**, *7*, 2372–2380.

[105] J. Tan, C. Huang, D. Liu, X. Zhang, Y. Bai, L. Zhang, *ACS Macro Lett.* **2016**, *5*, 894–899.
[106] J. Tan, J. He, X. Li, Q. Xu, C. Huang, D. Liu, L. Zhang, *Polym. Chem.* **2017**, *8*, 6853–6864.
[107] H. Agrawal, N. Thacker, A. Misra, in *Chall. Deliv. Ther. Genomics Proteomics* (Ed.: A. Misra), Elsevier, London, **2011**, pp. 531–622.
[108] V. Tkachenko, C. M. Ghimbeu, C. Vaulot, L. Vidal, J. Poly, A. Chemtob, *Polym. Chem.* **2019**, *10*, 2316–2326.
[109] F. Le Quéméner, D. Subervie, F. Morlet-Savary, J. Lalevée, M. Lansalot, E. Bourgeat-Lami, E. Lacôte, *Angew. Chem. Int. Ed.* **2018**, *57*, 957–961.
[110] I. Capek, S. H. Nguyen, D. Berek, *Polymer* **2000**, *41*, 7011–7016.
[111] P. Lacroix-Desmazes, A. Guyot, *Colloid Polym. Sci.* **1996**, *274*, 1129–1136.
[112] C. K. Ober, M. L. Hair, *J. Polym. Sci. Part Polym. Chem.* **1987**, *25*, 1395–1407.
[113] C.-H. Ho, S.-A. Chen, M. D. Amiridis, J. W. V. Zee, *J. Polym. Sci. Part Polym. Chem.* **1997**, *35*, 2907–2915.
[114] S. Chen, Y.-L. Yu, J.-H. Wang, *Anal. Chim. Acta* **2018**, *999*, 13–26.
[115] F. Jasinski, P. B. Zetterlund, A. M. Braun, A. Chemtob, *Prog. Polym. Sci.* **2018**, *84*, 47–88.
[116] C. Di, X. Jiang, J. Yin, *J. Appl. Polym. Sci.* **2010**, *115*, 1831–1840.
[117] J. P. Magnusson, A. Khan, G. Pasparakis, A. O. Saeed, W. Wang, C. Alexander, *J. Am. Chem. Soc.* **2008**, *130*, 10852–10853.
[118] S. Saeki, N. Kuwahara, M. Nakata, M. Kaneko, *Polymer* **1977**, *18*, 1027–1031.
[119] N. Zaquen, M. Rubens, N. Corrigan, J. Xu, P. B. Zetterlund, C. Boyer, T. Junkers, *Prog. Polym. Sci.* **2020**, *107*, 101256.

Chapter 4.

Polymer/inorganic hybrid latex particles via hydroalcoholic dispersion photopolymerization under visible light irradiation

Table of content

PART 1. LITERATURE REVIEW 193

I. INTRODUCTION 193

II. FORMATION OF ORGANIC/INORGANIC HYBRID LATEXES BY PICKERING POLYMERIZATION IN DISPERSED MEDIA 196

A. Pickering emulsions 196
B. Pioneering studies on heterogeneous Pickering polymerization in dispersed media 198
C. Pickering dispersion polymerization 198
1. Silica 198
2. Clay 200
3. Iron oxide 202

PART 2. CERIUM DIOXIDE AS PICKERING STABILIZER 203

I. CERIUM DIOXIDE 203

A. Nature of the CeO_2 sol 203
B. Particle size and morphology 203
C. Crystalline structure 204
D. Surface chemistry 206

II. SYNTHESIS OF CeO_2-ARMORED HYBRID LATEXES BY POLYMERIZATION OF PICKERING MINIEMULSIONS 208

A. Stabilization of miniemulsion droplets by CeO_2 nanoparticles 208
B. Polymerization of CeO_2-stabilized miniemulsions 209
C. Conclusion 213

III. SYNTHESIS OF CeO_2-ARMORED HYBRID LATEXES BY PICKERING EMULSION POLYMERIZATION 213

A. Functionalization of CeO_2 nanoparticles by MAA 214
B. Pickering emulsion polymerization with CeO_2 nanoparticles 215
C. Characteristics of CeO_2-armored P(*n*-BA-*co*-MMA) latex films 218

IV. SYNTHESIS OF CeO_2-ARMORED HYBRID LATEXES BY PICKERING EMULSION PHOTOPOLYMERIZATION 222

A. Functionalization of CeO_2 nanoparticles by disulfide 223
B. Pickering emulsion photopolymerization with CeO_2 nanoparticles 225

PART 3. SYNTHESIS OF CeO_2-ARMORED LATEXES *VIA* VISIBLE LIGHT-INDUCED PICKERING DISPERSION POLYMERIZATION 228

I. PREPARATION OF DICARBOXYLIC ACID DIPHENYL DISULFIDE MODIFIED CeO_2 NANOPARTICLES 229

A. Stabilization of CeO_2 nanoparticles in hydroalcoholic medium 229
1. Choice of the hydroalcoholic medium 229
2. Surface modification of CeO_2 nanoparticles by disulfide 230

II. SYNTHESIS OF CeO_2-ARMORED HYBRID LATEXES BY PICKERING DISPERSION PHOTOPOLYMERIZATION 236

A. Efficiency of our disulfide-modified CeO_2 nanoparticles for Pickering dispersion photocopolymerization of *n*-BA and MMA 237
B. Influence of the CeO_2 content 239
C. Influence of the disulfide concentration 241
D. Influence of the luminous flux 244
E. Towards very low CeO_2 contents 245

F. Influence of the monomer concentration 248
G. Proposed mechanism for the particle formation 250
H. Disulfide vs. three-component photoinitiating system 252

III. CHARACTERIZATION OF CEO_2-ARMORED P(*N*-BA-*CO*-MMA) LATEX FILMS 253

A. Structural characterization 254
B. Optical properties 255
C. Mechanical properties 257

GENERAL CONCLUSION 259

REFERENCES 261

In the previous chapters, we studied our three-component PIS in emulsion and dispersion polymerization processes and successfully obtained stable latexes with very narrow size distributions. These latexes produced in emulsion were stabilized by a surfactant, SDS, and in dispersion by two polymeric stabilizers, PEGMA and PVP. However, these species can negatively impact the final properties of the films formed from those latexes (*e.g.* surfactant migration). For that purpose, a new class of stabilizer (inorganic nanoparticles) has emerged. It is then possible to produce stable hybrid latexes and combine both properties of polymer and inorganic nanoparticles.

This chapter is organized in three specific parts. First, the different studies on the systems used for the formation of polymer/inorganic hybrid latexes by polymerization in dispersion will be discussed. Next, we will focus on cerium dioxide (CeO_2) nanoparticles (NPs) and their application in miniemulsion and emulsion polymerization, both under thermal and photo-activated initiation. The last section will report the use of our disulfide as photoinitiator under visible light irradiation in the presence of CeO_2 NPs for the preparation of poly(*n*-butyl acrylate-*co*-methyl methacrylate) particles through dispersion polymerization, and the effect of several parameters will be studied. Finally, we will discuss the characteristics of the films obtained from these hybrid latexes.

Part 1. Literature review

I. Introduction

Owing to their remarkable properties, hybrid nanomaterials occupy an increasingly important place in our daily life and cover various sectors of activity such as construction industry, biomedicine, or cosmetics. Moreover, nature is replete with examples of hybrid materials (nacre, bone, or corals). Organic/inorganic hybrid materials have been produced by humans since ancient times. For example, the Maya blue pigment shows a notable conservation in time which allowed the frescoes of pre-Columbian civilizations to come down through the centuries. Research has shown that its composition contains a mixture of natural indigo molecules attached to a mineral clay matric (palygorskite).[1] The combination of these two phases has made it possible to obtain new properties, especially the resistance over time, much more superior to what they would have been separately. However, the scientific interest in hybrid materials has developed relatively recently, specifically for paintings. These materials

have experienced a real boom in the 1980's with the development of new synthetic techniques. Indeed, based on a bio-inspired approach, several so-called "soft chemistry" processes carried out at mild temperatures have emerged to produce hybrid materials.[2,3] Herein, the preparation of polymer/inorganic hybrid particles which contain polymers as the organic component will be discussed.

Polymer/inorganic hybrid particles take full advantage of the polymer component properties (structural and mechanical features, and processability) which can be combined with those of the inorganic component to bring specific functionalities (magnetism, catalytic activity, luminescence …) and/or reinforce the mechanical and thermal properties of the polymer. The final properties of the hybrid materials result in synergetic effects from both components. Four synthetic routes are possible to form polymer/inorganic hybrid latexes as depicted in Figure 103.[4]

1- The formation of both polymer and inorganic components occurs *ex situ*, and the hybrid nanoparticles are formed by their combination. In that case, the polymers formed are either covalently (for example by "grafting to") or non-covalently bound to the inorganic particles.

2- The inorganic component is formed *ex situ* and the polymerization of the organic component takes place in its presence.

3- The polymer particles are formed *ex situ* and the precipitation/crystallization of the inorganic component occurs *in situ* on polymer particles which act as "template".

4- Both the polymer and the inorganic components are simultaneously formed *in situ* during hybrid nanoparticle formation.

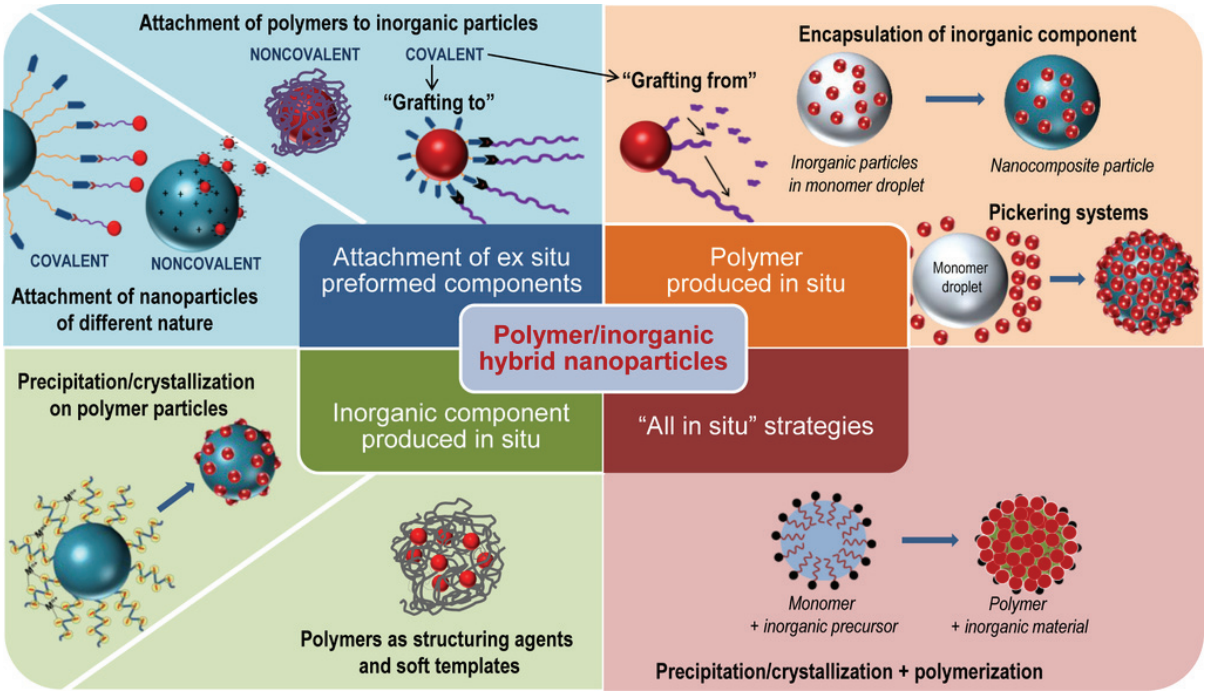

Figure 103. *Different synthetic strategies in the formation of polymer/inorganic hybrid particles.*[4]

In the second case, where the polymerization takes place in the presence of preformed inorganic particles, the key to efficiently form polymer/inorganic hybrid nanoparticles is the adjustment between the physical and chemical properties of the inorganic particle surface and those of the polymer matrix, so that the inorganic component is well wetted by the polymer chains. When these properties match (*via* surface energy minimizations), it is possible to selectively control the particle location within the latexes.[5] For example, the inorganic particles can be encapsulated by the polymer which provide them a protection from environmental aggressions or functional groups (from the polymer surface) to improve interactions with the surrounding medium. In the case where the inorganic particles are located at the polymer particle surface (core-shell morphology), hollow particles can be formed by removal of the core. The various possible morphologies obtained have an obvious interest in, for instance, drug delivery or encapsulation of pigments for the paint industry.

In this chapter, we will focus on the case where inorganic nanoparticles are used as stabilizer and this approach is based on the stabilization of Pickering emulsions, *i.e.*, the capacity of inorganic nanoparticles to adhere to soft deformable interfaces. It is important to keep in mind that Pickering emulsion polymerization is not the polymerization of emulsion droplets stabilized by inorganic nanoparticles. After a short introduction on the concepts underlying Pickering emulsions, we will discuss the preparation of organic/inorganic hybrid latexes prepared by dispersion polymerization using solid particles as stabilizer.

II. Formation of organic/inorganic hybrid latexes by Pickering polymerization in dispersed media

A. Pickering emulsions

The researches of Ramsden in 1903 and Pickering in 1907 have introduced a new class of emulsions characterized by the presence of particles at the oil/water (O/W) interfaces, so-called Pickering emulsions.[6,7] Pickering emulsions can be of any type, either oil-in-water, water-in-oil, or even multiple.[8,9] There is a wide variety of available particles (organic and inorganic) with different shape and/or size that can be used to form Pickering emulsions.[10] The interest arises from the fact that the particles located at the interface between the two liquids exert electrostatic forces, creating a physical barrier which prevents the emulsion droplets to coalesce. The wettability properties of the solid particles at the O/W interface is the main parameter determining the formation and stability of Pickering emulsions.[8,11] The particle wettability is characterized by the three-phase contact angle (θ – see Figure 104). For solid particles stabilizing Pickering emulsions, θ is the equivalent of the hydrophilic-lipophilic balance for surfactants.[12] When $\theta < 90°$, solid particles are mostly hydrophilic and stabilize O/W emulsions as a larger part of the particles is immersed in the aqueous phase. Conversely, when $\theta > 90°$, solid particles are mostly hydrophobic and stabilize W/O emulsions.

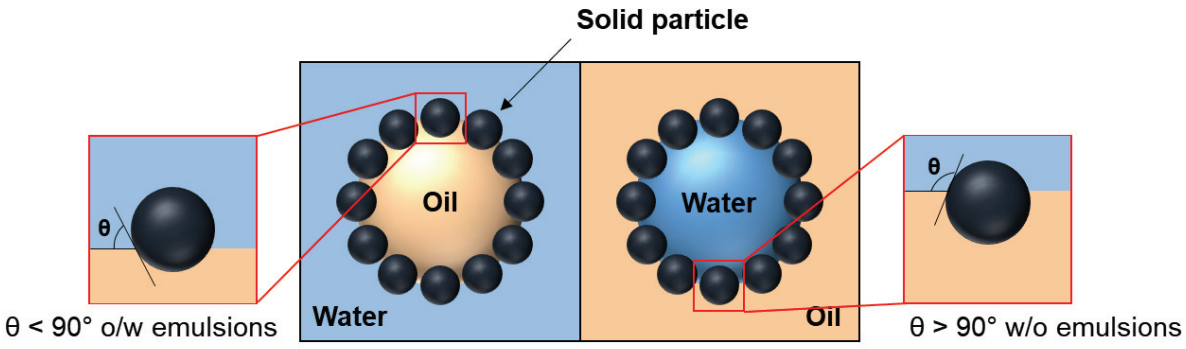

Figure 104. *Schematic representation of an O/W and a W/O Pickering emulsion as a function of the three-phase contact angle (θ).*

It is important to notice that emulsions can be stabilized with fully hydrophilic or fully hydrophobic particles.[13] It is also possible to have particles with $\theta = 90°$ (or very close) which can lead to the formation of double emulsions since they are capable to efficiently stabilize both types of interfaces (O/W and W/O).[14–16] The stabilization mechanism of Pickering emulsions is based on the adsorption of the particles at the O/W interface. The free energy of adsorption

ΔG_d[17] represents the energy required to remove a spherical particle of radius r and of three-phase contact angle θ, from an O/W interface with an interfacial tension γ_{OW} and is given by the following equation:

$$\Delta G_d = \pi r^2 \gamma_{OW} (1 \pm \cos\theta)^2 \quad (Eq.\,4.1)$$

The energy required to desorb the particles from the O/W interface is maximal for θ = 90° (Figure 105a). As the solid particle size increases, the energy of adsorption increases at a fixed contact angle (Figure 105b). In the case where the radius of the particles and the contact angle are fixed, the energy of adsorption is affected by the O/W interfacial tension, but the influence is less pronounced than for the radius (Figure 105c). The energy of adsorption is much higher than that of surfactants, which is equivalent to the thermal energy (k_BT). The adsorption of solid particles is thus considered to be irreversible unlike surfactants which are subject to continuous adsorption-desorption phenomena.[18,19]

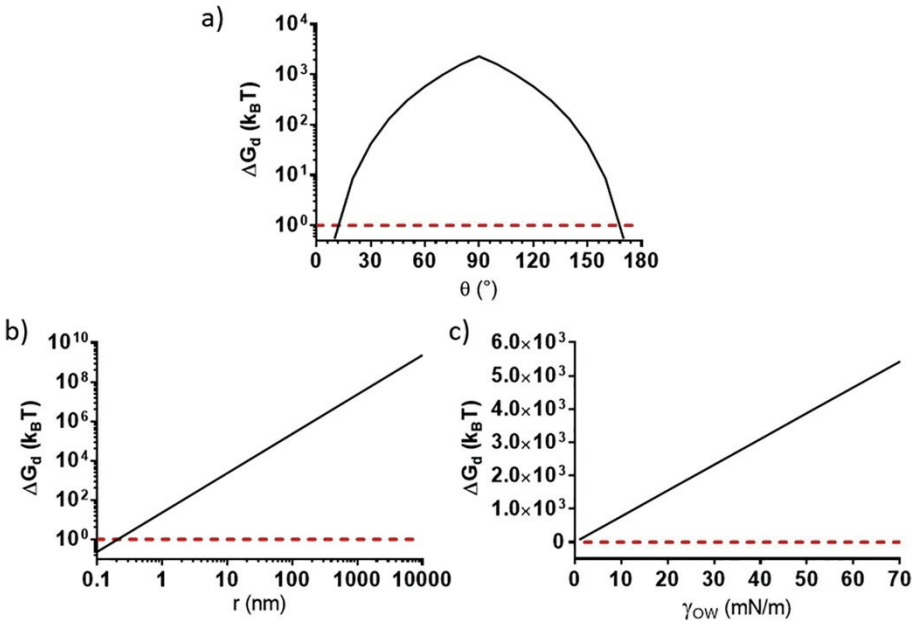

Figure 105. *Variation of the energy required to remove a particle from an O/W interface as a function of a) the three-phase contact angle (γ_{OW} = 30 mN m^{-1} and r = 10 nm), b) the radius of the particles (γ_{OW} = 30 mN m^{-1} and θ = 90°) and c) the interfacial tension at the O/W interface particles (r = 10 nm and θ = 90°). The horizontal dashed line corresponds to the k_BT value at 293 K.*[11]

We will show in the next sections how this type of stabilization has been used to synthesize polymer/inorganic hybrid particles by dispersion polymerization.

B. Pioneering studies on heterogeneous Pickering polymerization in dispersed media

The pioneering works on the preparation of hybrid latexes with solid particles as Pickering stabilizer in heterogeneous polymerization processes was described by Rohm and Trommsdorff in the mid of 1930's.[20] In their study, the authors used tale, barium sulphate, kaolin clay and aluminum oxide in the suspension polymerization of several monomers. Since then, two main techniques have been investigated to produce organic/inorganic hybrid latexes: the polymerization of Pickering miniemulsions[21–23], and emulsion[24–30] Pickering polymerizations using a variety of monomers and a range of inorganic particles such as silica, Laponite® clay, magnetite, or titanium dioxide.[31] The miniemulsion and emulsion processes will be not detailed in this thesis. The reader is referred to the recent reviews and textbooks for a comprehensive description of these techniques.[31–35]

To allow efficient adhesion of the inorganic nanoparticles with the polymer, it is common to introduce groups that are reactive in the polymerization process (*e.g.*, monomers, initiators, or chain transfer agents). These groups may be either chemically bound or physically adsorbed on the surface. In the following sections, a list of studies on relying on the concepts of Pickering stabilization to form such hybrid latexes will be presented in dispersion conditions.

C. Pickering dispersion polymerization

1. Silica

The first study on Pickering dispersion polymerization was reported by Armes and co-workers in 1992.[36] Indeed, this technique was used to produce polyaniline latexes stabilized by silica NPs (diameter = 38 nm). A minimum silica content of *ca*. 3 wt.% was necessary to form stable latexes with diameters in the 200–500 nm range. Unusual raspberry-like hybrid nanoparticles were observed with the silica NPs being held together by the polyaniline "binder".[37] The authors showed that for a sufficient silica content, the size of the hybrid particles and the size dispersity were only weakly dependent on the addition of more silica NPs, the acidity of the medium or the reaction temperature.[38]

Armes and co-workers then studied the synthesis of silica NPs-vinyl copolymer latexes via aqueous Pickering dispersion polymerization by using a water-soluble monomer 2-hydroxypropyl methacrylate (HPMA) and 4-VP (minimum 15 wt.%) as an auxiliary comonomer (Figure 106).[39,40] As previously mentioned, the presence of 4-VP improved the interaction between the silica nanoparticles and the polymer particles. The obtained core-shell hybrid nanoparticles showed uniform size distributions with diameters of 205–330 nm, and silica contents ranging from 5 to 42 wt.% (depending on the proportion of 4-VP). Finally, the films formed by annealing the latexes showed good transparency (greater than 80% transmittance over the visible wavelength range), even for high silica contents (30 wt.%).

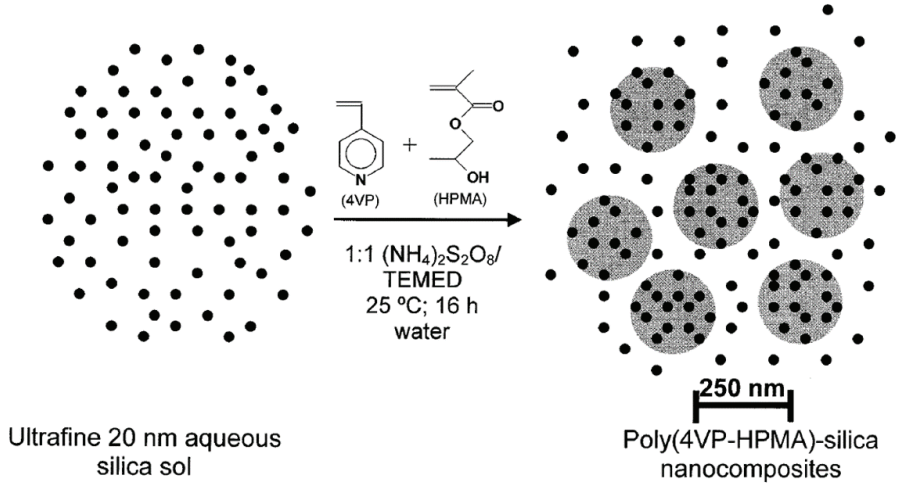

Figure 106. *Reaction scheme for the formation of poly(HPMA-co-4-VP)/silica hybrid particles by aqueous Pickering dispersion polymerization.*[39,40]

By using commercial alcoholic silica sols, Armes and co-workers carried out the Pickering dispersion polymerization of several monomers such as styrene, MMA, MAA, *n*-BuA and HPMA without the use of an auxiliary comonomer.[41] Stable inorganic/organic hybrid particles were obtained with reasonably narrow size distributions and silica contents of up to 58 wt.%. The authors further investigated the influence of the nature of the initiator on the formation of silica-polystyrene hybrid particles prepared by Pickering dispersion polymerization in methanol or 2-propanol. The use of a nonionic azo-initiator (AIBN) led to micron-sized hybrid particles containing very low silica contents (no more than 1.1%). However, the silica sol located at the particle surface was responsible for the colloidal stability. In that case, the silica incorporation efficiency was very low. By using an anionic azo-initiator 4,4'-azobis(4-cyanovaleric acid) (ACVA), precipitated amorphous polystyrene was obtained. Conversely, the use of a cationic azo-initiator, AAPH, led to submicron-sized hybrid particles containing high silica contents

(between 13 and 29 wt.%). According to the XPS and TEM analysis, well-defined core-shell morphologies for these silica/polystyrene hybrid latexes were obtained with particle size in the 262–464 nm range (Figure 107). Here again, the effect of a strong electrostatic interaction between the initiator/oligomers and the anionic silica sol for efficient hybrid particles formation was highlighted.

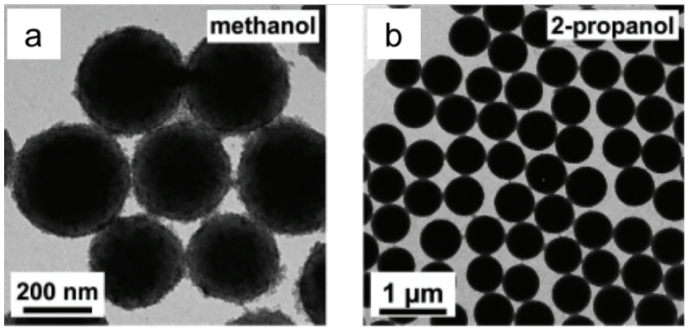

Figure 107. *TEM images of silica/polystyrene hybrid latexes prepared by Pickering dispersion polymerization in (a) methanol and (b) 2-propanol initiated with AAPH in the presence of 13 nm diameter silica particles.*[41]

2. Clay

Greesh *et al.*[42] reported for the first time the synthesis of fully exfoliated polymer/clay hybrid latexes via Pickering dispersion polymerization of styrene in polar medium (ethanol/water, 85/15 vol%). For that purpose, Na-MMT was functionalized by MPTMS to improve the interaction between clay and the polymer particles. The final particle size decreased from 1050 to 254 nm with narrower size distributions as the clay contents increased from 1 to 10 wt.% (relative to styrene) (Figure 108). The authors obtained two different morphologies depending on the clay content. At low clay content, exfoliated structures were obtained while intercalated structures were observed at high clay content. However, the particles obtained were not completely stable and the TEM images showed that most of the clay platelets were in the continuous phase.

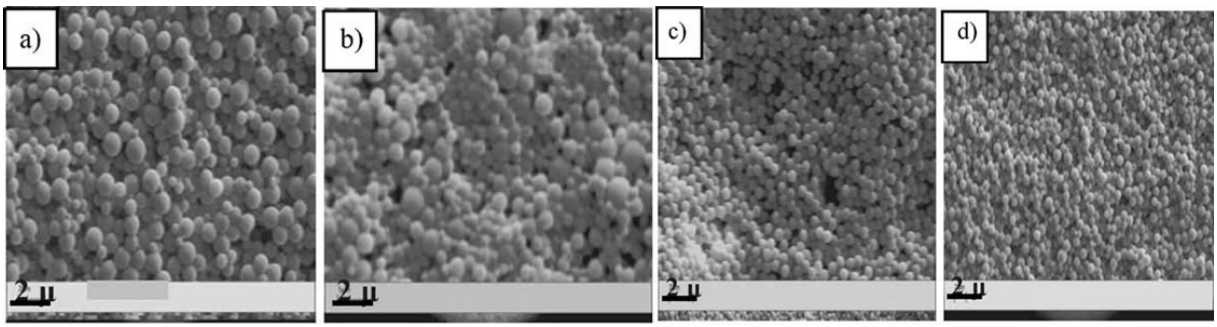

Figure 108. *SEM images of polystyrene containing: (a) 1, (b) 3, (c) 7, and (d) 10% clay content, respectively. Scale bar = 2 µm.*[42]

In order to improve the stability, the authors modified Na-MMT clay by using a cationic amphiphilic block copolymer of poly(styrene-b-2-hydroxyethyl acrylate) (PS-*b*-PHEA) *via* ion-exchange reaction and use this (PS-*b*-PHEA)-modified MMT clay as Pickering stabilizer to prepare polystyrene particles *via* dispersion polymerization.[43] Indeed, the polystyrene chains should adsorb strongly onto the polystyrene particle surface while the PHEA segments anchored to the MMT clay is soluble in the alcoholic medium and provides steric stabilization. The authors proposed a mechanism for hybrid particles formation (Figure 109). Styrene starts to polymerize in the homogenous medium and when the polymer chains reach a critical chain length, they precipitate to form the nuclei. Then, the polystyrene segments of the (PS-*b*-PHEA)-modified MMT clay adsorbs onto the surface of the primary polystyrene particles to prevent further aggregation. Finally, the polymerization proceeds within the polymer particles through monomer diffusion from the continuous phase.

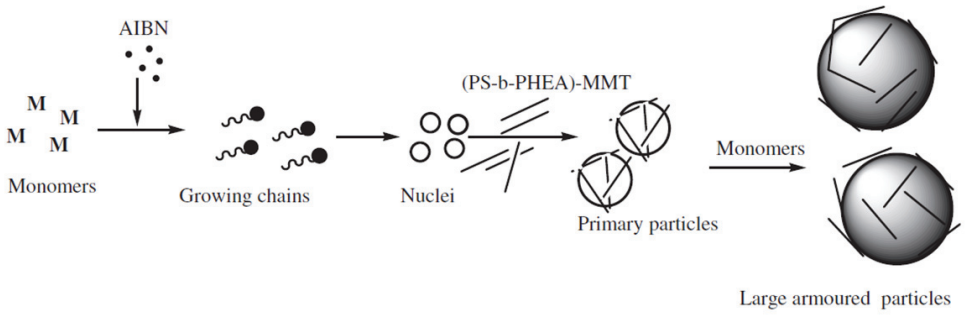

Figure 109. *Schematic mechanism of formation of (PS-b-PHEA)-modified MMT clay-armored polystyrene particles via Pickering dispersion polymerization.*[43]

Stable (PS-*b*-PHEA)-modified MMT clay armored polystyrene particles were obtained with an average diameter between 200 and 900 nm (depending on the concentration of (PS-*b*-PHEA)-MMT clay). By increasing the (PS-*b*-PHEA)-MMT clay content, the diameter of the hybrid particles decreased. This tendency has already been observed in previous studies. MMT clay platelets were observed on the surface of the hybrid nanoparticles as illustrated in Figure 110. At high clay content, the hybrid particles showed a quasi-spherical morphology, but irregular morphologies were obtained at low clay content. Moreover, both rate of polymerization and monomer conversion decreased as the amount of (PS-*b*-PHEA)-MMT clay increased. According to the authors, the presence of clay platelets may hinder the growth of the polymer chains and thus leading to a decrease in monomer conversion. In addition, an increase of the clay content could also lead to restricted diffusion of monomer to the polymer particles.

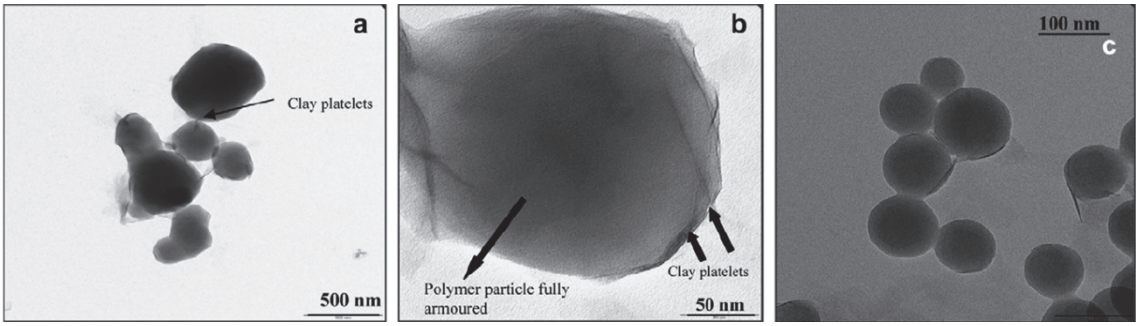

Figure 110. *TEM images of hybrid nanolatexes at different (PS-b-PHEA)-MMT clay content: (a) and (b) 3 wt.%, and (c) 7 wt.%.*[43]

3. Iron oxide

Yang *et al.*[44] proposed the synthesis of Fe_3O_4-polystyrene hybrid particles *via* Pickering dispersion polymerization in methanol/water medium (80/20 vol%) and in the presence of AIBN as initiator. A stable hybrid latex was obtained with a limited conversion (75%) and low molecular weight (M_n = 20 000 g mol^{-1}). The authors believed that the IO NPs inhibited the polymerization. IO-armored polystyrene particles were observed but as shown in Figure 111, it was difficult to estimate the exact amount of Fe_3O_4 nanoparticles that participated to the stabilization because of the magnetic attraction of the latter to the surface of the hybrid particles. However, the authors did not put the emphasis on the stabilizing role of the IO NPs.

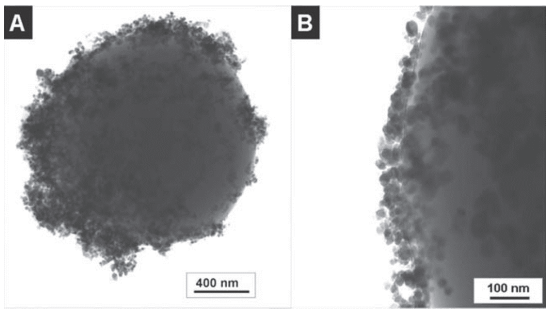

Figure 111. *(A) TEM images of Fe_3O_4-polystryene hybrid nanoparticles and (B) at higher magnification.*[44]

In summary, the dispersion polymerization process is barely described in the literature while it could be easily used to prepare monodisperse polymer particles of a range of sizes 1–20 µm with very good yield. Moreover, dispersion polymerization has been widely studied for the preparation of a variety of polymers (PS, PMMA, P(BuA), poly(acrylamide)…), but there are only a few articles reporting on the use of this technique in the field of nanocomposite.

In the following sections, we will introduce the cerium dioxide (CeO_2) sol used as solid stabilizer in the polymerization of Pickering miniemulsions and Pickering emulsion polymerizations thermally activated and under visible light irradiation.

Part 2. Cerium dioxide as Pickering stabilizer

Cerium dioxide (CeO_2) NPs have been studied over the past few years for their attractive properties in catalysis and UV-absorbing. In addition, they are used as polishing agents and exhibit excellent resistance to abrasion for coatings. More recently, CeO_2 have been developed in the biomedical sector (for their antioxidative properties).[45–50]

Several studies have been carried out at C2P2 on the use of CeO_2 as Pickering stabilizer. The thesis of Nancy Zgheib focused on the polymerization of Pickering miniemulsions and emulsion Pickering polymerization stabilized by CeO_2 NPs.[51,52] First, the main characteristic of the CeO_2 NPs, supplied by Rhodia-Solvay company, will be presented. Following detailed results from N. Zgheib's thesis, we will introduce the first example of Pickering emulsion photopolymerization successfully achieved by D. Subervie.[53]

I. Cerium dioxide

A. Nature of the CeO_2 sol

Rhodia-Solvay carried out the synthesis of the CeO_2 sol by thermo-hydrolysis of an acid solution of ceric nitrate salt $Ce^{4+}(NO_3^-)_4$ in an aqueous solution of nitric acid.[54–56] The obtained precipitate $CeO_2(NHO_3)_{0.5}(H_2O)_4$ spontaneously dispersed in water and a stable colloidal suspension was formed in a pH range between 0.5 and 2.5. The particle size was controlled by the excess of hydroxide ions introduced during the thermo-hydrolysis. The colloidal suspension is clear and yellow with a solids content of 13 wt.% and a pH value of 1.

B. Particle size and morphology

The morphology and size of the CeO_2 NPs were characterized by DLS, TEM and small angle X-ray scattering (SAXS) by N. Zgheib. The size of these clusters in suspension was determined by DLS. Their average hydrodynamic diameter was 7 nm, with a relatively narrow size distribution. This value agreed with the one determined with the TEM images. However, the CeO_2 NPs were observed as clusters with an equivalent diameter of 8 nm (Figure 112). A high magnification of the clusters shows the presence of nanoparticles of approximately 2 nm

(relatively isometric). However, it was not possible to determine the exact size of the CeO_2 NPs with the TEM images.

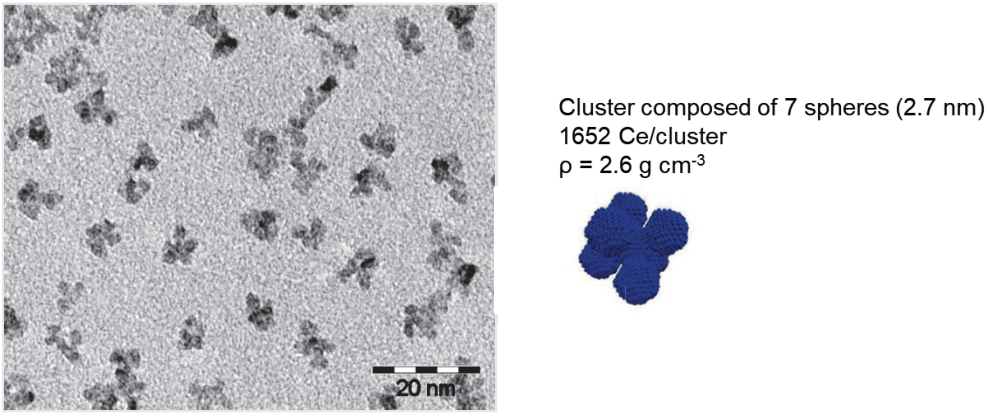

Figure 112. *TEM image of CeO_2 NPs from Solvay – Rhodia and the corresponding cluster composed of 7 spheres (2.7 nm) determined by SAXS.*[51,52]

The morphology of the CeO_2 NPs was then more precisely characterized by SAXS. SAXS is an efficient technique to determine the structural parameters of the CeO_2 NPs with a very high resolution. N. Zgheib showed that the clusters were composed of 7 nanoparticles (or crystallites) of about 2.7 nm in diameter, aggregated with each other.[51]

Then, the specific surface was determined by three methods: Brunauer, Emmet and Teller (BET), SAXS and geometrically. The results are reported in Table 30. The specific surface calculated by BET will be considered for the following study.

Table 30. *Specific surface of CeO_2 NPs determined by three methods.*[51,52]

Measurement	SAXS	BET	Geometric area
Specific surface (m^2 g^{-1})	285	219	250

C. Crystalline structure

The crystalline structure of the CeO_2 NPs was determined by X-ray diffraction (XRD) (Figure 113). The experimental spectrum was indexed by using the reference diagram 04-008-6551 from the crystallography database.[57]

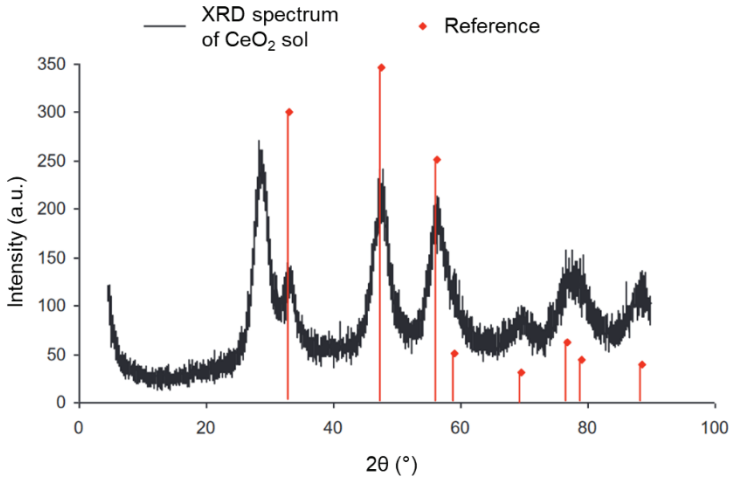

Figure 113. *XRD spectrum of the CeO_2 powder (obtained after drying in an oven at 100 °C).*[51,52]

The spectrum of the CeO_2 NPs in suspension is compatible with the theoretical spectrum of CeO_2. The characteristic bands of the CeO_2 are represented by the red lines.[57] These bands confirmed the monocrystal nature of the CeO_2 NPs in suspension. The CeO_2 NPs crystallize according to a CaF_2-type structure, *i.e.*, space group *Fm3m*. The Ce^{4+} ions occupy the regular sites of the face-centered cubic structure whereas the O^{2-} ions occupy the eight tetrahedral interstitial sites (Figure 114).

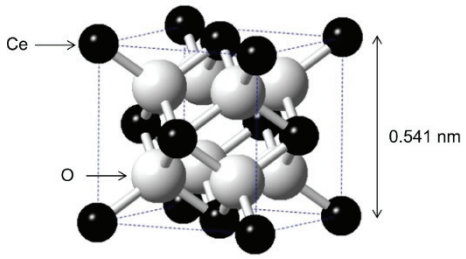

Figure 114. *The unit cell of CeO_2 (the spheres have been drawn at 50% space-filling to show the Ce-O bond).*

The (111)-index face of CeO_2 was identified *via* high-resolution (HR-)TEM (Figure 115). The repeat unit consists of three planes in a symmetrical configuration resulting in no net dipole moment perpendicular to the surface. The CeO_2(111) is the most stable surface.[58] In addition, single NPs with an average diameter of 2.7 nm were in the form of clusters, supporting the cluster-type morphology described above.

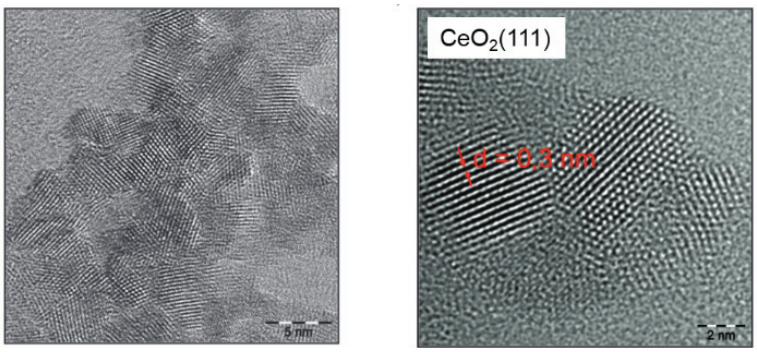

Figure 115. *HR-TEM images of the CeO_2 NPs.*[51,52]

D. Surface chemistry

The CeO_2 NPs surface is covered by hydroxyl and nitrate groups (Figure 116). At a pH value of 1, the CeO_2 NPs in suspension are in permanent equilibrium with several ions from the sol (H_3O^+ and NO_3^-), generated by the nitric acid during the synthesis of the CeO_2 sol. The zeta potential of the NPs surface charge at a pH of 1.8 in the presence of a KCl solution (ionic strength of 0.01 mol L^{-1}) is +45 mV. The surface of the CeO_2 NPs is thus positively charged since the pH of the solution is lower than the isoelectric point of the CeO_2 NPs (IEP ≈ 7).

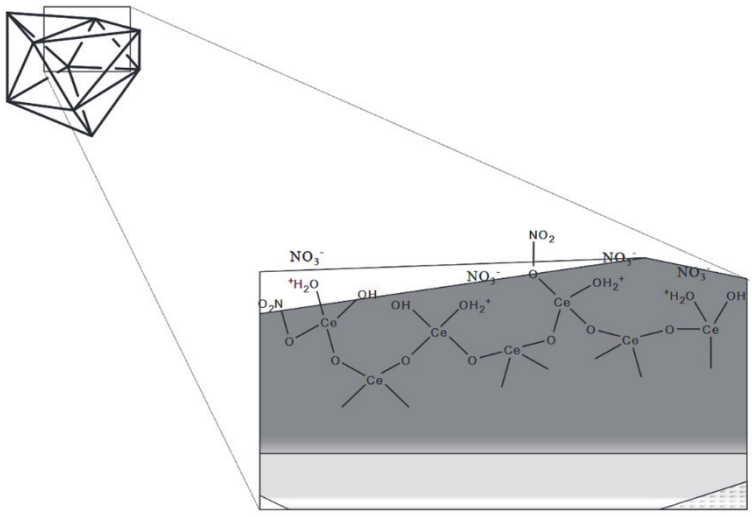

Figure 116*. Schematic representation of the CeO2 NPs surface in water at pH = 1.*[52]

The nature of the chemical groups on the CeO_2 NPs surface was characterized by Fourier-transform infrared (FTIR) spectroscopy (Figure 117). The broad absorption band between 3 600 and 3 100 cm^{-1} and the shoulder located at 1 620 cm^{-1} are characteristic absorption of H_2O molecules and hydroxyl groups.[59] The nitrate groups can be clearly identified from their intense and narrow peaks at 1 388 and 1 455 cm^{-1}, respectively, corresponding to the

symmetrical and asymmetrical vibrations of the N–O bond. The absorption band at 500 cm^{-1} corresponds to O–Ce–O stretching vibrations.[60]

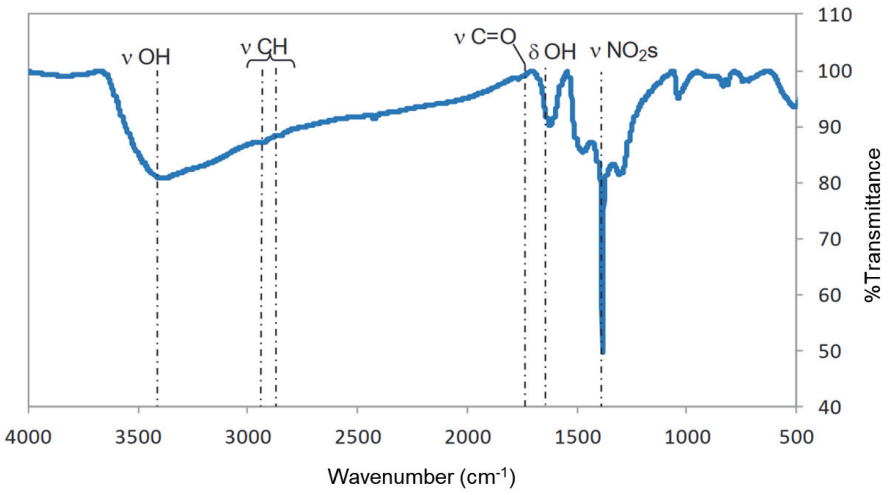

Figure 117. *FTIR spectrum of the CeO_2 NPs after ultra-centrifugation of the sol and drying at 100 °C.*[51,52]

Therefore, FTIR analysis showed that the surface of the "dry" CeO_2 NPs was mainly composed of hydroxyl and nitrate groups. These groups were probably adsorbed or bound onto the surface from the ceric nitrate precursor used for the formation of the CeO_2 sol. Moreover, the zeta potential indicated a positively charged surface of the CeO_2 NPs in suspension, resulting from the surface protonation.

To conclude, the CeO_2 NPs sol used in this study consists in clusters containing an average of 7 CeO_2 spheres of 2.7 nm in diameter. The surface of the CeO_2 NPs is covered by hydroxyl and nitrate groups. At a pH value between 0.5 and 2.5, the CeO_2 NPs form a stable suspension. All the main characteristics are presented in Table 31.

Table 31*. Characteristics of the CeO_2 sol used by N. Zgheib and D. Subervie for the Pickering miniemulsion and emulsion polymerization.*[51,52]

CeO_2 content in solution (wt.%)[a]	13
Particle size (nm)[b]	7
Polydispersity index[b]	0.09
BET specific surface (m^2 g^{-1})	219
pH	1
Bulk density of clusters (g cm^{-3})	2.6
Zeta potential (mV)	+45

[a] Determined by gravimetry.
[b] Determined by DLS.

II. Synthesis of CeO_2-armored hybrid latexes by polymerization of Pickering miniemulsions

A. Stabilization of miniemulsion droplets by CeO_2 nanoparticles

The miniemulsions were first prepared by mixing the monomers (MMA, MMA/*n*-BA, or *n*-BA) with the co-stabilizer octadecyl acrylate (ODA) (and the initiator if lipophilic). Then, this organic phase was added to the aqueous solution containing CeO_2 NPs (and the initiator if water-soluble) under vigorous stirring for 5 min (ultra-sonication). As for other systems described in the state-of-art part, N. Zgheib used an auxiliary comonomer, methacrylic acid (MAA), to improve the interaction between the MMA droplets and the CeO_2 NPs (Figure 118).[51,52] At acidic pH, MAA interacts with the CeO_2 NPs surface and forms a coordination complex (from the carboxylic acid groups of MAA). MAA can thereby act as a monodentate, bidentate or even bridging ligand. MAA is also a comonomer, enabling its copolymerization with MMA from the organic phase and thus consolidating the CeO_2-polymer bond during the polymerization.

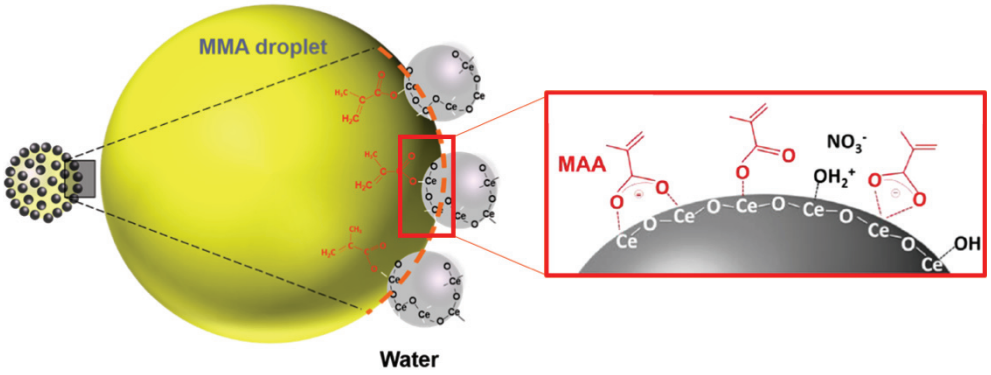

***Figure 118**. Schematic representation of the Pickering miniemulsion stabilized by MAA-modified CeO_2 NPs.*

First, N. Zgheib determined the amount of MAA required to form stable miniemulsions by varying the MAA concentration from 0 to 7 µmol m^{-2} at a fixed CeO_2 content of 25 wt.% based on MMA. When MAA was absent, no miniemulsion was obtained. An increase of MAA concentration led to a decrease of the droplet diameter until it reached a minimum value for 1.85 µmol m^{-2} before steadily increasing again (Figure 119). MAA mostly interacts with CeO_2 NPs in the water phase since it is highly soluble in water. The CeO_2 NPs thus become gradually

more hydrophobic, which favored their adhesion at the MMA/water interface. Beyond a concentration of 1.85 µmol m^{-2} in MAA, the CeO_2 NPs are completely covered by MAA, leading to aggregation, and resulting in a less efficient stabilization of the miniemulsion.

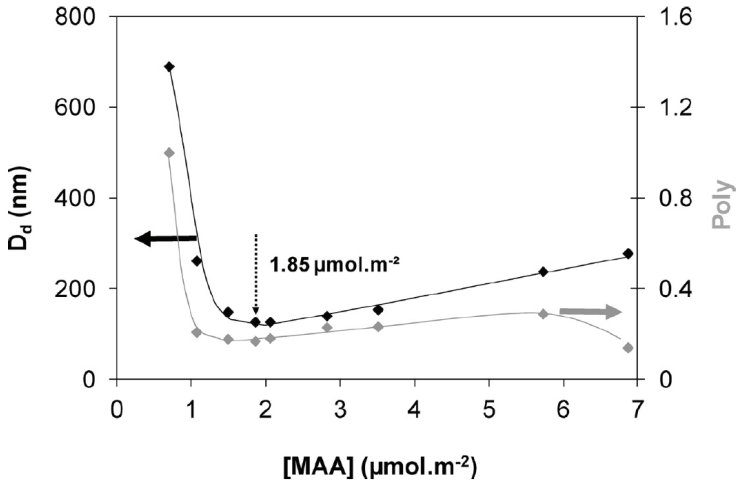

***Figure 119**. Evolution of the droplet diameter (dark line) and the size dispersity (gray line) as a function of MAA concentration for MMA miniemulsions stabilized by 25 wt.% of CeO_2 based on MMA (MMA: 20 wt.%/water, octadecyl acrylate: 4 wt.% based on MMA).*[51,52]

The influence of the CeO_2 content on the stability of the Pickering miniemulsions was then studied. An increase of the CeO_2 concentration led to a decrease of the droplet size and an increase of the surface coverage of the monomer droplets. However, it was noticed that even at high CeO_2 contents (35 wt.% based on MMA), a complete surface coverage of the monomer droplets was never achieved (only 37% of surface coverage). This observation suggested that CeO_2 NPs did not form a dense layer at the MMA/water interface probably due to the strong electrostatic repulsion between the positively charged CeO_2 NPs. However, this low surface coverage was sufficient to form stable miniemulsions.

B. Polymerization of CeO_2-stabilized miniemulsions

The following step was to polymerize the monomer droplets to obtain hybrid latexes in the presence of the cationic initiator, 2,2'-azobis(2-amidinopropane) dihydrochloride (AAPH). N. Zgheib investigated the influence of the CeO_2 content, the MAA concentration and the nature of the monomer. All the results are presented in **Table 32**.

***Table 32**. Influence of several parameters (CeO_2 content, MAA concentration and type of monomer) on the kinetic and the particle size in polymerization of Pickering miniemulsions stabilized by CeO_2 NPs.*[51,52]

Parameters		Time (h)	Conv. (%)	D_h[e] (nm) initial/final	PDI[e] initial/final	N_p (x 10^{16} L^{-1}) initial/final	Coverage (%) initial/final
CeO_2 content (wt.%/MMA)[a]	20	0.8	78	148/217	0.14/0.06	14/3.8	31/55
	25	1	85	139/202	0.17/0.05	18/4.8	37/65
	30	1.25	83	112/195	0.16/0.09	33/5.3	36/75
	35	3	85	101/200	0.22/0.05	47/5.0	37/90
***c*(MAA) (µmol m^{-2})**[b]	1.5	1.25	85	149/203[f]	0.18/0.08[f]	ND	ND
	1.9	1	85	139/202[f]	0.17/0.07[f]	18/4.8	37/65
	2.8	1.3	85	147/257[f]	0.21/0.08[f]	ND	ND
Monomer[c]	MMA	2	86	115/216	0.19/0.02	32/3.9	43/98
	MMA/*n*-BA[d]	4.5	96	150/198	0.19/0.09	15/5.4	54/88
	n-BA	6	92	190/211	0.26/0.06	7.3/4.8	67/89

[a] Experimental conditions: solids content of 20 wt.% and polymerization temperature at 70 °C. [MAA] = 1.9 µmol m^{-2}, ODA 4 wt.% and AAPH 1 wt.% both based on MMA.
[b] Experimental conditions: solids content of 20 wt.% and polymerization temperature at 70 °C. CeO_2 content of 25 wt.% relative to MMA, ODA 4 wt.% and AAPH 1 wt.% both based on MMA.
[c] Experimental conditions: solids content of 20 wt.% and polymerization temperature at 70 °C. CeO_2 content of 35 wt.% relative to monomer, [MAA] = 1.4 µmol m^{-2}, ODA 4 wt.% and AAPH 1 wt.% both based on monomer.
[d] Same experimental conditions as [c] with MMA/*n*-BA = 50/50 (wt.%).
[e] Determined by DLS.
[f] Determined by DLS at 80% conversion (before destabilization).

- ***Influence of the CeO_2 content***: The polymerizations were relatively fast and independent of the CeO_2 content (Figure 120a). The conversion reached a maximum of about 85%. Beyond this conversion, the latexes became systematically unstable for a CeO_2 content lower than 35 wt.%. The surface coverages were relatively low (except at 35 wt.% of CeO_2 – see **Table 32**). The cryo-TEM images (Figure 120b and c) showed two types of particles. All polymer particles were homogeneously covered with CeO_2 NPs, but their surface coverages seemed to vary depending on the particle diameter. Indeed, the smallest particles were not fully covered (Figure 120b). Most of the particles exhibited a spherical morphology and a broad size distribution while some of them, specially the biggest ones, exhibited a buckled morphology. This indicated that some residual monomer remained in the polymer particles before TEM observation, which is consistent with the limited conversion (85%).

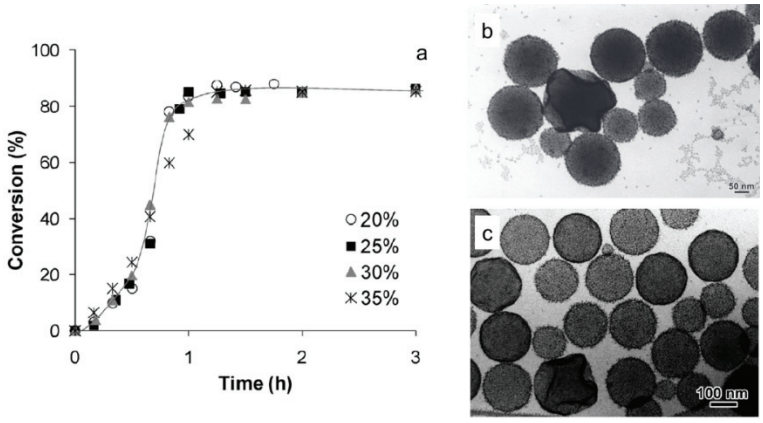

Figure 120. *(a) Evolution of conversion vs. time for MMA miniemulsion polymerization using various amounts of CeO_2 (wt.%/MMA) and the cryo-TEM images of CeO_2-armored PMMA latexes with (b) 30 and (c) 35 wt.% of CeO_2 based on MMA (see Table 32 for experimental details).*[51,52]

It was reported that the presence of a layer of inorganic NPs covering the polymer particles surface could affect the entry and exit events of the radicals.[22] In the present case, the oligoradicals formed in the aqueous phase can easily enter the MMA droplets at the beginning of the reaction if one assumes that the CeO_2 NPs are initially homogeneously but not too densely distributed onto the MMA droplets. As the polymerization proceeded, the polymer chains formed at the surface of MAA-modified CeO_2 NPs may screen their cationic charges. Moreover, the number of particles significantly decreased at low conversion (< 10%) suggesting partial coalescence. This effect became even more important when the initial amount of CeO_2 decreased. This partial coalescence was attributed to a change in the interfacial tension between MMA/water and PMMA/water, and thus in the adhesion of the CeO_2 NPs to the interface. The combination of the charge screening and the alteration of the interfacial tension resulted in a lower capability for the CeO_2 NPs to stabilize PMMA particles compared to MMA droplets. In addition, according to the cryo-TEM images, the polydispersity in size and the higher surface coverage of the larger particles may be related to the coalescence events. These observations indicated that the system probably did not follow the criteria of a miniemulsion polymerization, *i.e.*, a nucleation of all the droplets without significant variation of their number.

- ***Influence of MAA concentration***: The MAA concentration did not significantly influence the polymerization rate. The final conversion reached a plateau at 85%. Whatever the MAA concentration, the latexes were not stable at the end of the polymerization. However, less destabilization was observed for MAA concentrations lower than 1.9 µmol m^{-2}. The particle sizes before destabilization (80% – see **Table 32**) were slightly smaller with [MAA] < 1.9 µmol m^{-2} (*e.g.*, D_h = 203 nm for 1.5 µmol m^{-2}) than those obtained for

[MAA] = 2.8 µmol m^{-2} (D_h = 257 nm). Even if at the beginning of the reaction, the droplets diameters were similar for all MAA concentrations, the CeO_2 NPs surface was modified by complexation and started to aggregate at high MAA concentration, thus becoming less efficient for the stabilization of the polymer particles.

- ***Influence of the monomers***: The aim was to prepare latexes with lower glass transition temperatures (T_g) than that of PMMA-based latexes (T_g close to 100 °C) for coating applications. N. Zgheib and co-workers decided to use *n*-BA (T_g of P(*n*-BA) is close to -50 °C) and a mixture of MMA and *n*-BA (50/50 in wt.%, T_g of P(MMA-*co*-*n*-BA) close to 5 °C). The CeO_2 content was fixed at 35 wt.% based on the monomer and the MAA concentration at 1.4 µmol m^{-2} (concentration for which the stability of the miniemulsion was still ensured no matter the monomer(s) used). It was found that the size of the droplets formed in the presence of a more hydrophilic monomer, MMA (D_h = 115 nm) was smaller than in the presence of MMA-*n*-BA mixtures (D_h = 150 nm) or a more hydrophobic monomer, *n*-BA (D_h = 190 nm). Whatever the nature of the monomer, the latexes obtained were stable. Furthermore, the final conversion was higher for the MMA-*n*-BA mixture (96%) than for MMA (86%) and *n*-BA (92%) used alone. The polymerization was however slower in the presence of *n*-BA (Figure 121a). Indeed, the reactivity ratios of MMA/*n*-BA (r_{MMA} = 2.55 ± 0.35 and $r_{n\text{-BA}}$ = 0.36 ± 0.08)[61] show that MMA is more reactive than *n*-BA, leading to a composition drift. Therefore, the hydrophilic/hydrophobic nature of the monomer or of the mixture of monomers is an important parameter that can influence the polymerization rate and the stabilizing capability of the CeO_2 NPs.

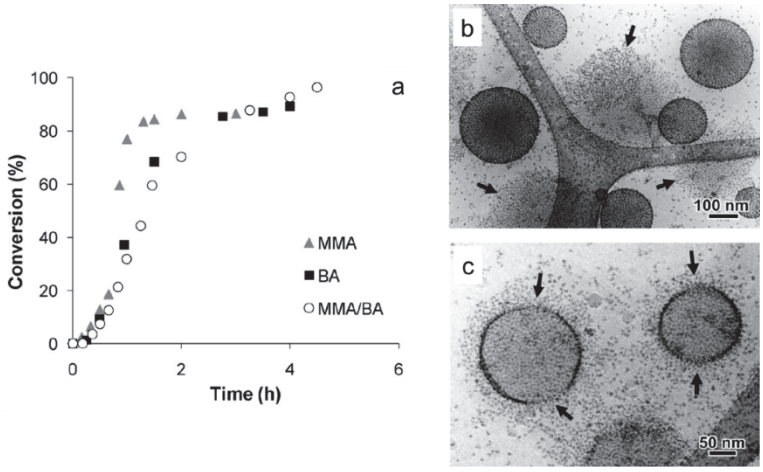

Figure 121. *(a) Evolution of conversion vs. time for the polymerizations of Pickering miniemulsions using different types of monomer and the cryo-TEM images of CeO_2-armored P(n-BA) latexes with 35 wt.% of CeO_2 based on monomer (see Table 32 for experimental details).*[51,52]

The P(*n*-BA) latexes were observed in cryo-TEM (Figure 121b and c). Spherical polydisperse latex particles were obtained and, on some particles, the CeO_2 armoring layer appeared to have been destabilized, perhaps due to shearing forces during the sample preparation. They started to detach from the P(*n*-BA) particle surface.

C. Conclusion

Stable Pickering miniemulsions were successfully formed using for the first time CeO_2 NPs as Pickering stabilizer and in the absence of any additional surfactant. This success was based on the use of MAA as an auxiliary comonomer and a complexing agent for CeO_2 NPs. The role of MAA was crucial since it improved the adhesion of the inorganic particles at monomer-water interface. MMA and CeO_2 NPs concentration had both an effect on the diameter and the stability of the monomer droplets.

Hybrid latexes were then obtained by polymerizing the Pickering-stabilized MMA miniemulsions at varied CeO_2 contents. Stable PMMA latexes were only formed at high CeO_2 content (> 35 wt.% based on MMA). Due to the screening of surface charges, high surface coverages were required to ensure the stability of the final particles. Finally, stable latexes in the presence of *n*-BA and a mixture of MMA/*n*-BA were successfully obtained, paving the way for the development of coating reinforced with CeO_2 NPs.

III. Synthesis of CeO_2-armored hybrid latexes by Pickering emulsion polymerization

The system developed by N. Zgheib was next transposed to emulsion polymerization process.[52] Indeed, miniemulsion polymerization is still poorly exploited industrially because of the specific equipment needed (homogenizer) which does not allow the preparation of large volumes for scale-up. The surface of the CeO_2 NPs was again functionalized using MAA which has an anchoring site (carboxyl group) and a polymerizable site (methacrylate function). For surfactant-free emulsion polymerization, the polymer particles are formed by homogeneous nucleation. The stabilization will be ensuring by the CeO_2 NPs, which become more hydrophilic

(growth of polymer chains from their surface), and therefore adsorb on the polymer particles. Note that the monomer droplets are too large and few to be stabilized by the CeO_2 NPs.

A. Functionalization of CeO_2 nanoparticles by MAA

The first step of the study consisted in investigating MAA and CeO_2 interaction in water (with no monomer present, unlike what was previously done for the miniemulsions). The complexation of MAA on CeO_2 involves interactions between the carboxyl groups of MAA and the cerium atom from the NPs. It leads to a reduction of the cationic charges as soon as the coverage by MAA becomes too high. As mentioned above, an increase of MAA molecules at the CeO_2 NPs surface leads to a decrease of the charge density, and the electrostatic repulsions responsible for the stabilization of the CeO_2 sol disappear, causing aggregation. The authors first determined the MAA concentration required to modify the CeO_2 NPs surface while maintaining their stability in solution (Figure 122).

The aggregation was visually accompanied by an increase in the turbidity of the suspension, as can be seen in the photographs in Figure 122. DLS analyzes confirmed that the MAA-modified CeO_2 NPs size increased with MAA concentration. Beyond a certain MAA concentration (around 5 µmol m^{-2}), MAA-modified CeO_2 NPs precipitated. The presence of MAA on the CeO_2 NPs surface was evidenced by FTIR spectroscopy. UV analyzes of the supernatant obtained after separating the MAA-modified CeO_2 NPs by ultra-centrifugation revealed the presence of free MAA in solution regardless of the MAA amount added. Thus, the latter partitioned between the aqueous phase and the CeO_2 NPs surface. The maximum concentration of MAA at which the CeO_2 sol did not aggregate was 1.9 µmol m^{-2}. Then, N. Zgheib and co-workers plotted the adsorption isotherm of MAA on the CeO_2 sol. The MAA concentration of 1.9 µmol m^{-2} gave the maximum ratio between MAA adsorbed on the inorganic surface ($[MAA]_{ads.}$ = 0.38 µmol m^{-2}) and free MAA in solution. This concentration was therefore chosen for the rest of the study.

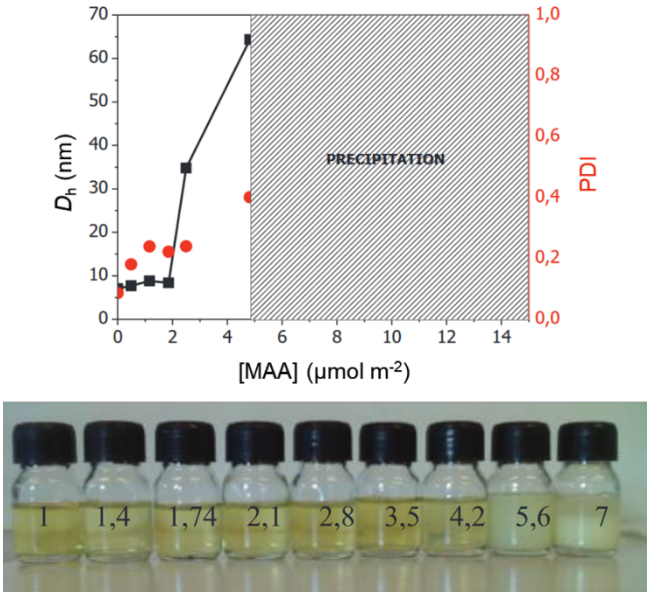

Figure 122. *Influence of the concentration of the auxiliary comonomer MAA (µmol m^{-2}) on the stability of the CeO_2 sol (5 wt.% of CeO_2 relative to water). The latter became destabilized beyond a certain concentration ([MAA] ≥ 5.6 µmol m^{-2}).*[52]

B. Pickering emulsion polymerization with CeO_2 nanoparticles

- ***Case of MMA***: N. Zgheib and co-workers first studied the Pickering emulsion polymerization of MMA initiated by the cationic initiator AAPH at different CeO_2 contents. For all the polymerizations, the final conversions were total (Figure 123). However, the DLS measurements showed a destabilization of the hybrid particles prepared with CeO_2 contents under 30 wt.% relative to MMA (Figure 123). This destabilization occurred at 60% monomer conversion for 15 wt.% of CeO_2 and 90% for 25 wt.% of CeO_2. It was therefore necessary to raise the CeO_2 content to 35 wt.% to prevent any destabilization at high monomer conversions.

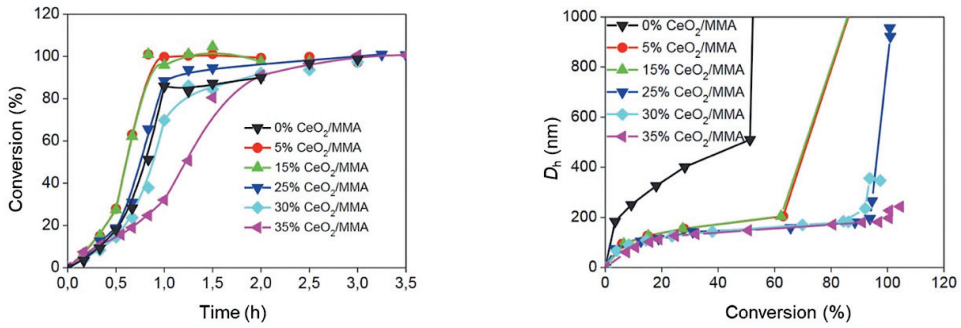

Figure 123. *Evolution of the conversion as a function of time (left) and of the particle diameter as a function of the conversion (right) during the Pickering emulsion polymerization of MMA at a fixed MAA concentration (1.9 µmol m^{-2}) and different CeO_2 content.*[52]

The polymerization rate decreased with increasing CeO_2 contents. To better understand this surprising observation, the authors investigated the influence of MAA concentration. They observed that for a fixed CeO_2 content (25 wt.% based on MMA), the higher the MAA concentration, the slower the polymerization. While under the same conditions but in the absence of CeO_2 NPs, MAA had no influence on the polymerization rates. Therefore, the presence of MAA adsorbed on the CeO_2 NPs surface clearly had an impact on the polymerization rate but this latter point remains to be clarified.

N. Zgheib *et al.* referred to studies which highlighted the role of Ce^{3+} as radical scavengers located in the vicinity of the CeO_2 NPs that could have an impact on the polymerization kinetics.[62,63] As the CeO_2 NPs surface is composed of Ce^{4+}, their reduction produces Ce^{3+} ions which are more stable than Ce^{4+} in acidic solution. To get rid of these Ce^{3+} ions, the CeO_2 sol was dialyzed. The authors determined the Ce^{3+} concentration by inductively coupled plasma mass spectrometry in the CeO_2 sol, in the dialyzed CeO_2 sol and in the hybrid PMMA latex prepared with the non-dialyzed CeO_2 sol (Table 33). According to these measurements Table 33, the dialysis eliminated almost all Ce^{3+} ions. It should also be noticed that the amount of Ce^{3+} presents in the final hybrid PMMA latex was higher than that measured before the Pickering emulsion polymerization (11.66 ppm *vs*. 3.77 ppm, respectively).

Table 33. *Ce^{3+} concentrations contained in the starting CeO_2 sol, in the CeO_2 dialyzed and in the final CeO_2-armored PMMA latex prepared with the non-dialyzed CeO_2 sol (CeO_2 content of 7 wt.% relative to water).*[a]

Solutions	***c*(Ce^{3+}) (ppm)**
CeO_2 sol	3.77
dialyzed CeO_2 sol	0.15
CeO_2-armored PMMA latex	11.66

[a] The solutions to be analyzed were all acidified (pH between 0 and 1) with a solution of HNO_3 (65%).

Then, the dialyzed CeO_2 sol was used to prepare a PMMA latex in the presence of 35 wt.% of CeO_2 and 1.9 µmol m^{-2} of MAA. The authors demonstrated that the Pickering emulsion polymerization was much faster with the dialyzed CeO_2 sol than with the initial CeO_2 sol, suggesting that the Ce^{3+} ions significantly influenced the polymerization rate.

The authors then extended the system to other monomers such as styrene and *n*-BA, as well as film-forming copolymers based on *n*-BA/MMA (60/40 in wt.%) or *n*-BA/styrene (70/30 in

wt.%) at a fixed CeO_2 content of 10 wt.% based on monomer and a MMA concentration of 1.9 µmol m^{-2} (Figure 124).

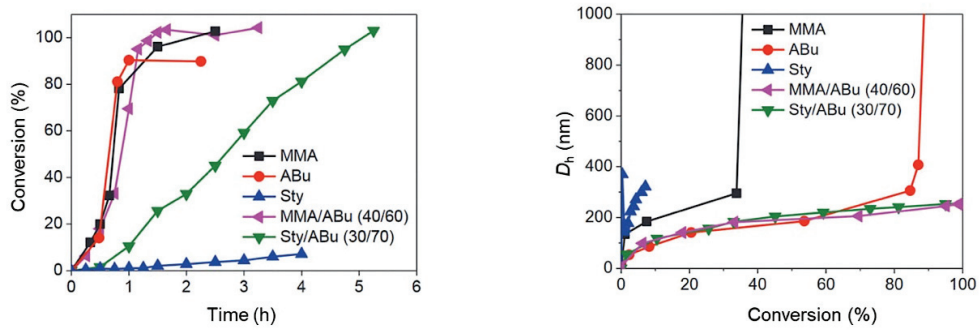

Figure 124. *Evolution of the conversion as a function of time (left) and of the particle diameter as a function of the conversion (right) during the Pickering emulsion polymerization of various monomers at a fixed CeO_2 (10 wt.% based on monomer) content and MAA concentration (1.9 µmol m^{-2}).*[52]

- ***Case of styrene***: The polymerization of styrene was inhibited (5% conversion after 4 h – see Figure 124). The authors suggested that the higher hydrophobicity of styrene compared to the other monomers strongly reduced the interactions of the MAA-modified CeO_2 NPs with the polymer particles. Therefore, there would be fewer styryl radicals in the vicinity of the CeO_2 NPs which could explain an inhibited nucleation phase. To get around this problem, the authors copolymerized styrene with *n*-BA. However, despite the obtention of a stable latex, the polymerization was slow in comparison with the other monomers. N. Zgheib studied the influence of CeO_2 content on the copolymerization of styrene and *n*-BA. An increase of CeO_2 content led to slower polymerizations (and low monomer conversions). Finally, the *n*-BA/styrene ratio was modified from 70/30 to 30/70 (wt.%) at a fixed CeO_2 content (10 wt.% based on monomer). Upon decreasing the *n*-BA/styrene ratio, the latexes were not stable, and the conversions were limited. These results therefore confirmed a strong inhibiting effect of styrene in the polymerizations.

- ***Case of n-BA/MMA***: For the copolymerization of *n*-BA/MMA (60/40 in wt.%), the polymerization was fast, leading to the formation of a stable latex at the end of the reaction (Figure 124). This notable difference in stability was attributed to the properties of the polymer formed. Indeed, the authors showed that the zeta potential of the CeO_2-armored PMMA latex was lower than that of the P(*n*-BA-*co*-MMA) hybrid latex, and they attributed this difference to the greater hydrophobicity of the copolymer compared to the homopolymer. Therefore, in the case of PMMA, the polymer chains would have more affinity for the CeO_2 NPs surface. The CeO_2 NPs would then be more wetted by the polymer and would consequently be more buried within the PMMA particles (Figure 125).

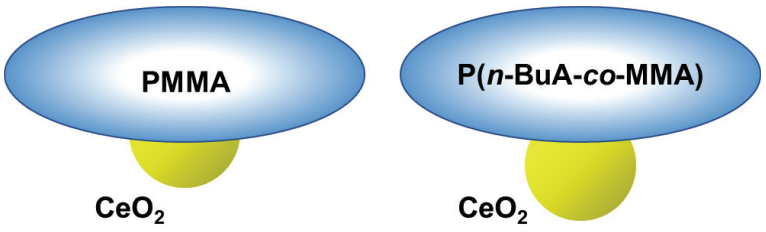

***Figure 125**. Schematic representation of the CeO_2 NPs positioning at the PMMA (left) and P(n-BA-co-MMA) (right) particle surface.*[52]

To prevent the CeO_2 NPs from aggregation, the electrostatic repulsion forces must be sufficiently high. Thus, in the case of PMMA latexes, there are less apparent cationic charges provided by the CeO_2 NPs than in the case of copolymer latexes and it is therefore necessary to increase the CeO_2 content up to 35 wt.% (based on MMA) to obtain a stable PMMA latex. Conversely, in the case of P(*n*-BA-*co*-MMA) particles, it was possible to decrease the CeO_2 content below 10 wt.% (based on monomers).

In summary, the work of N. Zgheib showed that it was possible to prepare stable CeO_2-armored latexes by Pickering emulsion polymerization of MMA, n-BA/MMA (60/40 in wt.%) and n-BA/styrene (70/30) using an auxiliary comonomer (MAA). The CeO_2 NPs gradually become more hydrophobic because the growing polymer chains chemically bind to the surface via MAA (methacrylate function). The more hydrophobic CeO_2 NPs then adsorb to the polymer particles, thus contributing to their stability. In the following section, the mechanical, and optical properties of CeO_2-armored P(n-BA-co-MMA) latex films will be discussed.

C. Characteristics of CeO_2-armored P(*n*-BA-*co*-MMA) latex films

Martín-Fabiani *et al.*[64] studied the mechanical and optical properties of CeO_2/polymer latex films depending on their nanostructures. For that purpose, the hybrid P(*n*-BA-*co*-MMA) latexes (with *n*-BA/MMA ratio of 60/40 in wt.%) were prepared *via* two methods (Figure 126).

- ***Pickering emulsion polymerization*** in the presence of MAA as auxiliary comonomer as described above.

- ***Physical blend process*** using a CeO_2 sol and a P(*n*-BA-*co*-MMA-*co*-MAA) latex without any surfactant. The hybrid particles were assembled by complexation involving

interactions between the cerium atoms from the acidic CeO_2 sol and the carboxyl groups of the MAA present at the surface of the latex particle.

Two types of sols were used: acidic CeO_2 sol (ACS), which was the one used by N. Zgheib, and the commercial Rhodigard basic CeO_2 sol (BCS) in which the CeO_2 NPs surface are already coated with citric acid molecules, providing their stability under basic pH. The aim was to determine which fabrication route should be chosen depending on the final film properties that are needed.

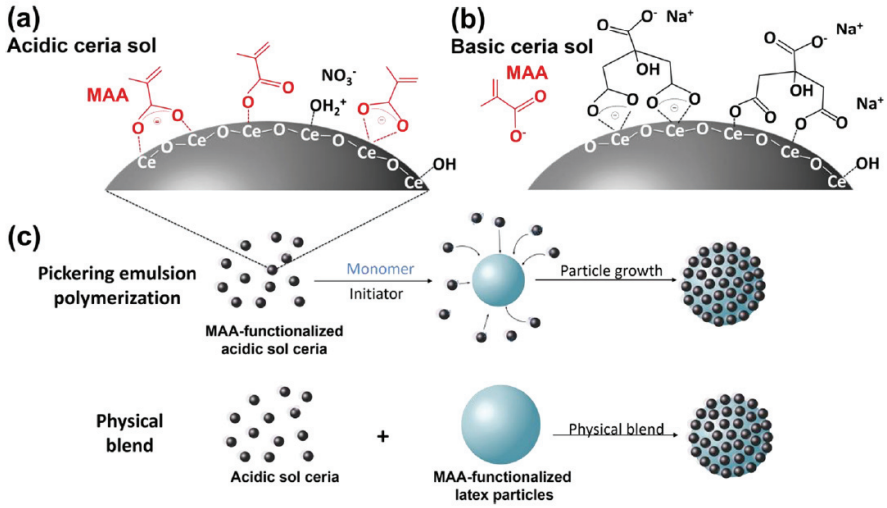

***Figure 126**. Schemes depicting the surface chemistry of the (a) ACS and (b) BCS NPs and interactions with MAA groups and (c) comparison between the Pickering emulsion polymerization and physical blend process using ACS.*[64]

- ***Structural characterization***: The authors first showed that free CeO_2 NPs were observed in cryo-TEM in the case where hybrid latexes were prepared by using the BCS. Indeed, the MAA auxiliary comonomer is unlikely to be able to adsorb at the negatively charged CeO_2 NPs surface (repulsions between charges). In addition, larger BCS Pickering latex particles were obtained (1 000 nm) than ACS Pickering latex particles (590 nm), which indicates a weaker interaction in the case of BCS.

Three hybrid latex films were prepared from the two types of CeO_2 NPs sols (ACS and BCS) latex dispersions and from the physical blend. The films were characterized by combining focused ion beam and scanning electron microscopy (FIB-SEM) and TEM (Figure 127). In the case of the ACS Pickering film, the CeO_2 NPs formed a honeycomb structure derived from the armored structure of the hybrid latex. However, in the case of BCS Pickering film, the CeO_2 NPs appeared to accumulate in clusters between the particles where they provide a physical barrier to particle deformation. Finally, the physical blend film also presented a honeycomb structure like the one seen in the ACS Pickering latex. In the physical blend process, the

carboxyl groups from MAA units were located at the polymer surface and could interact with the ACS surface *via* the cerium atoms. This process also resulted in CeO_2-armored P(*n*-BA-*co*-MMA) latexes that persisted during film formation. It should be noticed that some discontinuities in the CeO_2 NPs in the cellular wall structure were clearly observed in the case of the physical blend film, while it appeared to be more continuous in the case of ACS.

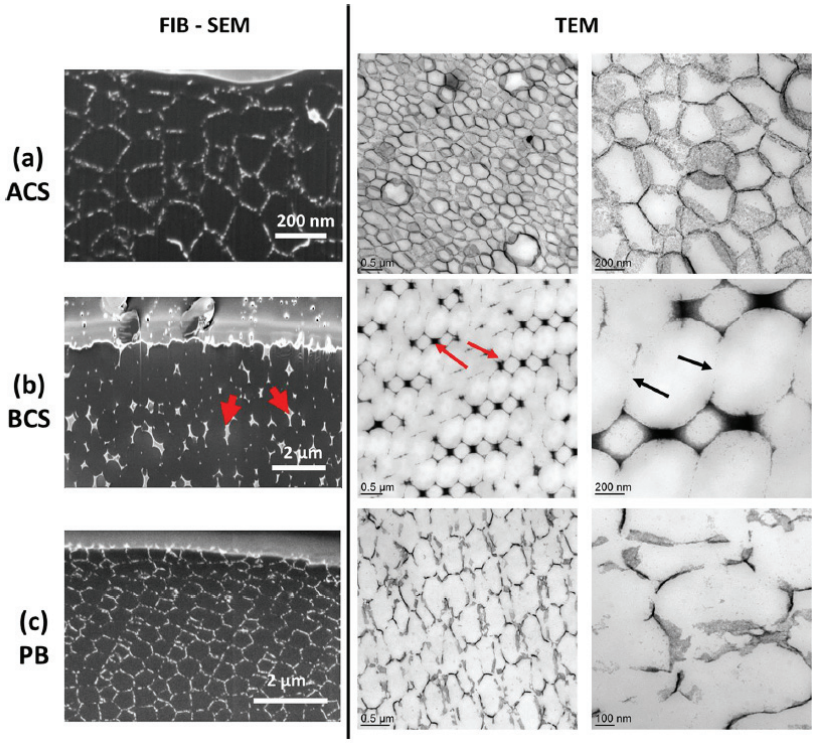

***Figure 127**. Microstructural characterization of the dried films of hybrid latexes containing CeO_2 NPs: (a) Pickering latex synthesized using ACS; (b) Pickering latex synthesized using BCS; (c) physical blend of the blank polymer and ACS. Left column: FIB−SEM images of film cross sections. Center and right columns: TEM images of thin cross-sectional slices. The red arrows in row b point to the ceria clusters (left and center columns); the black arrows point to the coalesced polymer boundaries, apparently free of ceria (right column).*[64]

- ***Mechanical properties***: Next, the authors investigated the dynamic mechanical analysis (DMA) properties under a low strain. Figure 128 represents the storage modulus (*E'*) and the loss factor (tan *δ*) as a function of the temperature for different films (note that SFB corresponds to surfactant-free blank latex, the one used for the physical blend). According to the tan δ curves, two peaks were obtained for SFB and the physical blend (PB) at around -5 °C and 40 °C, whereas only one broad peak appeared for the Pickering latex films synthesized using ACS and BCS. Moreover, the presence of CeO_2 NPs in the films raised their storage modulus in the rubbery state and reduced their main relaxation temperature (T_α). The higher T_α for the ACS Pickering film relative to the BCS Pickering and physical blend films was attributed to the immobilization of polymer chains at the CeO_2 NPs surface *via* the auxiliary comonomer MAA.

Despite their similar honeycomb structures, the physical blend film had a higher modulus at the rubbery plateau than the ACS Pickering film. According to Martín-Fabiani and co-workers, the CeO_2–CeO_2 contacts were strong in the blend which resulted in a more cohesive network than that in the ACS Pickering film. Interestingly, both the ACS and BCS Pickering films exhibited identical mechanical properties while their microstructures differed significantly. This was due to the large concentration of MAA used for the preparation of BCS Pickering latex (12 µmol m^{-2} *vs*. 1.9 µmol m^{-2} for ACS Pickering latex). Indeed, the presence of MAA has been proven to improve the mechanical properties of latex films.[65]

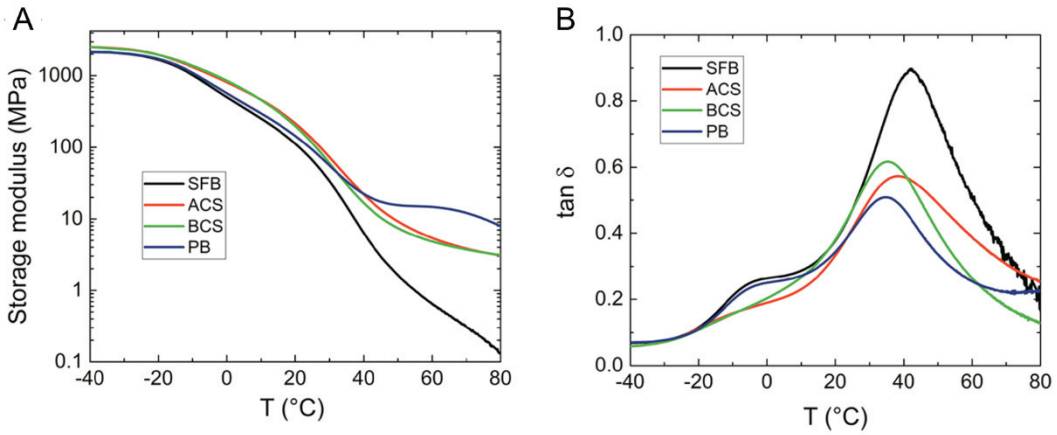

Figure 128. *DMA curves as a function of the temperature for the different films. A) storage modulus and B) loss tangent (tan δ).*[64]

- ***Optical properties and application as an UV-absorbing coating***: It is well-known that the CeO_2 NPs absorb UV photons (intensive peak at 210 nm decreasing until 400 nm). The authors thus studied the optical properties of the hybrid films for applications as UV-absorbing coatings. The size of the CeO_2 NPs has a strong impact on the reflectance and transmittance of the hybrid polymer films, depending on the wavelength. All latexes were film-forming and relatively transparent as shown in Figure 129. The yellowish tint was due to the CeO_2 NPs. The blank film showed a single absorption peak around 230 nm which was attributed to the absorption by the polymer. In the presence of CeO_2 NPs, the three other films showed a second peak at 300 nm (identical to the absorption band of the CeO_2 NPs alone), demonstrating that the transparent (in the visible region) films absorbed UVB (300 nm) and UVA (360 nm).

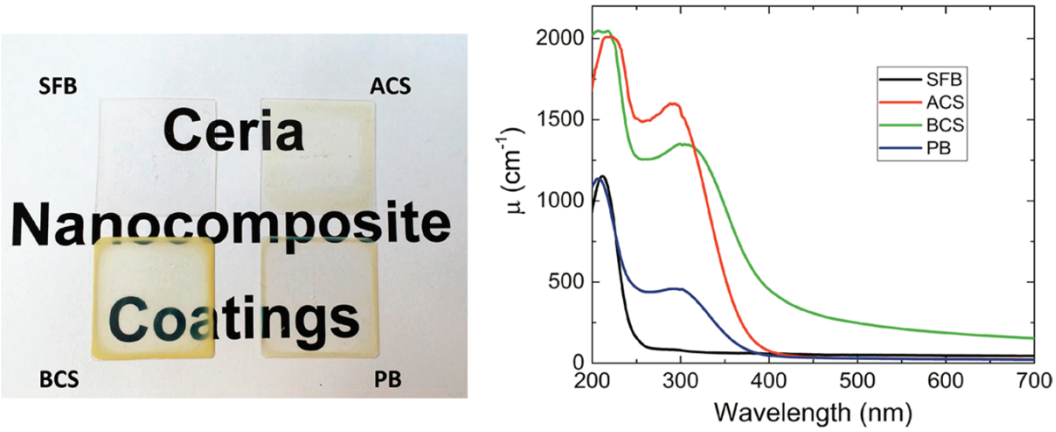

***Figure 129**. Optical properties of CeO_2/polymer films: photographs of the different nanocomposite coatings on quartz substrates (left); linear absorption coefficients for CeO_2/polymer films and the blank film as a function of the wavelength of the incident light (right).*[64]

To sum up, this study showed the properties of different types of Pickering latex films and the contribution of CeO_2 NPs depending on their interaction with an auxiliary comonomer. The films from the ACS Pickering latex and the physical blend exhibited CeO_2 NPs in a honeycomb structure. The BCS Pickering latex contained free CeO_2 NPs resulting in large clusters congregating at the particle interfaces in the film. The CeO_2 NPs distributions in the film directly impacted the mechanical properties.

IV. Synthesis of CeO_2-armored hybrid latexes by Pickering emulsion photopolymerization

As CeO_2 NPs intensively absorb the UV photons, the emulsion photopolymerization must be initiated by visible light irradiation. Taking into consideration that complexation involves interactions between the carboxyl group from the MAA auxiliary comonomer and the cerium atom, D. Subervie decided to make the most of this interaction by replacing MAA by the disulfide used in the three-component PIS.[53] Indeed, the latter can photoinitiate the emulsion photopolymerization of MMA and *n*-BA/MMA as described in Chapter 2 and in addition, the disulfide exhibits two carboxyl groups able to develop strong interactions with the CeO_2 NPs surface (Figure 130). The disulfide could thus play a dual role, as photoinitiator and anchoring agent to form CeO_2-armored latexes by Pickering emulsion photopolymerization. After decomposition of disulfide under visible light irradiation, thiyl radicals will react with monomer units on one hand at the CeO_2 NPs surface and the polymer will grow from there (grafting from), and on the other hand in the water phase. The surface of the CeO_2 NPs was

modified by the disulfide to then facilitate their adhesion to the polymer particles. The adsorption of the disulfide at the CeO_2 NPs surface involving the two carboxyl groups seems to be hardly feasible because of the conformation of the disulfide which must be able to combine with the CeO_2 NPs surface (distance between the cerium atoms, the curvature…).

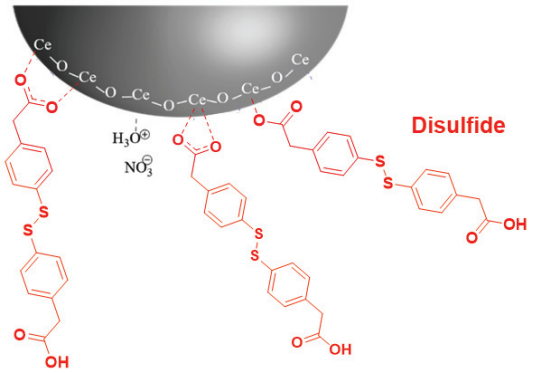

***Figure 130**. Scheme depicting the surface chemistry of the CeO_2 NPs and interactions with disulfide.*

A. Functionalization of CeO_2 nanoparticles by disulfide

The CeO_2 sol used by D. Subervie was the same as the one used by N. Zgheib. In the following sections, the concentration of carboxylic acid functions, *i.e.*, [COOH] = 2x [disulfide], was expressed in µmol m^{-2} based on the total surface area of the CeO_2 nanoparticles (specific surface of 218.6 m^2 g^{-1}, see Table 30).

As already mentioned, the anchoring of the disulfide at the CeO_2 NPs surface must lead to a reduction of the cationic charges, which may cause aggregation of the CeO_2 sol. D. Subervie determined the maximal disulfide concentration eligible to modify the CeO_2 NPs surface without destabilization of the suspension (Table 34). At the pH of the CeO_2 sol (pH = 1), the disulfide is however only slightly soluble (pK_a = 3.8), and a small fraction of disulfide precipitated. The disulfide concentration was varied from 0.036 to 0.45 µmol m^{-2} at a fixed CeO_2 content of 5 wt.% in water.

***Table 34**. Stability of CeO_2 NPs after 45 min in solution at different disulfide concentrations and fixed CeO_2 content of 5 wt.% based on water.[53]*

c(COOH) (µmol m^{-2})	Precipitation[a]	D_h[b] (nm)	Intensity[b] (%)
0.036	No	8.8	92
0.092	No	9.4	93
0.252	Yes	12.8	92
0.352	Yes	21.0	81
0.450	Yes	21.3	86

[a] Visible to the naked eye.
[b] Determined by DLS. The intensity corresponds to the peak value of D_h.

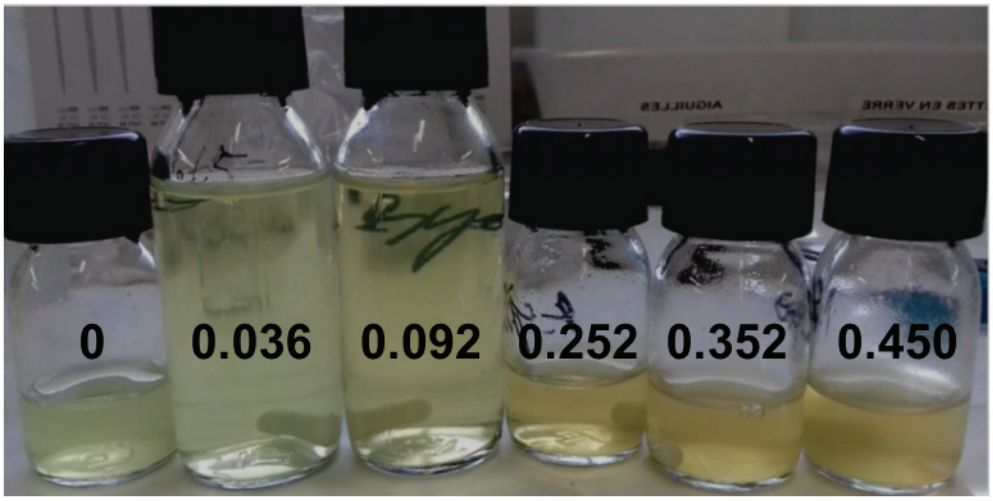

***Figure 131**. Influence of the disulfide concentration (µmol m^{-2}) on the stability of the CeO_2 sol. The latter became destabilized beyond a certain concentration ([disulfide] > 0.092 µmol m^{-2}).[53]*

The aggregation was visually accompanied by an increase in the turbidity of the suspension, as can be seen in Figure 131. DLS measurements confirmed that the disulfide modified CeO_2 NPs size increased with the disulfide concentration. Beyond a certain disulfide concentration (around 0.092 µmol m^{-2}), the suspension became destabilized and the particles precipitated. Moreover, the presence of a population of larger particles (200–500 nm in diameter) was observed in DLS with a variation from 7 to 19% of the total intensity, regardless of the disulfide concentration.

The presence of disulfide on the CeO_2 NPs surface was demonstrated by attenuated total reflectance (ATR)-IR spectroscopy. UV analyzes of the supernatant obtained after separating the disulfide modified CeO_2 NPs by ultra-centrifugation revealed the absence of free disulfide in solution regardless of the disulfide amount initially added. However, considering the poor solubility of the disulfide in the CeO_2 sol, one cannot however rule out the presence of free

disulfide aggregates that would precipitate together with the CeO_2 particles, which does not allow the quantification.

B. Pickering emulsion photopolymerization with CeO_2 nanoparticles

The water and monomer phases of the emulsion were first degassed separately to prevent the CeO_2 sol from destabilization. To a solution of water containing the disulfide was added dropwise the CeO_2 sol. This solution was introduced in the reactor with the monomer phase under stirring, and then the light was switched on.

- ***Case of MMA***: D. Subervie first investigated the Pickering emulsion photopolymerization of MMA in the presence of the disulfide modified CeO_2 NPs. The disulfide concentration was varied from 0.042 to 0.352 µmol m^{-2} at a fixed CeO_2 content of 21.7 wt.% based on MMA. An increase of the disulfide concentration led to faster photopolymerizations (Figure 132). The final conversion increased with the disulfide concentration (from 77% for 0.042 µmol m^{-2} to 95% for 0.352 µmol m^{-2}). However, DLS measurements showed a destabilization of the hybrid particles prepared at all disulfide concentrations, by the end of the reaction (Figure 132). This destabilization occurred at around 70% monomer conversion for a disulfide amount of 0.042 µmol m^{-2}, and at 90% for 0.252 µmol m^{-2}. N. Zgheib already explained this destabilization by a significant affinity of the CeO_2 NPs for the PMMA particles (because of the growing PMMA chains anchored at the CeO_2 NPs surface), leading the CeO_2 NPs to be buried in the latex particles and thus unable to stabilize the polymer particles.

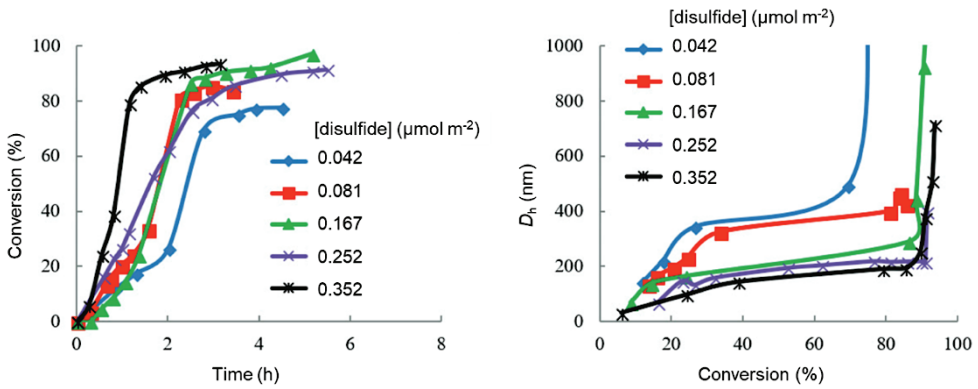

***Figure 132**. Influence of the disulfide concentration on the evolution of the conversion as a function of time (left) and of the diameter of the particles as a function of conversion (right) during the Pickering emulsion photopolymerization of MMA.[53]*

- ***Case of n-BA/MMA***: D. Subervie first investigated the effect of the disulfide concentration on the polymerization rate and the particle size for a *n*-BA/MMA mixture of 60/40 in wt.% at a fixed CeO_2 content of 21.7 wt.% based on monomers (**Figure 133**). For the lowest disulfide concentration, the polymerization rate was low, and the final conversion reached 92% after 7 h. Moreover, the particles were relatively large in diameter (400 nm) and after 80% conversion, the size continued to increase suggesting a destabilization of the latex. The polymerization rate increased, and the particle size decreased with increasing the disulfide concentration. Except for a disulfide concentration of 0.088 µmol m^{-2}, all the final latexes were stable. The P(*n*-BA-*co*-MMA) chains are more hydrophobic, which prevented CeO_2 NPs from burying themselves in the latex particles.

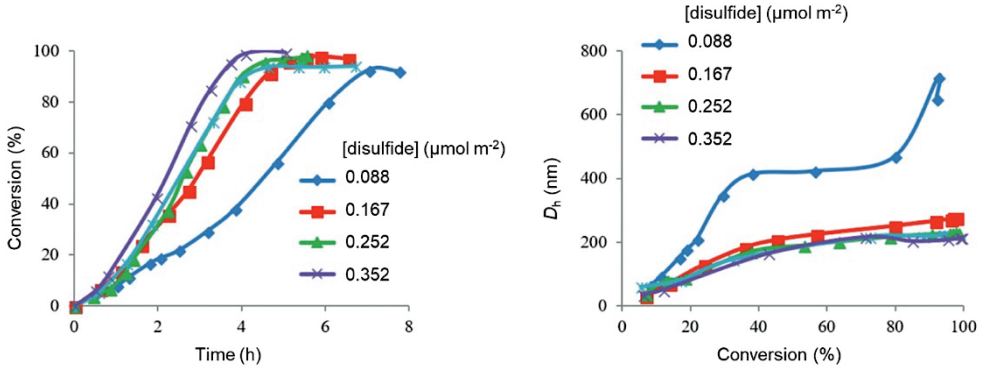

***Figure 133**. Influence of the disulfide concentration on the evolution of the conversion as a function of time (left) and the diameter of the particles as a function of conversion (right) during the Pickering emulsion photopolymerization of n-BA/MMA (60/40 in wt.%).[53]*

Finally, D. Subervie determined the minimum CeO_2 content allowing the formation of a stable latex. The disulfide concentration was fixed at 0.252 µmol m^{-2} and the CeO_2 content was varied from 10 to 21.7 wt.% based on monomers. The polymerization rate decreased by decreasing

the CeO_2 content and a destabilization of the latexes was observed at the end of the reaction below 21.7 wt.% of CeO_2. The best conditions were therefore a disulfide concentration of 0.252 µmol m^{-2} and a CeO_2 content of 21.7 wt.% based on monomers.

In summary, the Pickering emulsion photopolymerization described by D. Subervie is operationally very simple since it only requires the use of one compound, the disulfide, which has a dual role of anchoring agent to the CeO_2 NPs surface, and of photoinitiator. To our knowledge, this is the first example of hybrid latexes prepared by Pickering emulsion photopolymerization reported in the literature. However, this Pickering system deserves to be improved since at the beginning of the reaction, a non-negligible amount of CeO_2 NPs aggregates are present, phenomenon likely related to the poor solubility of the disulfide in the acidic CeO_2 sol. This is why we decided to study this reaction in a hydroalcoholic medium in which the disulfide is more soluble.

Part 3. Synthesis of CeO_2-armored latexes *via* visible light-induced Pickering dispersion polymerization

The recent years have seen an increasing interest for surfactant-free synthetic latexes. Indeed, low molar mass surfactants can be detrimental for some applications, *e.g.*, in the coating industry. The introduction of inorganic particles in the synthesis of latexes results in hybrid particles that take full advantage of both the polymer component properties (structural and mechanical features, and processability) and the inorganic component, which can introduce specific functionalities (magnetism, catalytic activity, luminescence …) and/or reinforce the mechanical and thermal properties of the polymer. New properties of the hybrid materials may thus result from synergetic effects from both components.

Pickering emulsion and miniemulsion polymerizations are the major methods to produce hybrid latexes in the absence of surfactant and only very few studies have been carried out in dispersion conditions. As previously discussed, there are a wide range of inorganic particles that can be used and among them, cerium dioxide has drawn particular attention due to its mechanical and UV absorbing properties.

To the best of our knowledge, no example of Pickering photopolymerization was reported in the literature. D. Subervie showed the feasibility of producing CeO_2-armored polymer latexes by Pickering emulsion photopolymerization but he faced some aggregation issues with the CeO_2 NPs. Taking advantage of the established affinity of dicarboxylic acid diphenyl disulfide with the CeO_2 NPs surface (section Part 2.IV), we attempted to prepare CeO_2-armored P(*n*-BA-*co*-MMA) particles by Pickering dispersion photopolymerization. In addition, compared to the emulsion process, the initial medium is transparent, which allows a maximum penetration of light.

In this part, we will first focus on the interaction of the dicarboxylic acid diphenyl disulfide and the CeO_2 NPs surface. Then, several parameters that should have an impact on the polymerization rates and the particle sizes will be studied to produce P(*n*-BA-*co*-MMA) hybrid particles by Pickering dispersion photopolymerization. Finally, we will characterize the films obtained from these hybrid latexes.

I. Preparation of dicarboxylic acid diphenyl disulfide modified CeO_2 nanoparticles

To improve the interactions between the CeO_2 NPs and the polymer particles, the CeO_2 NPs surface was functionalized with our dicarboxylic acid diphenyl disulfide photoinitiator. As previously described (section Part 2.I), the CeO_2 NPs form stable suspensions in water at a pH value between 0.5 and 2.5. In the previous case of D. Subervie, the emulsion polymerizations were carried out in water. However, the dispersion conditions involve hydroalcoholic media, and we cannot exclude that the CeO_2 sol could be destabilized by the addition of alcohol. We must therefore choose an appropriate hydroalcoholic composition to obtain a stable CeO_2 suspension and carry out another study on disulfide adsorption on the CeO_2 NPs in hydroalcoholic medium.

A. Stabilization of CeO_2 nanoparticles in hydroalcoholic medium

1. Choice of the hydroalcoholic medium

The CeO_2 NPs are positively charged and suspended in water. Therefore, we must consider an alcohol that will not destabilize the CeO_2 NPs. For that purpose, the solvent physical properties should be considered, and more specifically its dielectric constant (ε) which is a measure of the solvent's ability to separate charges. Two candidates have drawn our attention: methanol (MeOH) and ethanol (EtOH). They both have dielectric constants that are close to that of water, yet still significantly lower (ε_{MeOH} = 32.66, ε_{EtOH} = 24.28 and ε_{water} = 78.48 determined at 25 °C).[66,67]

In addition, to enable stable dispersions of the CeO_2 NPs, the composition of the hydroalcoholic medium must be a good solvent for the monomer and the initiator, but a non-solvent for the polymer. We therefore decided to select a 50/50 (wt.%) alcohol/water composition since the dielectric constants of these mixtures are only slightly lower than that of pure water according to Table 35. For hydroalcoholic solutions containing more water, the solubility limit of *n*-BA and MMA will be reached and phase separation in the reaction mixture could be observed.[68–70]

***Table 35**. Influence of the alcohol-water composition on the dielectric constant at 25 °C.* [66,67]

Dielectric constant	ε		
Composition	100/0 wt.%	70/30 wt.%	50/50 wt.%
MeOH/water	32.66	47.11	56.28
EtOH/water	24.28	41.76	53.44

We first chose a CeO_2 content so that the NPs remain in suspension in the water-methanol mixture. In the case of emulsion, the CeO_2 content was 5 wt.% relative to water. We decided to prepare an alcohol/water mixture (10 g/10 g) containing 2.8 wt.% of CeO_2 based on solvent (which corresponds to a content of 25 wt.% based on monomer for the following study on polymerization) as follows: the alcohol was added dropwise *via* a syringe pump (at a flow rate of 1 mL min^{-1}) to the CeO_2 sol under stirring. After 30 min, the dispersions were analyzed by DLS (Figure 134). No aggregation was observed when MeOH was added, whereas in the case of EtOH, a large second peak appeared between 100 and 200 nm indicating CeO_2 NPs aggregation. We therefore decided to use a MeOH-water mixture (50/50 in wt.%).

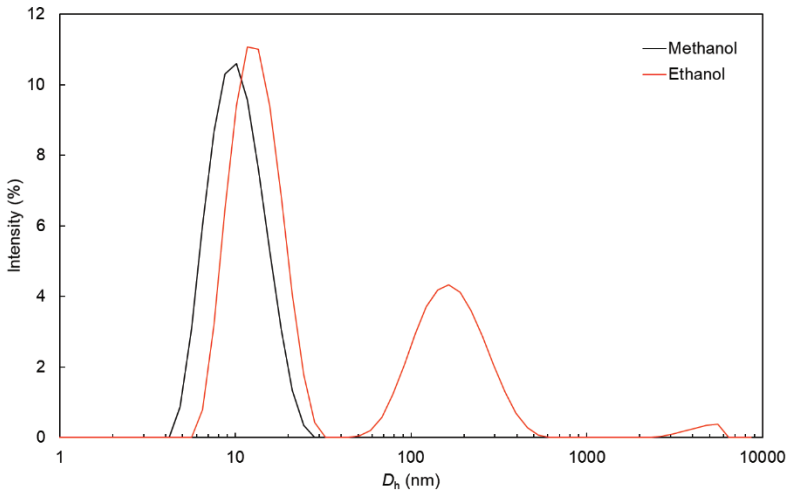

***Figure 134**. DLS measurements of MeOH/water (dark curve) and EtOH-water (red curve) solutions (50/50 in weight) containing 2.8 wt.% of CeO_2 based on solvent.*

2. Surface modification of CeO_2 nanoparticles by disulfide

In the following studies, the concentration of carboxylic acid functions, *i.e.*, *c*(COOH) = 2x *c*(disulfide), was expressed in µmol m^{-2} based on the total surface area of the CeO_2 NPs (specific surface area of 218.6 m^2 g^{-1}, see Table 30). The concentration of disulfide

required to cover the CeO_2 NPs surface without destabilization was determined by increasing gradually the amount of *c*(COOH) from 0.27 to 20 µmol m^{-2} (*i.e.*, from 1.45 to 107.2 mmol L^{-1} in 20 g of MeOH/water mixture 50/50 in wt.%). The disulfide was first dissolved in MeOH and the mixture was then added dropwise *via* a syringe pump (flow rate fixed at 1 mL min^{-1}) to the CeO_2 sol (2.8 wt.% of CeO_2 based on solvent). Note that the disulfide was totally soluble in methanol except for COOH concentrations higher than 26.8 mmol L^{-1}, equivalent to *c*(COOH) ≥ 5.0 µmol m^{-2}. The suspensions were then stirred for 30 min. The flasks of the CeO_2 sols shown in Figure 135A indicate that for an initial *c*(COOH) between 0 and 0.58 µmol m^{-2}, the CeO_2 sols were transparent and did not precipitate (with a cloudy appearance for 0.58 µmol m^{-2}). For concentrations of 1.01 µmol m^{-2} and above the sols became very cloudy, and beyond 4.99 µmol m^{-2}, completely unstable. After 4 days (Figure 135B), the CeO_2 sols remained stable for *c*(COOH) ≤ 0.58 µmol m^{-2} but beyond 1.01 µmol m^{-2}, the CeO_2 sols totally precipitated.

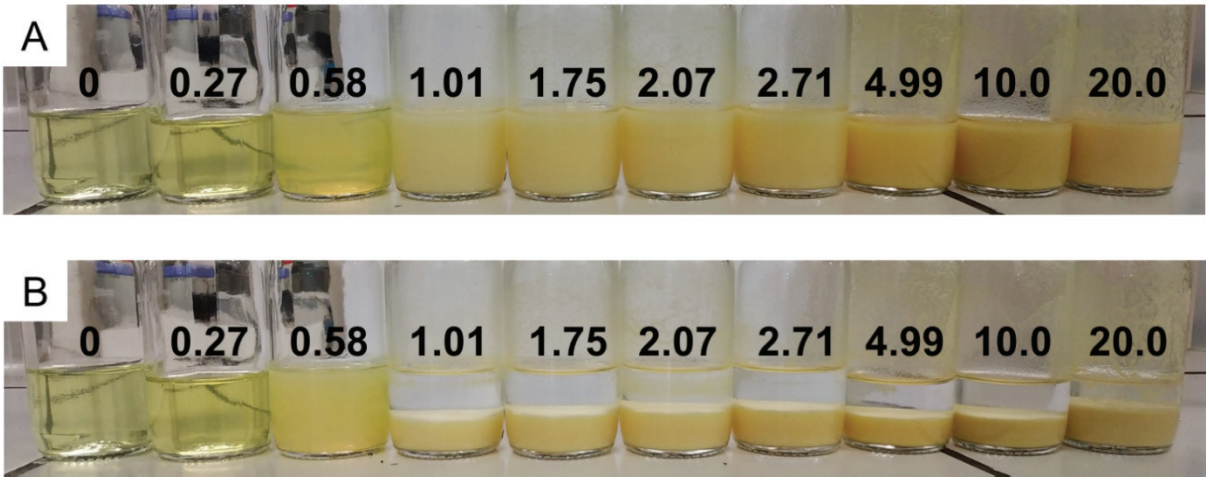

***Figure 135**. Appearance of the CeO_2 sols at 2.8 wt.% solids content as a function of c(COOH) (µmol m^{-2}) in MeOH/H_2O (50/50 wt./wt.): (A) directly after the addition of disulfide and (B) after 4 days.*

The cryo-TEM images showed that after the addition of disulfide at *c*(COOH) = 0.58 µmol m^{-2} in the MeOH/water mixture, individual CeO_2 NPs and a minor fraction of particles in interaction with each another, forming small clusters, were observed (Figure 136A, red circles). Two weeks later, the CeO_2 sol was very turbid but still had not precipitate. We observed larger aggregates with fractal geometry and no individual CeO_2 NPs. Some of the disulfide may act as a linker between two CeO_2 nanoparticles due to the dicarboxylic acid ended-groups, which would intensify the aggregation phenomenon. Thereafter, the CeO_2 sol was used directly after being prepared to prevent it from aggregation over time.

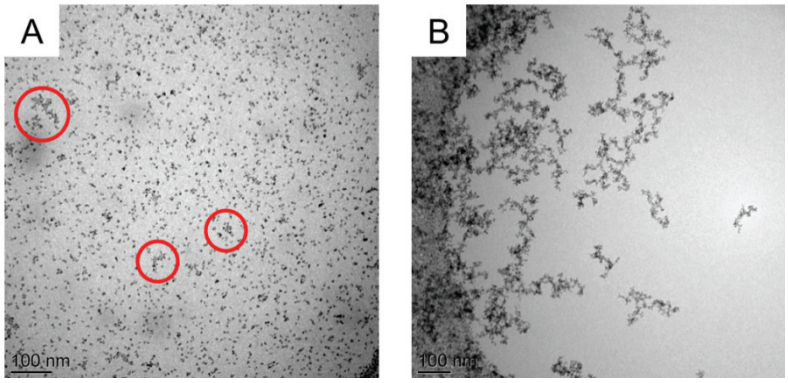

***Figure 136**. Cryo-TEM images of the CeO_2 sol at c(COOH) = 0.58 µmol m^{-2} in MeOH/water (50/50 in wt.%): (A) after 1 h of the addition of disulfide and (B) after 2 weeks.*

The particle size and the polydispersity index of the CeO_2 sols were determined directly after being prepared by DLS in the methanol-water mixture (50/50 in wt.%), after the addition of a gradually increased disulfide concentration. Figure 137 shows that an increase in carboxylic acid function concentration led to an increase in particle size. It increased drastically when c(COOH) > 0.58 µmol m^{-2}. In addition, even for c(COOH) < 1.01 µmol m^{-2}, we observed two populations, a main one at 10 nm corresponding to the CeO_2 NPs, and the presence of some aggregates near 100 nm, which explains a higher average hydrodynamic particle diameter (D_h = 30 nm at c(COOH) = 0.58 µmol m^{-2}). We therefore considered that the amount of COOH added to the CeO_2 sol must not exceed this value to maintain a good dispersion of the initial suspension. Indeed, when the CeO_2 NPs surface is covered by disulfide, the surface charges are screened resulting in a reduction of the electrostatic repulsions thus leading to important aggregation. There are also probably hydrophobic interactions between disulfide molecules that can involve aggregation.

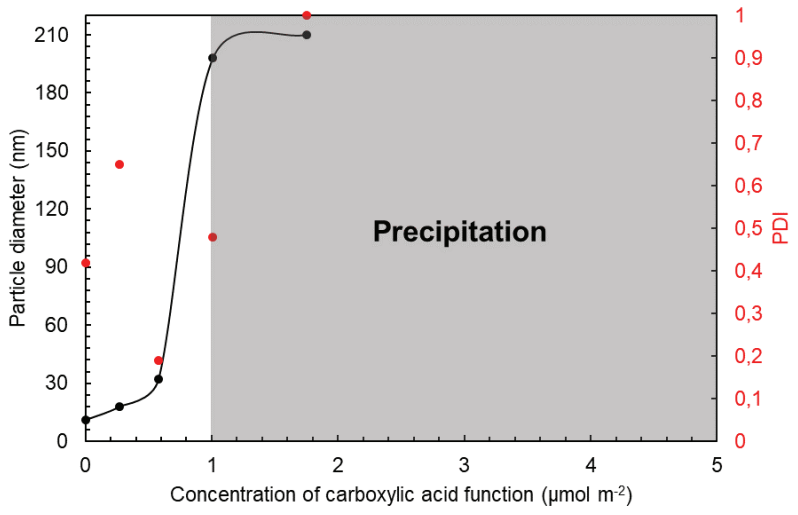

***Figure 137**. Evolution of the particle size determined directly after being prepared by DLS of the CeO_2 sols in MeOH/water (50/50 in wt.%) as a function of c(COOH) (µmol m^{-2}).*

It should be noticed that in these conditions, we were able to introduce a higher disulfide concentration (c(COOH) = 0.58 µmol m^{-2}) before destabilization, than when water was used as the continuous phase. Indeed, D. Subervie showed that CeO_2 precipitation occurred for c(COOH) = 0.252 µmol m^{-2}. in this case.

We then studied the affinity of the disulfide for the CeO_2 NPs surface. The previous mixtures prepared at different c(COOH) (from 0.27 to 20 µmol m^{-2}) were ultra-centrifugated. The supernatants were characterized by elemental analysis and the precipitates by FTIR. Figure 138 shows the adsorption isotherm. The amount of grafted carboxyl groups is plotted as a function of c(COOH) in the supernatant.

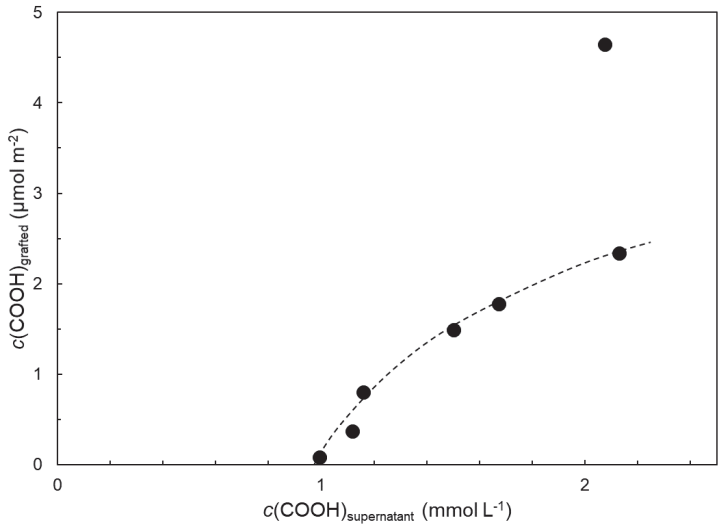

***Figure 138**. Binding isotherm of the disulfide on the CeO_2 sol in suspension (MeOH/water 50/50 in wt.%, at 20 °C and a CeO_2 content of 2.8 wt.% based on solvent).*

We observed that at low initial concentration, the grafted amount was very low, suggesting almost no affinity of the disulfide for the CeO_2 NPs surface in these diluted conditions (for an initial c(COOH) = 0.27 µmol m^{-2}, we obtained $c(COOH)_{grafted}$ = 0.08 µmol m^{-2}). As the initial c(COOH) increased, the adsorption of disulfide increased rapidly. The adsorbed molecules apparently favored the subsequent adsorption of other molecules through hydrophobic interactions. We expected the adsorbed amount to reach a plateau. However, we could not observe this plateau because, as mentioned previously, the disulfide was only partially soluble in methanol for initial COOH concentrations higher than 26.8 mmol L^{-1}, equivalent to c(COOH) ≥ 5.0 µmol m^{-2}, thus biasing the results.

The interaction between the CeO_2 NPs and the disulfide was also demonstrated by FTIR. The FTIR spectra of the precipitates collected after ultra-centrifugation (*i.e.*, disulfide-modified CeO_2 NPs) were compared with the spectra of the unmodified CeO_2 sol (Table 36, Figure 139)

and the disulfide (Table 37, Figure 140). We observed the evolution of the characteristic absorption peaks as a function of *c*(COOH) (0.58, 2.71 and 20.0 µmol m^{-2}). According to Figure 141, a peak characteristic of carboxyl group at 1 745 cm^{-1} (corresponding to the vibrations of "free" C=O) appeared for all disulfide concentrations. By increasing the initial *c*(COOH) at 2.71 and 20.0 µmol m^{-2}, we clearly observed a decrease of the ν_{NO} symmetric peak and the appearance of the $\nu_{C=C}$ peaks at 1 495 and 1420 (shoulder) cm^{-1} matching with the $\nu_{C=C}$ of the disulfide. Two single narrow peaks at 805 and 745 cm^{-1} corresponding C-$H_{arom.}$ in *para* position and the C-H bonds are also visible. The FTIR spectra therefore confirmed the presence of disulfide at the CeO_2 NPs surface.

***Table 36**. Characteristic absorption peaks obtained from FTIR spectrum of CeO_2 NPs.*

Wavenumber (cm^{-1})	Intensity	Bond assignment
3 350	strong, broad	O–H stretching
2 925, 2 850	weak	C–H stretching
1 620	medium	O–H bending
1 455	medium (shoulder)	N–O stretching asymmetric
1 388	strong, sharp	N–O stretching symmetric
500	strong	O–Ce–O stretching

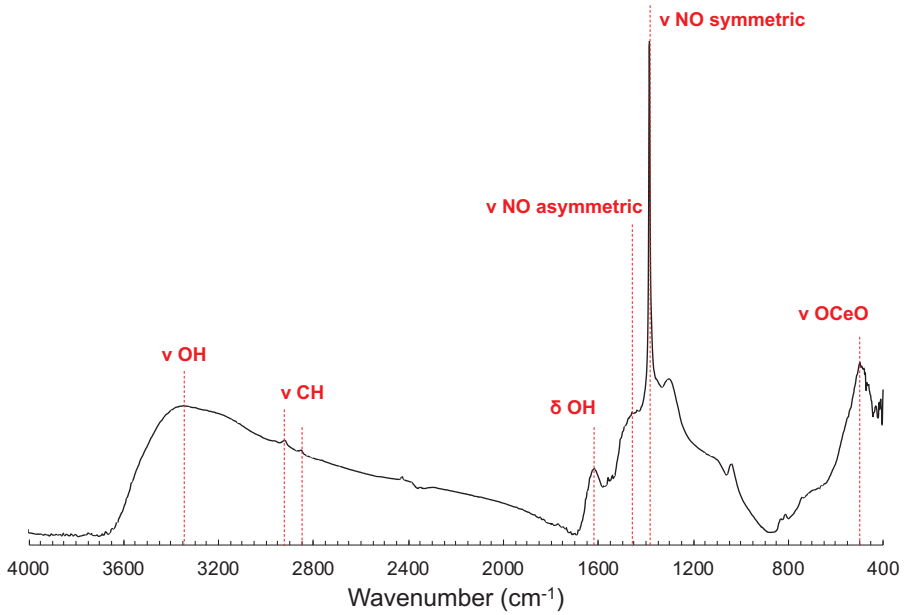

***Figure 139.** FTIR spectrum of the CeO_2 NPs after ultra-centrifugation of the sol and drying at 100 °C.*

***Table 37**. Characteristic FTIR absorption peaks of the diphenyl disulfide.*

Wavenumber (cm^{-1})	Intensity	Bond assignment
3 430	strong, broad	O–H stretching
2 900 – 3 100	medium	C–H stretching
2 350	medium	O=C=O stretching
1 720	strong, sharp	C=O stretching (free)
1 690	strong, sharp	C=O stretching (dimer)
1 495, 1 405	medium	C=C stretching (arom)
1 345	medium	O–H bending
1 255	medium	C–O stretching
805	medium	C–H bending (arom-*para*)
730	medium	C–H bending

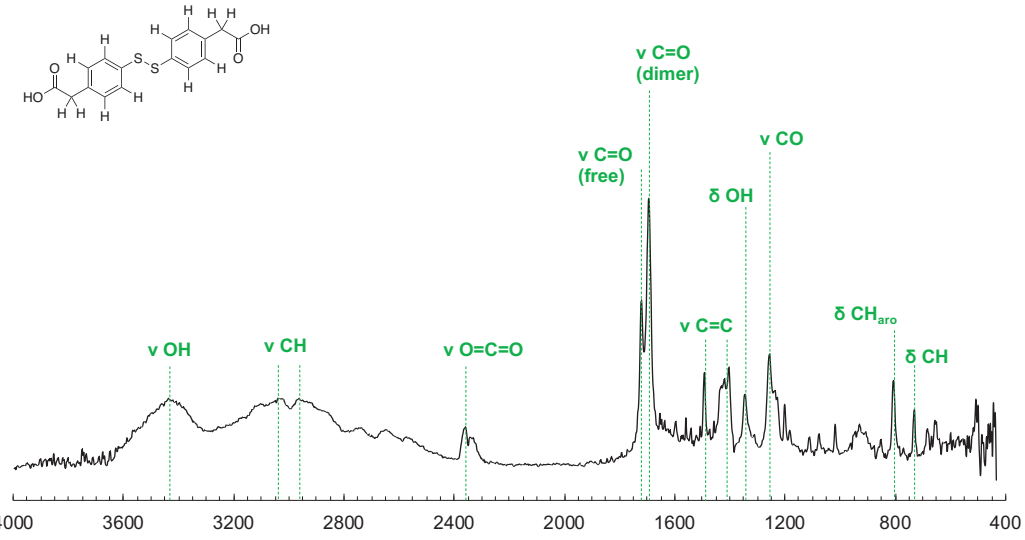

***Figure 140**. FTIR spectrum of the disulfide.*

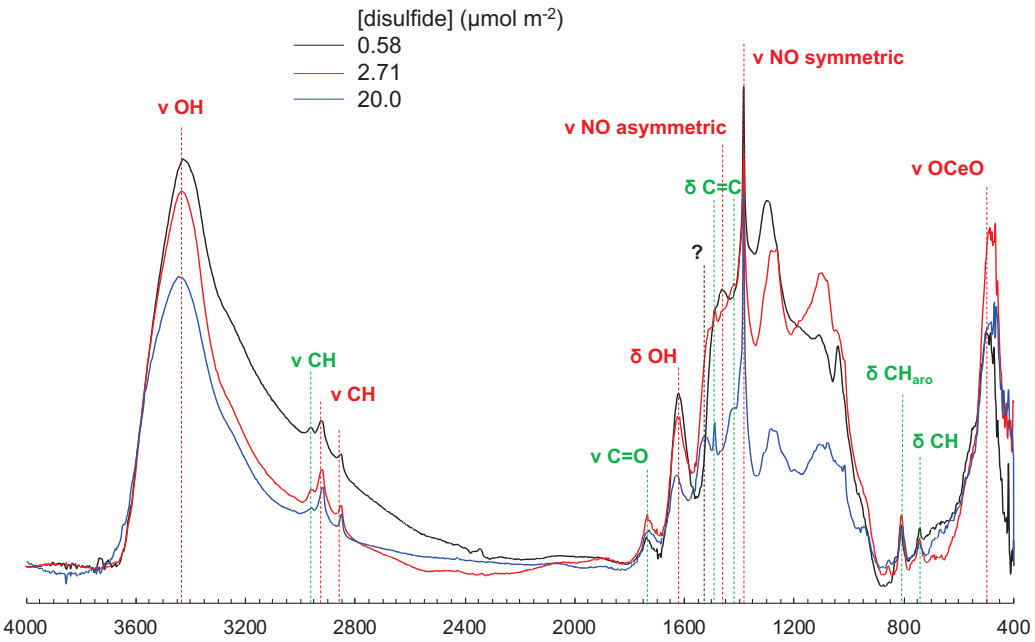

Figure 141. *FTIR spectra of the disulfide-modified CeO_2 NPs at different c(COOH): 0.58 (dark curve), 2.71 (red curve) and 20.0 µmol m^{-2} (blue curve).*

In summary, we identified the optimal conditions for the disulfide adsorption at the CeO_2 NPs surface. The maximum c(COOH) at which the CeO_2 sol does not aggregate is 0.58 µmol m^{-2}. We showed that c(COOH) = 0.58 µmol m^{-2} leads to the best ratio between disulfide adsorbed on the inorganic surface ($c(COOH)_{grafted}$ = 0.36 µmol m^{-2}) and free disulfide in solution. This c(COOH) was therefore chosen for the rest of the study. The presence of disulfide at the CeO_2 NPs surface was further supported by FTIR. However, the different techniques used did not allow us to clearly characterize the interaction between the disulfide and the CeO_2 NPs. What we know for sure is that the FTIR confirmed the presence of "free" carboxyl group.

II. Synthesis of CeO_2-armored hybrid latexes by Pickering dispersion photopolymerization

The copolymerization of *n*-BA and MMA was carried out in dispersion under visible light irradiation in the absence of steric stabilizer. The ratio *n*-BA/MMA of 60/40 (in wt.%) was chosen to subsequently make films.

A. Efficiency of our disulfide-modified CeO_2 nanoparticles for Pickering dispersion photo-copolymerization of *n*-BA and MMA

To demonstrate the crucial role of both disulfide and CeO_2 NPs to produce stable hybrid latexes, we prepared two blank latexes. For this study, we used the disulfide at c(COOH) = 0.58 µmol m^{-2} (which corresponds to c(COOH) = 3.10 mmol L^{-1}), the solids content was fixed at 10 wt.% and we first decided to work at CeO_2 content of 10 wt.% (based on monomers). The first blank was prepared without disulfide in the presence of the CeO_2 sol and the second with the disulfide in the absence of CeO_2 NPs. We observed that without disulfide, the photo-copolymerization of *n*-BA and MMA did not proceed. This proves that the disulfide was required to photoinitiate the polymerization. Conversely, when the CeO_2 NPs were absent, we obtained a polymer deposit at the bottom of the reactor, indicating that the polymer was formed but not stabilized in solution. In the presence of CeO_2 NPs and disulfide, the photopolymerization reached a final conversion of about 90% after 5 h. The hybrid latex was highly stable and contained particles with a mean diameter of 288 nm and a narrow size distribution (D_w/D_n = 1.03). As seen in the cryo-TEM image of Figure 142, the hybrid particles exhibit a spherical morphology with a stark contrast of their edge, corresponding to the CeO_2 NPs. On can also note the absence of free CeO_2 NPs. This experiment thus demonstrates the successful preparation of hybrid latexes in the presence of both the CeO_2 NPs and the disulfide.

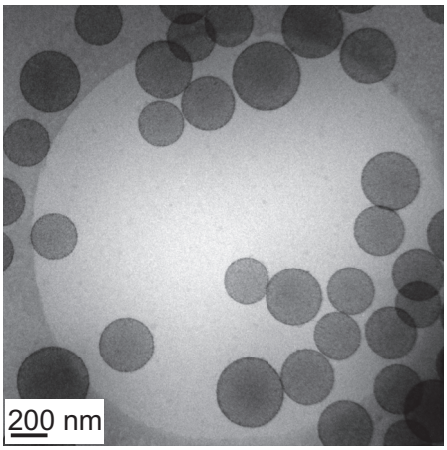

***Figure 142**. Cryo-TEM image of the CeO_2-armored P(n-BA-co-MMA) latex at CeO_2 content of 10 wt.% based on monomers and c(COOH) = 0.58 µmol m^{-2}.*

Next, we decided to compare our disulfide modified CeO_2 NPs Pickering stabilizer to PEGMA (M_n = 2 080 g mol^{-1}) and PVP-K30 (M_n = 40 000 g mol^{-1}), that both proved to be efficient stabilizers for dispersion photopolymerization of styrene in water-ethanol mixture (Chapter 3). The results are reported in Table 38.

***Table 38**. Influence of the type of stabilizer on the polymerization rate and the particle size.*

Run	Stabilizer	Time (h)	Conv. (%)	D_n[b] (nm)	D_w/D_n[b]	N_p (10^{14} cm^{-3})
1	CeO_2	5	90	288	1.03	6.76
2	PEGMA	27	71	540	1.22	0.81
3	PVP	7	60	518	1.03	0.78

[a] Experimental conditions: reaction temperature fixed at 40 °C, methanol/water = 50/50 (wt.%). The solids content was fixed at 10 wt.%. The stabilizer concentration was fixed at 10 wt.% based on monomers and c(COOH) = 0.58 µmol m^{-2}.
[b] Determined by TEM.

These three stabilizers were introduced at the same weight concentration, *i.e.*, 10 wt.% based on monomers, and the experimental conditions were similar. Figure 143 clearly shows that the photopolymerization carried out with the CeO_2 NPs was much faster. Indeed, the conversion reached 90% after 5 h in the case of CeO_2, whereas it only reached 70% and 60% after 25 and 7 h for respectively PEGMA and PVPK30. In addition, larger particles were obtained with the two polymeric stabilizers than with the CeO_2 NPs indicating that the Pickering dispersion photopolymerization in the presence of CeO_2 NPs as solid stabilizer was very efficient. In the case of PEGMA, a broad size distribution was observed (D_w/D_n = 1.22) whereas in the other cases, narrow size distributions were obtained (D_w/D_n = 1.03). As already shown in Chapter 3, PVP led to very narrow size distributions in the dispersion photopolymerization of styrene.

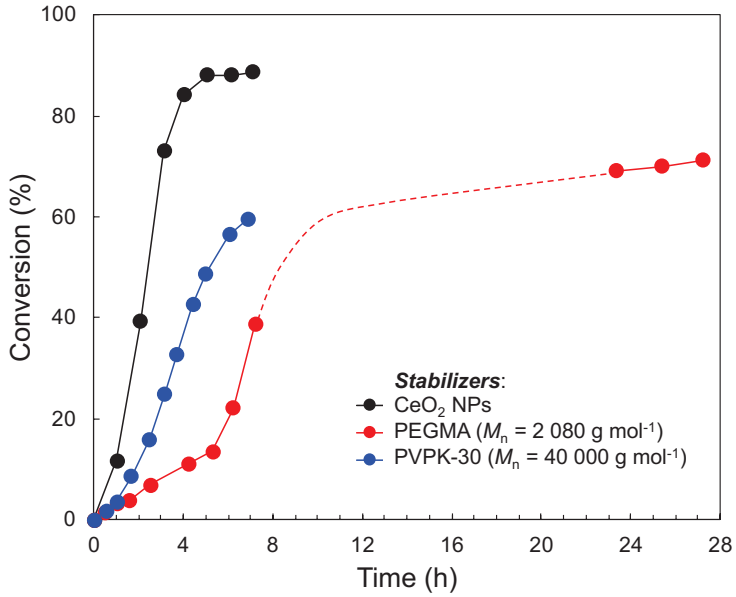

***Figure 143**. Evolution of the conversion as a function of time depending on the nature of the stabilizer: CeO_2 NPs (dark curve), PEGMA (red curve) and PVPK-30 (blue curve) for MMA/n-BA dispersion copolymerization under visible light irradiation. Each stabilizer was introduced at a concentration of 10 wt.% based on monomers.*

B. Influence of the CeO_2 content

We then studied the effect of the CeO_2 NPs content on the particles size and the polymerization rate. We varied the CeO_2 NPs content from 10 to 42 wt.% based on monomers and *c*(COOH) (in mmol L^{-1}) was adjusted to keep a constant concentration of 0.58 µmol m^{-2} of carboxyl function. The results are presented in Table 39.

Table 39. *Influence of the CeO_2 NPs content on the Pickering dispersion copolymerization of n-BA and MMA under visible light at c(COOH) = 0.58 µmol m^{-2}.*[a]

Run	CeO_2 (wt.%)	*c*(COOH) (mmol L^{-1})	Time (h)	Conv. (%)	D_n[b] (nm)	D_w/D_n[b]	N_p (10^{15} cm^{-3})
1	10	1.38	5	90	288	1.03	0.67
4	17	2.20	6	95	259	1.07	0.98
5	25	3.10	4.5	90	220	1.09	1.5
6	33	4.10	8.5	90	158	1.10	4.1
7	42	5.34	6	95	159	1.25	4.3

[a] Experimental conditions: reaction temperature fixed at 40 °C, methanol/water = 50/50 (wt.%). The solids content was fixed at 10 wt.%. The CeO_2 content was based on monomers and *c*(COOH) = 0.58 µmol m^{-2}.
[b] Determined by TEM.

In each case, we obtained stable hybrid latexes without any coagulum. The conversion curves in Figure 144 show that as the CeO_2 NPs content increased, the polymerization rate increased The particle size decreased when the CeO_2 NPs content increased (from 288 to 159 nm at CeO_2 of 10 and 42 wt.%, respectively). Moreover, we observed a gradual broadening of the size dispersity when the CeO_2 nanoparticle content increased (from D_w/D_n = 1.03 at 10 wt.% of CeO_2 to D_w/D_n = 1.25 at 42 wt.% of CeO_2).

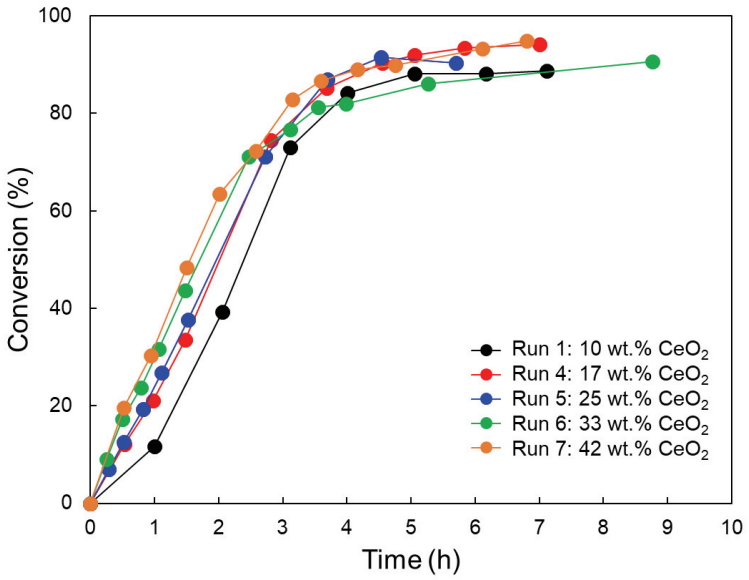

***Figure 144**. Conversion curves as a function of time at different CeO_2 NPs contents and at constant c(COOH) = 0.58 µmol m^{-2}. See Table 39 for experimental details.*

We expected a much faster photopolymerization at a CeO_2 NPs content of 42 wt.%, which corresponds to *c*(COOH) = 5.34 mmol L^{-1} than at 17 wt.% CeO_2 NPs content, which corresponds to *c*(COOH) = 2.20 mmol L^{-1}, since a more important number of thiyl radicals should be generated. However, Figure 144 indicates that the reaction rates increase with increasing the CeO2 content initially, but leveled off at higher concentrations. One possible explanation was the presence of Ce^{3+} ions in the CeO_2 NPs sols which could act as free radical scavengers. The higher the CeO_2 content, the greater the amount of Ce^{3+} ions. Indeed, as mentioned above, N. Zgheib demonstrated that a dialyzed CeO_2 NPs sol (free from Ce^{3+} ions) led to a faster copolymerization of *n*-BA and MMA in the presence of an auxiliary monomer MAA in emulsion conditions.[52] It should be interesting to carry out the synthesis in our experimental conditions with a dialyzed CeO_2 sol to confirm this hypothesis.

The cryo-TEM images in Figure 145 showed that no free CeO_2 NP was observed in all cases, suggesting that the selected *c*(COOH) = 0.58 µmol m^{-2} led to an optimal coverage of the CeO_2 NPs surface allowing an efficient adsorption of the latter at the polymer particles. The broadening of the size dispersity with increasing the CeO_2 content can be attributed to the greater number of CeO_2 NPs that could stabilize a greater number of polymer particles, extending consequently the nucleation period. In Figure 145e (CeO_2 content of 42 wt.%), we observed hybrid particles with different sizes and a few numbers of non-spherical particles.

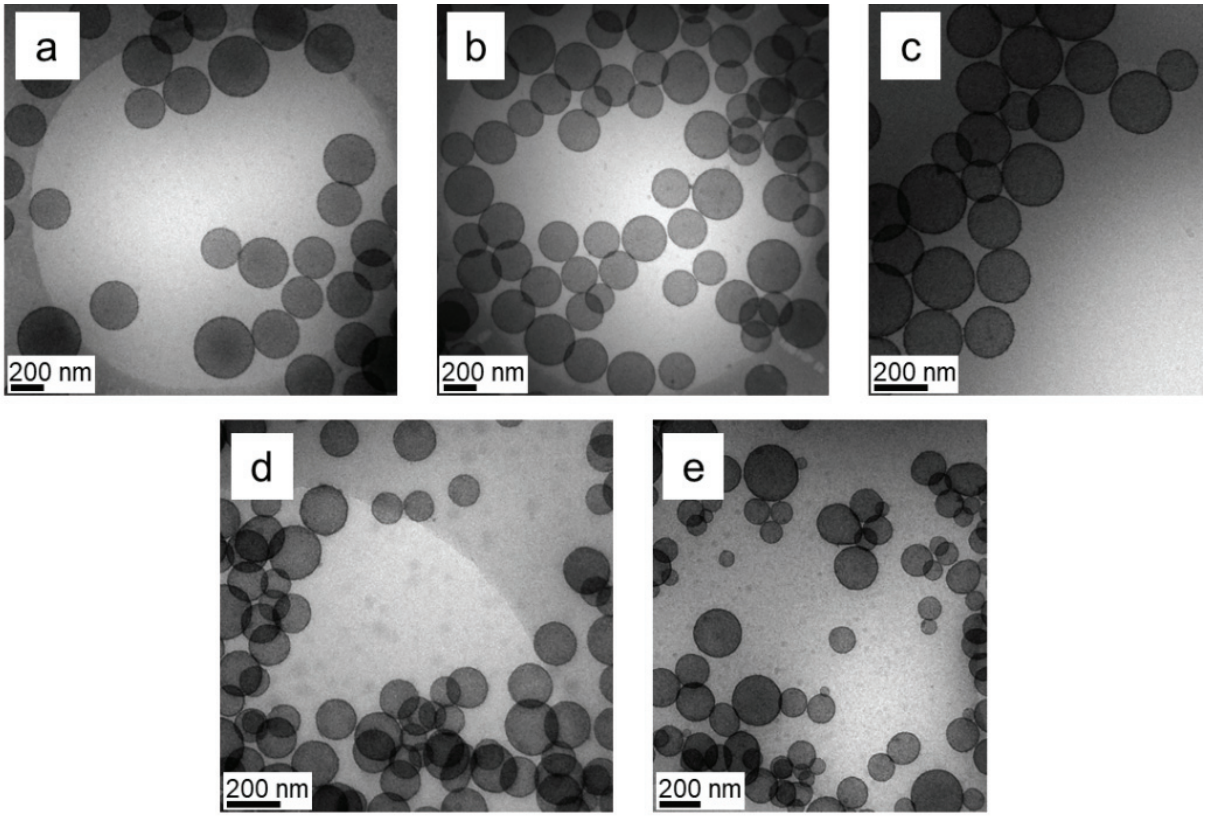

***Figure 145**. Cryo-TEM images of the CeO_2-armored P(n-BA-co-MMA) hybrid latexes at different CeO_2 NPs contents: (a) 10, (b) 17, (c) 25, (d) 33 and (e) 42 wt.% based on monomers at c(COOH) = 0.58 µmol m^{-2}.*

C. Influence of the disulfide concentration

Next, we varied *c*(COOH) from 1.08 to 5.36 mmol L^{-1}, with a fixed CeO_2 content (at 25 wt.% based on monomers). It is worth to notice that the range of disulfide concentrations is similar to that of the previous section. All the results are reported in Table 40.

***Table 40**. Influence of c(COOH) on the Pickering dispersion polymerization of n-BA and MMA under visible light in the presence of CeO_2 NPs (25 wt.% based on monomers).[a]*

Run	*c*(COOH) (mmol L^{-1})	*c*(COOH) (µmol m^{-2})	Time (h)	Conv. (%)	D_n[b] (nm)	D_w/D_n[b]	N_p (10^{15} cm^{-3})
8	1.08	0.2	8	90	150	2.45	4.8
9	1.74	0.32	7	90	267	1.11	0.84
10	2.46	0.4	6.5	90	216	1.11	1.6
5	3.10	0.58	4.5	90	220	1.09	1.5
11	5.36	1.01	3.5	100	284	1.17	0.8

[a] Experimental conditions: reaction temperature fixed at 40 °C, methanol/water = 50/50 (wt.%). The solids content was fixed at 10 wt.% and the CeO_2 content was fixed at 25 wt.% based on monomers.
[b] Determined by TEM.

In each case, we obtained stable hybrid latexes without any coagulum. The conversion curves shown in Figure 146 indicate that the kinetics of polymerization was highly dependent on the disulfide concentration. The polymerization rate increased with increasing the amount of disulfide. For example, at *c*(COOH) = 1.08 mmol L^{-1} (run 8), the final conversion reached 90 % after 8 h, whereas for a higher *c*(COOH) = 5.36 mmol L^{-1}, a full conversion was obtained after only 3.5 h (run 11).

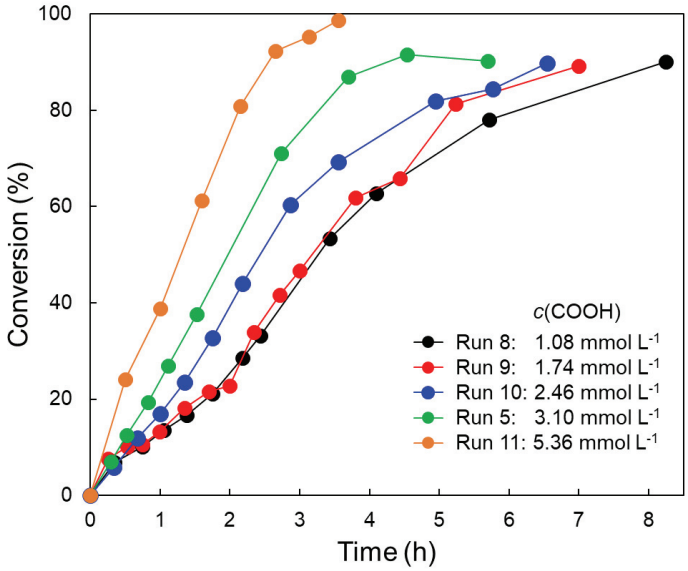

***Figure 146**. Conversion curves as a function of time at different initial COOH concentrations and a fixed CeO_2 NPs content (25 wt.% based on monomers). See Table 40 for experimental details.*

In comparison to the previous study where we varied the CeO_2 content and fixed the nominal grafting density leading *in fine* to roughly the same range of COOH concentrations, the effect of the disulfide on kinetics is much more pronounced here, indicating that the CeO_2 has a negative impact on the reaction rate. The influence of the amount of CeO_2 on the kinetics is best evidenced when comparing run 11 (Table 40) and run 7 (Table 39), carried out with the same *c*(COOH) = 5.36 mmol L^{-1} and two different CeO_2 contents (25 and 41 wt.%, respectively), or run 1 (Table 39) and run 8 (Table 40) for which *c*(COOH) was still again roughly the same (1.38 and 1.08 mmol L^{-1}, respectively) but the CeO_2 content again different (10 and 25 wt.%, respectively). In both cases, and as shown in Figure 147, the reaction rate decreased with increasing the CeO_2 content for a similar amount of disulfide, supporting the above hypothesis.

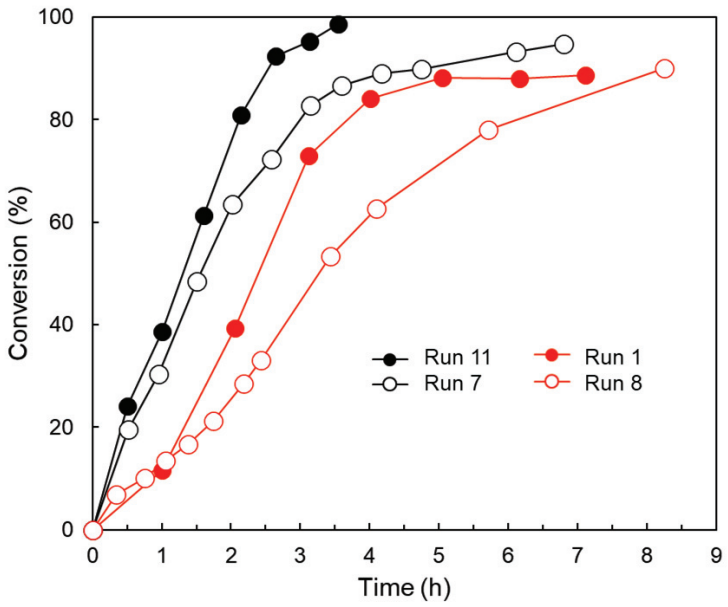

***Figure 147**. Influence of the CeO_2 content on the polymerization rates for run 11/run7 at c(COOH) = 5.36 mmol L^{-1} and run1/run8 at c(COOH) = 1.38 and 1.08 mmol L^{-1}, respectively.*

The hybrid latexes were observed by cryo-TEM (Figure 148). We first observed that the particles size increased from 150 to 267 nm with an increase of *c*(COOH) from 1.08 to 1.74 mmol L^{-1}, but as the COOH concentration continued to increase until *c*(COOH) = 3.10 mmol L^{-1}, the particles size decreased, and the size distributions narrowed. For the highest COOH concentration, *c*(COOH) = 5.36 mmol L^{-1}, the particles size increased again, but a relatively broad size dispersity (D_w/D_n = 1.17) was observed. For the highest *c*(COOH) = 2.68 mmol L^{-1}, we observed in Figure 148e, a potato-like morphology of the particles, which suggests an inefficient stabilization. Indeed, we have shown previously that the CeO2 particles tend to aggregate at high disulfide concentration, and are therefore likely less efficient as stabilizer, leading to a higher particle size. Moreover, at low COOH concentration, *c*(COOH) = 1.08 and 1.74 mmol L^{-1}, we clearly observed free CeO_2 NPs in these latexes (Figure 148a and b). A simple explanation would be the low adsorption of the disulfide at the CeO_2 NPs surface and thus, a low affinity of the CeO_2 NPs for the polymer particles. Therefore, an optimal *c*(COOH) was found between 2.46 and 3.10 mmol L^{-1} for which the final hybrid latex was efficiently stabilized with a spherical morphology and relatively narrow size distribution (see Table 40), and was devoid of any free CeO_2 NPs.

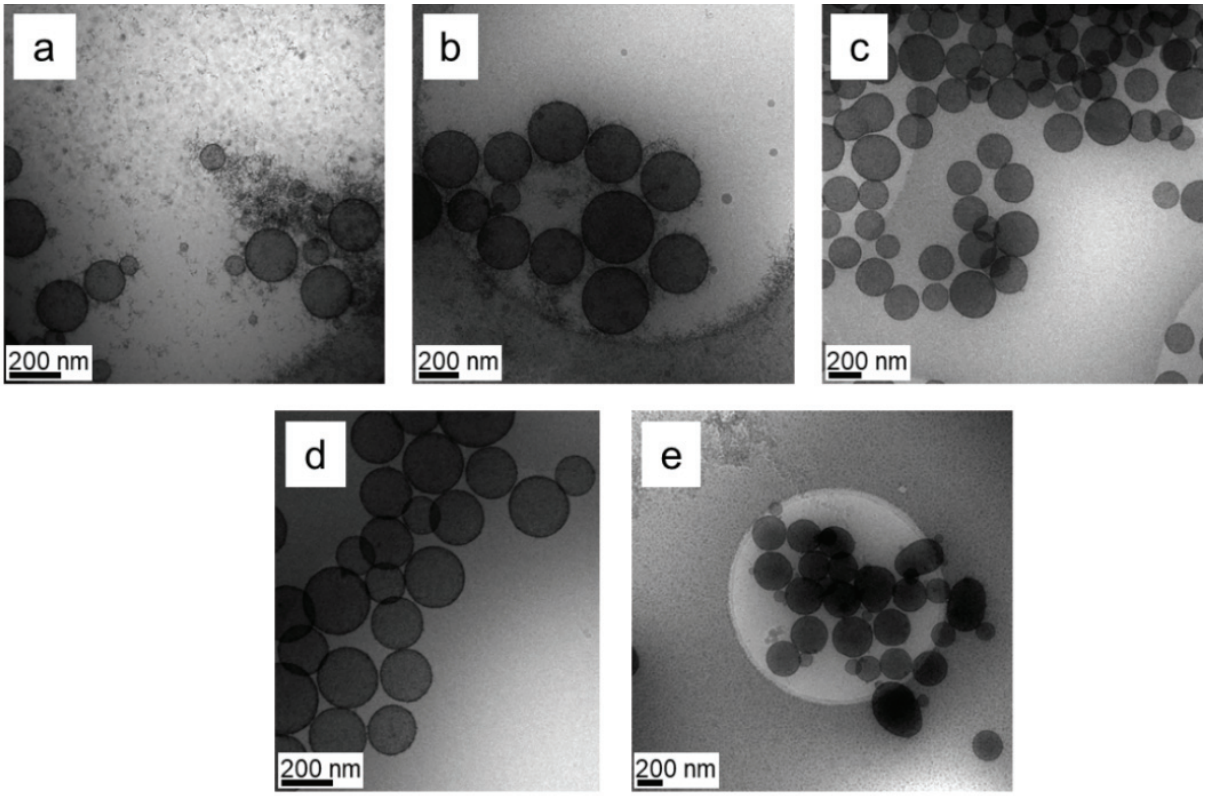

***Figure 148**. Cryo-TEM images of the CeO_2-armored P(n-BA-co-MMA) hybrid latexes at different c(COOH): (a) 1.08, (b) 1.74, (c) 2.46, (d) 3.10 and (e) 5.36 mmol L^{-1}. See Table 40 for experimental details.*

D. Influence of the luminous flux

During this thesis, the synthesis of CeO_2-armored P(*n*-BA-MMA) latexes were carried out with a LED ribbon composed of 94 LEDs (equivalent to an overall brightness of 1 692 Lumens). With the exception of run 11 (see Table 40), all the experiments were limited in conversion (~90%). Therefore, in order to approach full conversions, we decided to use a more powerful LED ribbon with the best experimental conditions found previously, *i.e.*, a CeO_2 content of 25 wt.% based on monomers and a disulfide concentration of 1.55 mmol L^{-1} (which corresponds to 0.58 µmol m^{-2} of COOH groups). The new ribbon was composed of 130 LEDs corresponding to an overall brightness of 2 015 Lumens according to the characteristics given by the supplier. We then performed the photo-copolymerization of *n*-BA and MMA in dispersion conditions at 40 °C. The results are reported in Table 41.

***Table 41**. Influence of the luminous flux on the Pickering dispersion copolymerization of n-BA and MMA under visible light in the presence of CeO_2 NPs (25 wt.% based on monomers).[a]*

Run	Luminous flux (Lumen)	Time (h)	Conv. (%)	D_n[b] (nm)	D_w/D_n[b]	N_p (10^{15} cm^{-3})
5	1 692	4.5	90	220	1.09	1.5
12	2 015	3.5	100	218	1.07	1.75

[a] Experimental conditions: reaction temperature fixed at 40 °C, methanol/water = 50/50 (wt.%). The solids content was fixed at 10 wt.%, the CeO_2 content at 25 wt.% based on monomers and c(COOH) = 0.58 µmol m^{-2}.
[b] Determined by TEM.

We observed that the photopolymerization was faster with the new LED ribbon, reaching complete monomer conversion after 3.5 h vs. 90% conversion after 4.5 h for the previous LED ribbon. We believe that the reactor mixture received a higher photon flux which led to more thiyl radicals and thereby, a faster photopolymerization. Moreover, we obtained a similar particles size, with slight improvement of the size dispersity. From that point on, all the Pickering dispersion photopolymerizations were carried out with the new LED ribbon.

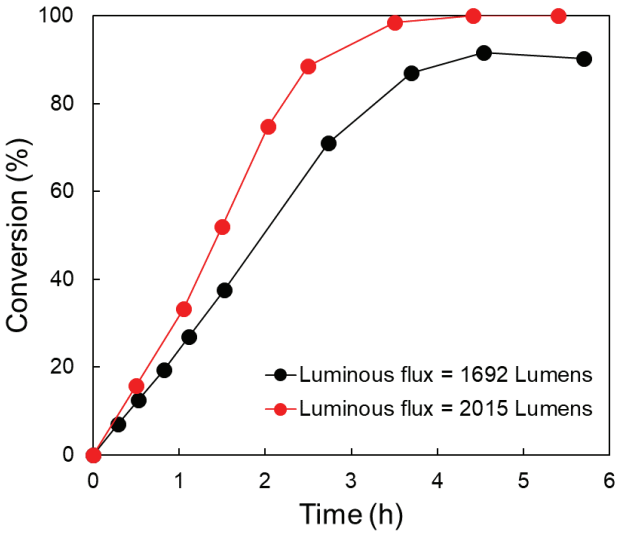

***Figure 149**. Conversion curves as a function of time at two different luminous flux: 1 692 Lumens (dark curve) and 2 015 (red curve). See Table 41 for experimental details.*

E. Towards very low CeO_2 contents

In this series of experiments, our aim was to strongly decrease the CeO_2 content and observe whether the colloidal stability of the hybrid particles was maintained. The CeO_2 content was varied from 1 to 25 wt.% (based on monomers) and the disulfide concentration adjusted to

keep a constant concentration of 0.58 µmol m^{-2} of carboxyl function. The results are presented in Table 42.

***Table 42**. Influence of the CeO_2 NPs content on the Pickering dispersion polymerization of n-BA and MMA under visible light at c(COOH) = 0.58 µmol m^{-2}.[a]*

Run	CeO_2 (wt.%)	*c*(COOH) (mmol L^{-1})	Time (h)	Conv. (%)	D_n[b] (nm)	D_w/D_n[b]	N_p (10^{15} cm^{-3})
13	1	0.12	6	28	565[c]	-	-
14	5	0.62	4.5	86	460	1.03	0.16
15	10	1.24	6	100	405	1.06	0.27
16	20	2.50	4.6	100	331	1.10	0.50
12	25	3.10	3.5	100	218	1.07	1.75

[a] Experimental conditions: reaction temperature fixed at 40 °C, methanol/water = 50/50 (wt.%). The solids content was fixed at 10 wt.%. The CeO_2 content was based on monomers and *c*(COOH) = 0.58 µmol m^{-2}.
[b] Determined by TEM.
[c] Average diameter determined by counting 25 particles.

We observed a significant effect of the CeO_2 content on the polymerization rates which substantially increased when the CeO_2 content was varied from 1 to 10 wt.%, but this effect tended to be moderate beyond 10 wt.% of CeO_2 (Figure 150). Indeed, at 1 wt.% (which corresponds to a very low *c*(COOH) of 0.12 mmol L^{-1}), the monomer conversion reached 28% after 6 h and we observed a substantial flocculation. We also observed this phenomenon at 5 wt.% of CeO_2 which corresponds to *c*(COOH) = 0.62 mmol L^{-1}, but the final monomer conversion reached 86% after 4.5 h. This difference in terms of kinetics can be explained by the fact that the disulfide concentration was about 5 times higher in the latter case, resulting in a much important generation of thiyl radicals and a much faster polymerization. On the other hand, when we compare run 15, *c*(COOH) = 1.24 mmol L^{-1} and run 12, *c*(COOH) = 3.10 mmol L^{-1}, we observe a slight increase in the reaction rate. We found that he minimal content of CeO_2 necessary to obtain stable hybrid latexes was 10 wt.% (based on monomers).

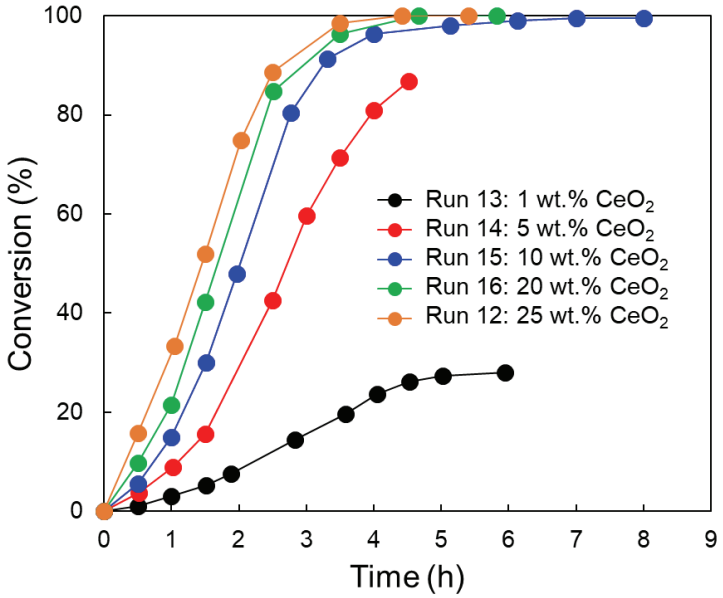

***Figure 150**. Conversion curves as a function of time for different CeO_2 NPs contents and c(COOH) = 0.58 µmol m^{-2}). See Table 42 for experimental details.*

As previously studied, the particles size decreased when the CeO_2 content increased (from 405 to 218 nm at CeO_2 contents of 10 and 25 wt.%, respectively), while the particles size distribution broadened. We obtained very similar trend with the previous study on the influence of CeO_2 content (see Table 39 and Figure 144). We can observe in Figure 151a (1 wt% of CeO_2 NPs) that the polymer particles are not completely covered by CeO_2 NPs. Moreover, the particles present a hairy-like morphology which it is very similar to the structure of CeO_2 NPs in methanol-water mixture in the presence of disulfide observed after 2 weeks (Figure 136). We believe that the amount of disulfide adsorbed at the CeO_2 NPs surface was not enough to improve the adhesion of the CeO_2 NPs at the polymer particles.

The destabilization of the hybrid latexes seemed to occur at a critical particle size, which in our experimental conditions was around 460 nm. The problem is that there are not enough of CeO_2 NPs to efficiently stabilize the polymer particles. In addition, we were faced to reproducibility issues in Chapter 3, probably due to the slow and continue generation of radicals, leading to a slow nucleation. In the present study, we developed a robust system that allow the obtention of large particles (up to 405 nm) and full conversions after 4 h. We believe that this robustness was due to the high overall polymerization rate.

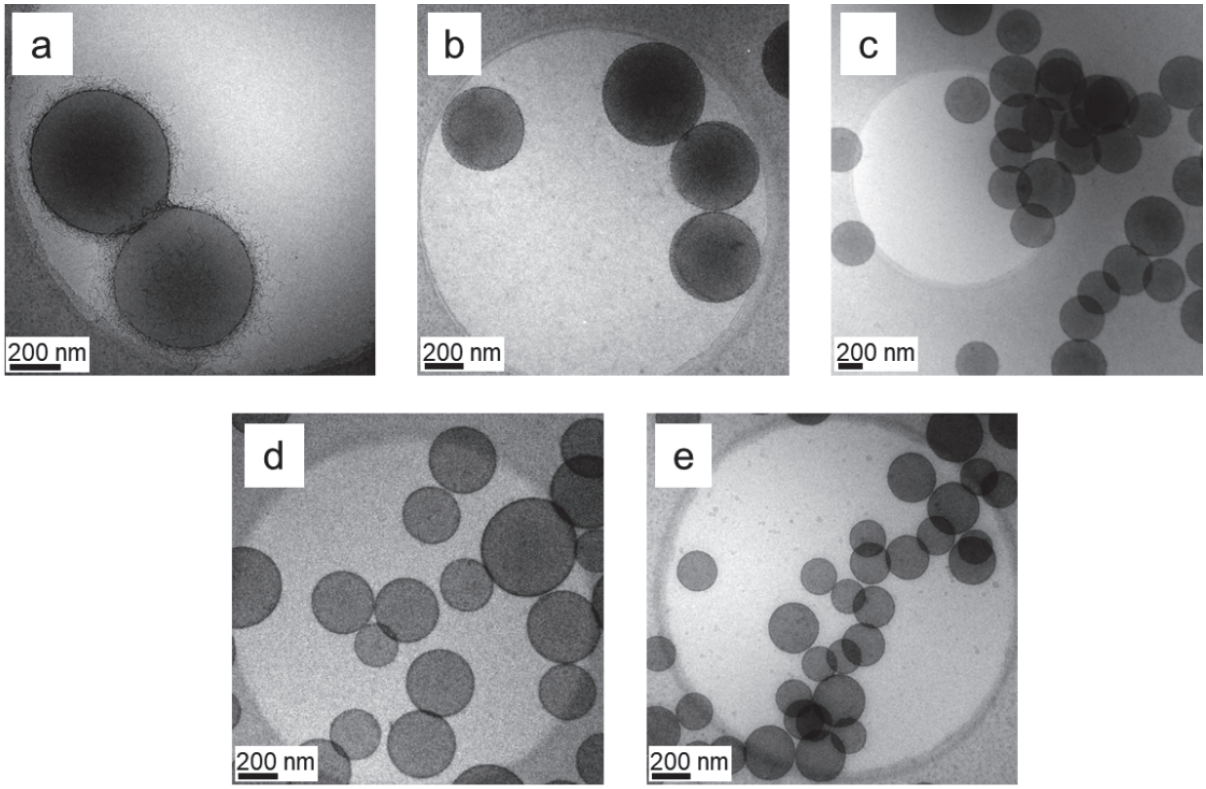

Figure 151. *Cryo-TEM images of the CeO_2-armored P(n-BA-co-MMA) hybrid latexes at c(COOH) = 0.58 µmol m^{-2} and for different CeO_2 NPs contents: (a) 1, (b) 5, (c) 10, (d) 20 and (e) 25 wt.% based on monomers. See Table 42 for experimental details.*

F. Influence of the monomer concentration

We then studied the effect of the monomer concentration on the polymerization rate and the particle size for two different CeO_2 contents. The COOH concentration adjusted to keep a constant concentration of 0.58 µmol m^{-2} of carboxyl function. In comparison with a solids content of 10 wt.%, the amount of disulfide was about twice higher at 20 wt.% solids content. The results are reported in Table 43.

Table 43. *Effect of monomer concentration for different CeO_2 contents on the Pickering dispersion polymerization of n-BA and MMA under visible light at c(COOH) = 0.58 µmol m^{-2}.[a]*

Run	Monomer (wt.%)	CeO_2 (wt.%)	*c*(COOH) (mmol L^{-1})	Time (h)	Conv. (%)	D_n[b] (nm)	D_w/D_n[b]	N_p (10^{15} cm^{-3})
15	10	10	1.24	6	100	405	1.06	0.27
16	10	20	2.5	4.6	100	331	1.10	0.50
17	20	10	3.10	5	100	455	2.15	3.5
18	20	20	5.60	5	100	196	3.21	4.8

[a] Experimental conditions: reaction temperature fixed at 40 °C, methanol/water = 50/50 (wt.%). The solids content was fixed at 10 or 20 wt.%. The CeO_2 content was based on monomers and *c*(COOH) = 0.58 µmol m^{-2}.
[b] Determined by TEM.

The conversion curves in Figure 152 show that the kinetics of polymerization was highly dependent on the monomer concentration at low CeO_2 contents. In all cases, c(COOH) = 0.58 µmol m^{-2}. For a similar disulfide concentration in mmol L^{-1} relative to monomer concentration and at the same CeO_2 content of 10 wt.% (runs 15 and 17), the photopolymerization carried out at 10 wt.% solids content was relatively faster than the one at 20 wt.% solids content. Similarly, by increasing the CeO_2 content at 20 wt.%, the photopolymerization was relatively faster at low monomer concentration. As described in Chapter 1, an increase of the solids content will lead to the formation of a greater quantity of particles and consequently increase the light scattering phenomena, especially multiple scattering. We believe that by increasing the solids content, we favor scatterings which would impact locally the generation of radicals, resulting in a diminution of the polymerization rate.

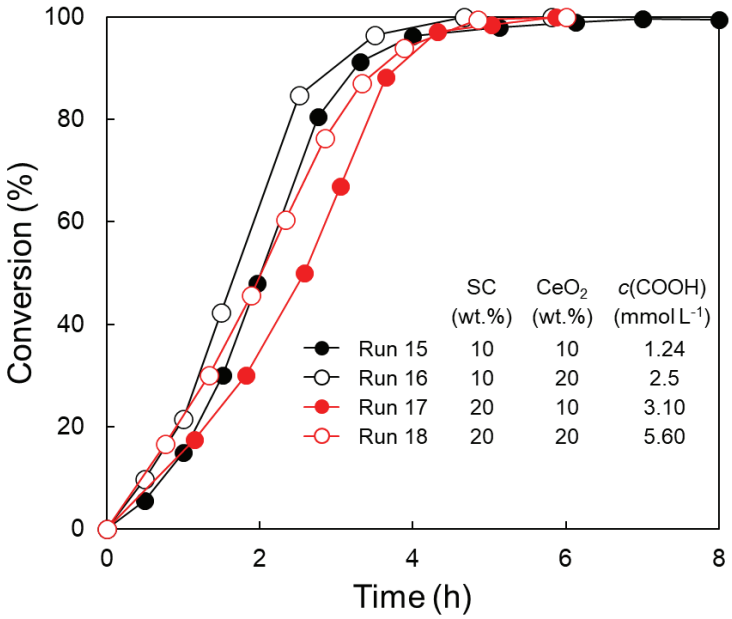

Figure 152. *Conversion curves as a function of time at 10 and 20 wt.% solids content and by varying the CeO_2 contents (c(COOH) = 0.58 µmol m^{-2}). See Table 43 for experimental details.*

The hybrid latexes were observed in cryo-TEM. As already mentioned for the 10 wt.% experiments (runs 15 and 16, Figure 151c and d), well-defined spherical particles covered with CeO_2 NPs were obtained. The latexes obtained in the 20 wt.% series were quite different (Figure 153). Stable hybrid latexes were obtained with sizes of D_n = 455 and 196 nm in diameter for 10 and 20 wt.% of CeO_2, respectively. However, as shown in Figure 153b and c, the particles size distributions were very broad. This can be explained by the fact that a higher amount of CeO_2 NPs can stabilize a greater number of polymer particles and thus extends the nucleation period.

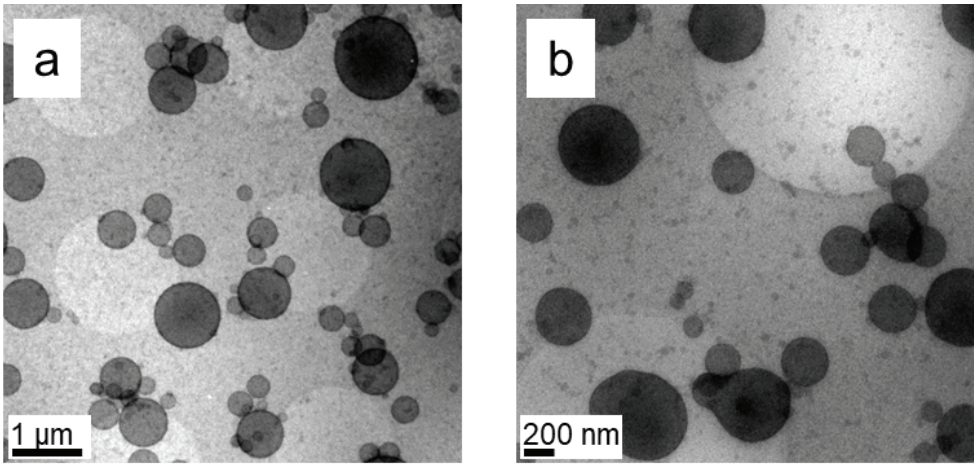

***Figure 153**. Cryo-TEM images of the CeO_2-armored P(n-BA-co-MMA) hybrid latexes for a solids content of 20 wt.%, c(COOH) = 0.58 µmol m^{-2} and for different CeO_2 contents: (a) 10 and (b) 20 wt.%.*

G. Proposed mechanism for the particle formation

Considering all our results, we propose a plausible mechanism for the formation of CeO_2-armored P(*n*-BA-*co*-MMA) latexes (Figure 154). Under visible light irradiation, some of the disulfide located at the CeO_2 NPs surface decomposes and generates two thiyl radicals. The one anchored onto the CeO_2 NPs surface initiates the polymerization from the NPs while the other initiates the polymerization in solution. In the former case, oligoradicals grow from the CeO_2 NPs surface on the surface until they reached a critical chain length and then precipitate, and/or the CeO_2 NPs containing oligomers at their surface adsorb on the polymer particles before precipitation. While the thiyl radical in solution adds to monomer units to form oligoradicals that continue to grow until reaching a critical length at which the oligoradicals are no longer soluble and precipitate. Then, the growing particles, partially stabilized by the CeO_2 NPs, should coagulate with each other and with CeO_2 modified with polymer chains until their surface is completely covered by the CeO_2 NPs. Once the mature particles are formed, the polymerization proceeds similarly to conventional dispersion polymerization.

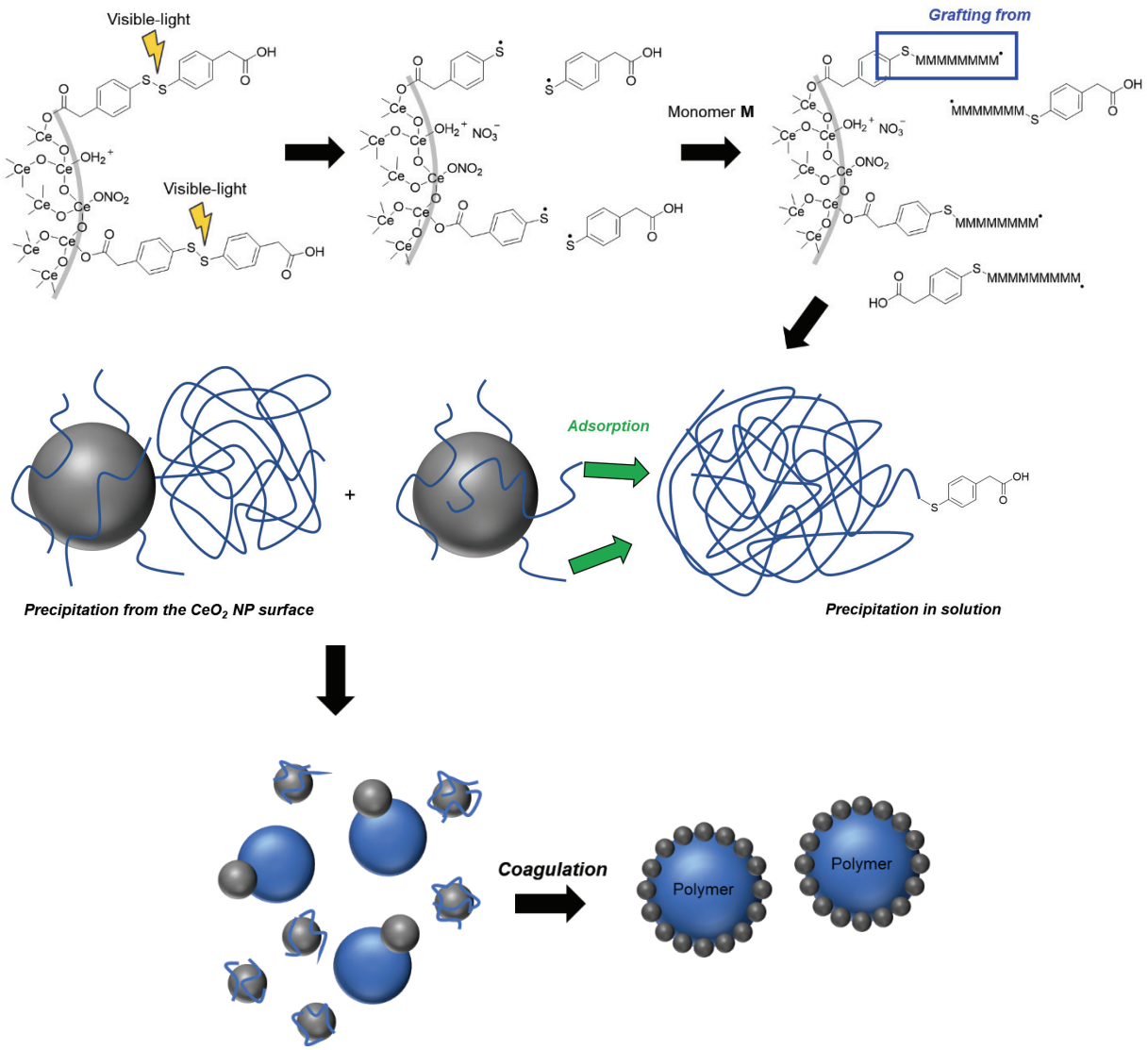

***Figure 154**. Schematic representation of the proposed mechanism for the formation of CeO_2-armored hybrid latexes via Pickering dispersion photopolymerization.*

This proposed mechanism was also based on the evolution of the photopolymerization with time observed by cryo-TEM (Figure 155) in the experimental conditions detailed in Table 41 (run 12). At the beginning of the reaction, we observe "deflated-like" objects as shown in Figure 155a and b (corresponding to conversion of 10 and 20% respectively), that could be due to the preparation of the sample. This was attributed to the large amount of residual monomer, which evaporated before the freezing step, resulting in a depression within the monomer swollen polymer particles. This "deflated-like" morphology was observed in Pickering emulsions when small amounts of oil were expelled from the droplet.[51,71] It should be noticed that free CeO_2 NPs were observed at 10% conversion and the free CeO_2 NPs gradually disappeared as the conversion increased. This showed that the CeO_2 NPs gradually adsorb to the surface of the

polymer particles as they grow. At 80% conversion, perfectly spherical CeO_2-armored polymer particles were observed.

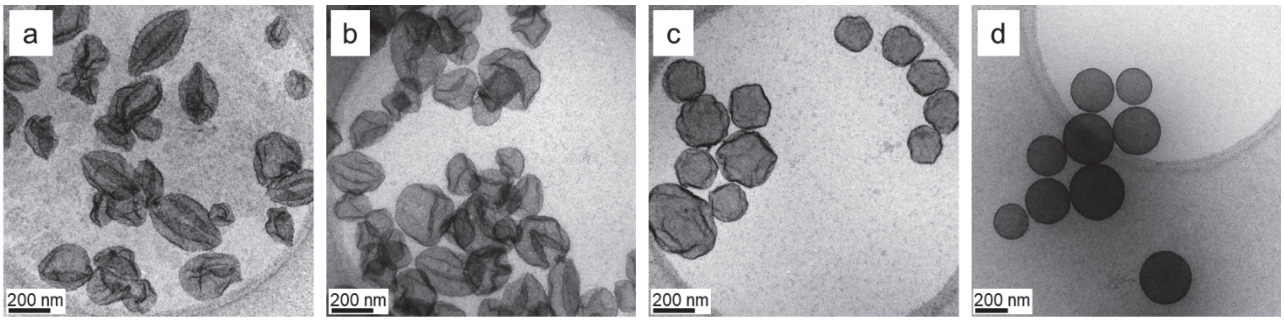

***Figure 155**. Evolution of the polymer particles in time at different conversions: (a) 10%, (b) 20%, (c) 40% and (d) 80% (run 12). The CeO_2 content was fixed at 25 wt.% and c(COOH) = 0.58 µmol m^{-2}, for a solids content of 10 wt.%.*

H. Disulfide vs. three-component photoinitiating system

Finally, we used our three-component photoinitiating system (acridine orange, disulfide, and NHC-borane) to prepare CeO_2-P(*n*-BA-*co*-MMA) hybrid particles. In that case, the NHC-boryl radicals are the initiating species and thus, the polymer should be formed mainly in solution and not at the CeO_2 NPs surface. The aim was to confirm the efficiency of the disulfide-modified CeO_2 NPs as Pickering stabilizer. The results are reported in Table 44.

***Table 44**. Effect of the three-component photoinitiating system on the preparation of CeO_2-P(n-BA-co-MMA) hybrid particles.[a]*

Run	Photoinitiating system	Time (h)	Conv. (%)	D_n[b] (nm)	D_w/D_n[b]	N_p (10^{14} cm^{-3})
15	Disulfide	6	100	405	1.06	2.7
20	AO/disulfide/NHC-BH_3	7.5	94	398	1.13	2.7

[a] Experimental conditions: reaction temperature fixed at 40 °C, methanol/water = 50/50 (wt.%). The solids content was fixed at 10. The CeO_2 content was fixed at 10 wt.% based on monomers and *c*(COOH) = 0.58 µmol m^{-2}).
[b] Determined by TEM.

In the presence of the full PIS, the polymerization rate was lower than with the disulfide alone. The final monomer conversion reached 94% after 7.5 h. Similar particle sizes were obtained in both cases, but the size dispersity was broader when the full system was used.

In addition, the cryo-TEM images in Figure 156 showed that the morphology of the hybrid particles was non-spherical. We also observed in Figure 156a, some polymer particles which were not covered by the CeO_2 NPs. We believe that the polymer chains grew from the NHC-

boryl radicals, resulting in a weak hydrophobization of the CeO_2 NPs. The use of the full PIS led to a different photoinitiation mechanism. Indeed, the AO photo-reduces the disulfide to generate one thiyl radical and one thiolate. This suggests that the disulfide anchored at the CeO_2 NPs should not add to monomer units. Therefore, the surface modification of the CeO_2 NPs by the disulfide only (without the formation of oligoradicals from its surface) is not enough to improve their interaction with the polymer particles. However, the formation of some spherical objects suggested that a small fraction of disulfide-modified CeO_2 NPs interacted with polymer but not enough to stabilize efficiently the particles.

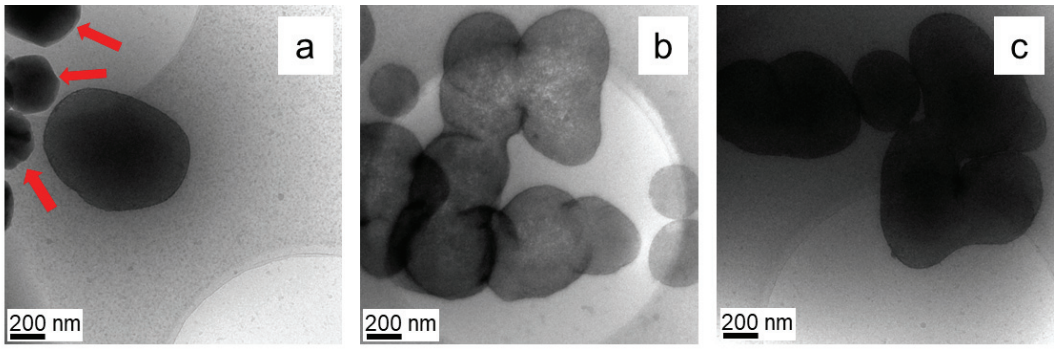

***Figure 156**. Cryo-TEM images of CeO_2-armored P(n-BA-co-MMA) latexes prepared with the three-component photoinitiating system via Pickering dispersion photopolymerization.*

Therefore, the use of disulfide alone led to highly stable hybrid latexes contrary to the full PIS, probably because the latter do not make the CeO_2 NPs hydrophobic enough *via* the growth of polymer chains anchored to their surface.

III. Characterization of CeO_2-armored P(*n*-BA-*co*-MMA) latex films

Finally, the CeO_2-armored hybrid latexes were cast into films and their mechanical and optical properties were investigated. Three films were formed from CeO_2-armored P(*n*-BA-*co*-MMA) hybrid latexes incorporating different CeO_2 contents (10, 20 and 25 wt.% based on monomer, see Table 42, runs 12, 15 and 16). All latexes containing CeO_2 NPs were film-forming and crack-free (Figure 157). The blank P(*n*-BA-*co*-MMA) was first prepared from the dissolution in THF of the CeO_2/P(*n*-BA-*co*-MMA) film. After centrifugation, the supernatant was collected to form a film without CeO_2 NPs (which precipitated). But the film was too sticky to be removed from the poly(tetrafluoroethylene) mold. We then decided to use the hybrid latex

prepared in the presence of PEGMA (at 10 wt.% based on monomers) as macromonomer stabilizer (see Table 38, run 2). In that case, the film was not sticky. The films containing CeO_2 NPs exhibited a uniform yellow tint, more or less pronounced depending on the CeO_2 content, whereas the film obtained from the blank latex was colorless.

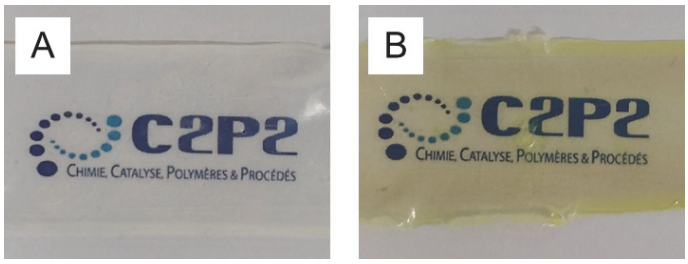

Figure 157*. Photographs of the two P(n-BA-co-MMA) latex coatings obtained after drying at room temperature during one week of the latexes prepared by Pickering dispersion photopolymerization of n-BA/MMA (60/40 in wt.%) containing (A) a macromonomer as stabilizer (PEGMA) and (B) CeO_2 NPs as Pickering stabilizer. See Table Table 38 and Table 42 for experimental details.*

A. Structural characterization

We first decided to characterize the structure of the films since their final properties are strongly dependent on the distribution of the CeO_2 NPs in the films.[64] For a copolymer composition *n*-BA/MMA of 60/40 in wt.%, the glass transition temperature (T_g) is expected to be –9.7 °C (according to the Fox equation). We measured a value of –5 °C by differential scanning calorimetry (DSC), in reasonable agreement with the theoretical value. Despite this low T_g, the films were formed without being sticky to the touch. The film cross-sections were characterized by cryo-TEM for the hybrid latexes synthesized with 10 and 25 wt.% of CeO_2 (Figure 158).

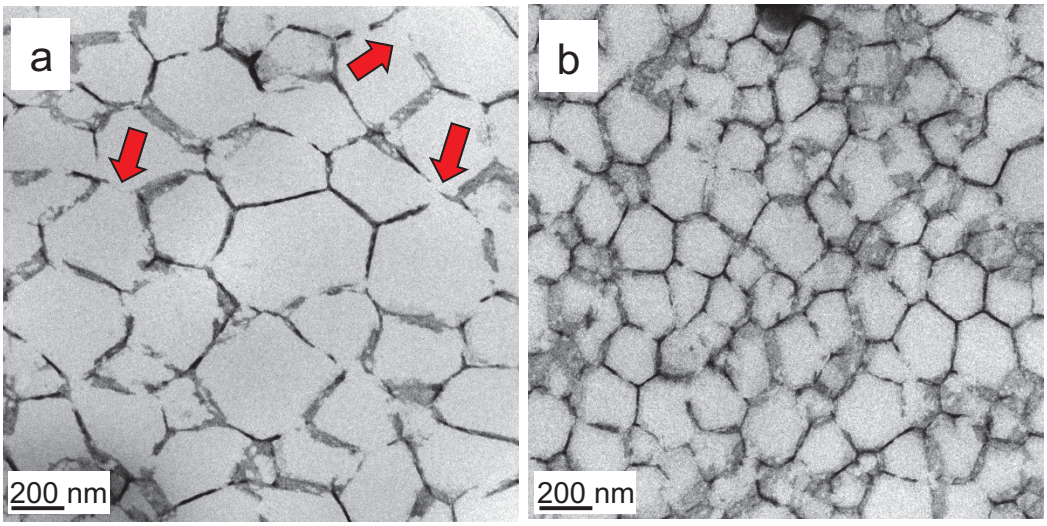

***Figure 158**. Cryo-TEM images of film cross-sections prepared from hybrid CeO_2/P(n-BA-co-MMA) latexes containing (a) 10 (run 15) and (b) 25 wt.% (run 12) of CeO_2 (based on monomers).*

In both cases, the CeO_2 NPs formed a honeycomb structure. According to Figure 158a and b, one might assume that the particle size distributions were broad but cryo-TEM analysis has proven that at least for the hybrid latex prepared with 10 wt.%, the particles exhibited a narrow size distribution with D_w/D_n = 1.03 (see Table 42, run 14). Martín-Fabiani *et al*.[64] suggested that the different sizes observed in the cryo-section were likely due to the cross-sectioning of the particles and not fully representative of the particle distribution. Moreover, for the film containing 10 wt.% of CeO_2 NPs, there are discontinuities in the CeO_2 NPs in the cellular wall (red arrows, Figure 158a), while it seems to be more continuous in the case where 25 wt.% of CeO_2 NPs were introduced (Figure 158b). Discontinuities in the cellular structure might be related to the lower CeO_2 content and the difference in disulfide available at the surface in both cases. The honeycomb structures with inorganic NPs in the cell walls were like those reported by González et al.[72] for Pickering particles with titanium dioxide NPs in the shells.

We next considered how these morphologies have an impact on the film properties.

B. Optical properties

We first investigated the optical properties of the hybrid films for applications as UV-absorbing coatings. Indeed, the CeO_2 NPs absorb intensively UV photons (in the 200–400 nm range). The oxidation state of cerium has a strong influence on the UV absorbance of CeO_2 NPs. It has been shown that a stronger UV absorption was obtained when Ce^{4+} was predominant compared to a combination of Ce^{3+} and Ce^{4+}.[73] At the same time, depending on the specifications, the coatings must be transparent in the visible region. It has also been reported that the reflectance and transmittance of the polymer films containing inorganic particles were influenced by the size of the latter component.[74,75]

Figure 159 clearly shows that the latex films resulting from the Pickering dispersion photopolymerization of *n*-BA/MMA in the presence of CeO_2 NPs completely absorb the UV photons, whereas the P(*n*-BA-*co*-MMA) latex film (in this case prepared from the dissolution in THF of the CeO_2/P(*n*-BA-*co*-MMA) film) only absorbed UV photons below 300 nm. In addition, in the range of visible light (from 450 to 800 nm), the films containing CeO_2 NPs exhibited a better transmittance by approximately 20%.

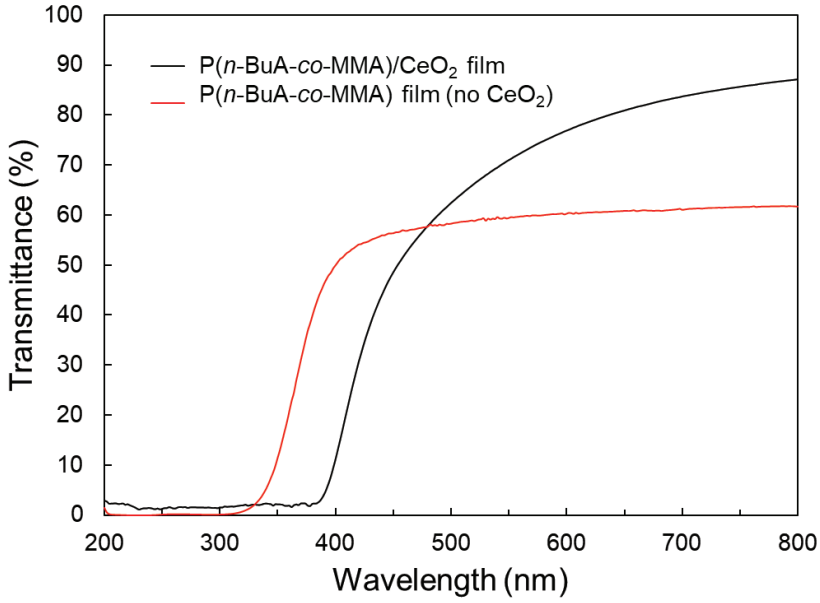

Figure 159. *Optical transmittance spectra of P(n-BA-co-MMA) films obtained from the hybrid latexes synthesized with CeO_2 NPs (dark) and prepared from the dissolution in THF of the CeO2/P(n-BA-co-MMA) film (red).*

C. Mechanical properties

Finally, we investigated the mechanical properties of our films by dynamic mechanical analysis (DMA) under a low strain. The storage modulus and loss factor (tan δ) measured for the films containing different CeO_2 contents as a function of the temperature are shown in Figure 160.

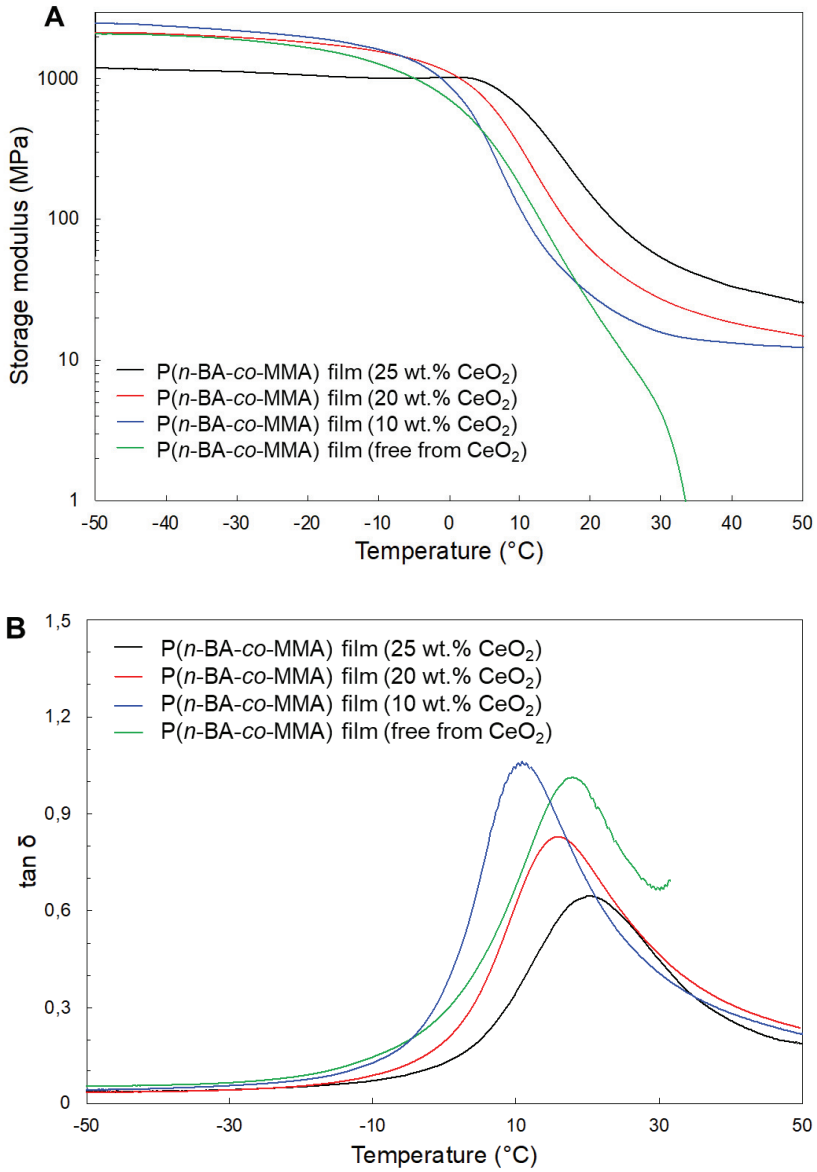

***Figure 160**. DMA curves as a function of the temperature for the different films investigated: (A) storage modulus and (B) loss tangent (tan δ).*

The storage modulus at the rubbery plateau increased with increasing the CeO_2 content in the films. Although the films containing CeO_2 NPs have similar microstructures as shown in Figure 158, at low CeO_2 content, the cryo-TEM images of the cross-sections showed discontinuities

in the CeO_2 NPs in the cellular wall which could explain the diminution of the storage modulus. It is important to notice that the presence of CeO_2 NPs in the films raised its storage modulus in the rubbery state. Indeed, at 30 °C, the storage modulus of the blank P(*n*-BA-*co*-MMA) was about 4 MPa whereas for a P(*n*-BA-*co*-MMA) latex film containing 25 wt.% of CeO_2, the storage modulus was about 30 MPa. Moreover, as the CeO_2 content decreased, the main relaxation temperature (T_α) was reduced. This can be attributed to the fact that the network of CeO_2 NPs in the cellular walls was large in comparison with higher CeO_2 content (final latex sizes of 405 nm *vs.* 218 nm).

General conclusion

In this chapter, we were able to make the most of our disulfide to both initiate dispersion photopolymerization and contribute to particle stabilization. Indeed, this molecule can adsorb onto the CeO_2 NPs surface *via* complexation of the cerium atoms by the carboxyl groups, thus allowing the NPS to act as solid stabilizer. The disulfide being able to photoinitiate emulsion polymerization of various (meth)acrylate monomers (Chapter 2), we therefore investigated the synthesis of CeO_2-armored P(*n*-BA-*co*-MMA) hybrid latexes by Pickering dispersion photopolymerization under visible light irradiation. This technique does not require the use of any polymeric stabilizer. A very few studies reported the use of inorganic NPs modified by an initiator. In addition, it is possible to combine both properties of polymer and inorganic nanoparticles.

The experiments were all performed in a hydroalcoholic medium composed of methanol and water (50/50 in wt.%), in which the CeO_2 sol was stable. The addition of increasing amounts of the disulfide, previously dissolved in methanol, to the CeO_2 sol first allowed us determining an optimum disulfide concentration to maintain the CeO_2 sol stable, corresponding 0.58 µmol of COOH functions m^{-2}. The presence of disulfide at the CeO_2 NPs was confirmed by FTIR spectroscopy. This suggests that the disulfide has almost no affinity for the CeO_2 NPs surface and the adsorption may be favored by the subsequent adsorption of other molecules. What we know for sure is that the FTIR confirmed the presence of "free" carboxyl group. We were not able to confirm the adsorption of the disulfide involving the two carboxyl groups. However, it seems to be hardly feasible because of the steric effects. What is possible is that after the disulfide decomposition, the thiyl radical which migrates in the continuous phase adds to monomer units and then could adsorb on the CeO_2 NPs due to the poor solubility of the oligomer generated (if available cerium atoms).

Highly stable CeO_2-armored P(*n*-BA-*co*-MMA) hybrid latexes were then successfully obtained (*n*-BA/MMA: 60/40 in wt.%) at 10 wt.% solids content and in a CeO_2 content range from 10 to 25 wt.% (based on monomers). The particles sizes were in the 200 – 400 nm range and relatively narrow size distributions were obtained. The disulfide concentration as well as the monomer content proved to be decisive. we observed the absence of free CeO_2 NPs in the final hybrid latex. The hybrid particles exhibited a spherical morphology with a stark contrast of their edge, which corresponds to the CeO_2 NPs. To our knowledge, this is the first example of Pickering dispersion photopolymerization reported in the literature. The Pickering initiation system was

very minimalistic since it only involved a single compound, the disulfide, which acted as both photoinitiator and anchoring agent. According to our results and the evolution of the particles during the photopolymerization observed by cryo-TEM, we proposed a mechanism of particle formation. Some other techniques could be exploited to validate our assumptions such as solid NMR or X-ray photoelectron spectrometry.

Finally, we formed films from our hybrid latexes and from a CeO_2-free latex used as a reference to evaluate the value added by the CeO_2 NPs to various properties. Our films exhibit excellent anti-UV properties while retaining high light transmission in the visible range. Moreover, the CeO_2 NPs formed a honeycomb structure, wherein every polymer particle was surrounded by CeO_2 NPs. This structure positively influenced the mechanical properties of the films.

References

[1] A. Doménech, M. T. Doménech-Carbó, M. S. del Río, M. L. V. de A. Pascual, E. Lima, *New J. Chem.* **2009**, *33*, 2371–2379.
[2] C. Sanchez, B. Julián, P. Belleville, M. Popall, *J. Mater. Chem.* **2005**, *15*, 3559–3592.
[3] C. Sanchez, C. Boissiere, S. Cassaignon, C. Chaneac, O. Durupthy, M. Faustini, D. Grosso, C. Laberty-Robert, L. Nicole, D. Portehault, F. Ribot, L. Rozes, C. Sassoye, *Chem. Mater.* **2014**, *26*, 221–238.
[4] M. A. Hood, M. Mari, R. Muñoz-Espí, *Materials* **2014**, *7*, 4057–4087.
[5] M. R. Bockstaller, R. A. Mickiewicz, E. L. Thomas, *Adv. Mater.* **2005**, *17*, 1331–1349.
[6] W. Ramsden, F. Gotch, *Proc. R. Soc. Lond.* **1904**, *72*, 156–164.
[7] S. U. Pickering, *J. Chem. Soc. Trans.* **1907**, *91*, 2001–2021.
[8] B. P. Binks, *Interface Sci.* **2002**, 21.
[9] R. Aveyard, B. P. Binks, J. H. Clint, *Adv. Colloid Interface Sci.* **2003**, *100–102*, 503–546.
[10] Y. Chevalier, M.-A. Bolzinger, *Colloids Surf. Physicochem. Eng. Asp.* **2013**, *439*, 23–34.
[11] C. Albert, M. Beladjine, N. Tsapis, E. Fattal, F. Agnely, N. Huang, *J. Controlled Release* **2019**, *309*, 302–332.
[12] W. C. Griffin, *J Soc Cosmet Chem* **1949**, *1*, 311–326.
[13] Q. Y. Xu, M. Nakajima, B. P. Binks, *Colloids Surf. Physicochem. Eng. Asp.* **2005**, *262*, 94–100.
[14] Y. Zhu, J. Sun, C. Yi, W. Wei, X. Liu, *Soft Matter* **2016**, *12*, 7577–7584.
[15] J. Chen, R. Vogel, S. Werner, G. Heinrich, D. Clausse, V. Dutschk, *Colloids Surf. Physicochem. Eng. Asp.* **2011**, *382*, 238–245.
[16] B. P. Binks, P. D. I. Fletcher, B. L. Holt, P. Beaussoubre, K. Wong, *Phys. Chem. Chem. Phys.* **2010**, *12*, 11954–11966.
[17] S. Levine, B. D. Bowen, S. J. Partridge, *Colloids Surf.* **1989**, *38*, 325–343.
[18] B. P. Binks, T. S. Horozov, *Colloidal Particles at Liquid Interfaces*, Cambridge University Press, **2006**.
[19] B. P. Binks, M. Kirkland, *Phys. Chem. Chem. Phys.* **2002**, *4*, 3727–3733.
[20] O. Rohm, E. Trommsdorff, *Process for the Polymerization of Methyl Methacrylate*, **1939**, US2171765A.
[21] S. Fortuna, C. A. L. Colard, A. Troisi, S. A. F. Bon, *Langmuir* **2009**, *25*, 12399–12403.
[22] S. A. F. Bon, P. J. Colver, *Langmuir* **2007**, *23*, 8316–8322.
[23] S. Cauvin, P. J. Colver, S. A. F. Bon, *Macromolecules* **2005**, *38*, 7887–7889.
[24] L. A. Fielding, J. Tonnar, S. P. Armes, *Langmuir* **2011**, *27*, 11129–11144.
[25] P. J. Colver, C. A. L. Colard, S. A. F. Bon, *J. Am. Chem. Soc.* **2008**, *130*, 16850–16851.
[26] R. F. A. Teixeira, H. S. McKenzie, A. A. Boyd, S. A. F. Bon, *Macromolecules* **2011**, *44*, 7415–7422.
[27] C. A. L. Colard, R. F. A. Teixeira, S. A. F. Bon, *Langmuir* **2010**, *26*, 7915–7921.
[28] N. Sheibat-Othman, E. Bourgeat-Lami, *Langmuir* **2009**, *25*, 10121–10133.
[29] S. C. Thickett, P. B. Zetterlund, *ACS Macro Lett.* **2013**, *2*, 630–634.
[30] B. Brunier, N. Sheibat-Othman, Y. Chevalier, E. Bourgeat-Lami, *Langmuir* **2016**, *32*, 112–124.
[31] A. Schrade, K. Landfester, U. Ziener, *Chem. Soc. Rev.* **2013**, *42*, 6823–6839.
[32] E. Bourgeat-Lami, in *Hybrid Mater. Synth. Charact. Appl.*, **n.d.**
[33] E. Bourgeat-Lami, M. Lansalot, in *Hybrid Latex Part. Prep. Miniemulsion Polym.* (Eds.: A.M. van Herk, K. Landfester), Springer, Berlin, Heidelberg, **2010**, pp. 53–123.

[34] S. A. F. Bon, in *Encycl. Polym. Nanomater.* (Eds.: S. Kobayashi, K. Müllen), Springer, Berlin, Heidelberg, **2014**, pp. 1–6.
[35] J. Hu, M. Chen, L. Wu, *Polym. Chem.* **2011**, *2*, 760–772.
[36] M. Gill, J. Mykytiuk, S. P. Armes, J. L. Edwards, T. Yeates, P. J. Moreland, C. Mollett, *J. Chem. Soc. Chem. Commun.* **1992**, 108–109.
[37] M. Gill, S. P. Armes, D. Fairhurst, S. N. Emmett, G. Idzorek, T. Pigott, *Langmuir* **1992**, *8*, 2178–2182.
[38] J. Stejskal, P. Kratochvíl, S. P. Armes, S. F. Lascelles, A. Riede, M. Helmstedt, J. Prokeš, I. Křivka, *Macromolecules* **1996**, *29*, 6814–6819.
[39] M. J. Percy, V. Michailidou, S. P. Armes, C. Perruchot, J. F. Watts, S. J. Greaves, *Langmuir* **2003**, *19*, 2072–2079.
[40] C. Barthet, A. J. Hickey, D. B. Cairns, S. P. Armes, *Adv. Mater.* **1999**, *11*, 408–410.
[41] M. J. Percy, J. I. Amalvy, D. P. Randall, S. P. Armes, S. J. Greaves, J. F. Watts, *Langmuir* **2004**, *20*, 2184–2190.
[42] N. Greesh, P. C. Hartmann, R. D. Sanderson, *Macromol. Mater. Eng.* **2009**, *294*, 787–794.
[43] N. Greesh, R. Sanderson, P. C. Hartmann, *Polymer* **2012**, *53*, 708–718.
[44] J. Yang, T. Hasell, W. Wang, J. Li, P. D. Brown, M. Poliakoff, E. Lester, S. M. Howdle, *J. Mater. Chem.* **2008**, *18*, 998–1001.
[45] M. Flytzani-Stephanopoulos, T. Zhu, Y. Li, *Catal. Today* **2000**, *62*, 145–158.
[46] K. Ouzaouit, Matériaux bi-fonctionnels pour applications catalytiques et piézoélectriques, à base d'oxydes de cérium, de lanthane et de langasite, phdthesis, Université du Sud Toulon Var, **2007**.
[47] P. Patsalas, S. Logothetidis, C. Metaxa, *Appl. Phys. Lett.* **2002**, *81*, 466–468.
[48] R. D. Robinson, J. E. Spanier, F. Zhang, S.-W. Chan, I. P. Herman, *J. Appl. Phys.* **2002**, *92*, 1936–1941.
[49] L. Truffault, Synthèse et caractérisation de nanoparticules à base d'oxydes de cérium et de fer pour la filtration des UV dans les produits solaires, phdthesis, Université d'Orléans, **2010**.
[50] V. Shah, S. Shah, H. Shah, F. J. Rispoli, K. T. McDonnell, S. Workeneh, A. Karakoti, A. Kumar, S. Seal, *PLOS ONE* **2012**, *7*, e47827.
[51] N. Zgheib, J.-L. Putaux, A. Thill, F. D'Agosto, M. Lansalot, E. Bourgeat-Lami, *Langmuir* **2012**, *28*, 6163–6174.
[52] N. Zgheib, Élaboration de Particules de Latex Composites à Base d'oxyde de Cérium Par Polymérisation Radicalaire En Milieu Aqueux Dispersé, These de doctorat, Lyon 1, **2011**.
[53] D. Subervie, NHC-Boranes : amorceurs de photopolymérisation en émulsion et nouveaux matériaux énergétiques, phdthesis, Université de Lyon, **2018**.
[54] J.-Y. Chane-Ching, *Sol-Forming Cerium Material*, **1992**, US5145605 (A).
[55] J.-Y. Chane-Ching, *Preparing a Dispersible, Sol-Forming Cerium (IV) Composition*, **1994**, US5308548 (A).
[56] A. Sehgal, Y. Lalatonne, J.-F. Berret, M. Morvan, *Langmuir* **2005**, *21*, 9359–9364.
[57] E. A. Kümmerle, G. Heger, *J. Solid State Chem.* **1999**, *147*, 485–500.
[58] D. R. Mullins, *Surf. Sci. Rep.* **2015**, *70*, 42–85.
[59] X. Zhang, X. Bi, W. Di, W. Qin, *Sens. Actuators B Chem.* **2016**, *231*, 714–722.
[60] R. Zamiri, H. Abbastabar Ahangar, A. Kaushal, A. Zakaria, G. Zamiri, D. Tobaldi, J. M. F. Ferreira, *PLoS ONE* **2015**, *10*, DOI 10.1371/journal.pone.0122989.
[61] M. Buback, A. Feldermann, C. Barner-Kowollik, I. Lacík, *Macromolecules* **2001**, *34*, 5439–5448.

[62] S. Babu, A. Velez, K. Wozniak, J. Szydlowska, S. Seal, *Chem. Phys. Lett.* **2007**, *442*, 405–408.
[63] Y. Xue, Q. Luan, D. Yang, X. Yao, K. Zhou, *J. Phys. Chem. C* **2011**, *115*, 4433–4438.
[64] I. Martín-Fabiani, M. L. Koh, F. Dalmas, K. L. Elidottir, S. J. Hinder, I. Jurewicz, M. Lansalot, E. Bourgeat-Lami, J. L. Keddie, *ACS Appl. Nano Mater.* **2018**, *1*, 3956–3968.
[65] A. Y. C. Koh, S. Mange, M. Bothe, R. J. Leyrer, R. G. Gilbert, *Polymer* **2006**, *47*, 1159–1165.
[66] P. S. Albright, L. J. Gosting, *J. Am. Chem. Soc.* **1946**, *68*, 1061–1063.
[67] Jeffries. Wyman, *J. Am. Chem. Soc.* **1931**, *53*, 3292–3301.
[68] D. Wang, V. L. Dimonie, E. D. Sudol, M. S. El-Aasser, *J. Appl. Polym. Sci.* **2002**, *84*, 2692–2709.
[69] S. Jiang, E. D. Sudol, V. L. Dimonie, M. S. El-Aasser, *J. Polym. Sci. Part Polym. Chem.* **2007**, *45*, 2105–2112.
[70] S. Jiang, E. D. Sudol, V. L. Dimonie, M. S. El-Aasser, *J. Polym. Sci. Part Polym. Chem.* **2008**, *46*, 3638–3647.
[71] S. S. Datta, H. C. Shum, D. A. Weitz, *Langmuir* **2010**, *26*, 18612–18616.
[72] E. González, A. Bonnefond, M. Barrado, A. M. Casado Barrasa, J. M. Asua, J. R. Leiza, *Chem. Eng. J.* **2015**, *281*, 209–217.
[73] S. V. N. T. Kuchibhatla, A. S. Karakoti, D. R. Baer, S. Samudrala, M. H. Engelhard, J. E. Amonette, S. Thevuthasan, S. Seal, *J. Phys. Chem. C* **2012**, *116*, 14108–14114.
[74] J. Sun, B. V. Velamakanni, W. W. Gerberich, L. F. Francis, *J. Colloid Interface Sci.* **2004**, *280*, 387–399.
[75] A. Tzitzinou, J. L. Keddie, J. M. Geurts, A. C. I. A. Peters, R. Satguru, *Macromolecules* **2000**, *33*, 2695–2708.

Chapter 5.

Experimental part

Table of Content

I. MATERIALS AND METHODS 269

II. OPERATING PROCEDURES 274

A. SYNTHESES OF PHOTOINITIATING SYSTEM 274
*1. Synthesis of disulfide (**4**) 274*
2. Synthesis of NHC-BH_3 275
B. PREPARATION OF SYNTHETIC LATEXES BY EMULSION PHOTOPOLYMERIZATION 281
C. PREPARATION OF SYNTHETIC LATEXES BY DISPERSION PHOTOPOLYMERIZATION 282
D. PREPARATION OF HYBRID LATEXES BY PICKERING DISPERSION PHOTOPOLYMERIZATION 282
1. Modification of the CeO2 nanoparticles surface by disulfide 282
2. Pickering dispersion polymerization of n-BA/MMA 283
3. Film formation 283

In this chapter, we will present the comprehensive list of materials and analytical methods used for the different parts of the work, *i.e.*, the preparation of the organic compounds, the synthesis of the polymer latexes by emulsion and dispersion (photo)polymerization and the synthesis of hybrid latexes by Pickering dispersion photopolymerization.

I. Materials and methods

The reagents and the solvents were purchased from Sigma Aldrich, Alfa Aesar and TCI, and used without any further purification. The LED ribbon used was purchased from LED's Go (Ruban LED blanches – très haute puissance – 24 V – 24 W m^{-1} – 3500 lum m^{-1} – 182 LED m^{-1} – Ref. RUB_THP_NW_BN and Ruban MED couleur (RGB) – haute puissance – 24 V – 20 w m^{-1} – 1300 lum m^{-1} – 84 LED m^{-1} – Ref. RUB_RGB_HP_NW).

Nuclear magnetic resonance (NMR) spectra (^{1}H, ^{13}C, ^{11}B) were recorded on a Bruker AC 300 spectrometer operating at 300 MHz equipped with a BBFO+ probe for 5 mm NMR tube. All chemical shifts were measured relative to residual ^{1}H or ^{13}C resonance in the deuterated solvent: DMSO-d_6, δ 2.5 ppm for ^{1}H and 39.52 ppm for ^{13}C, D_2O, δ 4.79 ppm for ^{1}H. ^{11}B NMR spectra were calibrated using BF_3 Et_2O (0.0 ppm) as external reference.

NMR measurements were mainly performed for the organic compounds synthesized in Chapter 2.

UV-Vis spectrophotometry was performed on Cary 100 UV-visible spectrophotometer from Agilent Technologies (from 180 to 900 nm). It is controlled by the Cary WinUV software. The measurements were carried out with quartz cells with an optical path of 10 mm (model 100-QS from the Hellma brand).

Chapters 2 and 4 contain information from UV-Vis analysis. To calculate the partition coefficients of the AO (**1**) and NHC-BH_3 (**3**), the UV spectrophotometry technique was used to determine the concentration of these compounds in the monomer phase (styrene and MMA). The absorbances of the monomer solutions containing these compounds at a precise concentration were first measured. The calibration curves were obtained by plotting the absorbance as a function of the concentration of these species for solution of know concentration.

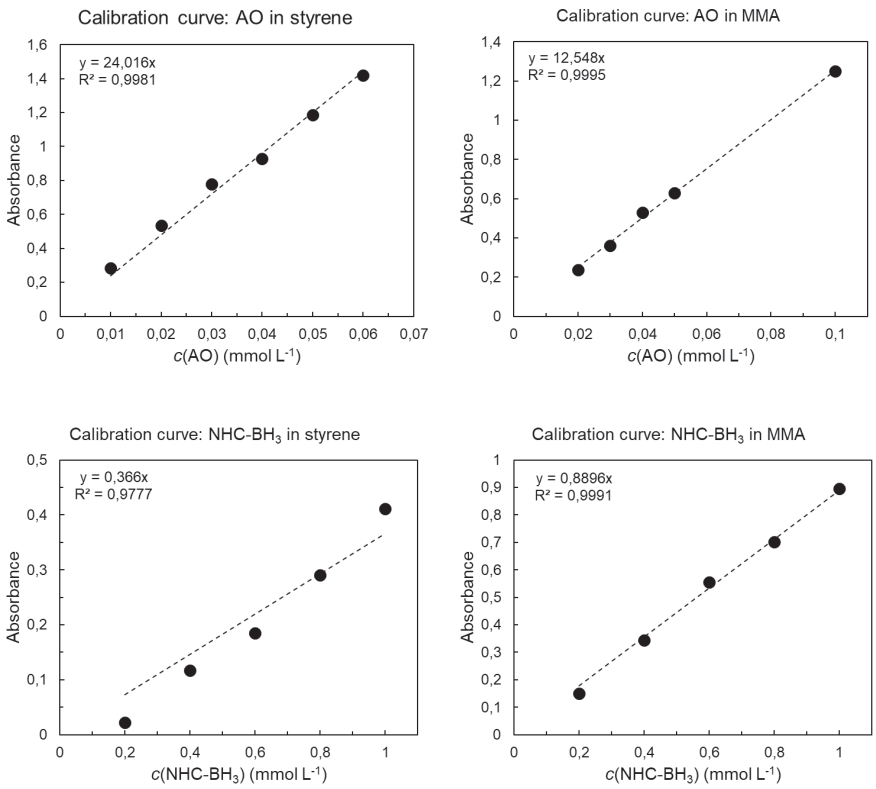

***Figure 161**. Calibration curves of the AO (**1**) and NHC-BH₃ (**3**) determined by UV spectrophotometry in styrene and MMA.*

Fourier-transform infrared spectroscopy (FTIR) measurements were performed at room temperature on a Nicolet i550 FT-IR apparatus. KBr pallets were used to record FTIR spectra. Each spectrum was the result of 16 scans from 4 000 to 400 cm^{-1} at the speed of 0.20 cm s^{-1}.

Measurements were performed on modified CeO_2 NPs to investigate the disulfide adsorption (Chapter 4).

Elemental analyses were performed at the Mikroanalytisches Laboratorium Kolbe (Oberhausen, Germany). The S atom content was measured by ion chromatography with 883 Basic IC Plus from Metrohm®.

Elemental analyses were performed to quantify the amount of disulfide adsorbed onto the CeO_2 NPs (Chapter 4), according to the following formula:

$$[disulfide]_{adsorbed}\ (\mu mol\ m^{-2}) = \frac{\Delta Z \times 10^6}{(n \times M_Z - \Delta Z \times M) \times S_{spec.}} \quad (Eq.5.1)$$

with ΔZ = %Z after adsorption – %Z before adsorption (weight content of the atomic element Z considered), S_{spec} the specific surface of the CeO_2 NPs, n the number of atoms of the element

Z containing in the disulfide compound, M the molar mass of disulfide and M_Z the molar mass of the atomic element Z.

Electrospray ionization mass spectrometry (ESI) was performed at the "Centre Commun de Spectrométrie de Masse de l'Université de Lyon 1" (UMR 5086). The measurements were carried out on a Burker MicrOTOF QII apparatus.

The compounds synthesized in Chapter 2 were analyzed by ESI mass spectrometry.

Dynamic light scattering (DLS) analyses were performed on a Zetasizer Nano ZS device from Malvern Instruments. DLS was used to measure the average hydrodynamic particle diameter (D_h) and the dispersity of the samples, given by the polydispersity index (PDI). To avoid multiple scattering effects, the sample was sufficiently diluted with ultrapure water or an ultrapure hydroalcoholic solution and introduced in a PS cuvette. The sample was then subjected to LASER irradiation (λ = 633 nm, He-Ne 5 mW). A detector installed at 173° from the light source collected the intensity of the light scattered by the particles. The intensity variation was due to the oscillation of the particles around an equilibrium point caused by Brownian motion. Thus, the speed of this movement depended on the scattering coefficient *D*. From this coefficient, it was possible to calculate the particles diameter by the Stokes-Einstein equation:

$$D_h = \frac{k_B T}{3\pi\eta D} \quad (Eq. 5.2)$$

with D_h the average hydrodynamic particle diameter (nm), k_B the Boltzmann constant (J K^{-1}), T the temperature (K), η the viscosity of the medium (Pa s) and *D* the scattering coefficient (m^2s^{-1}).

DLS analyses were conducted on (modified) CeO_2 NPs (Chapter 4) and for various polymer (hybrid) latexes (Chapters 2, 3 and 4).

Transmission electron microscopy (TEM) was performed at the Centre Technologique des Microstructures, platform of the Université Claude Bernard, Lyon 1. The polymer particles were imaged by TEM. A drop of the diluted latex was deposited on a carbon/Formvar®-coated copper grid, and the water was allowed to evaporate. The analysis was carried out at room

temperature with a Philips CM120 microscope operating at an accelerating voltage of 80 or 120 kV and equipped with GATAN Orius220 camera (2048x2048 pixels). The images were then analyzed by using the ImageJ software. Between 300 and 500 particle diameters were measured and the number and weight average particle diameters ($D_n = \frac{\sum n_i D_i}{\sum n_i}$ and $D_w = \frac{\sum n_i D_i^4}{\sum n_i D_i^3}$, where n_i is the number of particles with diameter D_i) and the diameter dispersity (D_w/D_n) were calculated using the following equations. A minimum of 200 particles was counted for each batch.

Chapters 2, 3 and 4 are concerned by TEM.

Cryogenic TEM (Cryo-TEM) for PMMA and P(*n*-BA-*co*-MMA) latexes was also was performed at the Centre Technologique des Microstructures, platform of the Université Claude Bernard, Lyon 1. The synthetic latexes observed by cryo-TEM were diluted in deionized water or hydroalcoholic solution until a concentration of between 1 and 3 wt.% was reached after deposition on a copper grid covered with a carbon film with holes and dipped in ethane liquid to trap particles in a film of ice. The grid is prepared on a GATAN 626 cryo-sample holder for insertion into the Philips CM120. Observations were realized at an accelerating voltage of 120 kV. The images were processed in the same way as in TEM.

Chapters 2 and 4 are concerned by TEM.

Gravimetric analyses provided the overall mass conversion of a polymerization reaction. It was used to follow the conversion as a function of time for the emulsion and dispersion polymerizations. The principle was based on the volatility of the water and the monomer(s) involved, unlike the solid polymer obtained. The sample of the reaction medium was weighed precisely in an aluminum pan. The volatile compounds were first pre-evaporated in a fume hood at room temperature and then the sample was dried in an oven at 100 °C. Weighing the mass of the dry polymer provided the conversion according to the following equation:

$$Conversion = \frac{m_0 - m_t}{m_0} = \frac{m_{polymer}}{m_0} = \frac{\frac{m_{dry}}{m_{aliquat}} - \tau_{NV}}{\tau_{solid}} \quad (Eq.\,5.3)$$

with m_0 the initial mass of monomer (g), m_t the reacted mass of monomer at time t (g), m_{dry} the mass of dry aliquot (g), $m_{aliquot}$ the mass of aliquot (g), τ_{NV} the non-volatile content apart polymer (*i.e.*, initiating system and surfactant) and τ_{solid} the theoretical solids content at 100% conversion (initial mass of monomer/overall system mass).

Chapters 2, 3 and 4 are concerned by gravimetric analyses.

Size exclusion chromatography (SEC) analyses were performed on a Viscotek GPCmax instrument from Malvern Instruments. It was used for evaluating the molar masses and molar mass distributions of dried polymers. The system is equipped with an online Triple Detector Array including a right and low angle light scattering detector (RALS and LALS), a four-capillary differential viscometer, and a differential refractive index detector (RI). THF was used as an eluent at a constant rate flow of 1 mL min^{-1}. The measurement was carried out at 35 °C. All polymers were prepared at a concentration of 5 mg mL^{-1}. They were filtrated through a 0.22 µm PTFE filter. The sample injection was set at 100 µL. The separation was carried out on three serial columns (PLgel Olexis, 300 x 7.5 mm) and a guard column (PLgel Olexis Guard, 300 x 7.5 mm). The OmniSEC software was used for data acquisition and data analysis. The average molar masses (number-average molar mass, M_n, and weight-average molar mass, M_w) and the molar mass dispersity, $Đ = M_w/M_n$, were calculated from the RI signal using conventional calibration with PS and PMMA standards.

Polymers synthesized in both Chapter 3 and 4 were analyzed by SEC-THF.

Differential scanning calorimeter (DSC) analyses were performed on a Mettler DSC 2 StarSyst apparatus. After initial equilibration at a low temperature (-50 °C), heating/cooling cycles between 200 and -50 °C were run at 10 °C min^{-1}. 40 µL aluminum crucibles containing between 5 and 20 mg of polymers was used.

The glass transition temperature (T_g) of P(*n*-BA-*co*-MMA) polymers from Chapter 4 was determined by DSC.

Dynamic mechanical analysis (DMA) was performed on DMA Q800 from TA Instruments at MATEIS laboratory, INSA Lyon. P(*n*-BA-*co*-MMA) latexes, with and without CeO_2 NPs, synthesized in Chapter 4, were cast in PTFE molds and allowed to dry under ambient conditions for 7 days. Then they were cut into strips with dimensions determined with a digital sliding caliper. Experiments were performed in the tensile mode at a frequency of 1 Hz with 0.01% strain. The temperature was ramped from -50 to 100 °C at 3 °C min^{-1}.

The storage modulus (*E'*) and the relaxation temperature ($T_α$) of P(*n*-BA-*co*-MMA) polymers from Chapter 4 was determined by DMA.

II. Operating procedures

Unless otherwise stated, all organic syntheses were conducted under inter atmosphere (argon) using standard techniques for manipulating air-sensitive compounds. All glassware was stored in an oven or was flame-dried prior to establishing an argon atmosphere. Yields refer to spectroscopically pure compounds (if possible). The polymeric syntheses were carried out under inter atmosphere (nitrogen) in a 250 mL double walled cylindrical glass reactor surrounding by a LED ribbon.

A. Syntheses of photoinitiating systems

1. Synthesis of disulfide (**4**)

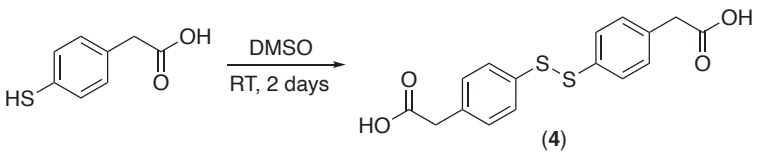

(**4**)

4-mercaptobenzylacetic acid (1.1 g) was introduced in a two-neck flask connected to a bleach trap, closed with a septum and flushed with argon. DMSO (3.5 g) was added and the reaction mixture was stirred under argon for 2 days. Excess solvents and byproducts (SMe_2 and H_2O) were removed under reduced pressure giving a yellow oil. Dichloromethane (DCM, 10 mL) was then added together with water (20 mL), and the obtained dispersion stirred vigorously. The product was precipitated, and then isolated by filtration, washed with water (2x10 mL) and dried at 70 °C to afford (**4**). Yield 85%. ^{1}H NMR (300 MHz, DMSO-d_6): δ = 7.46 (d, 4H), 7.26 (d, 4H), 3.55 (s, 4H) ppm. ^{13}C NMR (75.4 MHz, DMSO-d_6): δ = 172.9, 135.2, 134.4, 131.0, 127.9 ppm. HRMS calc. 334.0327 m/z found $[M + Na]^+$ 357.0225.

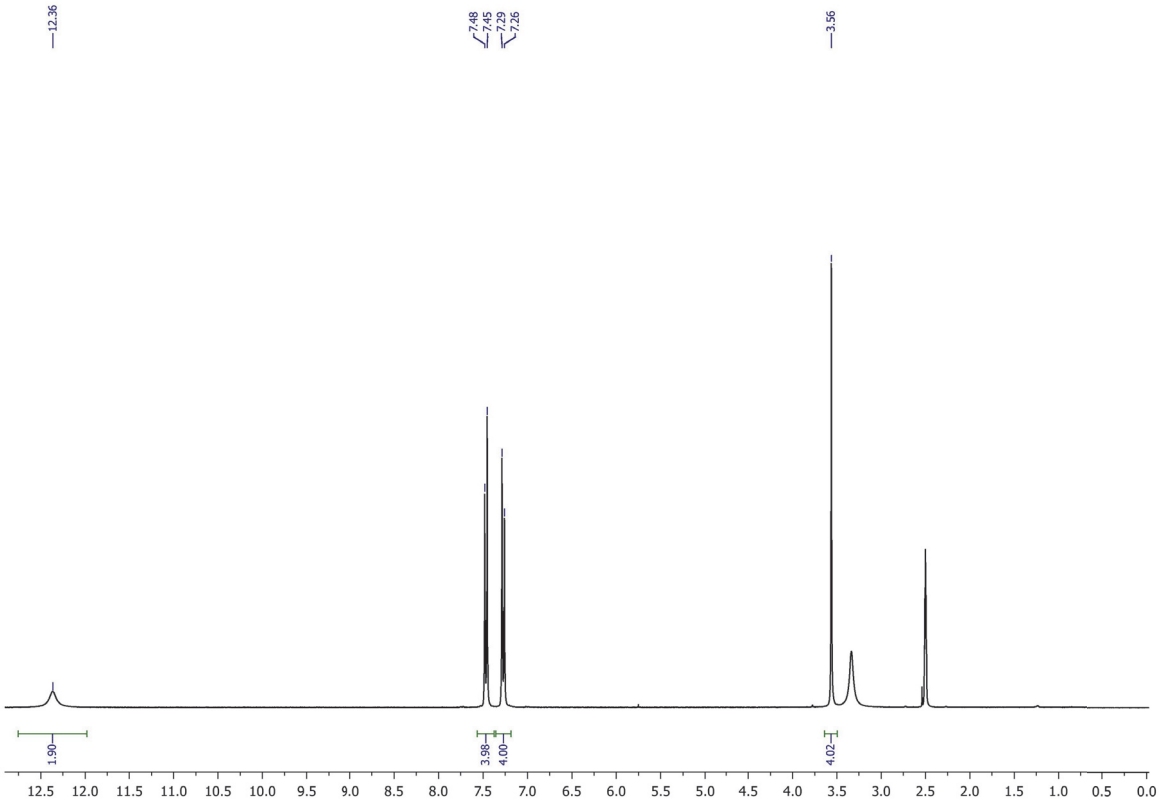

Figure 162. *^{1}H NMR spectrum of compound (4) in DMSO-d_6.*

2. Synthesis of NHC-BH_3

- Synthesis of 2,4-dimethyl-1,2,4-triazol-3-ylideneborane (**3**):

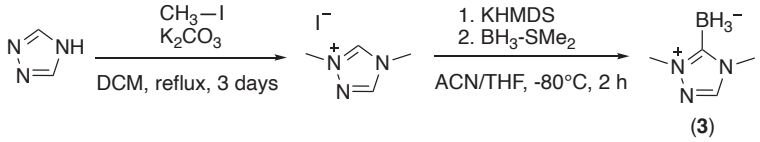

(**3**)

The synthesis of compound (**3**) has been slightly modified compared to the literature.[1] A solution of potassium hexamethyldisilazide (KMHDS, 1 mol L^{-1} in THF, 105 mL, 105 mmol) was first added to a solution containing 1,2,4-triazolium salt (21 g, 93 mmol) in THF (75 mL) and acetonitrile (ACN) (75 mL) at – 80 °C. Then, a solution of BH_3-SMe_2 (27 mL, 284 mmol) was added dropwise to the previous mixture. The reaction was stirred at –80 °C for 1 h. Then, the reaction medium was removed from the cooling batch and left at room temperature for 1 h. The solvent was evaporated under vacuum and the crude product was purified with silica gel column chromatography. The pure compound (**3**) was obtained as a white solid. Yield: 75%.

^{1}H NMR (300 MHz, DMSO-d_6): δ = 6.66 (s, 1H), 3.82 (s, 3H), 3.62 (s, 3H), 0.89 (q, 3H) ppm.

^{11}B NMR (96.3 MHz, $CDCl_3$): δ = -36.43 (q) ppm.

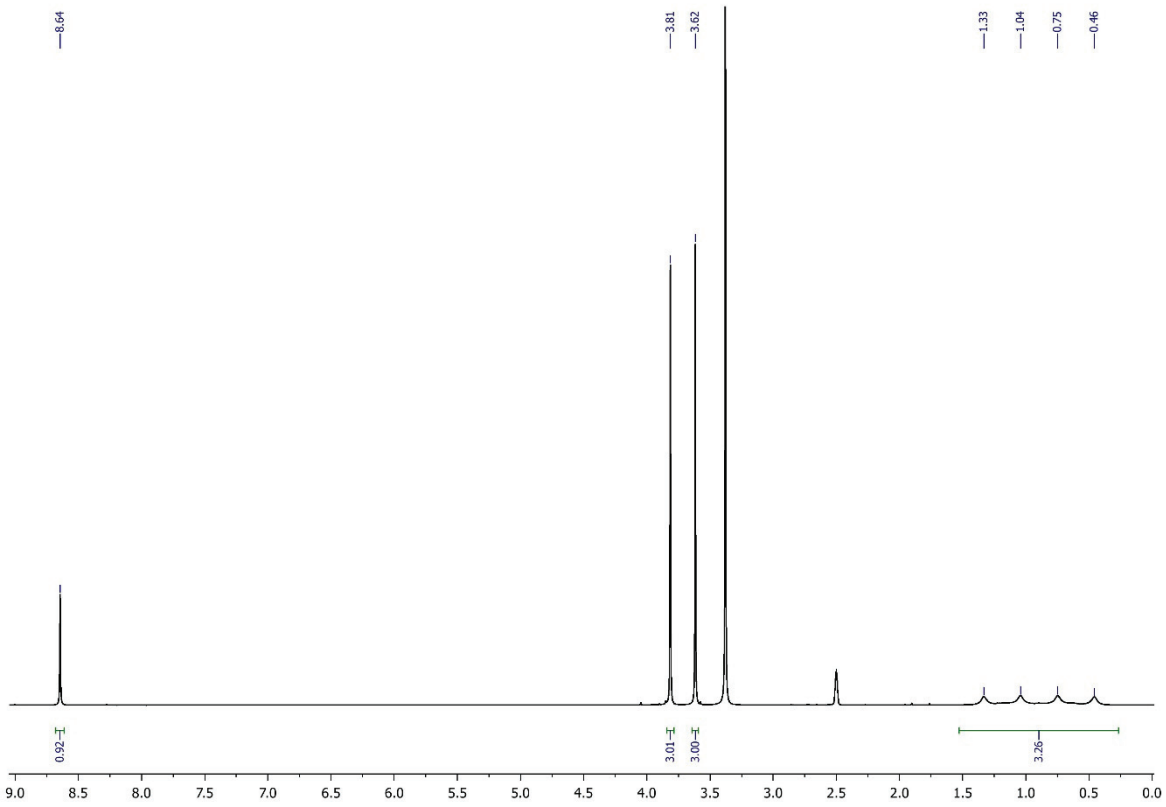

Figure 163. *^{1}H NMR spectrum of compound **(3)** in DMSO-d_6.*

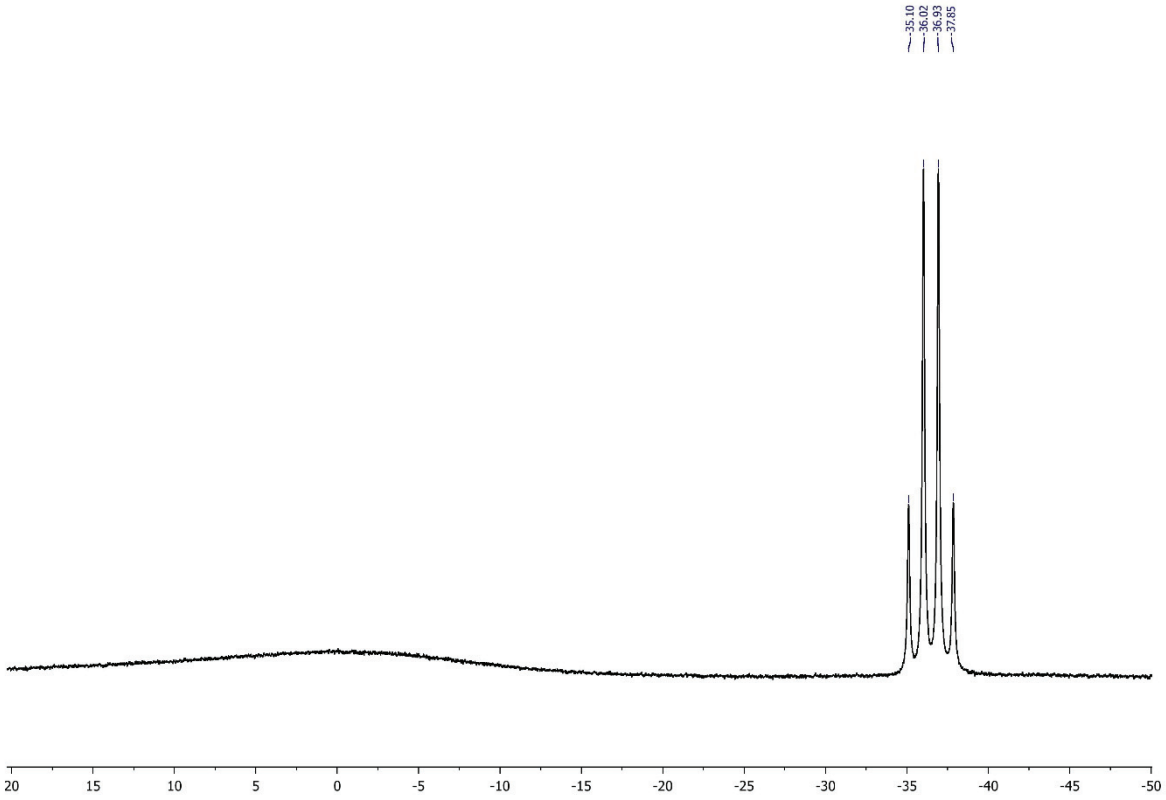

Figure 164. *^{11}B NMR spectrum of compound (**3**) in DMSO-d$_6$.*

- Synthesis of 1-methyl-3-(3-sulfonatopropryl)-1*H*-imidazol-2-ylideneborane (**13**):

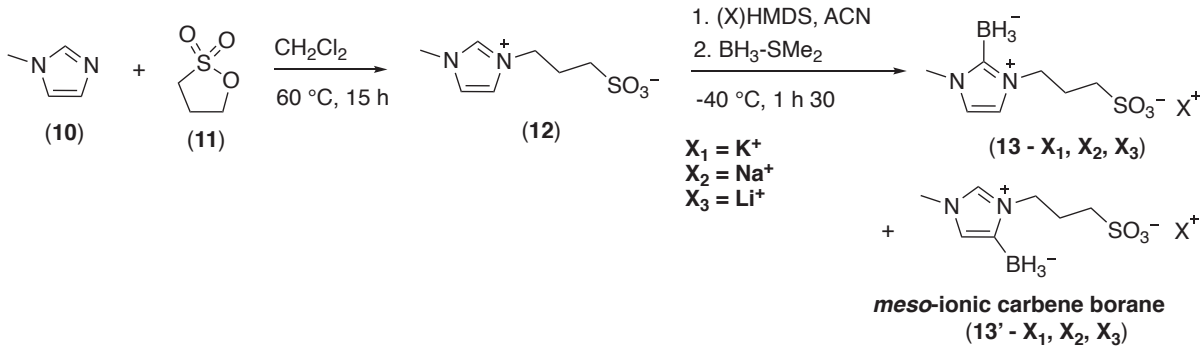

A solution of 1,3-propane sultone (**11**) (4.139 g, 33.6 mmol) and DCM (10 mL) was added to a round-bottom flask containing *N*-methylimidazole (**10**) (0.39 mL, 4.9 mmol). The reaction mixture was stirred at 60 °C for 15 h under argon atmosphere. The product was precipitated, and then isolated by filtration, washed with DCM (2 x 10 mL). A white powder was obtained as zwitterion (**12**) (1.01 g, Yield: 100%). A solution of KHMDS (1 mol L^{-1} in THF, 0.98 mL, 0.98 mmol) was first added to a solution containing zwitterion (**12**) (0.2 g, 0.98 mmol) in acetonitrile (20 mL) at – 40 °C. Then, a solution of BH_3-SMe_2 (0.3 mL, 3.16 mmol) was added dropwise to the previous mixture. The reaction was stirred at –40 °C for 1 h. Then, the reaction

medium was removed from the cooling batch (dry-ice acetone bath) and left at room temperature for 30 min. The solvent was evaporated under vacuum and the crude product (**13 – X_1 = K^+**) was obtained as a yellow powder (very sensitive to moisture). After several purification attempts (inverse column chromatography, evaporation, crystallization), the compound (**13 – X_1 = K^+**) was used as it is. Yield: 89%.

The same procedure was followed to prepare (**13 – X_2 = Na^+**) and (**13 – X_3 = Li^+**), replacing KHMDS by NaHMDS and LiHMDS, respectively. Despite various attempts, the purification of the crude products was not possible. Yield: 85% and 53 %, respectively.

- Synthesis of 2-methyl-4-(4-sulfonatopropryl)-1,2,4-triazol-3-ylideneborane (**16**):

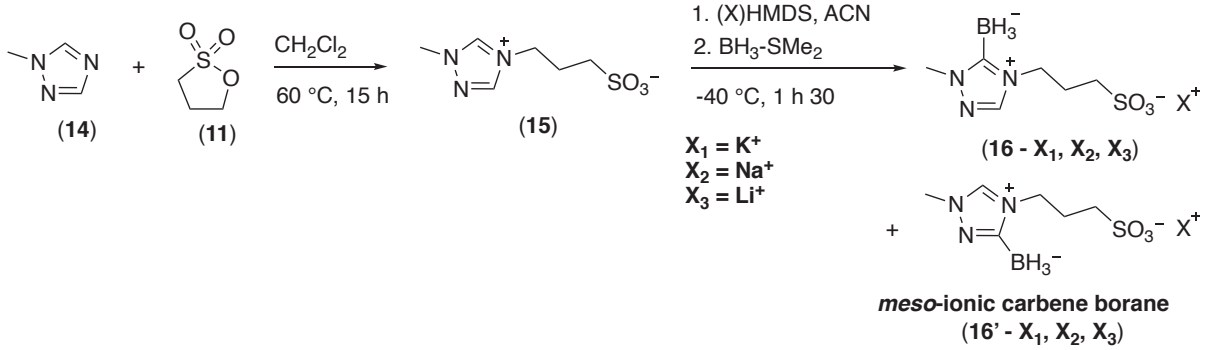

A solution of 1,3-propane sultone (**11**) (4.093 g, 33.5 mmol) and DCM (10 mL) was added to a round-bottom flask containing 1-methyl-1,2,4-triazole (**14**) (0.38 mL, 5.0 mmol). The reaction mixture was stirred at 60 °C for 15 h under argon atmosphere. The product was precipitated, and then isolated by filtration, washed with DCM (2 x 10 mL). A white powder was obtained as zwitterion (**15**) (1.03 g, Yield: 100%). A solution of KHMDS (1 mol L^{-1} in THF, 0.97 mL, 0.97 mmol) was first added to a solution containing zwitterion (**15**) (0.202 g, 0.98 mmol) in acetonitrile (20 mL) at – 40 °C. Then, a solution of BH_3-SMe_2 (0.28 mL, 2.95 mmol) was added dropwise to the previous mixture. The reaction was stirred at –40 °C for 1 h. Then, the reaction medium was removed from the cooling batch (dry-ice acetone bath) and left at room temperature for 30 min. The solvent was evaporated under vacuum and the crude product (**16 – X_1 = K^+**) was obtained as a yellow powder (very sensitive to moisture). After several purification attempts (inverse column chromatography, evaporation, crystallization), the compound (**16 – X_1 = K^+**) was used as it is. Yield: 69%.

The same procedure was followed to prepare (**16 – X_2 = Na^+**) and (**16 – X_3 = Li^+**), replacing KHMDS by NaHMDS and LiHMDS, respectively. Despite various attempts, the purification of the crude products was not possible. Yield: 99% and 59 %, respectively.

- Synthesis of 2-methyl-4-amino-1,2,4-triazol-3-ylideneborane (**21**):

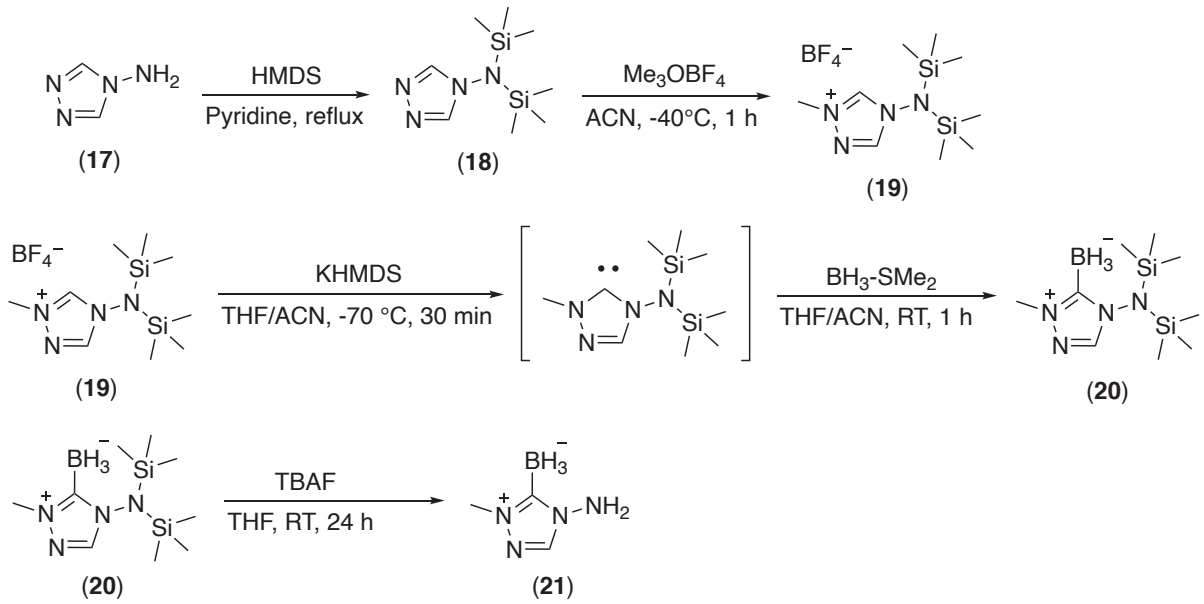

4-amino-1,2,4-triazole (**17**) (4.2 g, 49.9 mmol) was added to around-bottom flask containing a solution of hexamethyldisilazide (HMDS, 20 mL, 130.9 mmol) and pyridine (0.5 mL). The reaction mixture was stirred under reflux for 5 days. A brown precipitate was obtained without any purification (**18**) (6.23 g, 27.3 mmol, yield: 54%). Then, the compound (**18**) (0.5 g, 2.2 mmol) was added to a round-bottom flask containing trimethyloxonium tetrafluoroborate (Me_3OBF_4) (0.35, 2.3 mmol) and acetonitrile (40 mL). The reaction mixture was stirred at -40 °C (dry-ice acetone bath) during 1 h under argon atmosphere. The solvent was evaporated under vacuum and the salt (**19**) (0.72 g, 2.1 mmol, yield: 100%) was obtained without purification. Then, a solution of KHMDS (1 mol L^{-1} in THF, 2.5 mL, 2.5 mmol) was first added to a solution containing the salt (**19**) (0.72 g, 2.1 mmol) in THF (20 mL) and acetonitrile (20 mL) at –80 °C. Then, a solution of BH_3-SMe_2 (0.3 mL, 3.1 mmol) was added dropwise to the previous mixture. The reaction was stirred for 1 h. Then, the reaction medium was removed from the cooling batch and left at room temperature for 1 h. The solvent was evaporated under vacuum and the crude product was purified with silica gel column chromatography and the pure compound (**20**) was obtained as a white solid (0.101 g, 0.4 mmol, yield: 20%). Finally, a solution of tetrabutylammonium fluoride (1 mol L^{-1} in THF, 0.5 mL, 0.5 mmol) was added to a round-bottom flask containing the compound (**20**) (0.101 g, 0.4 mmol) and THF (5 mL). The reaction mixture was stirred at room temperature for 1 day. Then, the solvent was evaporated under vacuum and the crude product was purified with silica gel column chromatography. The pure compound (**21**) was obtained as a white solid. Yield: 10%. ^{1}H NMR (300 MHz, DMSO-d_6): δ

= 6.66 (s, 1H), 3.82 (s, 3H), 3.62 (s, 3H), 0.89 (q, 3H) ppm. ^{11}B NMR (96.3 MHz, $CDCl_3$): δ = -36.43 (q) ppm.

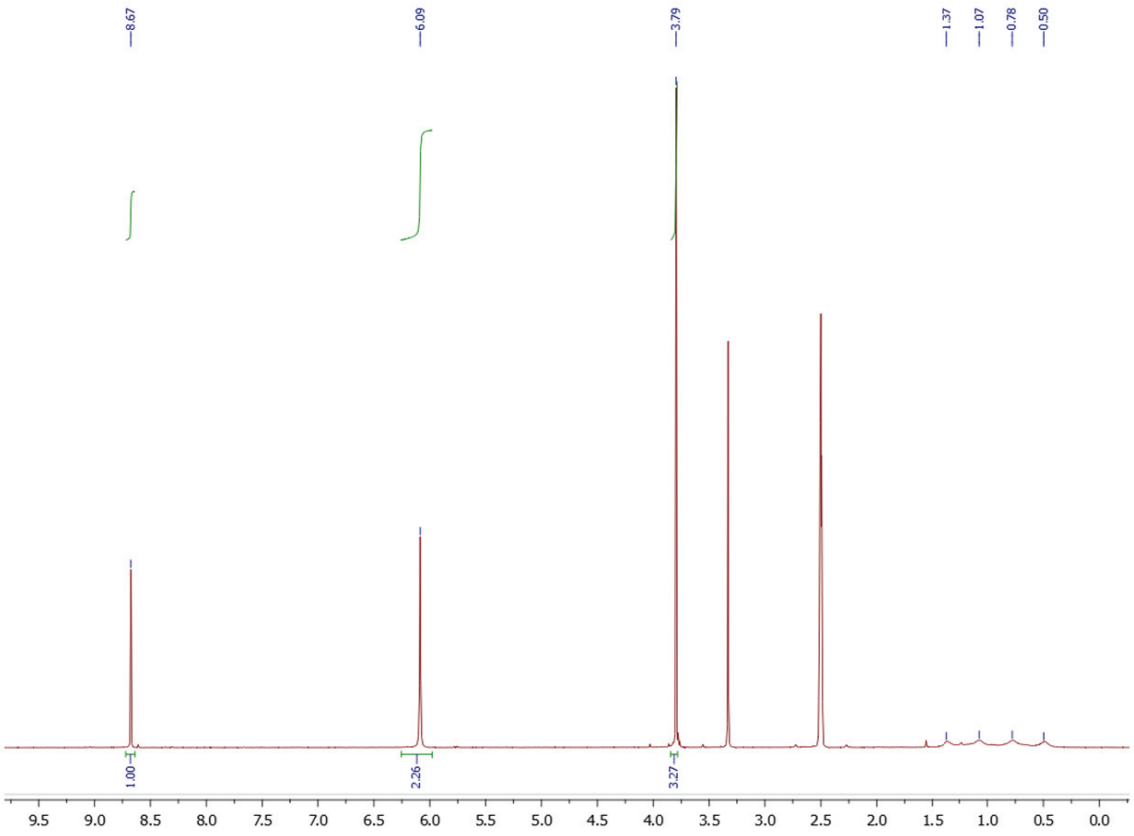

Figure 5. *^1H NMR spectrum of compound (**21**) in DMSO-d_6.*

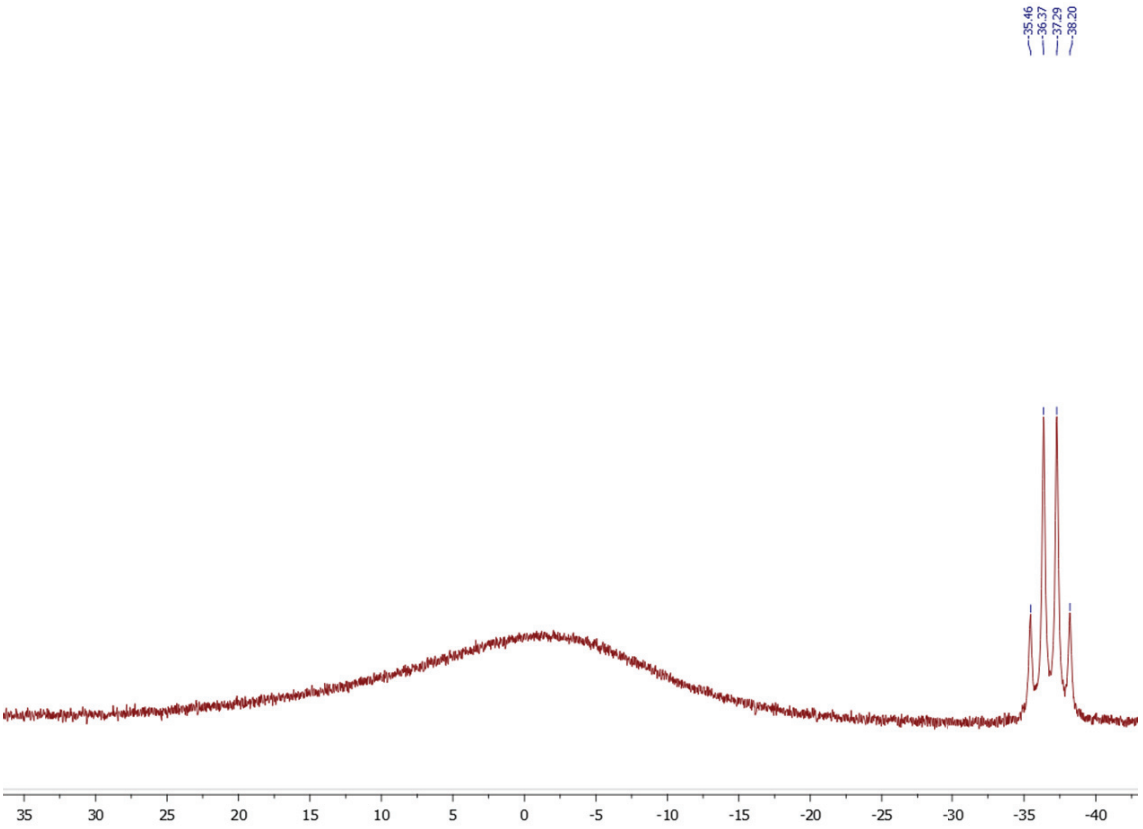

Figure 6. *^{11}B NMR spectrum of compound (**21**) in DMSO-d_6.*

B. Preparation of synthetic latexes by emulsion photopolymerization

The emulsion polymerization reactions were conducted in a 250 mL double wall reactor, mounted with a mechanical stirrer equipped with a glass anchor. A LED ribbon was coiled around the reactor. In a typical procedure, acridine orange (**1**) (8.8 mg, 9.95 x10^{-7} mol) was dissolved in 25 mL of styrene. Then 1 mL of this solution was added to monomer to get 25 g of the dispersed phase. On the other side, the continuous phase was composed of 100 mL of water, SDS, NHC-borane **(3)**, disulfide (**4**) and sodium carbonate. Both solutions were degassed by nitrogen bubbling prior to their transfer with a cannula to the reactor previously purged with nitrogen. The mixture was then stirred 5 min to form an emulsion, then light was switched on, setting the time zero of the reaction. Samples were periodically withdrawn from the reactor under nitrogen through a septum using a syringe and placed in an ice-water bath to stop the reaction, to determine the particle size by DLS and the monomer conversion by gravimetric

analysis according to the equation 5.3. Other dyes and NHC-boranes were used under experimental conditions detailed in Chapter 2.

C. Preparation of synthetic latexes by dispersion photopolymerization

The dispersion polymerization reactions were conducted in a 250 mL double wall reactor, mounted with a mechanical stirrer equipped with a glass anchor. A LED ribbon was coiled around the reactor. In a typical procedure, acridine orange (**1**) (13.2 mg, 1.48 x10^{-6} mol) was dissolved in 25 g of ethanol. Then 1 g of this solution was added the continuous phase composed of 70 g of ethanol, 30 g of water, stabilizer, NHC-borane (**3**), disulfide (**4**) and TBAH. The solution was degassed by nitrogen bubbling prior to its transfer with a cannula to the reactor previously purged with nitrogen. On the other side, the monomer was degased by nitrogen bubbling separately from the previous solution and transferred with a cannula to the reactor. The solution was then stirred, and the light was switched on, setting the time zero of the reaction. Samples were periodically withdrawn from the reactor under nitrogen through a septum using a syringe and placed in an ice-water bath to stop the reaction, to determine the particle size by DLS and the monomer conversion by gravimetric analysis according to the equation 5.3.

D. Preparation of hybrid latexes by Pickering dispersion photopolymerization

1. Modification of the CeO_2 nanoparticles surface by disulfide **(4)**

A suspension of CeO_2 (5.6 wt.% relative to water) was prepared in 10 g of water. The disulfide (**4**) was dissolved in 10 g of methanol in concentrations ranging from 1.29 to 96.02 mmol L^{-1}. The disulfide/methanol solution was then added dropwise *via* a syringe pump (flow rate fixed at 1 mL 15 min^{-1}) to the CeO_2 sol. The mixtures were stirred for 30 min. The size of the CeO_2 NPs was measured by DLS. 3 g of each solution were collected and then centrifugated at 80 000 rpm for 4 h to precipitate the disulfide modified CeO_2 NPs. After ultra-centrifugation, the supernatants were analyzed by elemental analysis and the precipitates by FTIR.

2. Pickering dispersion polymerization of *n*-BA/MMA

The Pickering dispersion polymerization reactions were conducted in a 250 mL double wall reactor, mounted with a mechanical stirrer equipped with a glass anchor. A LED ribbon was coiled around the reactor. In a typical procedure, disulfide was dissolved in 50 g of methanol and then, added dropwise *via* a syringe pump (flow rate fixed at 1 mL 15 min^{-1}) to the CeO_2 sol (50 g of water). The suspension was stirred and degassed by nitrogen bubbling for 45 min prior to its transfer with a cannula to the reactor previously purged with nitrogen. On the other side, the monomer was degased by nitrogen bubbling separately from the previous solution and transferred with a cannula to the reactor. The mixture was then stirred, and the light was switched on, setting the time zero of the reaction. Samples were periodically withdrawn from the reactor under nitrogen through a septum using a syringe and placed in an ice-water bath to stop the reaction. The particle size was determined by DLS and the monomer conversion by gravimetric analysis according to the equation 5.3.

3. Film formation

Film mold casts were prepared by using 3 mL of the (hybrid) latexes and left to dry in poly(tetrafluoroethylene) molds at ambient conditions over 7 days. The final films were obtained with a thickness < 150 mm.

Abstract

Photoinduced polymerization in dispersed media has been reported for the first time in the 1980s, while polymerization in dispersed media has found wide industrial applications for more than a century, allowing the production of various kinds of polymer colloids. Synthetic latexes are used in numerous fields such as coatings, paints, and adhesives. The studies on photoinduced polymerization in dispersed media remain rare, and only very few monomers such as methyl methacrylate and styrene have been investigated. However, photopolymerizations are attractive, since they are triggered by light, and as such subject to external temporal and spatial control. Efficient strategies must thus be developed to combine the advantages of photopolymerization with those of polymerization in dispersed media.

We have recently reported a new water-soluble photoinitiating system (PIS) capable of absorbing visible light at room temperature. It consists of a dye, a disulfide compound and a *N*-heterocyclic carbene borane. Compared to UV light sources, visible-light LEDs produce photons with longer wavelengths. The photons in the visible range are less subject than UV photons to the scattering effects induced by the presence of the particles, thus enabling a better light penetration. Our PIS has been shown to initiate the emulsion photo-polymerization of styrene and (meth)acrylic monomers. The obtained final latexes are highly stable, with particle sizes ranging from 50 to 300 nm and solids content up to 30%. The different species of the PIS were however shown to partition between the different phases of the system (water, monomer droplets and particles), resulting in some cases in broad particle size distributions.

In this work, we discuss new options that can lead not only to monodisperse but also larger particles. The introduction of a new more water-soluble PIS led to a substantial improvement of the size dispersity. Moreover, to push the boundaries of light penetration, the synthesis of both polymer particles and hybrid cerium dioxide–polymer latex particles was investigated in dispersion photopolymerization, where the mixture is initially totally homogeneous.

Résumé

La photopolymérisation en milieu dispersé a été reportée pour la première fois dans les années 1980, les procédés de synthèse de latex occupent depuis des décennies une place importante dans le secteur de l'industrie, permettant la production de divers types de dispersions colloïdales de polymère. Les latex synthétiques sont utilisés dans de nombreux domaines (revêtements, peintures, adhésifs). Les études sur la photopolymérisation en milieu dispersé restent rares et seuls quelques travaux sur des monomères tels que le méthacrylate de méthyle et le styrène ont été reportés jusqu'ici. Toutefois, les photopolymérisations sont attrayantes car elles sont déclenchées par la lumière, et permettent donc un contrôle externe de la polymérisation, du point de vue spatial comme temporel. Des stratégies doivent donc être mises en place pour combiner les avantages de la photopolymérisation avec ceux de la polymérisation en milieux dispersés.

Nous avons récemment développé un nouveau système photoamorceur hydrosoluble capable d'absorber la lumière visible à température ambiante. Il se compose d'un colorant, d'une espèce disulfure et d'un carbène *N*-hétérocyclique-borane. Par rapport aux sources de lumière UV, l'utilisation de LEDs en tant que source de lumière visible produit des photons ayant des longueurs d'onde plus longue. Les photons dans le domaine du visible sont moins soumis par rapport aux photons UV aux effets de diffusion induits par la présence de particules, permettant ainsi une meilleure pénétration de la lumière. Il a été démontré que notre système photoamorceur était ainsi capable d'amorcer la photopolymérisation en émulsion de monomères acryliques et du styrène. Les latex finaux obtenus sont très stables, avec des diamètres de particules compris entre 50 et 300 nm et avec des taux de solides allant jusqu'à 30%. Cependant, nous avons montré que les différentes espèces du PIS pouvaient se partager entre la phase monomère et la phase aqueuse, entraînant dans certains cas de larges distributions de tailles des particules.

Dans cette étude, nous discutons de nouvelles options pouvant conduire non seulement à des particules monodisperses, mais également à des particules plus grosses. L'étude d'un nouveau système photoamorceur plus hydrosoluble a conduit à une nette amélioration des distributions de tailles des particules. De plus, dans le but de repousser les limites de la pénétration de la lumière dans le milieu réactionnel, nous avons synthétisé des latex et des latex hybrides en présence de nanoparticules d'oxyde de cérium par un procédé de photopolymérisation en dispersion en milieu hydroalcoolique, pour lequel le mélange est initialement homogène.